Fast Assistance Search and Rescue

Final Report

Group S4

Design Synthesis Exercise

TU Delft

Fast Assistance Search and Rescue

Final Report

by

Group S4

Group members:

Eijkelhof, D.	4281446	Martin Mendez, M.	4179099
Gupta, A.	4355458	Mavrocordatos, N.	4350642
Haan, W. de	4296982	Pluijm, R. van der	4342313
Hak, J.A.H.R.	4391187	Seres, P.	4370716
Koreman, D.R.T.	4372328	Weijers, W.N.	4353730

DSE duration: April 24, 2017 – July 7, 2017

TU Delft

Preface

This report is part of the 2017 Spring A3200 Design Synthesis Exercise of the Delft University of Technology. Out of twenty-five exercises the DSE FASAR 04 exercise was selected to solve the problem SAR teams are coping with at the moment.
First, we would like to thank our DSE tutors Dr. Ir. F.F.J. Schrijer and Dr. Ir. A.H. van Zuijlen of the Faculty of Aerospace Engineering at the Delft University of Technology. They consistently allowed this project to be our own work, but steered us in the right direction whenever they thought we needed it. The purpose of the project is to develop an Unmanned Aerial Vehicle (UAV) that is able to provide assistance to search and rescue teams during a disaster.

Second, we would also like to acknowledge T. Steinke and B. Rattanagraikanakorn of the Faculty of Aerospace Engineering at the Delft University of Technology as the coaches of this project and we are gratefully indebted to them for their very valuable comments on our work and source recommendations whenever we got stuck. Also, we would like to thank Kyle from HFE internationals, who provided us with valuable information about the engine.

Finally, we must express our very profound gratitude to all the professors and lecturers for providing us with small but unfailing support. The final design would not have been possible without their help.
Hopefully the reader will see the effort we have put into this report. For the passed months we have been working on this report with a lot of enthusiasm.

Group S4
Delft, July 5, 2017

Executive summary

Just a few years ago Kathmandu suffered a 7.8-magnitude earthquake, followed by more than 120 aftershocks.[1] Thousands of inhabitants of the city and its surroundings were injured and the earthquake took lives of over 8,000 people. According to the Nepal Red Cross Society more than 17,000 were injured.[2] Search and rescue (SAR) teams from all over the world travelled to Nepal to search for survivors, including the Dutch rescue team.[3] However, life was tough for the SAR teams, as the media congested not only army choppers with journalists, where doctors and medical supplies were more needed, but also telecommunication satellites.[4] During these disasters with the infrastructure gone, communication between SAR teams is problematic due to the media using the much needed bandwidth used for satellite communications. This limits the efficiency SAR teams can work with and limits their ability to find people reported missing. The solution to these two problems is at hand. Nowadays, airspace is more and more occupied with Unmanned Aerial Vehicles (UAVs). Their application is widening with more relaxed UAV regulations, since UAVs are not only used for the military anymore. As an example, UAVs are now used for surveillance missions, agricultural missions and missions for search and rescue. However, existing search and rescue drones are limited in their flight envelope, their flight performance and endurance. Therefore,

a new design of a search and rescue drone is to be designed that flies autonomously

and copes with hard weather conditions and has the required performance. Along with the UAV design, a Ground Station (GS) with a pseudo-satellite is constructed. This design is explained soon after the description of the UAV. This Unmanned Aerial System (UAS) is designed to assist in SAR operations.

Concepts studied prior to the final design have been traded off depending on feasibility, performance, cost and more specific trade-off criteria as for instance mass, power and size. All concepts were based on a morphological diagram. Out of these concepts, three concepts were established to be looked further into. These concepts were the single fixed-wing aeroplane-like concept, the multiple fixed-wing aeroplane-like concept and the helicopter concept. Unfolding the tree to various configurations led to a trade-off within each concept and from both branches the best configuration was chosen. Namely, the fixed-wing aeroplane-like configuration and the single rotor configuration, were traded off against each other.

Requirements such as operating for more than 2 h successively and 72 h with a downtime of only 15 min were among the extensive list. It turned out operating in 10 Bft was unreasonable as people can not stand up right and trees become uprooted in these conditions.[5] Hence, the UAV is designed for 8 Bft. Furthermore, among the requirements were payload requirements such as fine and coarse mapping resolutions. Lastly, a cost constraint of € 500,000 and a weight constraint of 25 kg would make the UAV compatible for the market. Taking these requirements into account, a UAV design rolled off the assembly line as a twin-boom, aeroplane-like UAV with a petrol engine, taking up to 6 kg of fuel. An RGB-camera, a LIDAR-camera and an IR-camera are incorporated in the UAV, with the LIDAR being redundant but making the UAV more competitive on the market. Having a total cost below € 220,000 and a weight of less than 23 kg, the UAV meets the two last requirements.

Structural design

Performance analysis shows that the other requirements have been met as well. The structure is designed to deal with a load factor of 7 g. This means that the loads from launch of the emergency parachute does not destroy the structure. Examining the structural design of the UAV, the main wing turned out to be the most challenging. To withstand the hostile conditions, shear and bending moments have been identified along the main wing and have been designed accordingly. An adaptable discrete numerical model has been designed for the main wing, the horizontal tail and the vertical tail. The skin has been optimised for thickness to ultimately end up with the most lightweight UAV possible. However, limitations on manufacturability resulted in a step-wise decrease in thickness which is shown in fig. 1a. After the optimisation of the thickness, the geometry was updated and evaluated for stresses to make sure the yield stress were not exceeded. As a last step the method was completed by checking for additional loads on the UAV.

This procedure and model was validated by using a finite element analysis (FEA). This basically implies that a model was created in Ansys and compared to the discrete numerical model that was used for this project. Ansys was verified by checking for a simple geometry.

[1] http://www.bbc.com/news/world-asia-32479909
[2] http://timesofindia.indiatimes.com/world/south-asia/Nepal-earthquake-death-toll-rises-to-8413/articleshow/47187088.cms?from=mdr
[3] http://nltimes.nl/2015/04/26/dutch-rescue-team-to-aid-nepal-earthquake-response/
[4] http://www.thehindu.com/news/national/indian-media-jingoism-was-trigger-for-backlash-in-earthquakehit-nepal/article7171043.ece
[5] https://www.windfinder.com/wind/windspeed.htm

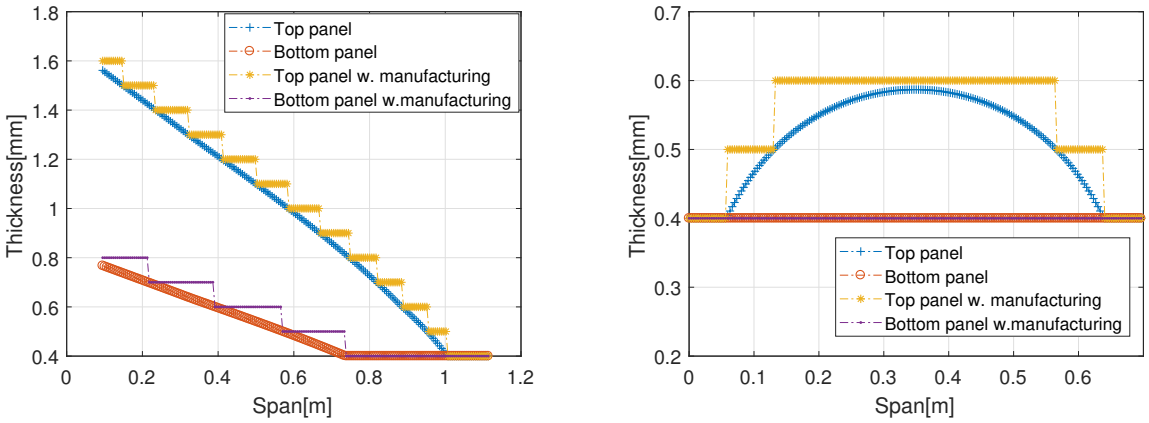

(a) Main wing.

(b) Tail wing.

Figure 1: Thickness optimisation along the half-span and the horizontal tail.

The structural design of the U-tailed, twin-boom empennage was less of a challenge. The reduced complexity compared to the main wing and the absence of the booms eased the computations. The thickness optimisation of the tail wing is depicted in fig. 1b. A step-wise thickness layout is shown again due to manufacturability limits. The booms have been designed for bending and checked for torsion. An I-beam was found optimal from a structural point of view, but lacked performance from an aerodynamic point of view. The booms were optimised for thickness as well and is depicted in fig. 2.

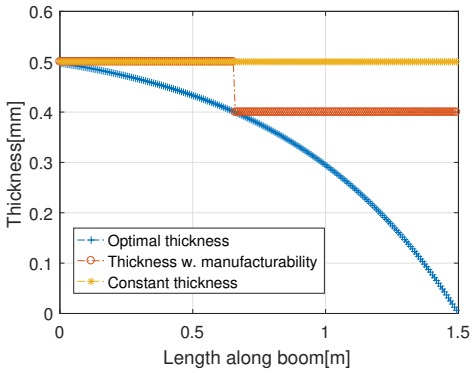

Figure 2: Ideal, step-wise and constant thickness along the boom.

Lastly, the fuselage was designed and structurally enforced to ensure take-of loads and provide placements for the payload. A summary of the required thickness is shown in table 1.

Table 1: Required thickness of fuselage skin for different stress modes

Stress Mode	Maximum load present	Required fuselage skin thickness [mm]
Bending	1,500 [N m]	0.052
Shear	2,000 [N]	0.015
Torsion	500 [N m]	0.019
Column Buckling	3,500 [N]	0.001
Axial	3,500 [N]	0.012

Aerodynamic design

In aerodynamics, the design of a custom-made propeller played an important role. By means of XROTOR 7.55 a propeller was designed to minimise induced losses, but still guaranteeing that the performance requirements were met. It turned out that manufacturability limited the rotor design to a tip chord of 0.06 m. The resulting geometry values are summarised in table 3. Here, the c- and β-column represent the chord length and the geometric blade pitch angle along the propeller blade respectively.

Furthermore, the main wing planform and its aerofoil have been devised to provide lift that counteracts the weight of the UAV. The geometry of the aerofoil has been selected based on its usability, controllability and stall characteristics in the low Reynolds regime at low Mach number missions. Even though a high thickness aerofoil has greater stability characteristics

in comparison to symmetrical, cambered and reflex cambered aerofoil, a semi-symmetric cambered aerofoil was picked. The conclusion was drawn based on cruise speed range and the high lift over drag coefficient.

Twenty-two aerofoils out of this branch of aerofoils were investigated using XFOIL V6.99. The aerofoil that stood out from the extensive list was the FX 63-110 Wortmann aerofoil, depicted in fig. 3a. The stall lift coefficient $C_{l_{max}}$ outperforms all other aerofoils and the C_l-C_d graphs shows the highest lift over drag in the full drag coefficient regime.

Table 2:
Cambered, semi-symmetric aerofoils selected for the main wing aerofoil.

Aerofoils			
RG 14	USA 48	S2027	FX 63-110
RAF-48	HQ3.0/11	GEMINI	FX 60-100
EPPLER E853	EPPLER 67	Curtis C-72	CLARK V
S40222	AG37	NACA 2408	NACA 2409
NACA 2410	NACA 2411	NACA 2412	NACA2413
NACA 2414	NACA2415		

Table 3: Final geometry of the chord and pitch angle of three blade sections.

	c [m]	β [°]
Root (hub)	0.062	72.83
0.5 · R	0.050	35.68
Tip	0.006	25.09

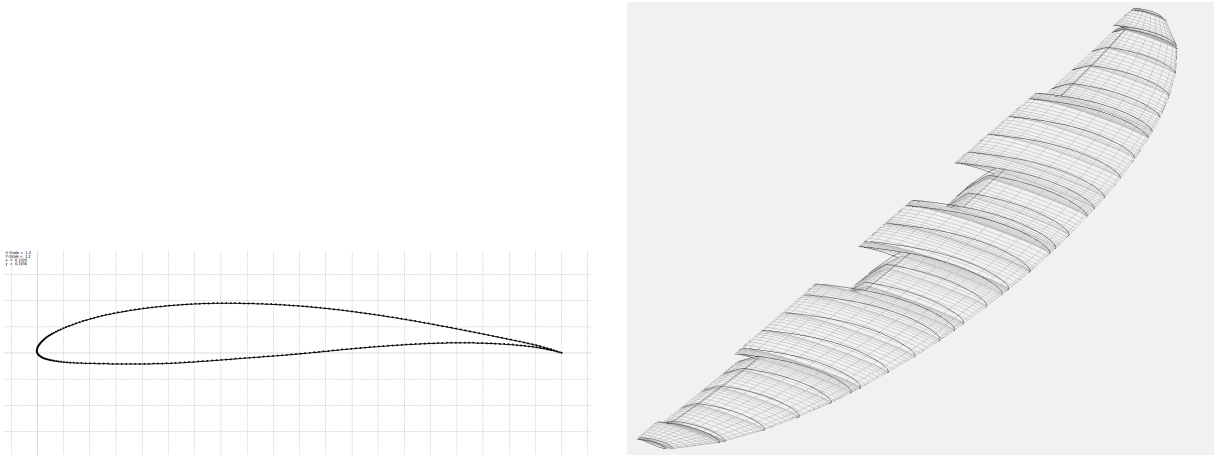

(a) Two-dimensional layout of the FX 63-110 Wortmann aerofoil.

(b) Three-dimensional

Figure 3: Two- and three-dimensional layout of the main wing.

For converting the two-dimensional aerofoil to the three-dimensional planform an investigation on the shape of the planform was required. The semi-elliptical planform was chosen due to its constant elliptical lift distribution. Including the tail, the configuration has been optimised to make sure the aeroplane is stable. It shows that the aeroplane is stable by having a negative C_{m_α} around the centre of gravity. Furthermore, the UAV flies with a zero moment in cruise condition and it was checked that the UAV still provides positive lift at $C_m = 0$. These are shown in fig. 4a and fig. 4b.

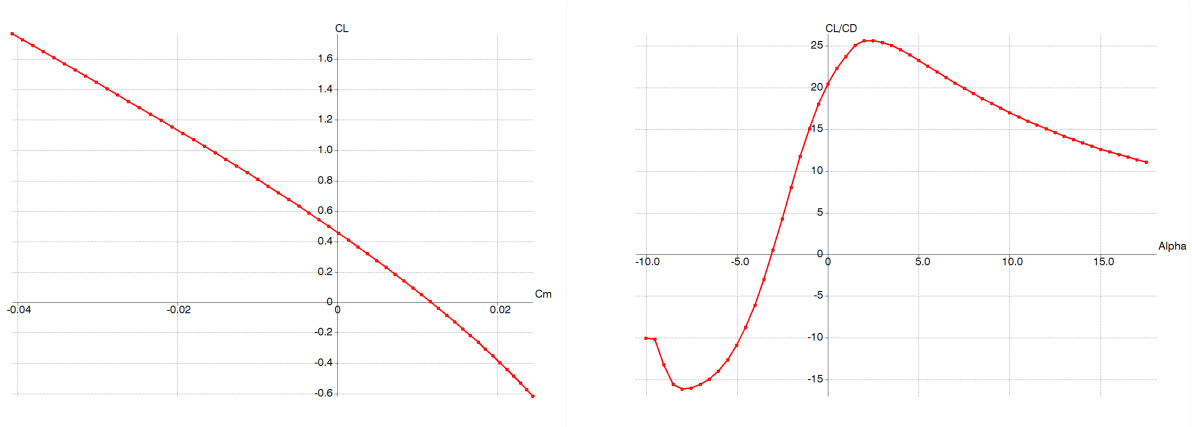

(a) C_m- C_L polar graph.

(b) $C_L C_D$-α polar graph.

Figure 4: Polar graph of the main wing and tail wing together.

Controllability of the UAV

Aerodynamics is not only relevant for cruise condition, but also plays a major role in controlling the aircraft. By altering the camber locally along the trailing edge, the wind direction is altered and lift is produced locally. This is done by means of

ailerons, flaps and elevators. The elevators are designed in such a way it can still assure controllability in landing configuration. Based on requirement **REQ.U.SYS.22**, the ailerons were designed and the flaps were constrained by the distance between the engines and the booms. The aileron sizing is depicted in fig. 5, where the horizontal line indicates the required roll rate compared to the available roll rate, shown along the half-span, by means of the inner dimension of the aileron b_1.

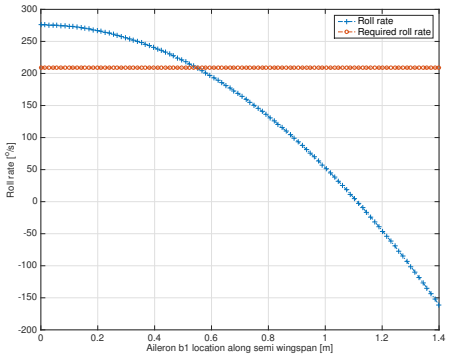

Figure 5: Required and available roll rate along the half-span, by means of the inner dimenions of the aileron b_1.

However, it is much more convenient to look at the dynamic stability of the aeroplane by means of eigenvalues. The eigenvalues have been established using XFLR5 V6.38. It has to be noted that the Vortex Lattice Method (VLM) was not able to perform calculations near the stall angle of attack (AoA), the linear region of the lift polar curve came out valuable.[14] The dynamic analysis eigenvalues are tabulated in table 4. The emphasis needs to be stressed on all the negative, damping real parts of the eigenvalues, except the spiral stability. However, as the spiral is a slow diverging eigenmotion, it can be controlled easily and is not necessarily needed to be corrected. The imaginary parts of the eigenvalues show the level of oscillation of the eigenmotion.

Table 4: Eigenvalues for the different eigenmotions.

	Motion	Eigenvalues	Period [s]	Damping coefficient ζ	$T_{\frac{1}{2}}$ [s]
Longitudinal	Short motion	-4.034 +/- 5.256i	1.195	0.6088	0.1718
	Phugoid	-0.0063 +/- 0.328i	19.162	0.0012	110.585
Lateral	Asymmetric roll	-12.17	-	1	0.0570
	Dutch roll	-0.2965 +/- 3.267i	1.923	0.0904	2.3378
	Spiral	0.06221	-	-	-11.142

The importance of the time-to-half-amplitude is significant because it is a measure of the length of the eigenmotion. These have also been summarised in table 4. Shown in the last column, the phugoid motion hardly damps out and takes over 100 min. Moreover, it is essential to note the negative time-to-half-amplitude that actually means the time-to-double-amplitude, indicating that the eigenmotion is indeed divergent.

Payload

As the objective states that the UAV is there to assist the SAR team and hence is equipped with mapping, sensing, communication and avionics payload to map, sense and communicate. These systems have been thoroughly analysed and merged together to have the most valuable layout of the payload. Among the mapping payload there is an RGB-camera for high resolution pictures, but is vulnerable to weather conditions. Furthermore, the UAV is equipped with an IR-camera for heat detection that is particularly of importance to locate survivors. Lastly, to make the UAV more valuable on the market, the UAV is completed with a LIDAR-camera to provide the SAR teams with three-dimensional mapping point cloud.

Regarding the sensing payload, a radar, a Global Positioning System (GPS) and a pitot tube are included and with respect to communications, transceivers and antennas are on-board of the UAV.

The payload is carefully placed to balance the UAV, guarantee stability and also provide the best vantage point. The payload has been placed closed to the nose since the engine provides a nose-up moment. The placement of all systems on-board of the UAV is depicted in fig. 6. The fuel tank is placed directly at the centre of gravity, meaning that the centre of gravity will be the same, irrespective of being filled or empty. The power required is served by a 325W generator that is attached to the engine and LiPo batteries are included for emergency situations to still provide power to the main subsystems.

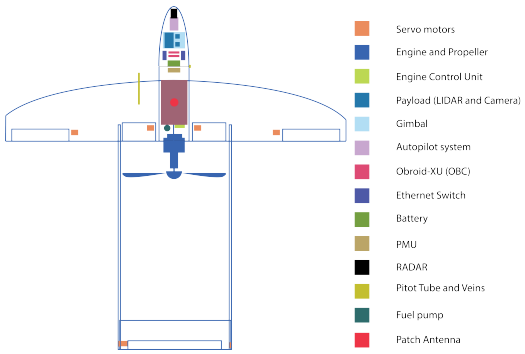

Figure 6: Subsystem placement of the UAV.

Ground station

The GS has been designed to provide a data link between the UAV and the GS. An innovative system has been developed to comply with the requirement **REQ.U.SYS.6** that states that the UAV needs to have a communication link of 50 km. To comply with this requirement, the GS is equipped with a pseudo-satellite in the shape of a kite. This kite contains multiple safety measures to guarantee tether-visibility and has a payload to provide the communication between the GS and the SAR-teams. The payload is tabulated in table 5.

Table 5: The payload of the kite.

Component	Weight [g]	Power consumption[W]	Cost[€]
Battery pack	1,900	-	500
Transponder	78	2.0	3,500
Transceiver	120	40.0	7,500
Transceiver	120	4.8	7,500
Antennas	400	-	-
LED	100	9.5	50
Total	2,718	56.3	19,050

For the kite to be useful in all weather conditions, it was chosen to go for multiple kites that cope with all weather conditions. A Helikite is suitable in low wind conditions but drifts off at higher wind speeds. To be able to cope with severe wind conditions a Delta Kite is used. Both are suitable and proven concepts.

An inventive landing procedure was designed that makes the landing feasible without depending on the surroundings where the GS is situated. A large landing net with dimensions of 7 by 10 m absorbs the energy of the UAV and slows it down. The net is shown in fig. 7a, including the target zone where the UAV is able to land safely. The blue circles represent the IR emitters, which are sensed by the UAV to have a coordinated landing. Peripherals have been thought off, such as tension belts, a variety of pins, tubes and attachment ropes.
The launching procedure is an off-the-shelf catapult launcher that is able to give the UAV a launch speed of 21 m s^{-1}.

Lastly, the GS has been equipped with a command station in which operators can analyse, intervene and programme flight paths. The command station comes with a 1.7 kW GP2200i generator from Generac to provide power to the portable ground station, illustrated in fig. 7b.[6] Durably integrated in to a military case, the command station is indestructible and used as a docking station. Components such as a laptop, a flightstick and a hard disk are put in the command station, meaning that everything is at hand for the operators. The GS can be operated by three people only and is set up in 75 min.

[6] http://www.generac.com/all-products/generators/portable-generators/gp-series/gp2200i

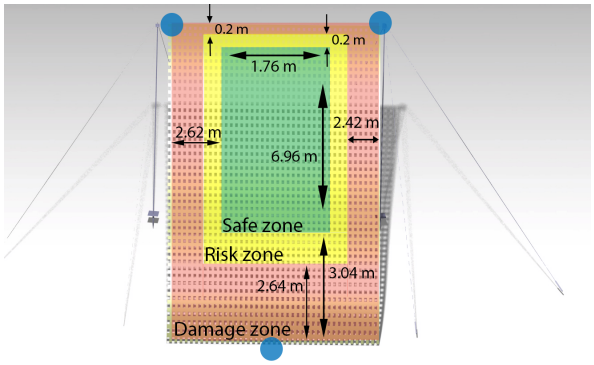

(a) Illustration of safe, risky and damaging spots of the landing procedure.

(b) Command station layout.

Figure 7: Illustration of the landing net and the command station that are part of the GS.

Manufacturability and assembly

Manufacturability limits posed some limitations on the design. Regarding structures and aerodynamics, it would end up beneficial when the manufacturability limits are decreased.

Taking a look at the assembly of the UAV, it can be seen that the UAV is easily assembled. This has been guaranteed by using a push and pull configuration for the main wing. The assembly for the main wing is depicted in fig. 8a. Note that the push and pull method also ensures that the UAV can be fitted in a case with the dimensions shown in fig. 9.

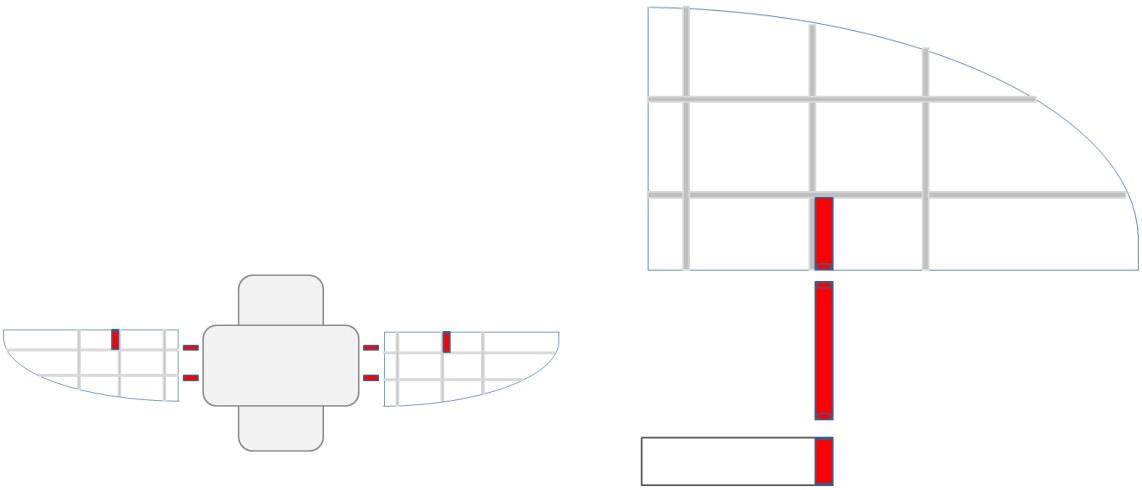

(a) Main wing assembly.

(b) Tail wing assembly.

Figure 8: Assembly layout for the main wing and tail wing.

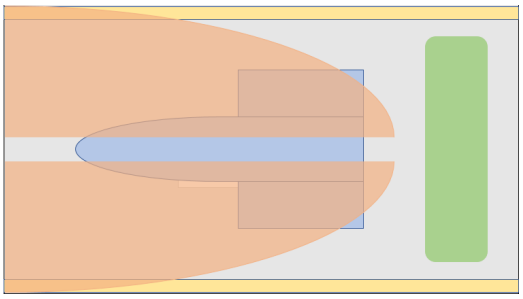

Figure 9: Layout in the box when the UAV is disassembled.

Important parameters

All important parameters w.r.t. the UAS are listed below. Volume, mass and cost budgets are shown in table 6 for the entire system. The UAV is broken down even further and tabulated in table 7. The big picture in table 7 and table 6 shows that the UAV complies with requirement **REQ.U.SYS.1** and requirement **REQ.O.SYS.10**.

Table 6: Total volume, mass and costs of the UAS.

Subpart	Volume [m^3]	Price [€]	Mass [kg]
Total UAVs	0.864	162000	34.14
Total control station	0.1137	8649	50.05
Total landing net	0.158	1046	97.5
Total redundant parachute	0.005	800	1.2
Total catapult launcher	0.5	20950	110
Total kite payload	0.00187	19001	2.718
Total kite	0.365	10149	96.2
Total fuel	0.250	N.I.	192.5
Total	**2.26**	**222600**	**585**

Table 7: Total mass, costs and power budget of the UAV.

Subpart	Mass [kg]	Price [€]	Power [W]
Total Fuselage	1.98	5,500	-
Total Main Wing	4.035	12,000	-
Total Empennage	0.350	1,000	-
Total Booms	0.382	1,700	-
Total Propeller	0.300	900	-
Total Structure	**7.24**	**21,000**	**-**
Engine,Generator and PMU	4.398	21500	+325
Fuel Tank	0.658	1,948	-
Fuel	6	N.I.	-
Lights	0.200	50	-10
OBC	1.128	14,000	-179
Mapping Payload	1.22	15,500	-19.4
Radar	0.05	500	-1
Pitot Tube	0.16	3,090	-0.7
Antennas	0.5	250	-
Parachute	1.2	800	-
Servo	0.133	2,450	-8.75
Total Systems	**15.65**	**60,090**	**+106**
Total	**22.89**	**81,088**	**+106**

Table 8: Comparison of primary performance specifications of the UAV to competitors.

Specification	Product
Propulsion type [-]	Combustion
MTOW [kg]	22.89
Wingspan [m]	2.42
Wing Area [m^2]	0.777
Power consumption engine [$kg\,kW^{-1}$]	0.675
Endurance [h]	9.6
Flight Range [km]	840
Cruise speed [$m\,s^{-1}$]	31-34
Max level speed [$m\,s^{-1}$]	42.3
Max wind resistance [Bft]	8
Ceiling [m]	5000
Takeoff Method [-]	Pneumatic Catapult
Maximum takeoff altitude [m]	3548
Landing Method [-]	Net & Parachute

Evaluation and recommendation

Evaluating the system shows that it complies with most of the main requirements set in the beginning. Focusing only on the requirements that have not been met, means more elaboration needs to be given to requirements **REQ.U.SYS.9**, **REQ.O.SYS.7** and **REQ.G.SYS.3**. Out of these, the 10 Bft is the most severe requirement that could not have been met. The reason for it has already been elaborated earlier on. Requirement **REQ.O.SYS.7** has not been met because the possibility to locate and save survivors turned out to be higher when a petrol engine was used compared to an electrical engine. As the product is designed for saving lives, priority was given to performance over sustainability.

Table 9: Compliance matrix showing whether the requirements are met.

Requirement	Target performance	Actual Performance	Compliance
Costumer requirements			
Requirement **REQ.U.SYS.5**	2 h	9.6 h	**Yes**
Requirement **REQ.O.SYS.1**	72 h	Unlimited	**Yes**
Requirement **REQ.U.SYS.3**	10 km^2 in 3 h	37.4 km^2 in 3 h	**Yes**
Requirement **REQ.U.SYS.2**	1000 m^2 in 30 min	6.23 km^2 in 30 min	**Yes**
Requirement **REQ.U.SYS.4**	-	Autonomous flight computer in OBC	**Yes**
Requirement **REQ.U.SYS.9**	10 Bft	8 Bft	**No**
Requirement **REQ.U.SYS.18**	-	Parachute for emergencies	**Yes**
Requirement **REQ.O.SYS.6**	15 min	12 min	**Yes**
Requirement **REQ.O.SYS.7**	-	-	**No**
Requirement **REQ.O.SYS.11**	-	Reusable in different scenarios	**Yes**
Requirement **REQ.O.SYS.12**	3.15 m^3	2.26 m^3	**Yes**
Requirement **REQ.O.SYS.13**	-	COTS used consistently in GS and UAV	**Yes**
Requirement **REQ.O.SYS.10**	500,000.- €	220,000.- €	**Yes**
Requirement **REQ.U.SYS.6**	50 km	50 km	**Yes**
Regulation requirements			
Requirement **REQ.U.SYS.1**	25 kg	22.89 kg	**Yes**
Requirement **REQ.U.SYS.19**	-	2 pilots at ground station	**Yes**
Requirement **REQ.U.SYS.17**	-	LED lights are added for 24 h visibility	**Yes**
Technical requirements			
Requirement **REQ.O.SYS.3**	3,500 m	3,548 m (GS), 5,000 m (UAV)	**Yes**
Requirement **REQ.U.SYS.16**	15 min	10 min	**Yes**
Requirement **REQ.G.SYS.3**	15 min two people	55 min three people	**No**
Requirement **REQ.U.SYS.22**	156 ° s^{-1}	209 ° s^{-1}	**Yes**

As recommendations further research on both the vertical tail shape and its volume, and winglets from an aerodynamics point of view has to be performed. Moreover, the engine used for this UAV is overpowered and on the heavy side because the generator comes along with the engine. Besides, from a structural point of view more research could have been done on carbon honeycomb structures to provide the UAV with a lighter wing.

Contents

Nomenclature

Abbreviations

AC	Alternating Current	
AMC	Aerial Medical Certification	
AoA	Angle of Attack	
BMP	Bit Map	
BSE	Big Single Engine	
BW	Bandwidth	[Hz]
CDMA	Code Division Multiple Access	
CEF	Cost Escalation Factor	
CFD	Computational Fluid Dynamics	
CFR	Code of Federal Regulations	
CG	Centre of Gravity	
COTS	Commercial Off-the-Shelf	
CPI	Consumer Price Index	
CPM	Computational Processing Module	
CPU	Central Processing Unit	
CR	Close Range	
CRUD	Cumulative result of undesirable drag	
CST	Computer Simulation Technology	
DC	Direct Current	
DNG	Digital Negative	
DOT	Design Option Tree	
FAA	Federal Aviation Administration	
FASAR	Fast Assistance Search and Rescue	
FC	Flight Computer	
FEA	Finite Element Analysis	
F	fineness ratio	
FF	Form Factor	
FOV	Field of View	
GNSS	Global Navigation Satellite System	
GPS	Global Positioning System	
GS	Ground Station	
GSM	Global System for Mobile Communications	
HP	Horsepower	[W]
HTOL	Horizontal Take-off and Landing	
IF	Interference Factor	
ILS	Instrument Landing System	
ECU	Engine Control Unit	
IMU	Inertial Measurement Unit	
IR	Infrared	
LIDAR	Light Detection and Ranging, Laser Imaging Detection and Ranging	
LiPo	Lithium-ion-Polymer	
LOS	Line of Sight	
MAC	Mean Aerodynamic Chord	[m]
MCS	Modulation Code Scheme	
MSL	Mean Sea Level	
MTOW	Maximum Take-off Weight	
OBC	On-Board Computer	
OTS	Off-the-shelf	
PFC	Primary Flight Control	
PLC	Payload Computer	
PMU	Power Management Unit	
POA	Plan of Action	
PSFC	Power Specific Fuel Consumption	
RAM	Random-access Memory	

RGB	Red-Green-Blue
ROC	Rate of Climb
ROD	Rate of Descent
ROI	Region of Interest
RPM	Rotations per Minute
RSSI	Received Signal Strength Indication
RTK	Real Time Kinematic
RTMS	Real Time executed for Multiprocessor Systems
RTOS	Real Time Operating System
RX	Receiver
SAR	Search and Rescue
SM	Specific Modulus
SNR	Signal to Noise Ratio
SS	Spacial Streams
SS	Specific Strength
STUA	Small Tactical Unmanned Aircraft
SUA	Small Unmanned Aircraft
sUAV	Small-sized Unmanned Aerial Vehicle
TIFF	Tagged Image File Format
trc	Tail Rotor Correction
TSFC	Thrust Specific Fuel Consumption
TX	Transmitter
UAS	Unmanned Aerial System
UAV	Unmanned Aerial Vehicle
UHF	Ultra High Frequency
VTOL	Vertical Take-off and Landing

Constants

a	Lapse Rate	$[\mathrm{K\,m^{-1}}]$
g_0	Gravitational Acceleration	$[\mathrm{m\,s^{-2}}]$
k	Boltzmann's Constant	$[\mathrm{m^2\,kg\,s^{-2}\,K^{-1}}]$
k	Induced Drag Power Factor	

Greek symbols

α	Angle of Attack	
α_{accel}	Angular acceleration about x-axis	$[\mathrm{^\circ\,s^{-2}}]$
β	geometric blade pitch angle	
$\frac{d\epsilon}{d\alpha}$	Downwash Coefficient	
η_p	Propeller Engine Efficiency Factor	
η_P	Propeller Efficiency	
λ	Wavelength	[nm]
λ	Eigenvalue	
μ	Tip Speed Ratio	
μ	Gust Alleviation Coefficient	
Ω	Rotor Rotational Velocity	$[\mathrm{rad\,s^{-1}}]$
ϕ	Roll angle	[°]
ρ	Density	$[\mathrm{kg\,m^{-3}}]$
ρ_0	Density at Sea Level	$[\mathrm{kg\,m^{-3}}]$
σ	Rotor Solidity	
σ	Ultimate Tensile Stress	
σ_y	Normal Stress	[Pa]
σ_{crit}	Critical Stress	[Pa]
τ_{xy}	Shear Stress in XY-plane	[Pa]
τ_{xz}	Shear Stress in XZ-plane	[Pa]
τ_{yz}	Shear Stress in YZ-plane	[Pa]
θ	Pitch angle	[°]

ζ	Damping Coefficient	

Latin symbols

A	Aspect Ratio	
A	Cross-sectional Area	[m^2]
A_{encl}	Enclosed Area	[m^2]
b	Plate Short Dimension	[m]
b	Wingspan	[m]
b_e	Span Elevator	[m]
b_h	Span Horizontal Tail	[m]
c	Mean Aerodynamic Chord	[m]
C_{AV}	Average Cost	[€]
$\bar{c}$	Mean Aerodynamic Chord	[m]
c	Chord length	[m]
C_{COM}	Communication Cost	[€]
C_D	3-Dimensional Drag Coefficient	
C_d	2-Dimensional Drag Coefficient	
C_{d_0}	Zero lift drag	
C_{D_0}	3-Dimensional Basic Drag Coefficient	
C_{D_f}	3-Dimensional Skin Friction Drag Coefficient	
C_{D_i}	3-Dimensional Induced Drag Coefficient	
$C_{D_{misc}}$	3-Dimensional Miscellaneous or additive Drag Coefficient	
$\overline{C_{D_p}}$	Mean Aerodynamic Drag Coefficient	
C_{D_w}	3-Dimensional wave drag	
c_e	Chord Elevator	[m]
c_h	Chord Horizontal Tail	[m]
C_{HT}	Horizontal Tail Volume	
C_L	3-Dimensional Lift Coefficient	
C_{L_α}	3-Dimensional Lift Curve Slope	[rad^{-1}]
C_{l_α}	2-Dimensional Lift Curve Slope	
$C_{L_{\alpha_h}}$	3-Dimensional Lift Coefficient Horizontal Tail	[rad^{-1}]
C_l	2-Dimensional Lift Coefficient	
$C_{Le_{max}}$	Maximum C_L From Maximum Deflected Elevator	
C_{L_h}	3-Dimensional Lift Coefficient Horizontal Tail	
$C_{L_{h_{tot}}}$	Total C_L Horizontal Tail Including Elevator With Maximum Deflection	
$C_{L_{max}}$	Maximum 3-Dimensional Lift coefficient	
$C_{m_{ac}}$	Moment Coefficient Around Aerodynamic Centre	
C_{m_α}	2-Dimensional Moment Curve Slope	
C_m	2-Dimensional Moment Coefficient	
C_P	Power coefficient	
C_{PL}	Payload Cost	[€]
c_r	Root Chord Length	[m]
C_T	Thrust coefficient	
C_{TOT}	Total Cost	[€]
C_x	Shock Load Coefficient	
D	Drag	[N]
D	Rotor Diameter	[m]
d	Distance	[m]
dy_{seg}	Panel segment length	[m]
E	Endurance	[s]
E	Young's modulus	[MPa]
e	Oswald Efficiency Factor	
E	Young's Modulus	[MPa]
h	Altitude	[m]
h	Height	[m]
i	Panel indels in a cross-section	
I_{xx}	Moment of Inertia about the x-axis	[m^4]
I_{xx}	Mass moment of inertia about the x-axis	[kg m^2]
I_{xz}	Product Moment of Inertia	[m^4]

I_{zz}	Moment of Inertia about the z-axis	[m^4]
J	Propeller Advance Ratio	
j	Wing Segment Index	
K	Gust Alleviation Factor	
K	Buckling Coefficient	
L	Lift	[N]
l_h	Tail Length	[m]
L	Length of the Column	[m]
l_w	Distance Aerodynamic Centre From Centre Of Gravity	[m]
M_x	Moment about x-axis	[N m]
M_z	Moment about z-axis	[N m]
n	Load Factor	[m s^{-1}]
n_{gust}	Gust Load Factor	
n	Buckling Mode Coefficient	
n_{pull}	Pull Load Factor	
n_{turn}	Turn Load Factor	[m s^{-1}]
P	Power	[W]
P_{br}	Brake Shaft Power	
P	Period Of Oscillation	[s]
P	Axial Load	[N]
P_{par}	Parasite Drag Power	[W]
P_{p+d}	Profile Drag Power	[W]
P_i	Induced Drag Power	[W]
P_{req}	Power Required	
$P_{r_{tot}}$	Propeller Total Required Power	[kW]
P_{tot}	Total Power	[W]
q_{s0}	Constant Shearflow	[N m^{-1}]
R	Ideal Gas Constant	[J kg^{-1}]
R	Range	[m]
R	Distance from Propeller Centre	[m]
S	Wing Area, Rotor Area	[m^2]
S_h	Surface Area Horizontal Tail	[m^2]
S_{par}	Surface Area Parachute	[m^2]
T_0	Temperature at Sea Level	[K]
$T_{\frac{1}{2}}$	Time To Half Amplitude	[s]
T	Torsion	[N m]
t	Plate Thickness	[m]
U	Gust Velocity	[m s^{-1}]
U_{max}	Maximum Gust Velocity	[m s^{-1}]
V	Airspeed	[m s^{-1}]
V_{cruise}	Cruise Velocity	[m s^{-1}]
V_D	Dive Velocity	[m s^{-1}]
V_e	Poisson Ratio	
V_h	Airspeed Horizontal Tail	[m s^{-1}]
V_i	Induced Velocity	[m s^{-1}]
V_{stall}	Stall Velocity	[m s^{-1}]
V_{turn}	Turn Velocity	[m s^{-1}]
V_z	Internal Shear Loading	[N]
W	Weight	[N]
W_E	Empty Weight	[N]
W_f	Fuel Weight	[kg]
W_{TO}	Take-off Weight	[N]
$\bar{x_{ac}}$	Aerodynamic Centre Position With Respect To The MAC	
x_{ac}	Position Aerodynamic Centre From Nose UAV	[m]
$\bar{x_{cg}}$	Position of Centre of Gravity With Respect To The MAC	
x_n	Position Neutral Point From Nose UAV	[m]
X	Force Reduction Coefficient	
y(j)	Panel location	[m]
Y	Von Mises Stress	[Pa]

Chapter 1: Introduction

Natural disasters have affected millions of lives over the years. In the occurrence of such a disaster, search and rescue (SAR) teams risk their lives to save the ones of others. During SAR missions, knowledge about the infrastructure of the struck area is often highly limited due to the damage caused by the disaster. This lack of information introduces many additional challenges to the SAR missions.

Furthermore, the communication infrastructure in affected areas is prone to fail. Establishing proper communication between SAR teams can be the difference between life and death. This has been seen in the events following the 7.8 Richter scale earthquake that struck Kathmandu, Nepal in 2015. The majority of the communication infrastructure was either destroyed by the disaster or congested by the media and individuals trying to contact one another. K.R. Sigdel and Dol Raj Kafle claim that many lives could have been saved if proper communication could have been established between SAR teams.[7]

In order to address the challenges arising from disasters, group 04 of Delft University of Technology has developed an unmanned aerial system (UAS) that provides SAR teams with 2D and 3D mapping to gather knowledge about the local infrastructure to SAR teams as well as to locate victims of the disaster. Additionally, a communication framework has been implemented in the system to allow SAR teams to establish communication between each other.

Portugal was recently struck by a wildfire, killing at least 62 people. The frequency of such a tragic event proves the relevance of the design to be needed fast. [8]

To allow SAR teams to perform missions to the best of their ability, a robust system that can operate reliably in harsh weather conditions was required. To match this, the system consists of two fixed wing unmanned aerial vehicles (UAV), four kites and a ground station.

Part I of the report describes the mission along with a performance overview of the developed system. A market analysis is first carried out in chapter 2 which is followed by a requirement analysis in chapter 3. Part I is then concluded with a more detailed overview of the mission through a functional block analysis in chapter 5 in which a mission simulation is also provided.

Furthermore, part II deals with the actual design of the system. Chapter 6 first provides information about the trade-offs which have lead to the final system configuration. This is followed by chapters 7 to 9, 11 and 12 which provide detailed explanations of its aerodynamics, stability & control, its structural integrity, electronics as well as the ground station, respectively.

In the aerodynamics chapter, the entire surface of the aircraft is analysed; this includes the fuselage, main wing, vertical and horizontal tails as well as the propeller. The stability and control covers the sizing of each control surface as well as the dynamics of the UAV. The structural integrity is then considered by considering the dynamic loads the aircraft has to sustain. The electronics department covers the entire electronics of the UAV as well as the power management and positioning of components inside of it. Finally the ground station covers all ground equipment required to fulfil the mission as well as the kites required to establish a communication network.

Lastly, part III presents an assessment of the designed product and its design logic. First of all, the concurrent engineering design strategy that was utilised throughout the development of the project is found in chapter 13. A risk assessment of the mission is then provided in chapter 14. Following the risk assessment, RAMS (Reliability, Availability, Maintainability, and Safety) characteristics are discussed in chapter 16. Finally, a project design and development logic as well as a cost breakdown of the project is considered in chapter 17.

[7] http://www.waccglobal.org/articles/nepal-needs-better-communication-infrastructure-to-respond-to-disaster
[8] http://edition.cnn.com/2017/06/18/europe/portugal-fire/index.html

PART I
Mission description & performance overview

The first part of the report includes the description of the mission. A market analysis is conducted to show the relevance of the product. Additionally, the requirements set by the customer and the requirements that led from the several design phases are elaborated upon. Following is an investigation on the performance of the product. This includes a requirement compliance analysis. Moreover, a simulation of the mission reflecting the performance of the product is also included. Part I is concluded with a chapter on the functional analysis of the product providing an overview of which functions are implemented within the system.

Chapter 2: Market analysis

Before designing the UAS (Unmanned Aerial System), a careful market analysis has been carried out to determine how well the market is performing and in which areas it is lacking. This information has carefully been taken into account when writing requirements in order to design an attractive product to customers and allow growth of the company. This chapter covers the market analysis for the UAS under development.

2.1. Defining the market

Prior to carrying out the market analysis, the market itself must be defined. The needs statement of the mission states "The mission needs to provide an autonomous system that aids search and rescue (SAR) teams by mapping the disaster impact zone and enables communication between different teams.". To fulfil this need, an autonomous UAS system is going to be designed. As a result, the product is located in the UAS market.

Moreover, the system is primarily designed to aid SAR teams in their missions. The product is therefore located in the intersection between the UAS and SAR markets. The target market is therefore defined and will be reffered to as the UAS SAR market.

2.2. Market dynamics

Having defined the market, its size should be determined. Knowing the market size and current technological developments allows a market forecast to be built.

2.2.1. Market volume

Using Teal analysts 2012 global UAV market analysis, it is estimated that as of today (June 2017), the global UAV market is worth €37.7 billion, [8]. Moreover, the market size prediction of [8] is close to Mercelo Ballve's prediction, [6]. Lucintel [10] has carried out a segmentation of the global UAV market per contininent as illustrated below in fig. 2.1.

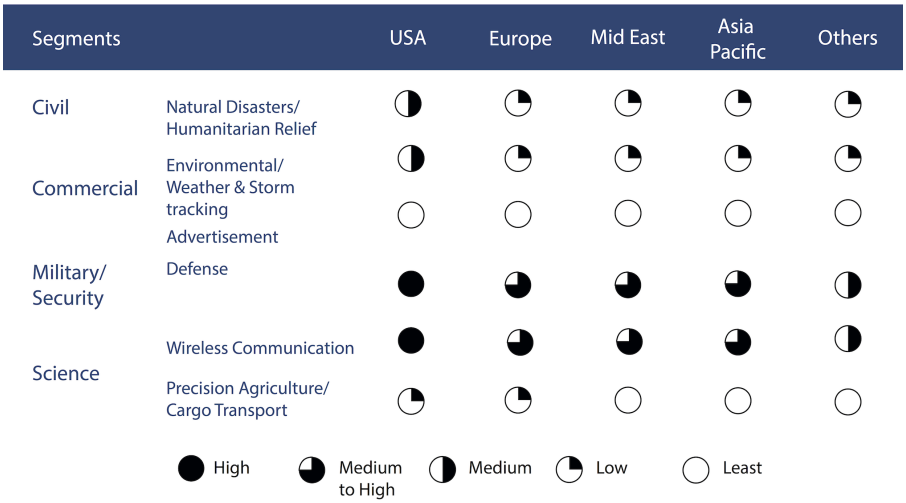

Figure 2.1: Global UAV market segmentation in different continents.

As it can be seen from fig. 2.1, the civil segment corresponds to the target market. However, the UAS is being designed for any SAR mission and not just natural disasters. Whilst this is said, it can still be assumed that since natural disasters affect a significantly greater fraction of the population, man-caused disasters are assumed to have negligible size in the market.

Additionally, fig. 2.1 shows that natural disasters constitute of a significant part of the UAV market in every continent. However, this analysis is qualitative and more quantitative values are preferable in order to obtain a better estimation of the SAR market segment.

The department of defence (DOD) is estimated to hold around 40% of the global UAV market, [21]. Using this value and comparing it to fig. 2.1, it can be approximated that the UAS SAR market holds 5-10% of the global UAV market. The UAS market has therefore been valued at €1.88 to €3.77 billion in 2017.

2.2.2. Market forecast

A growth in the UAV market of €5.92 to €10.22 billion is expected annually until 2022. It is therefore forecast that the market will be worth €79.82 billion by 2022, [8]. Another source, [48], estimates a market size of €87.90 billion by 2024 which appears to match the prediction from [8].

On top of the market growth, according to the international disaster data base [28], the number of individuals affected by natural disasters is expected to increase in the future. This increasing trend is due to both the increase of natural disasters [28] as well as due to the growing world population.[9]

Considering the fact that both the number of civilians affected by disasters and the global UAV markets are growing, it is estimated that the SAR segment will retain its 5-10% share in the global UAV market. With a global UAV market forecast at €87.90 billion in 2024, this yields a UAS SAR market size of €4.40 billion to €8.79 billion by 2024.

2.2.3. Potential customers

In order to have a successful product, it is important to understand who the customer is and what the customer needs. To do so, a heat map has been drawn to determine how different regions of the world are affected by natural disasters. In these regions, potential customers are largely defined to be governmental institutions, since search and rescue operations are mainly funded by the government.

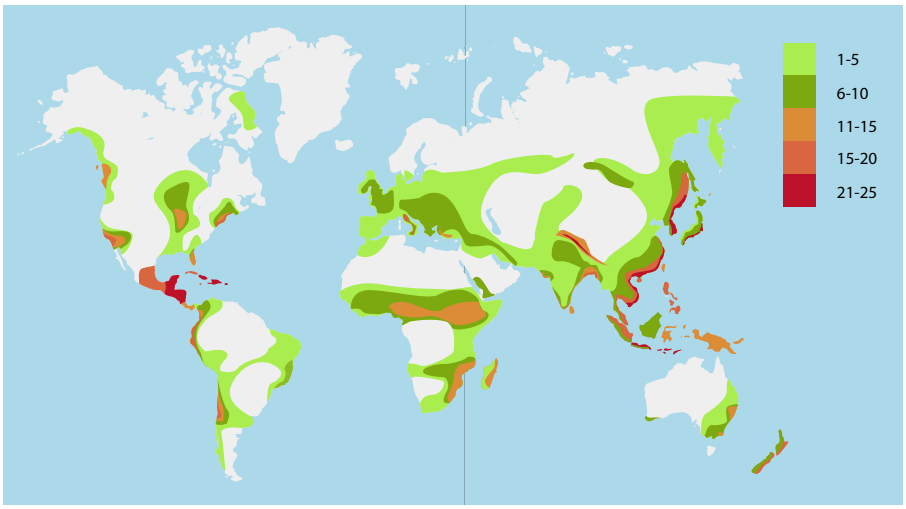

Figure 2.2: Heat map of the effects of natural disasters.

To generate the heat map as shown above in fig. 2.2, a large amount of statistical data over the past two decades has been taken into account. The data consider consists of five disasters, namely: earthquakes, cyclones, wildfires, volcanic eruptions and tsunamis. Data for each disaster type has been taken from [10,11,12,13] with the scale shown in table 2.1. The data was then merged with a population chart. The population density has been multiplied by the averaged disaster scale, yielding a new scale from 1-25 for the final heat map. A value of 1 represents and low population density which is not likely to be affected by disasters. On the other side of the scale, 25 represents a highly populated area which is eminently prone to a natural disaster.

Table 2.1: Disaster scale conversion.

Disaster/Scale	1	2	3	4	5
Earthquake (Ritcher scale)	1-3	3-5	5-7	7-9	9+
Floods	no damage	minor damage	causes property damage and epidemic outbreak	many fatalities	high fatalities and long term damage to the affected area
Cyclones (Category and wind speeds)	1 (153 km/hr)	2 (177 km/hr)	3 (210 km/hr)	4 (250 km/hr)	5 (250+ km/hr)
Volcanoes (VEI - eruption volume)	0-2 (<10^6 m^3)	2-4 (<10^9 m^3)	4-6 (<10^12 m^3)	6-7 (<10^15 m^3)	7-8 (>10^15 m^3)
Wildfire (Wildland urban interface hazard scale)	E0	E1	E2	E3	E4

[9] https://ourworldindata.org/world-population-growth/
[10] https://www.arcgis.com/home/webmap/viewer.html?useExisting=1&layers=30e5fe3149c34df1ba922e6f5bbf808f
[11] http://www.emdat.be/country_profile/index.html
[12] https://www.ngdc.noaa.gov/mgg/global/
[13] https://www.munichre.com/site/touch-naturalhazards/get/documents_E756103778/mr/assetpool.shared/Documents/0_Corporate_Website/Publications/302-05972_en.pdf

Looking at fig. 2.2, it can be expected that the UAS would be of most use in Asia, the west coast of the Americas and in eastern Asia. These regions are highly populated and it can be that often, these may not have enough economic and technological infrastructure to control the catastrophe. Additionally, according to the heat map, it appears coastal and mountainous regions are at most risk of disasters. This must be kept into account when designing the autonomous control system.

2.2.4. Competition

The UAS Sar market is a very competitive one. In the past decade, the use and need of UAS for SAR missions has grown significantly. Prior to the breakthrough of UAVs into the aviation industry, helicopters and large aircraft (relative to UAV size) were the only alternatives to carry out mapping missions for SAR purposes. With the rapid advancements in technology and new developments for UAS, the UAS market has managed to make an impact on SAR market.

Manned helicopters

SAR manned helicopters can perform a wide range of missions in harsh environments. However, these missions present additional risks to human life due to the crew having to be on board of the helicopter. Moreover, helicopters are extremely costly to purchase, operate and maintain.

One of the main advantages of helicopters is the fact that they can access remote locations. Additionally, their size allows the use of a wide range of payloads and the possibility to process data directly from the helicopter. Furthermore, depending on the type of rescue mission, it may be performed directly from the helicopter itself.

On of the goals is to develop a system can perform faster, better, safer and cheaper than a manned helicopter. If it is not possible to do this in a certain area such as direct rescue, it is important to improve other areas further. Doing so will provide a competitive edge to the product being designed and allow the UAS SAR market to grow and outperform manned helicopters.

Unmanned helicopters

Some companies have attempted to outperform manned helicopters by developing unmanned helicopters. The company Schiebel for example was provided a budget by the US military to develop an automated multi-purpose UAS.[14] Following this investment, Schiebel has developed the Camcopter S-100 which is able to carry out fine mapping operations whilst down-linking the data up to distance of 200 km. The S-100 has an endurance of up to 6 hours and is configurable thanks to its modular payload.

This product presents many benefits to SAR missions. However, it is extremely costly and mostly suitable for the military which has the budget to operate the S-100. The production of the helicopter alone costs around €400k. The total cost of the system including the ground station is likely to rise above €2 million, [31]. Additionally, specialised operators with thorough training are required to operate the UAV and ground station.

Multicopters

Many UAS have already entered the SAR market. Some of these companies which are viewed as competitors are Aerialtronics, Avinc and Microdrones.[15] [16] [17]

Microdrones is a company that designs and produces state of the art UAVs. Their quad-copters are used for professional applications such as surveying, mapping, LIDAR applications and more. Microdrones is viewed as a major competitor due to the wide range of tasks their UAV's are able to perform and the efficiency at which they do so. Additionally, the company boasts its ability to perform operations in harsh environments and its flight time of 45 minutes which is significant for quad-copters.

Moreover, Aerialtronics focuses on the production of cheap (±€2,000) quadcopters. Their SAR quadcopter allows for interchangeable payloads. One of which is a thermal imaging camera that allows real time visualisation from the ground. One of their most appreciable payloads is the Dupla Vista which allows instantaneous change between infrared thermal and vision camera. However, their UAV can only fly for up to 35 minutes.

The US military has invested a significant amount of money into Avinc to developed a UAV. The Puma AE RQ-20B aircraft shows great performances and also has the possibility of carrying multiple payloads. It is practical, cheap and easy to operate.

Despite all of the advantages presented for each company, none of them meet the requirements of the customers. They are mostly specialised to carry out either one or two types of missions. This suggests they are focused on either one or two niche markets whereas the customer wants a product that can fulfil requirements for the entire UAS SAR market. This will often be seen by areas which are prone to a wide range of disasters. The development of this UAS is necessary in order to fill an important gap in the UAS SAR market.

[14] https://schiebel.net
[15] http://aerialtronics.com
[16] https://www.avinc.com
[17] https://www.microdrones.com/en/home/

Unmanned aeroplanes

Unmanned aeroplanes are becoming more widely used. UAV Factory is known for its high performance UAVs.[18] One of their designs has a maximum endurance of 20 hours and can travel at speeds up to 32 m s^{-1}. Their UAVs have a modular payload which allows the operators to configure the UAV according to the mission needed to be performed. UAV Factory's UAV alone costs in the region of €40k. The target customer is able to purchase multiple UAV's and operate them simultaneously. This makes UAV Factory one of the strongest competitors due to their products' high performance and low price. Other companies produce similar UAVs such as Latitude Engineering which is also able to perform vertical take-offs and landings (VTOL).[19]

2.3. Market analysis conclusion

It has been determined that the UAS, UAV market is projected to grow significantly in the coming 7 years. This growth is expected to remain in the years following that. This provides a great opportunities for new products to be designed. Many UAVs can already be found on the market for a wide range of different missions. However, it has been noticed that often times, the UAVs are designed to perform one specific type of mission. Designing a multi-purpose UAV would therefore be highly beneficial.

Moreover, none of the UAVs stand out with respect to the weather conditions they are able to perform in. The majority of them are limited to 6 Bft wind conditions. Having SAR as part of the target market, it is important to be able to be able to operate quickly and in any weather condition. For this reason, a large amount of focus should be given to being able to operate in those conditions.

Finally, none of the systems mentioned have shown are currently being used as communication relays. Being one of the requirements of the customers, incorporating this system will allow the UAS being designed to stand out over the competition. By incorporating all of these factors into the design of the UAS, the product should be able to penetrate the market and allow the company to grow by outperforming competition.

[18] `http://www.uavfactory.com`
[19] `https://latitudeengineering.com`

Chapter 3: Requirement analysis

This chapter includes all the requirements for the product. The use of requirements is that it gives the design project hard guidelines to design for. Keeping the design process within these boundaries reduces the risk of for example over-designing, having a system that does not comply with the customers needs or a system that can not be certified because it does not comply with regulations.

The requirements have been derived in different ways. For clarity of this chapter three types of requirements have been identified. There are customer requirements which were set in the beginning by the customer. From the customer requirements other requirements have been derived. All these requirements are denoted with **C** behind it. When applicable, a short explanation is written in italics behind it. There are also requirements that originated in the project phases. These requirements can for example come from certain subsystems that have influence on other subsystems. Other possibilities are that the requirement is derived as a result of a mission analysis, a literature review or regulations. All these requirements are denoted with **D** behind it. The final type of requirement is the requirement that is a result of a trade-off. These requirements are denoted with **TO** behind it.

This chapter is structured as follows. The UAV system and subsystem requirements are documented in section 3.1. The ground station system and subsystem requirements are listed in section 3.2. The general operations requirements of the system are included in section 3.3.

For clarity, the symbols used are mentioned another time. A more elaborate explanation can be found above. C = customer requirement D = requirement derived during design project TO = requirement derived from trade-off

3.1. UAV (U) system requirements

REQ.U.SYS.1 The UAV shall have an MTOW of 25 kg at most. **TO** *Due to regulations for small UAVs [2].*

REQ.U.SYS.2 The UAV shall map an area of a 1,000 m^2 in 30 min with a resolution of 10 cm. **C**

REQ.U.SYS.3 The UAV shall map an area of a 10 km^2 in 3 h with a resolution for of 2 m. **C**

REQ.U.SYS.4 The UAV shall operate autonomously from take-off to landing with the exception of manual target inputs. **C** *The exception is derived and increases the operational flexibility of the UAV.*

REQ.U.SYS.5 The UAV shall have an endurance of at least 2 h. **C**

REQ.U.SYS.6 Communication relay shall be possible within 50 km from the GS. **C**

REQ.U.SYS.7 The UAV shall reach a rate of climb of at least 3 $m\,s^{-1}$. **D** *Due to regulations [2].*

REQ.U.SYS.8 The UAV shall have a top speed of at most 44.7 $m\,s^{-1}$. **D** *Due to regulations [2].*

REQ.U.SYS.9 The UAV shall operate in wind conditions up to 8 Bft. **TO** *A changed customer requirement. It was originally 10 Bft. (section 6.2)*

REQ.U.SYS.10 The UAV shall operate in a temperature range of –20 °C to 50 °C. **D** *Derived from the different disaster conditions the UAV operates in.*

REQ.U.SYS.11 The UAV shall operate in rain conditions of at least 5 $mm\,h^{-1}$. **D** *Derived from the different disaster conditions the UAV operates in.*

REQ.U.SYS.12 The UAV shall have a maximum take-off distance of 7 m at sea-level. **TO** *Derived from the take-off subsystem trade-off (subsection 6.4.6).*

REQ.U.SYS.13 The UAV shall have a maximum landing distance of 5 m at sea-level. **TO** *Derived from landing subsystem trade-off. (subsection 6.4.7).*

REQ.U.SYS.14 The UAV shall have a maximum noise pollution of 65 dB. **D** *Due to regulations [2].*

REQ.U.SYS.15 The UAV shall identify possible survivors on the ground in the target area. **C**

REQ.U.SYS.16 The UAV shall be assembled by two people in less than 15 min. **D** *Derived by project to ensure the ease-of-use of the system.*

REQ.U.SYS.17 The UAV shall have lights attached to provide visibility. **D** *Due to regulations [2].*

REQ.U.SYS.18 The UAV shall not endanger people on the ground or other vehicles.

REQ.U.SYS.19 The UAV shall be controllable by means of manual override. **D** *Due to regulations [2].*

REQ.U.SYS.20 The UAV shall continuously send its GPS location to the GS. **D**

REQ.U.SYS.21 The UAV shall have a maximum volume of 1.9 m^3. **C** *This volume is 60% of a mini-van (including packing inefficiencies), derived from customer requirement.*

REQ.U.SYS.22 The UAV shall have a roll rate of at least 156°. **D** *Explanation: subsection 8.3.1.*

REQ.U.SYS.23 The UAV shall have a minimum turn radius of 65 m. **D** *Explanation: section 9.1.*

3.1.1. Mapping payload (PL.M) subsystem requirements

REQ.U.PL.M.1 The mapping payload shall have a combined power usage of at most 25 W. **D** *Due to a preliminary power budget derived in early design phase.*

REQ.U.PL.M.2 The mapping payload shall be integrated in the UAV. **D** *Reduce drag and risk of damage during landing and take-off.*

REQ.U.PL.M.3 The mapping payload shall have a maximum combined weight of 1.5 kg. **D** *Preliminary mass budget derived in early design phase.*

REQ.U.PL.M.4 The mapping payload shall have a maximum combined volume of 0.01 m^3 **D** *Preliminary size budget derived in early design phase.*

REQ.U.PL.M.5 The mapping payload shall have a maximum combined bandwidth usage of 8 MB s^{-1} @ 50 km. **D** *Derived from preliminary link budget.*

REQ.U.PL.M.6 The mapping payload shall send data to the ground station with a maximum of 4 s delay. **D** *To provide feedback during manual control of UAV.*

REQ.U.PL.M.7 The mapping payload that provides pixel based data shall have a maximum of 0.5 a pixel of motion blur per pixel. **D** *To provide clear images.*

3.1.1.1. Mapping payload subsystem - RGB camera sub-subsystem requirements:

REQ.U.PL.RGB.1 The RGB camera shall be used for mapping under nominal weather conditions **TO** *Explanation: subsection 6.1.1.*

REQ.U.PL.RGB.2 The RGB camera shall provide raw data of at most 5 MB per image. **D** *Based on a preliminary band-with budget.*

REQ.U.PL.RGB.3 The RGB camera shall have a shutter speed of at least 1/700 seconds. **D** *Explanation: subsection 6.1.2.*

3.1.1.2. Mapping payload subsystem - IR camera sub-subsystem requirements:

REQ.U.PL.IR.1 The IR camera shall have a wavelength in the range of 400 nm to 1.000 nm. **TO** *Derived from trade-off on IR systems and their wavelengths. (subsection 6.1.1)*

REQ.U.PL.IR.2 The IR camera shall provide video stream with at least 7 fps. **D** *Based on requirement **REQ.U.PL.M.5** and parameters such as cruise speed.*

REQ.U.PL.IR.3 The IR camera shall have a registration time of at least 1/700 seconds. **D** *Explanation: subsection 6.1.2.*

3.1.1.3. Mapping payload subsystem - LIDAR (L) sensor sub-subsystem requirements:

REQ.U.PL.L.1 The LIDAR sensor shall generate a maximum data rate of 3 MB s^{-1}. **D** *Based on a preliminary band-with budget.*

REQ.U.PL.L.2 The LIDAR sensor shall have a minimum range of 150 m at 80% reflectivity. **D**

REQ.U.PL.L.3 The LIDAR sensor shall be operable regardless of weather conditions. **D**

3.1.2. OBC subsystem requirements:

REQ.U.OBC.1 The OBC shall handle and execute commands from the GS. **D**

REQ.U.OBC.2 The OBC processors shall be equipped with thermal management devices. **D** *Explanation: section 11.3.*

REQ.U.OBC.3 The OBC shall have an RTOS. **D** *Explanation: subsection 11.1.2.*

3.1.2.1. OBC subsystem - PFC sub-subsystem requirements:

REQ.U.OBC.PFC.1 The PFC shall have atleast two separate CPUs to achieve a fail-safe design. **D**

REQ.U.OBC.PFC.2 The PFC shall have a storage capacity larger than 2 GB. **D** *Explanation: section 11.2.*

REQ.U.OBC.PFC.3 The PFC shall have at least two storage devices to achieve a fail-safe design. **D**

REQ.U.OBC.PFC.4 The PFC shall have a minimum of 15 digital and 15 analogue input/output ports. **D** *Explanation: section 11.2.*

3.1.2.2. OBC subsystem - PLC sub-subsystem requirements:

REQ.U.OBC.PLC.1 The PLC shall have a storage capacity such that the last 10 minutes of payload data can be stored. **D** *Explanation: section 11.2.*

REQ.U.OBC.PLC.2 The PLC shall have a storage capacity larger than 16 GB. **D** *Explanation: section 11.2.*

REQ.U.OBC.PLC.3 The PLC storage device shall a write/read speed larger than 16 MB s^{-1}. **D** *Explanation: section 11.2.*

REQ.U.OBC.PLC.4 The PLC shall have at least two storage devices to achieve a fail-safe design. **D**

3.1.3. Control subsystem sensor(CS) requirements

REQ.U.CS.1 The CS shall have a maximum weight of 1.0 kg. **D** *This is the weight budget allocated to the CS system*

REQ.U.CS.2 The CS shall have a maximum power usage of 10 W. **D** *This is the power usage allocated to the CS system*

REQ.U.CS.3 The CS shall have a maximum cost of 20,000 €. **D** *This is the cost budget allocated to the CS system*

REQ.U.CS.4 The CS shall be able to measure the position (longitude, latitude and height) of the UAV with an accuracy of 1 m. **D** *The position needs to be known in order to accurately guide the UAV to the landing site and the area of interest. The accuracy of 1 m is also needed in order to geotag the sensor data. If a lower accuracy would be used, then directing the SAR teams and overlaying the data will be harder and the UAV will be unable to land.*

REQ.U.CS.5 The CS shall be able to measure the airspeed of the UAV with an accuracy of 0.1 $m\,s^{-1}$. **D** *The airspeed has to be known in order to know whether the UAV is flying at its stall speed. A higher accuracy would not add much more value, and a lower accuracy can increase the minimum airspeed.*

REQ.U.CS.6 The CS shall be able to measure the ground speed of the UAV with an accuracy of 0.1 $m\,s^{-1}$. **D** *This velocity is important to know how fast the UAV is approaching the landing site in order not to exceed the maximum velocity.*

REQ.U.CS.7 The CS shall be able to measure the distance from the UAV to the ground station (landing site) with a minimum sensing range of 30 meter. **D** *In order for the UAV to be able to determine the location of the landing site, it has to be able to detect it in time when flying at approximately 20 $m\,s^{-1}$. This takes the adjustments to the flight path and the actual sensing of the landing site into account.*

REQ.U.CS.8 The CS shall be able to detect potential collisions from a distance of 120 meters. **D** *Described in: subsection 6.1.4, subsection 8.3.1.*

REQ.U.CS.9 The CS shall be able to detect potential collisions with a minimum frontal area of 100 cm^2. **D** *This requirement is based on the frontal area of a bird, which is one of the most common obstacles to be found at the flight altitude.*

REQ.U.CS.10 The CS shall be able to measure the altitude of the UAV from the surface with an accuracy of 0.5 m. **D** *The altitude determination is especially important to know how far the UAV is above the ground in order to be able to land in the net and avoid the ground in its approach.*

3.2. Ground station(G) system requirements:

REQ.G.SYS.1 The GS shall be able to render images with a minimum of 15 million Pixels. **D** *The hardware and software need to be able to cope with the image size that is being used by the RGB camera for mapping.*

REQ.G.SYS.2 The GS shall be able to store at least 5 TB of data. **D** *Based on section 6.5 and contingencies.*

REQ.G.SYS.3 The GS shall be assembled by two people in less than 15 min. **D** *Based on early design phase time management budget.*

REQ.G.SYS.4 The system shall be capable of manually overriding the control of the UAV. **D** *Due to regulations.[2]*

REQ.G.SYS.5 The GS shall have a maximum volume of 1.25 m^3. **C** *This volume is 40% of a mini-van (including packing inefficiencies), derived from customer requirement.*

REQ.G.SYS.6 The cost of the ground station shall not be more than 70,000 euros. **C** *Derived from customer requirement **REQ.O.SYS.10** and the financial budget in table 6.16.*

3.2.1. Communication subsystem - Kite (K) sub-subsystem requirements:

REQ.G.Com.K.1 The kite shall be able to withstand at most 8 Bft winds **C**

REQ.G.Com.K.2 The kite shall not cost more than 70,000 euros. **C** *Derived from customer requirement **REQ.O.SYS.10** and the financial budget in table 6.16.*

3.2.1.1. Landing subsystem - Parachute (LA.PAR) sub-subsystem requirements:

REQ.U.LA.PAR.1 The parachute shall provide a landing with a maximum impact energy of 260 J at 25 kg. **D** *To reduce the risk of damage to UAV and its payload.*

REQ.U.LA.PAR.2 The parachute (including bag) shall have a weight of at most 1.5 kg. **D** *Based on preliminary mass budget.*

REQ.U.LA.PAR.3 The parachute and its cables shall not have interference with the propulsion or air frame system. **D**

REQ.U.LA.PAR.4 The parachute shall have a maximum volume of 0.004 m^3 when folded. **D** *Based on preliminary size budget.*

3.2.1.2. Landing subsystem - Net (LA.NET) sub-subsystem requirements:

REQ.U.LA.NET.1 The UAV shall be able to land with its nose forward in a rectangle of 6.96 m length and 1.76 m width. **D** *Explanation: sub-subsection 12.1.1.2.*

REQ.U.LA.NET.2 One spring loaded reel shall be able to absorb 3450 J over a length of four m. **D** *Explanation: sub-subsection 12.1.1.3.*

REQ.U.LA.NET.3 The IR emitters shall have a range of at least 300 m. **D** *Explanation: sub-subsection 12.1.1.2.*

3.3. Operations(O) system requirements:

REQ.O.SYS.1 The endurance of the mission shall be up to 72 hours. **C**

REQ.O.SYS.2 The UAV shall operate below 122 m altitude from the surface. **D** *Due to regulations. [2]*

REQ.O.SYS.3 The UAV shall operate up to 3,500 m MSL altitude. **TO** *Derived from trade-off based on heat map (fig. 2.2) of the market analysis and further explained in section 4.5.*

REQ.O.SYS.4 The UAV shall operate safely, such that it does not do any harm to its surroundings or humans on the ground. **C**

REQ.O.SYS.5 A minimum of four individuals shall be present during operations at the GS. **D** *Explanation: section 12.5.*

REQ.O.SYS.6 The turn-around time of the UAV shall be less than 15 min. **C**

REQ.O.SYS.7 The system shall be designed according to the circular economy paradigm. **C** *Is assessed in chapter 15.*

REQ.O.SYS.8 The used frequency shall comply with legal regulations. **D**

REQ.O.SYS.9 The used bandwidth shall comply with legal regulations. **D**

REQ.O.SYS.10 The complete system production costs shall be no more than € 500,000.-. **C**

REQ.O.SYS.11 The system should be re-usable **C**

REQ.O.SYS.12 The volume of the entire UAS shall be less than 3.15 m^3. **C** *A volume requirement given by customer. Volume of a mini-van. Contingencies have been included for packing inefficiencies.*

REQ.O.SYS.13 The UAS shall include of the shelf products where-ever possible. **C**

Chapter 4: Performance of the UAS

This chapter gives an overview of the achieved performance of the UAS. Its purpose is to provide the reader with a clear overview of the designed product as a whole, without diving into technical details. These are elaborated on in part II, the detailed technical design. Chronologically, these performance and simulation results follow from this detailed technical design.

4.1. Main UAV performance

Although in general, the UAS is reviewed as a full system, most resources have been invested in designing the UAVs. Therefore main technical specifications of these UAVs are derived in this section. Also these specifications are of great value to the product's comparison to competitors, which is elaborated on in section 4.4.

The most important performance specification include the MTOW, wing span and area, the cruise and maximum speed, the range and endurance, the UAV and GS ceilings, and the takeoff and landing methods. These values are summarised in table 4.6.

MTOW

During the design of the UAV, a MTOW of 25 kg has been used for design purposes, which follows from requirement **REQ.U.SYS.1**. However, as the final structural weight is lower than the assumed value, the actual MTOW equals 22.89 kg. By adding more fuel, it would be possible to increase the range and endurance with a 25 kg MTOW. However, this would lead to a decreased ceiling of the mission and would require a redesign of the fuel tank. Also, when additional structural reinforcements are required, it is possible to easily redesign the UAV with a design space of 2.11 kg. For now, for all performance calculations, a MTOW of 22.89 kg is used.

Wing span and Area

The wing span and area follow mostly from the required stall speed. In order to ensure a net landing, a stall speed of 18 m s^{-1} during landing is required at high altitudes. This drives the required surface area of the main wing, which equals 0.777 m^2. Than, the wing span follows from a trade-off between structural feasibility and aerodynamic efficiency and equals 2.42 m. A further analysis of the wing span and area is performed in chapter 7.

Cruise and maximum speed

The cruise speed equals the speed at which maximum range is achieved, provided all systems function properly at that speed, which is assessed in section 4.6 . This optimal speed typically changes by altitude and the amount of fuel burned. The optimal cruise speed at sea level ranges from 31 to 34 m s^{-1}, this follows from the the drag-velocity graph shown in fig. 4.1. The maximum speed follows from requirement **REQ.U.SYS.8** and section 9.1 and equals 42.3 m s^{-1}.

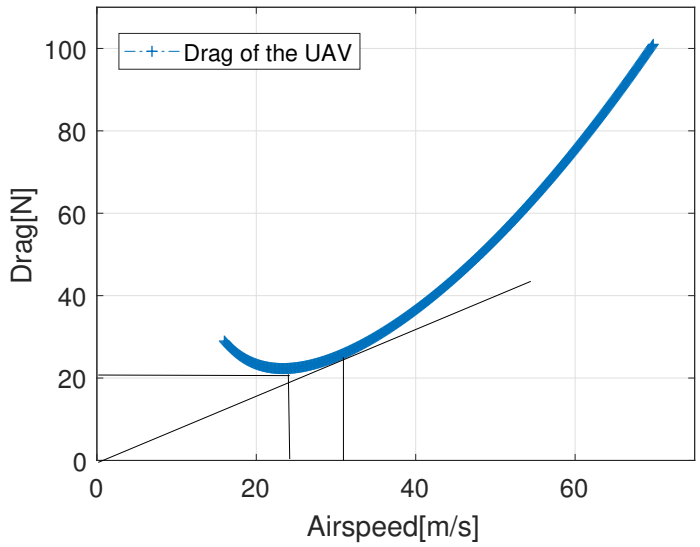

Figure 4.1: Total drag at different velocities.

Endurance and Range

As specified already, the cruise speed equals the speed at maximum range conditions. The maximum range is achieved at the minimum D/V-ratio and the maximum endurance is achieved at the minimum absolute drag, both follow from fig. 4.1. Then, the range and endurance are found by eq. (4.1) and eq. (4.2).

$$Range = \frac{v_{cruise} \cdot m_{fuel}}{PSFC \cdot (P_{prop_{maxrange}} + P_{gen})} = 840\text{km} \tag{4.1}$$

$$Endurance = \frac{m_{fuel}}{PSFC \cdot (P_{prop_{maxendu}} + P_{gen})} = 9.6\text{h} \tag{4.2}$$

Where v_{cruise} is the speed during maximum range conditions in m s^{-1}, m_{fuel} is the total fuel mass available in kg, PSFC is the power specific fuel consumption in kg kW^{-1} h^{-1}. $P_{prop_{maxrange}}$, $P_{prop_{maxendu}}$ and P_{gen} equals the required power by the propeller at maximum range, the required power by the propeller at maximum endurance and the required power of the generator respectively in kW. Most importantly, the power specific fuel consumption of the engine equals 0.675 kg kW^{-1} h^{-1}.

UAV and GS ceiling

In order to be able to operate at all areas of interest, the ceiling of the UAV and the GS is of primary importance. The ceiling of the GS is 3548 m and is limited by the takeoff speed of the pneumatic catapult launch. This is elaborated on in section 4.5. The ceiling of the sole UAV lies significantly higher. However, as there is no use of flying above 5000 meter altitude and in nearly every occasion, flying at this altitude does not comply with requirement **REQ.O.SYS.2**, the ceiling of the UAV is fixed at that altitude.

Take-off and landing

For small UAVs, take-off and landing can be performed in numerous different ways. This configuration launches with a pneumatic catapult and is retrieved with a net landing. Also, a parachute can be used in emergency situations. Take-off and landing with a catapult and net has as a large advantage that no runway is required. Therefore, the UAS can be operated everywhere, no matter what infrastructure is present in the disaster location. This adds largely to the value of the UAS.

4.2. Requirement assessment

In order to compare the performance of the system with the requirements set in chapter 3, a compliance matrix is given in this chapter. Table 4.1 evaluates the driving costumer, technical and regulation requirements. It compares the target requirements to the actual performance of the UAS, where all costumer requirements and the most vital regulation and technical requirements are included. Qualitative requirements have a concise explanation on how they are met. Quantitative requirements compare target and actual performance to assess compliance. A slight overlap occurs here with section 4.1 however, this compliance matrix aims to assess the requirements on the UAS, whereas section 4.1 aims to supply the reader with technical specification of the UAV.

Table 4.1: Compliance matrix showing whether the requirements are met.

Requirement	Target performance	Actual Performance	Compliance
Costumer requirements			
Requirement **REQ.U.SYS.5**	2 h	9.6 h	**Yes**
Requirement **REQ.O.SYS.1**	72 h	Unlimited	**Yes**
Requirement **REQ.U.SYS.3**	10 km^2 in 3 h	37.4 km^2 in 3 h	**Yes**
Requirement **REQ.U.SYS.2**	1,000 m^2 in 30 min	6.23 km^2 in 30 min	**Yes**
Requirement **REQ.U.SYS.4**	-	Autonomous flight computer in OBC	**Yes**
Requirement **REQ.U.SYS.9**	10 Bft	8 Bft	**No**
Requirement **REQ.U.SYS.18**	-	Parachute for emergencies	**Yes**
Requirement **REQ.O.SYS.6**	15 min	12 min	**Yes**
Requirement **REQ.O.SYS.7**	-	-	**No**
Requirement **REQ.O.SYS.11**	-	Reusable in different scenarios	**Yes**
Requirement **REQ.O.SYS.12**	3.15 m^3	2.26 m^3	**Yes**
Requirement **REQ.O.SYS.13**	-	COTS used consistently in GS and UAV	**Yes**
Requirement **REQ.O.SYS.10**	500,000.- €	220,000.- €	**Yes**
Requirement **REQ.U.SYS.6**	50 km	50 km	**Yes**
Regulation requirements			
Requirement **REQ.U.SYS.1**	25 kg	22.89 kg	**Yes**
Requirement **REQ.U.SYS.19**	-	2 pilots at ground station	**Yes**
Requirement **REQ.U.SYS.17**	-	LED lights are added for 24 h visibility	**Yes**
Technical requirements			
Requirement **REQ.O.SYS.3**	3,500 m	3,548 m (GS), 5,000 m(UAV)	**Yes**
Requirement **REQ.U.SYS.16**	15 min	10 min	**Yes**
Requirement **REQ.G.SYS.3**	15 min two people	55 min three people	**No**
Requirement **REQ.U.SYS.22**	156 ° s^{-1}	209 ° s^{-1}	**Yes**

As can be seen in the final column of table 4.1, three different requirements have not been met. This is due to different reasons. Costumer requirement **REQ.U.SYS.9**, originally being able to operate at 10 Bft, has not been met. This requirement has been lowered in cooperation with the costumers to 8 Bft as discussed in section 6.2 Satisfying this requirement would have greatly jeopardised the performance of the UAV. Also, designing a SAR UAS for wind conditions above 8 Bft is of little usage as most

SAR teams do not operate at these wind conditions at all. Still, the current UAV outperforms its competitors in wind resistance, as is assessed in section 4.4. Costumer requirement **REQ.O.SYS.7**, designing a system in the circular economy paradigm, neither has been met. This is due to the design priority, discussed extensively in chapter 15. In short, designing a fully circular system would have been possible. However, it would have decreased the performance of the system by an unacceptable amount. As this system is designed to safe lifes, the relatively small amount of fossil fuels burned by the system is accepted. Still, apart from the usage of fossil fuels, the system incorporates circular design. Technical requirement **REQ.G.SYS.3**, setting up the ground station in 15 minutes by two people, has neither been met. This requirement has been drafted in the design phase when the ground station was perceived as a control computer mostly. However, with the addition of different kites, a launch catapult and a landing net, all discussed in chapter 12, this requirement has become unrealistic. The current 55 min of assembly by the three present operators is an acceptable duration for this extensive ground station. Apart from these three requirements, all requirements have been met. Often, the UAS outperforms the set requirements drastically.

4.3. Summarising budgets

This section serves as a comprehensive overview of the designed product. It summarises all relevant masses, costs, power, link and size budgets used throughout the report. To the reader, this concise section gives an overview of the resource allocation of the product.

4.3.1. Unmanned Aerial System

For the entire UAS, mostly the mass, size and price are relevant. Obviously, the price is relevant to possible customers. The mass and size are important to the transportability of the system. All of these budgets should meet the requirements specified in chapter 3. The aforementioned budgets are shown in table 4.2. Most of these volume, price and mass contributions follow from chapter 12. The mass of the UAV equals twice the MTOW except for the fuel, the costs of the UAV are analysed in table 4.3 and the size of the UAV consists of a designed casing for each UAV, fitting all UAV components before assembly as listed in section 10.1.

Table 4.2: Total volume, mass and costs of the UAS.

Subpart	Volume [m^3]	Price [€]	Mass [kg]
Total UAVs	0.864	162,000	34.14
Total control station	0.114	8,649	50.05
Total landing net	0.158	1,046	97.50
Total redundant parachute	0.005	800	1.20
Total catapult launcher	0.500	20,950	110.00
Total kite payload	0.002	19,001	2.72
Total kite	0.365	10,149	96.20
Total fuel	0.250	N.I.	192.50
Total	**2.258**	**222,600**	**585**

4.3.2. Unmanned Aerial Vehicles

In contrast to the ground station, the UAVs are mostly designed and not of the shelf. As it concerns an aerial system, its budgets for mass and on board power are very limited, resulting also in quickly increasing costs. These three budgets are given in table 4.3 for one UAV. The masses of the structure subparts follow from their respective sections in chapter 9. The prices of the structure subparts follow from the manufacturing approach discussed in section 10.2. The prices and power of the systems in the fuselage are elaborated on in chapter 11.

Table 4.3: Total mass, costs and power budget of the UAV.

Subpart	Mass [kg]	Price [€]	Power [W]
Total Fuselage	1.98	5,500	-
Total Main Wing	4.035	12,000	-
Total Empennage	0.350	1,000	-
Total Booms	0.382	1,700	-
Total Propeller	0.300	900	-
Total Structure	**7.24**	**21,000**	**-**
Engine,Generator and PMU	4.398	21500	+325
Fuel Tank	0.658	1,948	-
Fuel	6	N.I.	-
Lights	0.200	50	-10
OBC	1.128	14,000	-179
Mapping Payload	1.22	15,500	-19.4
Radar	0.05	500	-1
Pitot Tube	0.16	3,090	-0.7
Antennas	0.5	250	-
Parachute	1.2	800	-
Servo	0.133	2,450	-8.75
Total Systems	**15.65**	**60,090**	**+106**
Total	**22.89**	**81,088**	**+106**

4.3.3. Link budget summary

The link budget is calculated for the most extreme case at which the UAV will be flying during the mission. Requirement **REQ.U.SYS.6** states that the system has to operate up to a distance of 50 km from the GS. Table 4.4 and table 4.5 gives the value for which the link budget is calculated and the final results. The link budget is extensively discussed in section 11.9.

Table 4.4: Given link parameters.

Inputs	**Value**
Frequency [MHz]	2,400
Max TX power [W]	40
TX antenna gain [dBi]	5.7
RX antenna gain [dBi]	5.4
TX antenna height [m]	122
RX antenna height [m]	300
Target Distance [km]	50

Table 4.5: Final link-performance values.

Link Performance Results	**20 MHz**	
(at max distance)	**2SS**	**1SS**
RSSI [dB m]	-83	
SNR [dB]	10	
MCS [-]	9	2
Link Capacity [MB s^{-1}]	20	15
Duty cycle [%]	76	102

4.4. Comparison to competitors

In order to assess the viability to the market, the performance of the product is compared to current market leaders. The specifications of the market leaders follow from the technical specification sheets of the competitors.[20] [21] The results are given in table 4.6.

Table 4.6: Comparison of primary performance specifications of the UAV to competitors.

Specification	Product	Penguin C	Precision Hawk
Propulsion type [-]	Combustion	Combustion	Electrical
MTOW [kg]	22.89	22.5	3.55
Wingspan [m]	2.42	3.3	1.5
Wing Area [m^2]	0.777		
Power consumption engine [kg kW^{-1}]	0.675		
Endurance [h]	9.6	20+	0.75
Flight Range [km]	840	1300+	32
Cruise speed [m s^{-1}]	31-34	19-22	12-16
Max level speed [m s^{-1}]	42.3	32	22
Max wind resistance [Bft]	8	6	4
Ceiling [m]	5,000	5,000	2,500
Takeoff Method [-]	Pneumatic Catapult	Pneumatic Catapult	Thrown
Maximum takeoff altitude [m]	3,548	3,000	2,500
Landing Method [-]	Net & Parachute	Parachute	Hard landing

The most comparable UAV currently on the market is the penguin C. The penguin C has similar specifications as the designed UAV. However, the penguin C has better performance in endurance and range. On most other specifications, the designed UAV outperforms the penguin C. It can be used at higher wind speeds, which makes it usable in an increased number of occasions, it can be launched from a 550 m higher altitude and the cruise and maximum speeds are significantly higher. These speeds determine the mapping rate of the disaster area, which is of primary importance. As such, it can be concluded that the Penguin C outperforms the designed UAV in high endurance surveillance missions. However, the FASAR application for which this product is designed has different priorities. For that application, the UAV outperform the penguin C both in usability in different conditions and in its mapping rate, which are of the highest importance.

Also, the precision hawk is added to the competitor analysis. The precision hawk is a different, smaller type of UAV. However, its usage as agricultural UAV closely resembles the purposes of the designed FASAR UAV. It is mostly added to analyse the performance of a significantly cheaper and smaller option. The main advantages of using a smaller UAV like the precision hawk are the ease of takeoff and landing, which require significantly less ground station operations, the increased sustainability and its low cost. However, the low wind resistance, low ceiling and low range make it an inconvenient system compared to the designed UAV.

In conclusion, the designed UAV has a clear added advantage to the current market leaders, making it a viable product to the market.

4.5. Performance at different altitudes

As a requirement, it is determined that the UAS has to be operable at an altitude of 3,500 m (requirement **REQ.O.SYS.3**). This requirement is based on a trade-off as the higher the required altitude, the more challenging the design of the UAV would be. In this trade-off, the natural disaster heat map of fig. 2.2 is taken into account. From this map, it is found that nearly the entire area of interest is located at altitudes below 3,500 m, but that relevant interesting areas in the world do have altitudes up to this design altitude.

[20] `http://www.precisionhawk.com/lancaster`
[21] `http://www.uavfactory.com/product/74`

In order to reach these high altitudes, the UAV design uses the fact that fuel is burned during the mission, lowering the weight of the UAV during the mission. As the required stall speed during take-off is 19.7 m s^{-1} and during landing is 18 m s^{-1}, this effect can be used to higher the required stall speed at high altitudes. The ceiling of the GS is then limited by the required stall speed for take-off of 19.7 m s^{-1} at 3,548 m. Below altitudes of 1,780 m, the UAV will be able to directly perform a safe net landing. Then, in the range of 1,780 to 3,548 m altitude, the UAV will have to burn a certain amount of fuel before it can land. Of course, emergency landings remain possible by deploying the emergency parachute, such that the safety of the system is not jeopardised. The amount of fuel that needs to be burned before landing at different altitudes is given in fig. 4.2. This figure also shows that at the maximum GS altitude of 3,548 m, the maximum take-off altitude becomes the limiting factor instead of the maximum landing altitude.

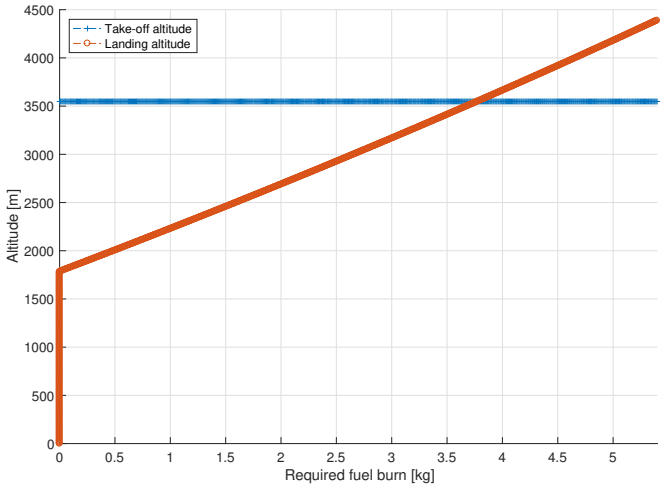

Figure 4.2: Total drag at different velocities.

4.6. Simulation

Having the UAV completely designed it is important to simulate stages of the mission in order to investigate different expected and unexpected scenarios. This section hence reports on most common and extreme situations during the mission. With regards to mission the simulation is split in two parts: mapping simulation and communication simulation.

4.6.1. Mapping simulation

For mapping primarily an optical camera and an infrared camera are used. Combined, these are able to perform the mission. Additionally, a LIDAR is added to provide accurate topological data which can be used in tandem with the other cameras. For the mission, fine and coarse mapping needs to be performed. As shown in table 4.1 and explained in chapter 11, the RGB and IR camera only fine map, as their resolution always is of fine mapping quality. The LIDAR has different coarse and fine mapping performance.

4.6.1.1. Fine mapping

The fine mapping needs a resolution of 10 cm and from the requirements this should be done in 30 min on an area of 1,000 m^2 (requirement **REQ.U.SYS.2**). LIDAR is specially sensitive to the height at which the UAV is flying. For this reason the resolution available at different height is plotted. With this the number of passes needed to acquire the necessary resolution is calculated. In section 11.2 the LIDAR sub-system is explained in more detail. It is evident from fig. 4.5 that even at the highest distance it is possible to obtain the required resolution. The area covered at each height is then plotted with time. Sub-subsection 4.6.1.1 shows that even at a height of 150 m the required resolution is met after 15 min, but at lower altitudes useful data is obtained faster than at higher altitudes.

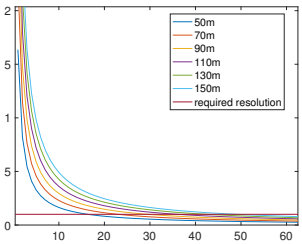

(a) LIDAR resolution with overlapped passes (fine).

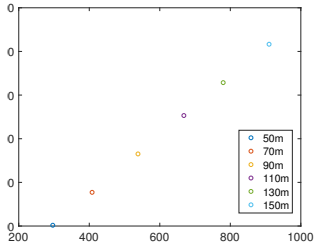

(b) LIDAR mapped area.

Figure 4.3: LIDAR simulation.

Graphs were plotted for the infrared and optical camera as seen in sub-subsection 4.6.1.1. Both the images show that in order to have a fine resolution the UAV has to fly at around 110 m altitude.

(a) Optical camera resolution.

(b) Infrared camera resolution.

Figure 4.4: Optical and infrared camera simulation.

4.6.1.2. Coarse mapping

The coarse mapping on the other hand needs a resolution of 2 m and an area of 10 km^2 needs to be mapped in 3 h. The same approach as above is used for coarse mapping for which the number of passes needed to obtain the resolution is calculated. For coarse mapping very few passes are needed to obtain the necessary resolution as seen in fig. 4.5. From sub-subsection 4.6.1.1 it can be already seen that the optical and the infrared cameras meet the requirement for coarse mapping.

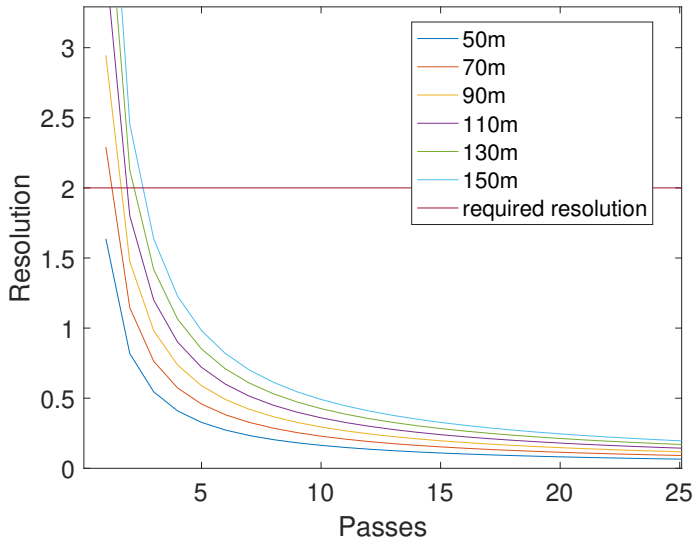

Figure 4.5: LIDAR resolution with overlapped passes (coarse).

4.6.2. Communication simulation

For communication the UAV has to transmit the data collected over a distance of up to 50 km. For this reason a pair of antennas is designed. The collinear antenna is to be placed on the kite to transmit in 360°along the ground plane. In the other end on the UAV, there is a four patch antenna facing four different directions. This orientation ensures radiation in all directions along the ground plane and the antenna itself is in a small form factor.

With the equipment on-board the UAV, the biggest variation in throughput (data transfer) that takes place is with respect to the distance it travels away from the ground station. There is also changes with respect to the attitude. The gain changes of the antenna with respect to orientation is first calculated and then this gain is used in the link budget to simulate and get data for different scenarios. Two angles will affect the gain of the patch array antenna on the UAV - roll and pitch. During the mission there is a maximum roll angle of 70°and a maximum pitch of 16°which is the stall angle. During these angle deflections the gain changes from 2.13 to 5.67. A plot is made to visualise the throughput (data rate) that can be transferred at maximum distance. This is illustrated in fig. 4.6. With the required data rate at 20 Mbit s there is enough throughput even at maximum pitch and row angles.

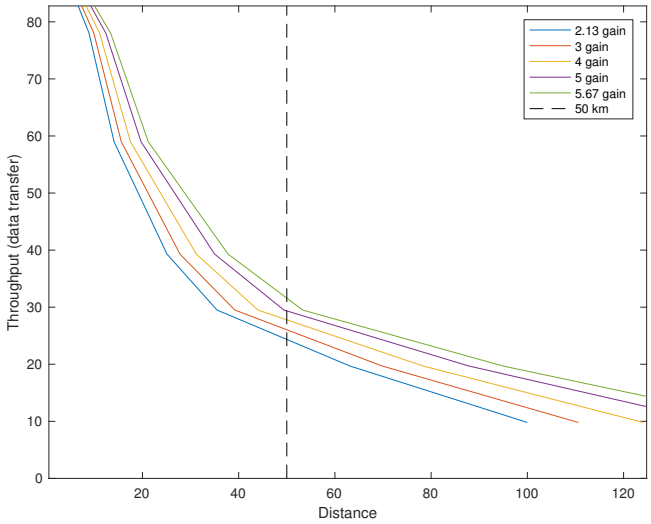

Figure 4.6: Throughput at different gains.

Chapter 5: Functional block analysis

In this chapter, the functional block analysis is performed. This will explain how the system will function, and describe these functions in two different ways. First, the functional flow diagram of the system is described in section 5.1. After this, the functional breakdown structure is described in section 5.2.

5.1. Functional flow diagram

A functional flow diagram is used to get a clear view of what the system has to do from the beginning of the mission to the end. It is also used to show in what order they will be executed. This is done by first describing the functions in a very generic way at the top level, while giving more detail about every main function in the levels below, as can be seen the functional flow diagram.

All the blocks in the diagram have a unique code, which makes it easier to reference to. The blocks with a **ref** on the top right are references to a block in a higher level, and is described in more detail after the **ref** block.

In fig. 5.1 a legend is provided, explaining the different blocks and symbols used to make the functional flow diagram.

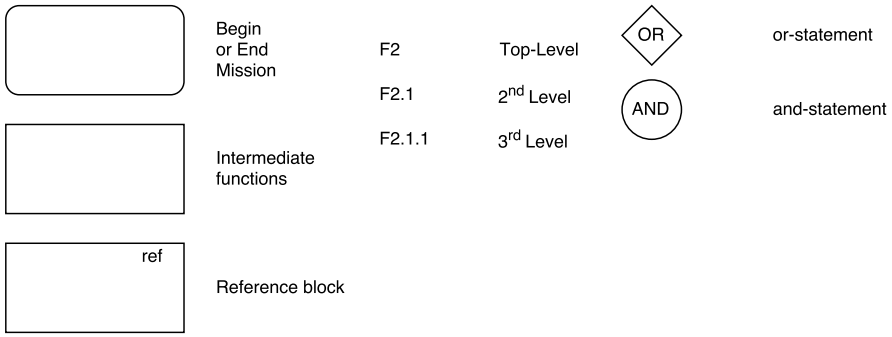

Figure 5.1: Functional flow diagram legend.

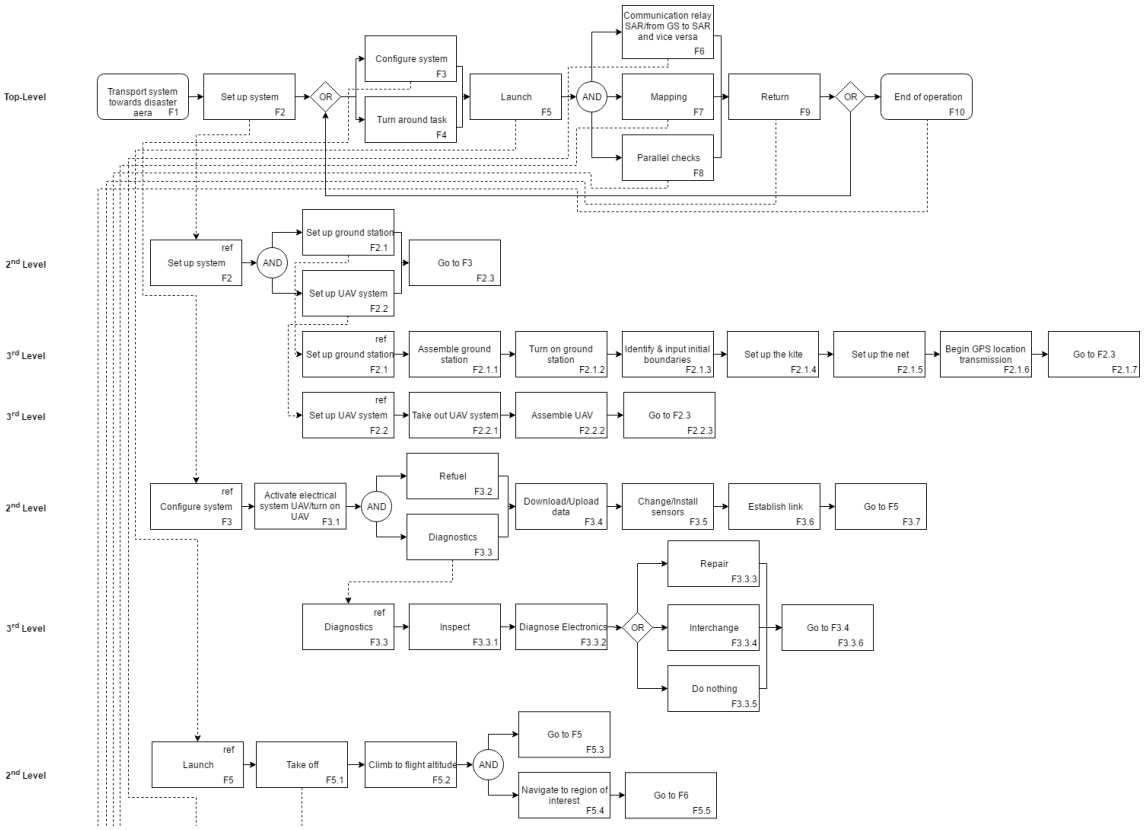

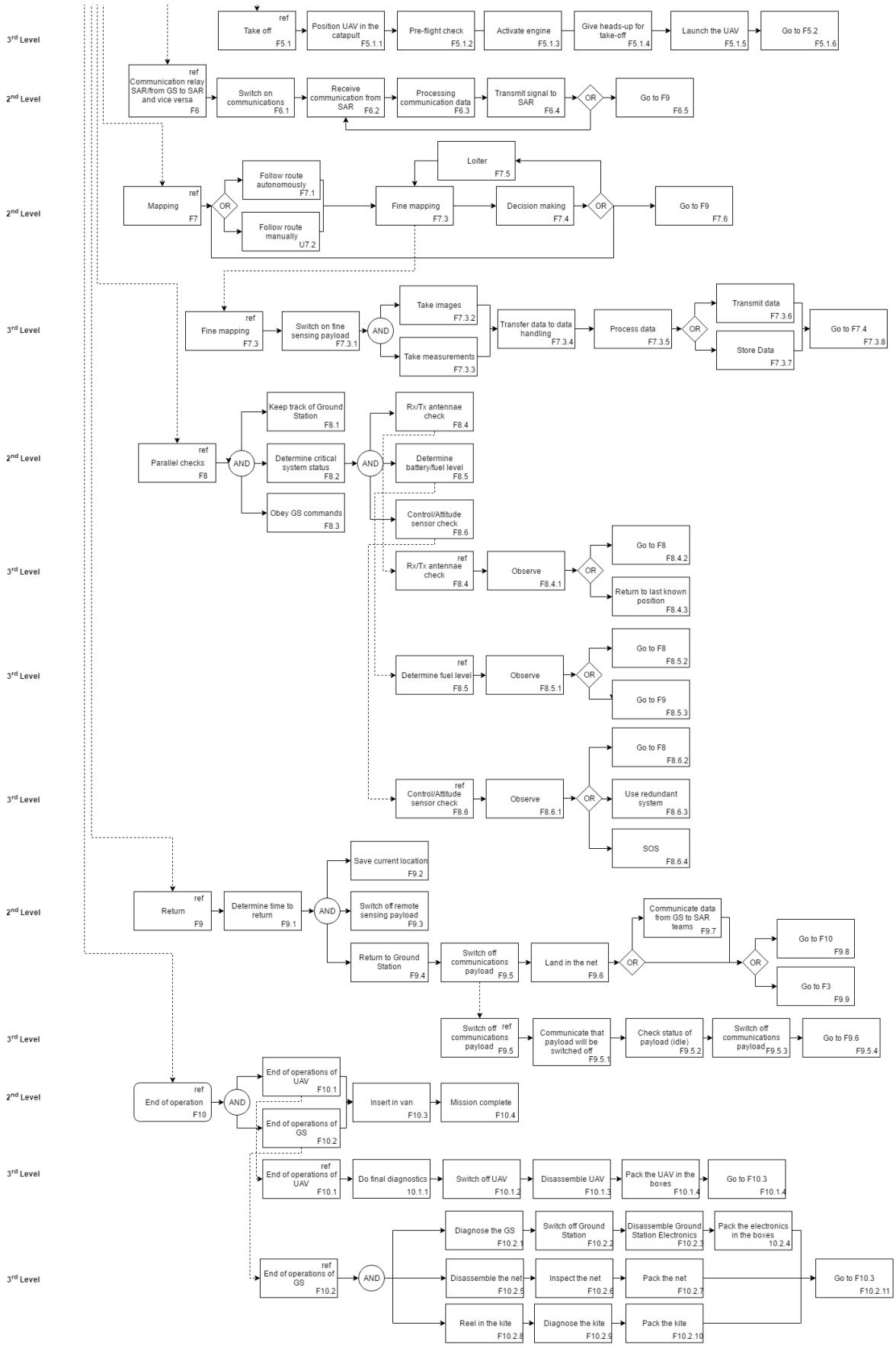

Figure 5.2: Functional flow diagram stating the mission from transportation to end of mission.

5.2. Functional breakdown structure

In the functional breakdown structure, all the required functions of the FASAR-mission are listed. First, an overview of all of these tasks is given, after which the most important of these are explained.

The mission composes of different phases. These phases are the same phases as the ones used in the functional flow diagram: Transport system towards area (F1), set up of the system (F2), configure the system (F3), turn around task(F4), launch UAV (F5), provide SAR communication relay/from GS to SAR and vice versa (F6), perform mapping (F6), do parallel checks (F8), return to ground station (F9) and end of operations task (F10). The top-level breakdown structure can be seen in fig. 5.3.

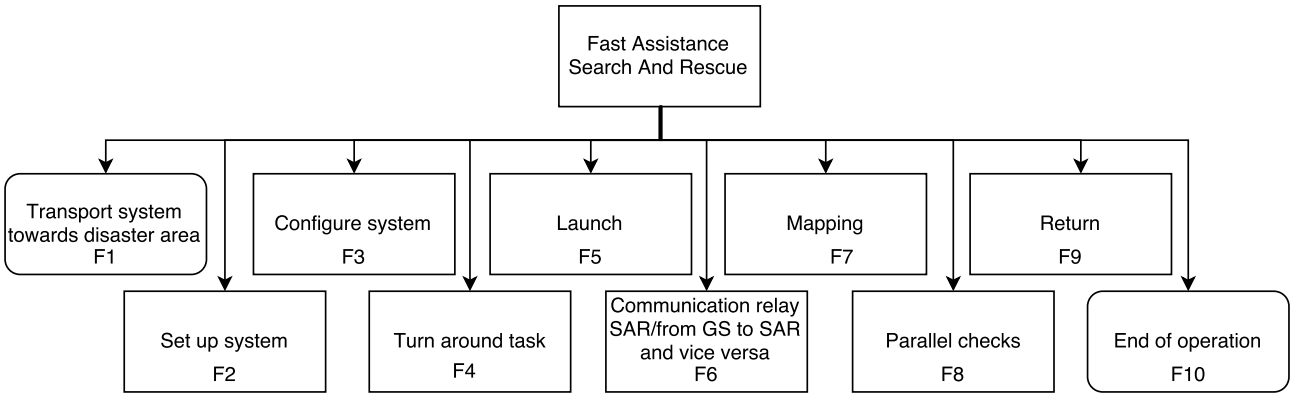

Figure 5.3: The functional breakdown structure for the top level functions.

The several functions which have to be executed by the system are explained and broken up in the next subsections. The functions can be broken down in different levels, representing a higher level of detail of what function or activity the system has to perform.

To refer to the specific tasks, a unique code is used. This code composes of two parts: a letter and a number. The letter is the same for all functions and is represented by an "F". The "F" is followed by a series of numbers, representing the level of detail and a unique identifier for each function. For example, F3.3.1 is a function which has a detail level of three. The "Go to" blocks in the functional flow diagram were given a code as well. Since these blocks are not functions themselves, but are used to refer back to another function, these are not included in the functional breakdown structure. This causes some function codes to be mission, like function F3.7.

In appendix A, the break-down of top level functions into first and second level functions are described in fig. A.1a up to fig. A.7.

Transport system towards area (F1)

The transportation of the system towards the area includes both a decision on where to place the ground station and the transportation itself. It does not yet include the setup of the system or the unloading of the boxes.

Set up system (F2)

The set-up of the system consists of all the performed activities associated with setting up both the UAV and the ground station. The diagram can be seen in fig. A.1a. This function has to be performed for both the ground station and UAV. For btoh the ground station and UAV, the setup is described below.

- Setting up the ground station consists of a number of tasks in order to make it functional. First, the ground station needs to be assembled. After this, the power system of the ground station is turned on. Then, the initial search area can be identified and put in the system to define the boundaries of the search area. After the electronics and power systems of the ground station are set up, the kite and net can be deployed. The GPS location of the ground station can then be transmitted to the SAR-teams and media in order to indicate that this base has become operational.
- The UAV needs a different approach on how to set up the system. This task only consists of the unpacking of the UAV from the transportation vehicle and an assembly of the UAV, since further tasks performed on the UAV are executed in function F3.

Configure System (F3)

The configuring of the system includes all activities which are performed to set up the UAV for its mission. These activities also have to be performed after the UAV has landed and is prepared for another flight. The activities which are performed in this system can be seen in fig. A.2.

- The refuelling of the UAV consists of providing the UAV enough fuel such that it can perform its mission.
- The diagnostics are performed in order to diagnose whether or not the UAV can perform its main tasks, and to assess the operational status of the different systems. This is mainly an observation for defects in the system.
- Switching on the UAV implies that the electrical system is activated.
- Uploading and downloading the data is composed of transferring the sensor data which could not be transmitted during flight, and the downloading of the geographical data of the area.

- Removing/installing sensors consists of the determination of the needed sensors, the removal/attachment of the sensors and the calibration of the sensors. This task can be useful in case different types of disasters are considered, which require different types of sensors.
- The final task of the configuration is the establishment of the communication link in order to make sure that the communication system is operative.

Turn around task (F4)

The turn around task is similar to the configuration of the system. However, this task is performed when the UAV has landed and returns to the air to resume the mission.

Launch (F5)

Included in the launch of the UAV are all the activities considered with take-off and flying to the region of interest. The functional breakdown for the launch can be seen in fig. A.1b.

- The take-off consists of the positioning of the UAV, the pre-flight checks and the take-off itself.
- Another subtask of the launch is climbing to the flight altitude after the launch has been performed.
- Immediately after lifting off the UAV will navigate its way to the region of interest. This will be done by determining the own position of the UAV, and receiving the target location. Then, the UAV can determine the route and fly to the region of interest itself.

SAR communication relay/communication from GS to SAR and vice versa (F6)

Once in the area, one of the main tasks of the UAV can be executed: providing a communication relay for SAR-teams and providing a communication link between GS to SAR and vice versa. This communication will go from the SAR team to the UAV, through the kite and ground station. This function can be divided into different sub-tasks as shown in fig. A.3.

- The communication relay is activated such that a communication signal can be received or transmitted to and from different SAR-teams.
- Receive signal from SAR: A signal, for example a recorded voice, is received from a SAR team.
- The processing of the signal is performed to make sure the message of the signal is not lost, and can be sent again without losing too much data.
- Transmit signal: A signal is transmitted to another SAR team.

Mapping (F7)

Another main task of the system is mapping the area in order provide search advice to the SAR-teams. The breakdown of this task can be seen in fig. A.4. This function consists of the following tasks:

- The first decision which needs to be made is: either the UAV is to fly autonomous or manually, which can be useful if a specific area needs to be investigated.
- The mapping function consists of switching on the sensing payload and determining the right velocity, followed by the mapping itself. Since both the coarse and fine mapping can be performed by the same payload, these will be grouped together under this function.
  Next to the mapping, this data is transferred to the data handling, where it is processed and transmitted to the ground station. The data is stored at the ground station and only the data from at least the last five minutes remains stored on-board of the UAV. This is done in order to prevent data-loss if the data can not be received by the ground station. In case the ground station does not receive the data, the UAV will not get a confirmation of the ground station receiving this data. When this happens, the UAV will return to the ground station to download the data and diagnose the problem. It can also happen that this was an interruption of the signal. If this is the case, then the data can be transferred when the connection is stable again.
- During mapping, decisions on where to look for survivors and the usage of the UAV have to be made. In order to support these decisions the route data, the endurance and the probability map of potential have to be analysed. Using the analysis the algorithm can also be optimised. This data will be given to the operator, which can then make a choice based on this.
- If the operator chooses to further investigate an area, the UAV can loiter above the area to gather more and more detailed data.

Parallel Checks (F8)

In order to guarantee continuity of the system the UAV is monitored continuously via a number of parallel checks. These can be seen in fig. A.5.

- In order to make sure that the UAV has enough fuel to return to the base at any time, preventing it to run without fuel, it has to determine its distance from the ground station. In the meanwhile, the fuel needed to overcome this distance is calculated and compared with the fuel levels at all times.
- When the UAV is in operation, checks on the most critical subsystems will be performed to make sure whether or not the task these subsystems can perform their task properly.

- The communications subsystem is regularly checked. This includes both the receiver (Rx) and transmitter (Tx).
- The control and attitude sensors are regularly checked in order to maintain attitude and to control the UAV.
- Also, the ground station commands have to be obeyed in order to set waypoints or to enable the operator to assume manual control.

Return (F9)

Due to the fact that the endurance of a UAV is less than the duration of the mission, the UAV has to return to the ground station. This phase considers all the activities from the beginning of the return from the mission up to the possible relaunching of the UAV or the end of the mission (F9). The functional breakdown structure can be seen in fig. A.6.

- The first thing the UAV needs to do when it returns to the ground station, is to determine the time it takes to return. This will give a estimated time of arrival, and will also determine if there is enough fuel to return.
- After this is done, the current location is saved. This is done to continue from this point when returning from the ground station with, for example, a full fuel tank.
- Then, the remote sensing payload is switched off. For this, it is first communicated that the payload will be switched off in order to, for example, let the relay communication be handled by a different UAV. Then, the status of the payload is checked and is shut off if it is idle.
- Then the UAV can return to the ground station by first determining the route back. This is done by determining the own location and the one of the ground station. Then the route is flown and the UAV can land.
- After the landing, the communications subsystem (communication with the ground station) is shut off, which will first be communicated in order to avoid open unused channels.
- The communication of the data from GS to the SAR teams is still going on while the UAV returns to the ground station.

End of operations (F10)

The end of operation-activities include all the tasks performed from the landing of the UAV up to the insertion of the system in the transportation vehicle. The functional breakdown structure of this can be seen in fig. A.7.

- At the end of the mission, the UAV has to be transported again, and should be ready for a new mission when needed. This is why final diagnostics are done to check the systems, including a visual inspection of the UAV and a check of the components like the sensors and batteries. Then the UAV's electrical systems are switched off and disassembled so it can be transported to a new location.
- For the ground station, the activities are similar. A diagnostic test has to be done, including a visual check, and a check of the radio and power systems. Then the ground station is switched off and disassembled to be able to transport it to a new location.
- Then, the UAVs are put in the van with the ground station.
- After this, the mission is completed and the system is ready for a new mission.

5.3. Operations and logistics

In this chapter, the operations and logistics of the system are discussed. The operation-cycle is explained in subsection 5.3.1 and the support is described in subsection 5.3.2. After this, the logistics are discussed in subsection 5.3.3

5.3.1. Operation Cycle

The user-flow of the system is important to make an efficient and user-friendly system and will also help in creating a clear image of the system and its possibilities and its possible limitations.

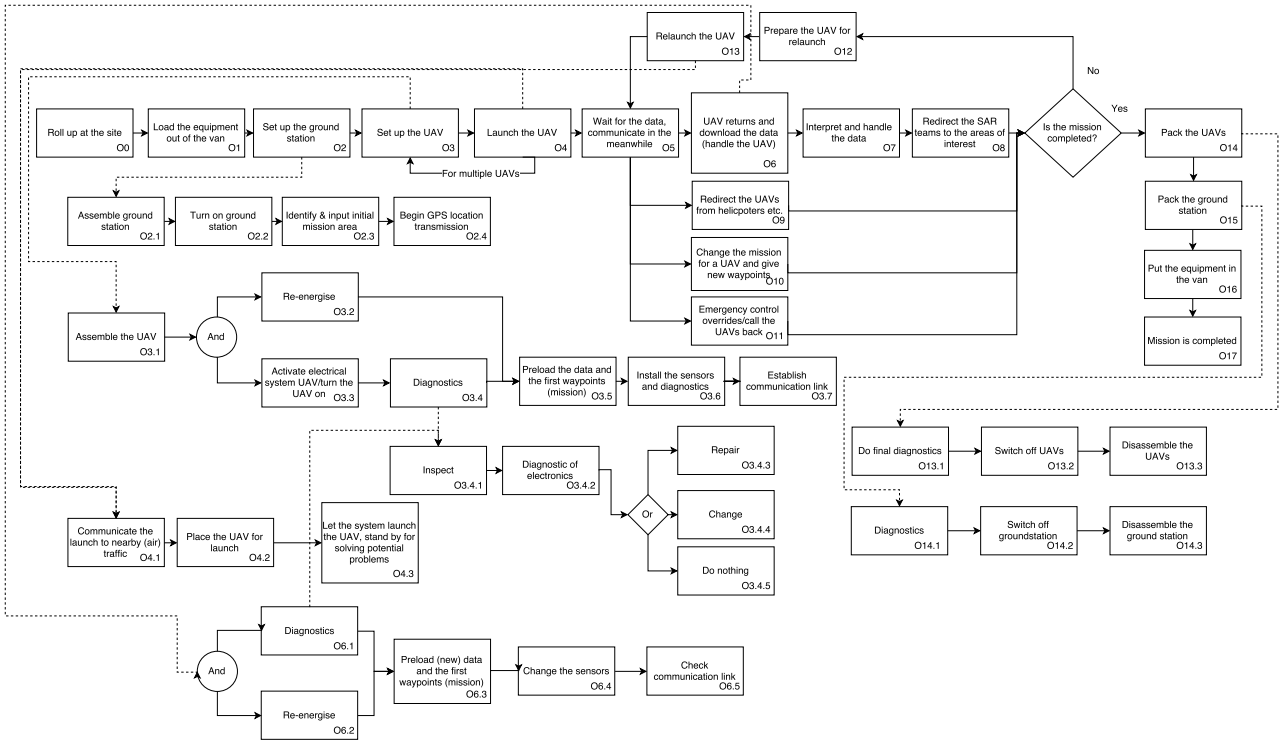

Figure 5.4: Operations flow diagram describing the flow of actions to operate the system.

As can be seen in fig. 5.4, there are about 15 different main tasks the operator can do, some with specific subtasks listed. The main tasks and their potential subtasks are listed below:

- **O0: Roll up**: This is the moment when the operator arrives at the base site, and is regarded as the beginning of the mission.
- **O1: Unload the equipment**: Before the system can be operated, the system first has to be unloaded from the van. The whole system can get unloaded in one time, or the ground station can be unloaded first.
- **O2: Set up the ground station**: The ground system has to be set up first, since then the UAVs can be launched after setting them up immediately. To set up the ground station, it first has to be assembled by attaching the antenna and starting the generator/van to use as a power supply. The ground station can then be switched on. The boundaries of the mission are then set into the system as inputs in order to allow the UAV to complete its mission. The GPS location of the ground station must then be transmitted in order to allow the UAV to know its location.
- **O3: Set up the UAV**: Now the UAVs can be set up after which they are launched to begin their mission, which is done one UAV at a time in case of multiple UAVs. To set up the UAV, it is first assembled. This includes the planform, avionics and other main systems which need to be attached to the UAV. The UAV must then be refuelled. This consists of re-charging any batteries and filling the fuel tank. The electrical system of the UAV is then switched on. Finally, diagnostics are run to check whether the system is able to operate nominally and perform its mission. The diagnostic itself comprises of multiple parts. The UAV is first checked visually for any abnormalities. The electronics are then diagnosed for potential problems. If any issues have been found, parts are either repaired or changed. If the damage is not critical, it is also possible to not take any action. Once this has been done, the data and inputs may be pre-loaded into the UAV in order to allow the UAV to perform its mission. The sensors are then set up in the UAV and further diagnostics are run. Finally, the communication link is checked.
- **O4: Launch the UAV**: The UAV is being launched to fulfil its mission. In order to launch, the intended actions must first be communicated to the surrounding (air) traffic control in order to avoid accidents. The UAV is then placed for launch. Finally, the automatic launch is initiated and the UAV flies to its first way-point. The operate must remain on stand-by in case of any malfunction of the system.
- **O5: Waiting**: After launching all the aircraft, the operator can wait until the UAVs return or data to come in.
- **O6: UAV returns, handling**: When a UAV returns, the data is downloaded if needed.
- **O7: Interpret and handle the data**: The operator can interpret and handle the data, which means he evaluates the data from the UAVs and sends the SAR teams to the areas of interest.
- **O8: Redirect the SAR teams to the areas of interest**: The SAR teams are redirected to the areas of interest, where people need help.
- **O9: Redirect the UAVs from helicopters**: If there is (air) traffic, the operator will redirect the UAVs away from these areas to avoid accidents.
- **O10: Redirect the UAVs for flying a different mission**: The UAVs can be redirected by the operator to map a different area, for example because he has new information of the locations of people.

- **O11: Emergency control overrides**: In case of emergency, the operator can take manual control of the UAVs to manually fly it. This might happen because there is an engine failure. This also includes a callback option to let all the UAVs return and land.
- **O12: Set up the UAV for relaunch**: The UAV has to be set up again for the next flight. Setting up the UAV for relaunch consists of running diagnostics for potential problems again. This is done in the same way as described in O3.4. The UAV is then refuelled and the new flight plan is pre-loaded. If needed, the sensors/payload may be changed. Finally, the communication link must be re-checked.
- **O13: Re-launch the UAV**: The UAV is launched again and O3.4-O3.11 are repeated.
- **O14: Pack the UAV**: The UAV is packed first after the mission is completed. When packing the UAV, final diagnostics must first be carried out and any problems should be solved prior the next mission. The UAV is then switched off, disassembled and placed into the van.
- **O15: Pack the ground station**: Then the ground station is packed using a similar procedure as for the UAVs. Similarly to the UAV, diagnostics are performed. The ground station is then switched off, dissambled and also loaded into the van.
- **O16: Put the equipment in the van**: Now the equipment is ready for a new mission, or problems are known which can be fixed, the system is placed in the van for transport.
- **O17: Mission is completed**: Now the mission is completed and the system can be transported back to the "central base".

5.3.2. Support of the System

The support of the system includes the way the system is maintained and supported to make sure it is operable. The two stages to this are

- Mission duration support: The support that is provided during the run of the mission. As mentioned under operations diagnostic data is constantly collected to monitor the state of the system. During turn-over period any repair/switch is performed and another set of diagnostic tests are done. In case of drastic weather change a decision is made to change route or change/add payload.
- Out of mission support: The support that is provided when the system is in standby-mode. The system will need weekly checks and firmware updates to make sure for compatibilities (required especially when open source software are used).

5.3.3. Logistics

One of the biggest challenges during a search and rescue operation is the logistics of equipment and man-power. Since disasters are accompanied by large damage to property, normal procedures of travel cannot be arranged. Transportation by air is the most convenient measure in these circumstances.

5.3.4. Air Plan

An operation Plan of Action is made before deployment.[22] This is needed to identify the necessary equipment and gear that need to be carried along. In the POA the type of contract for equipment and personal transfer needs to be stated. There are three types of contracts:

- Air Freight Service Agreements: Here special space is made available for cargo in an aircraft. These can be commercial airlines or fright forwarders.
- Aircraft Charter Agreement: Here aircraft are chartered to perform air transport services.
- In some situations the logistics of the SAR team is merged with that of the nations' defense personnel.

The POA also includes various information regarding inventory, responsibilities, check-in points, procedures, costs and support needed. Commonly used aircraft and their capacity is summarised in table 5.1.

Table 5.1: Aircraft cargo capacity.

Aircraft type	**Cargo Weight** [kg]	**Cargo Volume** [m^3]	**Door Dimension** [m×m]	**Pallet Size** [m×m]	**Pallet Qty**
L-100-10 Commercial Herc	11,400	127.5	2.75 x 3	2.25 x 2.75	6
L-188 Electra	14,500	105	2 x 3.56	2.25 x 2.75	8
B-727-100	15,875	230	2.26 x 3.4	2.25 x 3.17	9
Antonov-124	136,078	850	4.4 x 6	All	-
Helio Courier	545	3.96	-	-	-
Cessna 185	408	-	-	-	-

5.3.5. General procedures

In case of emergency situations an Air Coordination Center is set up to coordinate the massive influx of air traffic into a disaster zone. The traffic influx mainly consists of relief operators. They give priorities to the different humanitarian activities and also communicate and update the Civil Aviation Authorities.

[22] http://dlca.logcluster.org/display/LOG/Air+Operations/

5.3.6. Logistics UAV

The UAV will be disassembled to make sure it is transportable to the emergence locations. The UAV is assembled in such a way that it fits in a single box and still complies with the The Netherlands Law on Working Conditions.[23] The box in which the UAV is put has a length of 1.8 m, a width of 0.3 m and a height of 0.8 m. The box will weigh less than 20 kg, and hence can be carried by a single person. Since the UAV has multiple parts, it all fits together properly. The booms will be placed along the length of the box on either side. The fuselage will be placed in the middle of the two booms at one end of the box. Next to the fuselage, on either side, the wings are placed on top of the booms. Last, the tail wing and vertical wings are placed at the side of the box. All parts are protected from damaging by means of foam rubber. The layout is shown in fig. 5.5. The wing are shown in red, the fuselage is blue, the booms are yellow and the tail is green.

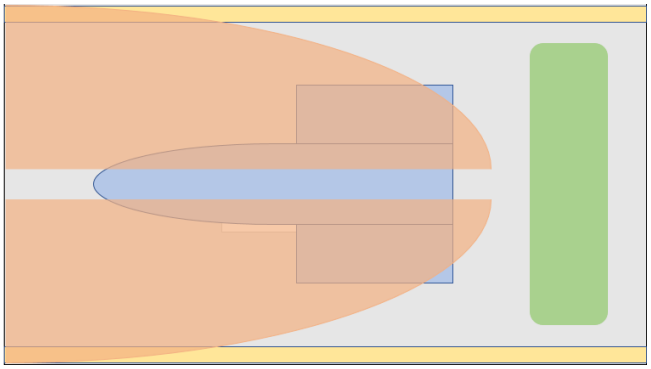

Figure 5.5: Placement on how the UAV is put in the box.

[23] https://www.arboportaal.nl/onderwerpen/tillen-en-dragen

PART II
Configuration trade-off & technical design

Part II includes the major configuration trade-offs of the UAV and ground station that has been conducted in the previous design phase. Once the configuration has been selected, its detailed technical design from final design phase is reported.

Chapter 6: Design choice procedure

This chapter summarises the second design phase of the project. This design phase included the trade-off that lead to a final concept choice. In an earlier design phase all the different possible configurations and sub-configurations were discovered using a morphological diagram. After all the non feasible options were eliminated there were still options left to investigate. This chapter aims to elaborate on all these different trade-offs and use quantitative arguing based on literature studies and knowledge of the team to perform this trade-off. Finally these trade-offs have led to a configuration choice for the final design of the UAV, payload and ground station.

This chapter is structured as follows: In section 6.1 the trade-off of the UAV payload is summarised. This trade-off led to a UAV configuration concept trade-off in section 6.2. In section 6.3 the number of UAVs is chosen. In section 6.4 a trade-off is done on the subsystems of the UAV that is chosen in section 6.2. In section 6.5 the ground station trade-off is done.

6.1. Payload

During the second phase of the design process the payloads that the UAV needs to carry were traded off based on the mission and design constraints. This section provides a brief overview of how this was handled. The mission dictates the payload that needs to be carried and two separate subsystems have been drawn from this - mapping payload and the communication payload.

6.1.1. Mapping payload

The trade-off here was done primarily based on technology where the best available product from each technique was traded off against each other.
A closer look was taken into RGB, Infrared and LIDAR since these systems have no major drawback and can fulfil the requirements. A trade-off was conducted on these different systems against several criteria.
Mass has the highest weight of 5, masses below 0.5 kg receive a good score, masses between 0.5 and 2.5 kg receive a medium score and masses above 2.5 kg receive a poor score.
Power has a weight of 3. The fact that a generator will be used on the UAV assures that it is not critical to slightly overshoot the power budget. Power usage between 5 and 25 W receive a medium score. Less power consuming sensors receive a good score and more power consuming sensors receive a poor score.
Costs has a weight of 2. Sensors pricing below $ 5,000 (4,500 €)receive a good score, below $ 15,000 (13,500 €) receive a medium score and more expensive sensors receive a poor score.
Size has a weight of 1. It has such a low weight because it correlates mass. Still, large sensors are hard to integrate and are therefore undesirable. Sensors with a 250 cm^3 receive a good rating. Sensors with more than a 4,000 cm^3 volume receive a poor rating.
Data rate has a weight of 2. If the data received from the payload is too large to actually send to the ground station, the data needs to be compressed, which decreases resolution. Data rates under 1 MB s^{-1} receive a good score, data rates between 1 and 3 MB s^{-1} receive a medium score and higher data rates receive a poor score. In the table the unit MB/f means MB per frame. It is denoted like this because the RGB camera will not be used for video streaming but just for taking pictures.
Maximum Flying Altitude has a weight of 3. In order to meet the main resolution requirements a certain sensor can operate from a certain maximum distance. If a sensor can be above an altitude of 150 m it receives a good score. Flying altitudes below 30 m receive a poor score because of the increase in obstacles on these flying altitudes.
Maximum Flying velocity has a weight of 3. Different sensors have different maximum flying speeds in order to achieve the main resolution requirements. This is the only trade off criterion where there is a clear difference between the helicopter and winged aircraft UAV concepts. Stall risks do not apply to helicopters. Poor scores are received for maximum flight speeds of under 15 m s^{-1}. Good scores are given to a maximum flight speed of over 40 m s^{-1}.
Mapping rate has a weight of 2. The mapping rate is crucial for the time at which SAR teams receive the vital mapping images. The mapping rate of a sensor is defined by its maximum flying velocity and maximum flying altitude, which have already been included in the criteria. There is only one remaining variable which is the field of view (FOV). Mapping rates that receive a good score are able to map 1,000 m^2 s^{-1}.
Vulnerability to environmental conditions has a weight of 4. Sensors that are not effected by environmental conditions receive a good score. Medium scores are given to sensors that have reduced capabilities but still properly function under harsh environmental conditions. Poor scores are given to sensors that do not fulfil its function under harsh environmental conditions.
Note that in all trade-offs, poor, medium and good scores represent scores of values 1, 2, and 3 respectively. The subsystem with the highest cumulative score is therefore the winner of the trade-off.

Table 6.1: Trade-off table for mapping payload.

	Budget Contribution					Sensor Performance				
	Mass (5) [kg]	Power (3) [W]	Costs (2) [$]	Size (1) [cm^3]	Data rate (2) [$MB\,s^{-1}$]	Max flying altitude (3) [m]	Max ground speed (3) [$m\,s^{-1}$]	Mapping Rate (1) [$m^2\,s^{-1}$]	Vulnerability to Environment (4) [-]	Total
RGB	0.36	5.5	5,000	200	0.60	>150	>35	5,300		61
Hyperspectral IR	5	41	14,000	5,200	2	>150	10	1,860		44
Thermal IR	0.12	2.1	4,400	150	4.9	>150	30	1,740		64
LIDAR	0.59	8	10,000	600	1-2	150	25	>1,000		54

Judging from table 6.1 the hyper-spectral infra-red was traded away due to the high weight of the system. A RGB camera was selected in particular due to its high mapping rate. An infrared camera was selected because of the night vision abilities, the ability to quickly detect humans and because it can look through smoke. The LIDAR was chosen as an extra addition (the aforementioned cameras already fulfil the requirements) to the system since it increases the value of the whole system by adding the possibility of 3D mapping. A LIDAR sensor can look through the canopy of a forest and can generate a very detailed three-dimensional map of an area of interest. It also works in almost any weather condition. For mapping it will not reach the required resolution in one fly over but it will still be within the time constraints.

6.1.2. Motion Blur

Since the UAV is a moving object, motion blur occurs during optical mapping. For the RGB camera this is mainly dependant on the shutter-speed. To obtain some sense on the effect of motion blur an investigation has been done on this matter. If the UAV flies with tailwind it will have a ground speed of at least 35 $m\,s^{-1}$. The 35 $m\,s^{-1}$ is the combined tailwind speed and stall speed and is just a rough estimated number to show how the motion blur has been determined. Requirement **REQ.U.PL.M.7** states that a maximum of 0.5 a pixel of blur per pixel should be present. Requirement **REQ.U.SYS.2** states that the fine mapping should have a resolution of 10 cm per pixel, which means the motion blur should be at most 5 cm. Using that number a shutter speed of at least 1/700 seconds is determined (which is also stated in requirement **REQ.U.PL.RGB.3**). A short investigation in existing RGB cameras on their shutter speeds finds that the B1942, which is also used for reference calculations for the data rate in section 11.2, has an adjustable shutter speed ranging from 1/500,000 to 1/32 seconds. Also a look was taken at the integration time (which is analogous to shutter speed for an RGB camera) of existing IR cameras. These also fall within a similar range. Concluding, to prevent motion blur at high ground speeds the system has to meet the above stated requirements.

6.1.3. Communication payload

The biggest constraint when it comes to communication is the range and the data rate. Radio signals will be used. From literature the higher the frequency, the smaller the size of the antenna needed but the lower the range. It was found that frequencies in the ultra high frequency spectrum (UHF) are the best choice for the application at hand. As the UAV should communicate with the ground system, it should have a communication system on-board which is able to receive data, transmit data and if possible, encode and amplify data. Research was done in possible off-the-shelf devices. From table 6.2 it can be quickly seen that SC-4200[24] performs best in all aspects and is therefore chosen.

Table 6.2: Available options for communication payload.

Device	Technology	Frequency [MHz]	Data rate [$MB\,s^{-1}$]	Power output [W]	Voltage [V_{DC}]	Consumption [W]	Weight [kg]	Range [km]
SC-4200	MN-MIMO	400 - 6,000	100	0.010 - 0.5	9 - 20	4.8 - 24	0.120	50
SC-4400	MN-MIMO	400 - 6,000	100	0.010 - 0.5	9 - 20	8 - 43	0.260	50
Airlink	Digital IP data link	2,400 - 5,800	12	1	10 - 16	5	0.108	30
Digi XBee-PRO XSC		902 - 928	0.010 - 0.020	0.250	2.4 - 3.6	-	0.020	45

Moreover, a trade-off was done on possible antennas. A high gain is needed due to the possible large distance between the UAV and the ground station. Directional antennas can get to a high range but their field of view is limited. Additionally, it is not reasonable to have a device that provides tracking for the antenna on the UAV. It was therefore decided to use an omni-directional antenna. The off-the-shelf antennas that have been found do not provide the required gain. Therefore an antenna will be designed in CST Studio Suite to get enough gain for transmission.

6.1.4. Control System Sensors

This section elaborates on the control system sensors for sensing the state of the UAV. Below, obstacle avoidance, position, attitude, heading, altitude and close range sensing are discussed.

Obstacle avoidance is used to prevent the UAV from colliding with other objects. The different sensors which can be used are described below for obstacle avoidance:

[24] `http://silvustechnologies.com/products/streamcaster-4200`

Radar: Radar uses radio waves to determine its relative position with respect to the object.
Sonar: Sonar uses uses high frequency sound waves.
LIDAR: LIDAR uses light waves instead of radio waves or sound.
Radio-location: The radio location uses the radio waves emitted by other SAR flying vehicles to determine their position. This requires these to communicate their frequencies used or use a transponder which could be given to them, which both could pose problems, since the frequencies might change, or not every helicopter/vehicle has a transponder, or the transponders might fail. Also, the system can not determine the presence of objects not emitting radio waves. For these reasons, this option is mentioned in the design option tree but is not regarded.
Visual/Optical: The optical method uses the optical camera to determine whether there is an object in the flight path of the UAV or not. This method is currently in development and can not see through fog or smoke.
The trade-off table is shown in table 6.3. The trade-off criteria on which the trade-off is based are:
Mass has the highest weight of 5 out of 5, masses below 100 g receive a good score, masses between 100 and 500 g receive a medium score and masses above 500 g receive a poor score.
Power has a weight of 3. Power usage between 5 and 25 W receive a medium score. More power consuming sensors receive a poor score.
Costs has a weight of 2. Sensors pricing below €1,000 receive a good score, below €5,000 receive a medium score and more expensive sensors receive a poor score.
Size has a weight of 1. On a volume scale, sensors with a 10 cm^3 receive a good rating. Sensors with more than a 300 cm^3 volume receive a poor rating.
Cope with meteorological precipitation has a weight of 4. This trade-off criterion represents how the obstacle avoidance system copes with of any product of the condensation of atmospheric water vapour that falls under gravity such as rain or snow. The poor, medium and good score of meteorological precipitation of different systems is based on [20].
Sensing range has a weight of 4. A large sensing range means that the UAV can avoid the obstacle with a certain safety factor. Values lower than requirement **REQ.U.CS.8** are poor because these are too close to react safely in time and values higher than 500 meter are considered good.
Visual conditions has a weight of 3, since certain systems handle visual conditions such as smoke and fog better. The poor choice of visual conditions for an optical/visual system is based on the fact that the sensing range is limited by the visibility.
Off-the-shelf has a weight of 3. The poor choice of the off-the-shelf category is because most of these systems are still in development.

Table 6.3: Trade-off table for obstacle avoidance payload.

	Budget contribution				Sensor performance				
	Mass (5)[g]	Power (3)[W]	Costs (2)[€]	Size(1)[cm^3]	Cope with rain/snow (4)[-]	Sensing range (5)[m]	Visual conditions (3)[-]	Off-the-shelf (3)[-]	Total
Radar system	50	1	500	23.4		200			66
Sonar system	5	0.025	60	4.8		10			68
LIDAR system	600	60	8,000	600		300			43
Optical/visual	360	5.5		190.8		6,000			51

Due to the low range of the sonar system, this option is be neglected. Furthermore, the LIDAR system receives a poor score for multiple criteria and is therefore excluded. The optical obstacle system is excluded due to poor score. This means that the radar system is the most suitable for obstacle detection since the contribution of the radar system to the budgets is minimal and the range requirements are met.

Following to the trade-off for different systems the specific sensor needs to be chosen. The radar systems applicable to the UAV and the helicopter are displayed in table 6.4.

Table 6.4: Radar sensors applicable to the UAV.

on-board radar systems	Manufacturer	Mass [kg]	Power [W]	Cost[€]	Size [cm^3]	Sensing Range [m]
μSharp Patch	Aerotenna	0.050	1	500	23.4	200
MESA-DAA	Echodyne	0.817	30	20,000	905	3,400

After clearly visualising the applicable sensors it was decided that the **μSharp Patch**-sensor is chosen due to the minimal contribution to the mass, cost, power and size budgets and the fact that it meets the sensing range requirement.

6.1.5. Position

For determining the position of the UAV there are two options: a GPS/GNSS system or an inertial measurement unit (IMU).

- GPS/GNSS: The GPS/GNSS a space-based radio-navigation system. A disadvantage is the possibility of losing a satellite lock, or the total loss of communication with the satellites due to for example dust. This is solved by setting up an RTK system, which will guarantee the operation ability of the system.
- IMU : The IMU can determine the velocity by integrating the measured accelerations from the accelerometers from which the position is determined. Due to the fact that this is an inertial system this creates an error which will accumulate over time. This error is not big in the beginning, but might increase to an unreliable extend for long term missions.

Because the GPS/GNSS system is not an inertial system, the position is continuously updated, such that errors will not accumulate. For determining the position the GPS/GNSS-system is preferred over the IMU.

6.1.6. Attitude

Different types of sensors may be used for attitude determination. Inertial systems show higher performances than individual sensors on their own. Combining data from multiple sensors as inertial systems do, allows for higher accuracy and precise attitude determination which is necessary for an automated UAV.

The attitude of the system can be determined with respect to both the earth centered reference frame and to the airflow. The attitude with respect to the earth centered reference frame is important to measure since the mapping sensors need to be pointed relative to the attitude of the UAV. In this case there is only one choice: an IMU.

Because it is decided that a GPS and an IMU are chosen, these sensors can be integrated. In table 6.5 a list of IMU/GPS sensors is provided.

Table 6.5: Integrated GPS and IMU sensors.

Name	Mass [kg]	Power [W]	Cost [€]	Accuracy [°] roll/pitch	Accuracy heading [°]	Position m	Altitude m	Velocity m s^{-1}	GPS
Ellipse II A	0.045	0.460	15,000	0.1	0.8	-	-	-	No
Ellipse II N	0.047	0.650	15,000	0.1	0.5	2	-	0.1	Yes
Ellipse II E	0.049	0.460	15,000	0.1	0.5	-	-	0.1	No
Ellipse II D	0.18	2.5	15,000	0.1	0.2	0.02	-	0.03	Yes
Ekinox A	0.4	3	30,000	0.015	0.03	0.02	-	-	No
Ekinox E	0.4	3	30,000	0.015	0.03	0.02	-	-	No
Ekinox N	0.6	6	30,000	0.015	0.03	0.02	-	-	Yes
Ekinox D	0.6	6	30,000	0.015	0.03	0.02	-	-	Yes
Apogee A	0.69	3	70,000	0.008	0.025	0.01	0.03	-	Yes
Apogee E	0.69	3	70,000	0.008	0.025	0.01	0.03	-	No
Apogee N	0.9	5	70,000	0.008	0.025	0.01	0.03	-	Yes
Apogee D	0.9	7	70,000	0.008	0.025	0.01	0.03	-	Yes

The Ellipse II D is chosen due to the accurate heading with dual antenna GNSS and also has the capability of receiving correction data (RTK).

The attitude with respect to the airflow is of a vital importance for the control system, therefore α and β vanes are used to determine the angle of attack and the angle of sideslip during flight. This can be integrated in a data boom with the pitot tube to have a self-contained system.

6.1.7. Heading

In order to determine the heading a GPS/GNSS system and an IMU can be used, which both have been covered in subsection 6.1.5. A third option for a heading sensor is a magnetometer, because the magnetometer can determine the attitude of the UAV with respect to the magnetic North. Due to the fact that the GPS/GNSS-system and the IMU are both already included in the system in subsection 6.1.5 and subsection 6.1.6 and that the magnetometer is often included in the IMU the magnetometer will not be included seperately in the UAV.

6.1.8. Airspeed and Ground Speed

For the UAV there are two types of speed which need to be determined: airspeed and ground speed. The pitot tube can determine the airspeed. Besides the pitot tube, there are no instruments found that could determine the airspeed. The pitot tube is also used often, which makes this technology very reliable. A disadvantage is that this method is not reliable when choosing for a helicopter design, since at a low airspeed the pitot tube might be in the wake of the main rotor, which influences the measurement. The pitot tube will have a weight of 155 g, cost €3,090 and will have a power consumption of 0.7 W

For ground speed there are three different options considered: GPS/GNSS, IMU and Doppler radar.[25]

- The GPS/GNSS system determines the ground velocity of the UAV in three dimensions, meaning that the course of the UAV can be determined with an accuracy of a few mm s^{-1}. [26] [27]
- As discussed in subsection 6.1.5 the IMU can determine the velocity by integrating the measured accelerations from the accelerometers.
- Doppler radar: The Doppler radar determines the ground speed by using the Doppler effect on the terrain the UAV flies above. The system is a self contained system, but requires difficult software algorithms and may yield errors if a non-stationary object moves into sight of the radar.

[25] http://www.vectornav.com/support/library/imu-and-ins
[26] http://www.insidegnss.com/node/4433
[27] http://gauss2.gge.unb.ca/papers.pdf/ionntm2004.serrano.pdf

Table 6.6 is generated to see the effect of the Doppler radar on the budgets. Due to the fact that the GPS and IMU are already included in the design and that the Doppler radar has a significant influence on the mass, power and cost budgets it is decided that it will not be included.

Table 6.6: Trade-off table for the ground speed sensor payload.

	Budget contribution				Sensor performance	
	Mass(3)[g]	Power(2)[W]	Cost(2)[€]	Size(1)[cm^3]	Accuracy(3)[-]	Total
GPS/GNSS with IMU	180	2.5	15,000	183	0.1 deg	26
Doppler Radar	50	1	500	23.4	-	20

6.1.9. Altitude

Two different types of altitude must be considered when choosing instruments to measure this parameter. First, the height above sea level, second, the height above the ground surface. Multiple methods may be used to determine the altitude of the UAV.

For the altitude above sea level the pitot tube is used, because it is included in subsection 6.1.8 already. Determining the ground speed can be done using a GPS system, a sonar sensor or a radar altimeter. The GPS-system is already included. However, for redundancy, one can include a second sensor which is discussed below.
Sonar: This method relies on high frequency sound waves to determine the distance from the ground. The range is small and it is vulnerable to weather conditions.
Radar altimeter: The radar altimeter measures the distance from the ground using radar. This method determines the distance to the ground for more than 100 meters. It may be integrated with the other radar systems on board of the UAV.
In the trade-off table in table 6.7 the radar altimeter has a significant contribution to the power budget and the sonar system fails to sense ranges larger than 10 meters. Therefore, it is decided that these systems are not included in the design.

Table 6.7: Trade-off table for the altitude sensing payload.

	Budget contribution				Sensor performance		
	Mass (3)[g]	Power (2)[W]	Cost (2)[€]	Size (1)[cm^3]	Accuracy (3)[-]	Range (4)[m]	Total
Sonar	0-50	0.025	30	11.3	Typically 3.5%	10	34
Radar altimeter	160	3.7	500	23.4	Typically 0.25m	500	35

6.1.10. Close Range Sensing

Close range sensing is used to land. This can be done using different methods and sensors, as described below:
Sonar: Sonar has a range of about 10 meters, which means that this method is not suitable for landing.
LIDAR: LIDAR has a larger range, but if there is fog or smoke, the system may not work as wanted and is not used (often) for landing UAVs.
CR radar: The close range radar can "visualise" the area where the UAV should land and determine the height the UAV is flying at. However, this method is not used (often) for landing UAVs.
Optical/Visual: This method uses a camera to identify the landing area. This method is promising, but it is still being researched and weather dependant.
Transponder: The transponder would ping its location to the UAV, which could locate it and try to land exactly. This system is not being used (often) for landing UAVs. For this reason, this system will not be used.
ILS: The Instrument Landing System (ILS) is being used for guiding normal aircraft on airports. The system is rarely being used for landing UAVs. Also, the system would require multiple pieces of equipment, which are larger than other systems. For these reasons, this system will not be taken into account.
IR: Infrared cameras can be used for close range sensing and allow the UAV to land. There are multiple ways of doing this. These different methods are listed below:

- **Beacon:** A beacon can be used, which the UAV can see with the IR camera, and land based on this reference point. This method can be used, but requires a very heavy system (in the order of 5 kg for a suitable IR-camera for this kind of beacon). For this reason this method is not included.
- **Ranging:** Ranging is done by off-the-shelf products and works like the beacon method. A sensor is used on the UAV to detect an infrared point on the landing platform. This method also only works for the helicopter concept.
- **Guiding:** The UAV can be guided by the GS by having a stereo IR-camera at the GS to determine where the UAV is, and send this data to the UAV, which can then land based on this information. This method is less accurate [38], very heavy (for the GS) and is being researched too. This makes this method not suited for this subsystem.

Table 6.8: Trade-off table for the close range sensing payload.

	Budget contribution				Sensor performance		Additional information		
	Mass (5)[g]	Power (3)[W]	Cost (2)[€]	Size (1)[cm^3]	Range (2)[m]	Operationality (5)[-]	Helicopter/Conventional UAV (2)[-]	Additional (5)[-]	Total
Sonar	0 - 50	0.025	30	4.8	10	Does not work well in rain	Helicopter		61
LIDAR	600	60	8,000	600	300	Does not work with fog/smoke and rain	All		48
Close Range Radar	50	1	500	79.56	45	Can detect through fog/smoke	All		73
Optical/Visual	360	5.5	-	190.8	Depends on visual situation and specific camera/software	Does not work with fog/smoke and rain	All	Is under development	44
IR: Ranging	200	4	200	40	15	Can detect through fog/smoke	Helicopter		73

The IR ranging method was chosen in case of the helicopter design, since this will guide the UAV to the landing location when close (in the order of 10 meters). Since this will not work as well for the conventional UAV as for the helicopter concept, the close range radar was chosen for the close range sensing of the conventional UAV to obtain the height from the surface and what is in front of the UAV fast and reliably. The geographical location data from the GPS/GNSS can be used to direct the UAV to its landing site, since this is present on the system already, following from results of previous sections.

The sensor that will be used for the IR ranging is an IR-lock-sensor.[28] For the close range radar, a product from Aerotenna (μSharp) is used, which is already used for obstacle avoidance.[29] Additionally, since it can be used to detect objects, it can also detect the landing site in combination with GPS/GNSS coordinates.

6.1.11. On-Board Computer

The On-Board Computer (OBC) is the central hub in the UAV where all incoming data is processed. In the design choices there had to be a pick between two options. 1. Buy off-the-shelf flight processing unit vs. build one on our own. 2. One processor does everything vs. multiple processors (e.g. flight computer and payload computer). A design choice was made for building a system and using multiple processors for a couple of reasons. Having a system that is build from scratch makes it more versatile and configurable. The on-board computer can be designed to take particular shapes which is useful because it is integrated in the UAV. Multiple processors help mitigate problems from data overload and running out of processing power. Also when one processors fails there is still enough contingency.

6.2. UAV concept choice

Aeroplane concepts and helicopter concepts have been considered. The three configurations to be investigated are a single and multiple aeroplane fixed wing configuration and a helicopter concept. Before the best concept choice is decided, a close look is taken at the wind requirement **REQ.U.SYS.9**. 10 Bft means wind speeds ranging from 24.5 m s^{-1} to 28.4 m s^{-1}. Difficulties such as humans not able to walk already become reality at 9 Bft. This means that the use of the UAV is very limited. At 8 Bft SAR missions can still be carried out, although walking in these conditions is still difficult.[40]
The flight envelope for the concept choice is established to determine the minimum and maximum load factors of the UAV. Both the load flight manoeuvre diagram and the gust load diagram are plotted to see the critical load factor. According to the FAA regulations Sec 23.337 [50] the limit load factors the aircraft has to be designed for shall not be lower than 4.4 and shall not be higher than -1.8. The flight manoeuvre diagram is created by means of eq. (6.1), which defines the load factor due to the lift over weight ratio. These are indicated in fig. 6.1 as curves 1 and 2. Furthermore, the maximum and minimum load factors (-1.8 and 4.4) limit the flight envelope of the UAV, as indicated in the diagram with lines 3 and 4. Additionally, the diagram is limited by the dive speed V_D because the UAV should never exceed this speed limit. This is represented as line 5.

$$n = \frac{L}{W} = \frac{C_L \frac{1}{2} \rho V^2 S}{W} \tag{6.1}$$

The gust diagram consists of four different lines, which are all described by eq. (6.2). This equation describes the load factor induced by a change in the angle of attack due to a gust. The gust diagram is drawn by calculating the minimum and maximum gust loads factors at V_{cruise} and V_D. These lines are indicated in fig. 6.1 by lines 6, 7, 8 and 9. All variable explanations can be found in the nomenclature.

$$n_{gust} = 1 \pm C_{L_\alpha} \cdot \frac{\rho}{2} \cdot \frac{S}{W} \cdot K \cdot V \cdot U \tag{6.2}$$

Krayer and Marshall determined wind speeds 1.5 times the mean wind speed when observing a hurricane [39]. FAA load factor requirements state that a maximum gust speed of 9.4 m s^{-1} can be used. This means that a wind speed of 18.8 m s^{-1} is the limiting speed the UAV can fly in. This falls in the 8 Bft range. Figure fig. 6.1 shows the total manoeuvre diagram.

[28] https://irlock.com/
[29] http://aerotenna.com/sensors/

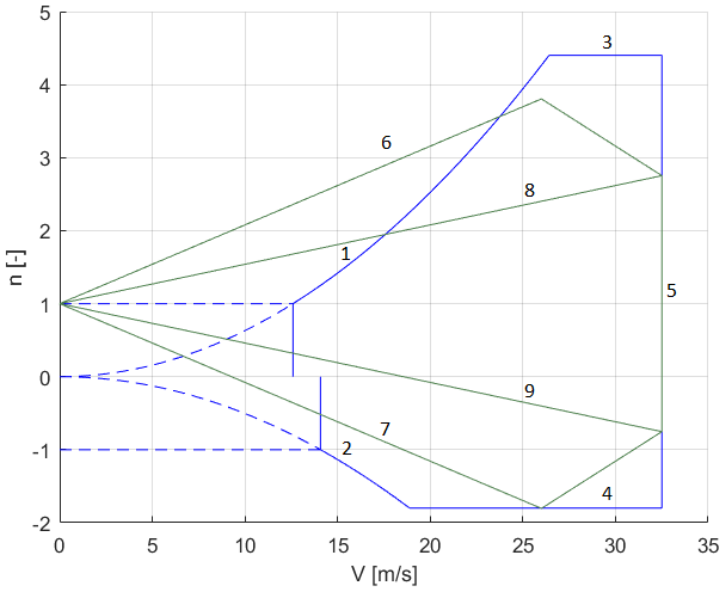

Figure 6.1: Flight envelope diagram with manoeuvre (blue) and gust (green) diagrams for a gust velocity of 9.4 m s^{-1}.

In order to fulfil this flight envelope, the UAV should be limited to flying in wind conditions up to 8 Bft only. As a result, item **REQ.U.SYS.9** is changed to 8 Bft.

6.2.1. Mapping Requirements

A lawnmower mapping method is used with all tracks parallel to each other and an overlay of 10%. The UAV flies following FAA regulations, meaning it flies at an altitude of 120 m resulting in a minimum field of view (FOV) of 47°. To fulfill the critical mapping requirement item **REQ.U.SYS.3**, an airspeed of 26.3 m s^{-1} must be reached and the UAV is required to have a stall speed less than 24.2 m s^{-1}.

6.2.2. Fixed Wing UAVs

This section summarises the design options for the fixed wing configuration. These configurations can still be combined with the pseudo-satellite option; meaning either a kite or a balloon above the GS. The kite/balloon is not taken into account at this moment since it is considered to be part of the GS. Next, six feasible configurations for the fixed wing UAV are summarised and taken to the next step or disregarded.

The most common configuration, the conventional aeroplane is referred to as a large lift generating main wing and a small stabilising tail. This concept is a proven concept in the aviation industry. It is considered later on.

The delta wing is a configuration used for high speed aircraft. Nowadays it is possible to fly at lower velocities, however, it suffers heavily from inefficiency. [30]

The canard configuration is a concept that has the advantage of performing more aggressive manoeuvres and having a reduced trim drag compared to a conventional tail. However, the canard is most effective at high Mach numbers, it has a high induced drag, complex stall behaviour and a high wing surface. ([4], [30]) No such abrupt manoeuvres are required and the mission will not be performed at high Mach values. It was therefore not taken into account further on.

A blended body design has a smooth transition between fuselage and main wing which itself is connected to the tail by means of extended winglets. The main wing has backward sweep, whereas the tail surface has forward sweep to be able to combine the two. An increased parasite drag leads to a big disadvantage but the most severe disadvantages are the structural and aerodynamic complexities it entails. Currently, this concept is still in development.

Lastly, the fixed wing with multiple copters is considered. Its main advantage is the possibility to perform a VTOL. Low stall speeds are reachable as well for the use of hovering. The performance however is less efficient to the conventional aeroplane. Its main question is therefore whether is is beneficial to go for efficiency loss and reduced performance. A quantitative calculation is performed to see the difference. P_{req} for VTOL equals 7.5 HP whereas a conventional aeroplane uses 3 HP. The difference is too large and the multiple copters are disregarded as a configuration option.

6.2.3. Helicopter UAVs

Four different helicopter configurations have been explored in detail. These are the conventional helicopter, the tandem rotor design, the intermeshing rotor helicopter and the coaxial design. These will be elaborated below.

[30] `http://docs.desktop.aero/appliedaero/preface/welcome.html`

The conventional helicopter has the advantage that it is a proven concept and that there is a lot of knowledge present. One of its disadvantages, however, is the need for a tail rotor to counteract torque caused by the main rotor. P_{req} for the tail rotor is generally 5% to 10% of the main rotor power. [42]

The tandem rotor design consists of two in-line counter-rotating rotors. An advantage of this design is its large CG range. One the other hand, due to its complexity and its low efficiency for low payload weights, it is not considered as a design option.

The intermeshing rotor design is too complex and neither of the two rotors provided vertical lift, meaning the efficiency of the design is significantly lower. However, a small fuselage can be used that decreases parasite drag significantly. [12]

The coaxial design is a where to propellers are put on top of each other, leading to great disadvantages. The efficiency of the second rotor is significantly lower w.r.t. the top rotor due to wake interference. The compact layout for the propulsion subsystem is, however, an advantage of this concept. Additionally, no tail rotor is required and shorter blades can be used w.r.t. the conventional design [36].

6.2.4. Preliminary Elimination Helicopter UAVs

The tandem and the intermeshing rotor designs are eliminated preliminary. It is not necessary for the FASAR UAV to have a large CG. range; hence the elimination fo the tandem rotor. Moreover, intermeshing rotors are complex and large difficulties arise when designing small scaled versions. There have not been any proven concepts for UAVs yet and they do not have favourable stability and control characteristics due to the missing tail rotor, [54].

6.2.5. Trade-off between Helicopter Concepts

[36] and [54] show that under the same conditions, P_{req} is less for the conventional helicopter w.r.t. the coaxial helicopter. The complexity of the coaxial design is higher and item **REQ.O.SYS.6** states quick repairs need to be possible. Concerning complexity, the conventional design is in favour. Taking size into account, a tail rotor is required for a conventional helicopter and therefore the size of the coaxial is smaller w.r.t. the conventional helicopter. Regarding manoeuvrability, the single rotor is favourable due to the tail rotor, [54].

Boris N. Bourtsev et al. compared the two designs. The flight envelope and operating speeds are larger and wider for the conventional helicopter, [9]. table 6.9 shows that the conventional is in favour regarding the helicopter designs.

Table 6.9: Trade-off table for the helicopter configuration.

	Power required (3)[-]	Complexity (3)[-]	Size (2)[-]	Manoeuvrability (2)[-]	Maximum speed (1)[-]	Total
Single rotor	2	3	2	3	3	26
Coaxial rotor	3	1	3	2	2	24

6.2.6. Performance Analysis

An initial look is taken at the flight profile as depicted in fig. 6.2. Contingency is shown for a two different possible landing methods. Moreover, the flight profile shows different operating heights by means of the dotted lines.

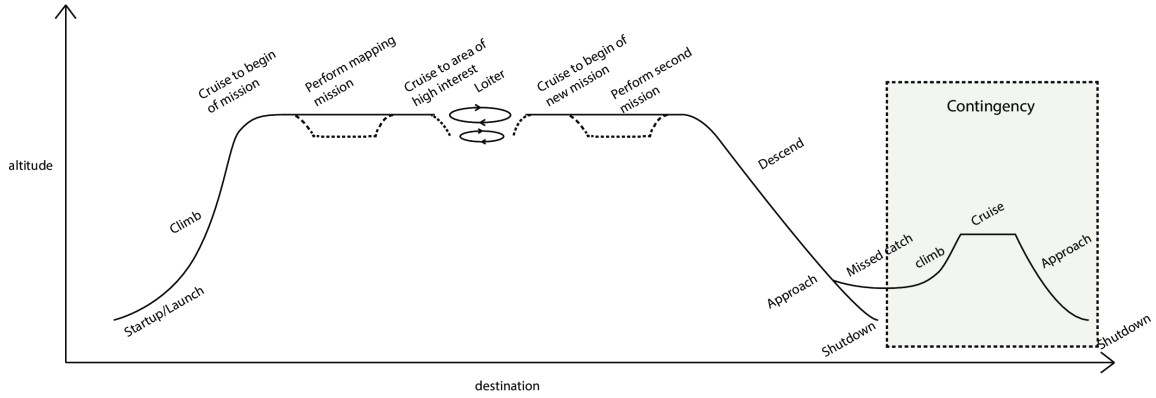

Figure 6.2: Typical mapping and comminucation relay flight profile.

For choosing between the two configurations, certain parameters have been set for both configurations and are summarised in table 6.10.

Table 6.10: Set parameters for both configurations.

Parameter	Value	Unit
MTOW	25	[kg]
W_f	3	[kg]
Altitude (MSL)	3,500	[m]
a	-0.0065	[K m^{-1}]
T_0	288.15	[K]
ρ_0	1.225	[kg m^{-3}]
R	287.00	[J kg^{-1}]
g_0	9.80665	[m s^{-2}]
PSFC	0.45	[kg kW^{-1} h^{-1}]
TSFC	0.45	[kg kW^{-1} h^{-1}]

Table 6.11: Typical values used for the initial sizing of the UAV.

Parameter	Value	Unit
C_D	0.03	[-]
η_p	0.7	[-]
A	8	[-]
e	0.8	[-]
CL_{max}	1.5	[-]
V_{stall}	15	[m s^{-1}]
V_{turn}	34	[m s^{-1}]
n_{turn}	1.4	[-]

6.2.6.1. Fixed wing performance

For a fixed wing aeroplane the initial sizing of the propulsion system and wing area can be done regardless of the chosen more detailed configuration. The values used for the initial sizing are based on typical values used for UAVs and can be seen in table 6.11.

The stall speed was obtained from general flight conditions the UAV has to be able to fly and was fine tuned to obtain a reasonable wing size, assuming the $C_{L_{max}}$ mentioned in table 6.11.

The turn speed shown is obtained using control sensing estimations. There is a maximum range at which automatic obstacle avoidance is possible. This poses a required turn radius and load factor at a given airspeed. This airspeed was chosen such that even after several iterations it will be within the cruise speed used during operations and the maximum speed capabilities of the aeroplane.

The following equation is used to determine the required HP/W for a given wing loading during a turn with a specified load factor n [40]:

$$\frac{P}{W} = \frac{1}{550\eta_p}\left(0.5\rho V^3 C_{D_0}\frac{S}{W} + \frac{2}{\pi Ae}\frac{n^2}{\rho V}\frac{W}{S}\right) \tag{6.3}$$

Where P is the power delivered by the propulsion system in units of HP. The wing loading is determined using the stall condition which can be obtained by the following relation [40]:

$$\frac{W}{S} = 0.5\rho V_{stall}^2 C_{L_{max}} \tag{6.4}$$

The horsepower requirements for endurance and cruise conditions are also taken into account, however they do not pose any further constraints on the design space for wing loading and horsepower requirements. The calculations are verified using [40]. Assuming a turn with a load factor of 1.4 and a turning speed of 34 m s^{-1} we find that 3.0 HP is needed at a wing loading of 145 N m^{-2}. For a MTOW of 25 kg a wing surface of about 1.7 m^2 is obtained.

Knowing the power output of the propulsion system and the estimated wing area, the power curve of the fixed wing UAV can be constructed. The power available is assumed to be constant with respect to airspeed at low mach numbers for propeller aeroplanes, however the propeller efficiency has to be adjusted for a difference in density at a higher altitude of 3,500 m. The following relation is used for power available:

$$P_a = \eta_p P_{br}\left(\frac{\rho}{\rho_0}\right)^{0.75} \tag{6.5}$$

P_{br} is the shaft power of the engine that is used for propulsion only (as the use of a generator is a possibility and is taken into account using a safety factor).

The power required for a given airspeed is given by the following equations [40]:

$$P_r = DV \tag{6.6}$$

$$D = 0.5C_{D_0}\rho V^2 S + \frac{W^2}{\left(\pi Ae 0.5\rho V^2 S\right)} \tag{6.7}$$

The following figure is constructed. From fig. 6.3 the optimum speed to fly at for both endurance and range can be obtained: the optimum condition for endurance is when drag is minimum (thus P_r is minimum) and for range it is when $\frac{D}{V}$ is minimum. The latter corresponds to the intersection of P_r with its tangent drawn from the origin.

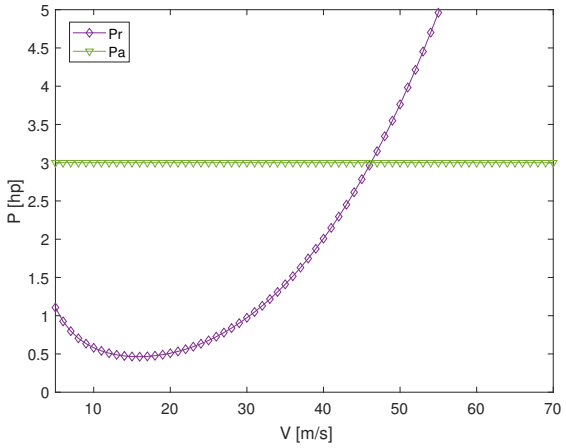

Figure 6.3: Power curve estimation of a small sized fixed wing UAV.

The endurance and range estimations are done using the Breguet equations [60].

$$E = \frac{\eta_p}{gV}\frac{1}{PSFC}\frac{L}{D}\ln\left(\frac{MTOW}{MTOW - W_f}\right)\frac{1}{3600} \tag{6.8}$$

$$R = \frac{V}{g}\frac{1}{TSFC}\frac{L}{D}\ln\left(\frac{MTOW}{MTOW - W_f}\right)\frac{1}{1000} \tag{6.9}$$

where W_f is the fuel used, $PSFC$ is the power specific fuel consumption and $TSFC$ is the power specific fuel consumption. For the fuel consumption an estimation has to be made, which will vary once an engine is selected, however if the same value is used for helicopter and fixed wing a comparison on performance can be made. The PSFC and TSFC are characteristic values for piston engines.

The lift over drag ratio is determined using a steady flight condition at that speed, using the wing surface area previously calculated and using the assumed C_L–C_D characteristics listed in table 6.10. It is obtained for the two optimum speeds corresponding to the optimum endurance and range conditions.

The resulting endurance and range estimations are then 13 h and 730 km. Also, the ROC can be obtained from the power curve using the maximum difference between power available and power required, and is about 10 m s^{-1}. If we assume that the maximum range condition will be used for cruise, than the cruise speed is estimated to be 27 m s^{-1}. The horsepower to be delivered by the engine to the propellers to obtain the required power available at an altitude of 3,500 m is estimated to be 6 HP. These values are used for the trade-off in subsection 6.2.7. The results obtained from this estimation are verified using [40] by inserting the same values to the method used.

6.2.6.2. Helicopter performance

Equations (6.10) to (6.13) [69] in addition with the general parameters and below are used to compute the power curve of the single rotor helicopter.

$$P_{\text{par}} = \sum (C_D S)_S \cdot \frac{1}{2} \cdot \rho \cdot V^3 \tag{6.10}$$

$$P_{\text{p+d}} = \sigma \cdot \frac{C_d}{8} \cdot \rho \cdot (\Omega \cdot \frac{1}{2} \cdot D^3) \cdot S \cdot (1 + 4.65 \cdot \mu^2) \tag{6.11}$$

$$P_{\text{i}} = k \cdot W \cdot V_i \cdot \sqrt{\frac{W}{2 \cdot \rho \cdot S}} \tag{6.12}$$

$$P_{\text{r,tot}} = \text{trc} \cdot (P_{\text{par}} + P_{\text{p+d}} + P_{\text{i}}) \tag{6.13}$$

Parameter	Value	Unit	
trc	1.1	[-]	[42]
P_{shaft}	6.5	[HP]	
η	0.91	[-]	[34]
D	1.8	[m]	
σ	0.027	[-]	[42]
$\overline{C_{D_p}}$	0.01	[-]	[42]
Ω	400	[rpm]	
$\sum (C_D S)_S$	0.0280	[m^2]	
k	1.15	[-]	[69]
$\frac{L}{D}$	4.5	[-]	[69]

The shaft power is determined for the case where requirement **REQ.U.SYS.7** is still met at take-off. Engine choices are made when the helicopter outperforms the aeroplane configuration. Figure 6.4 is generated from the given inputs.

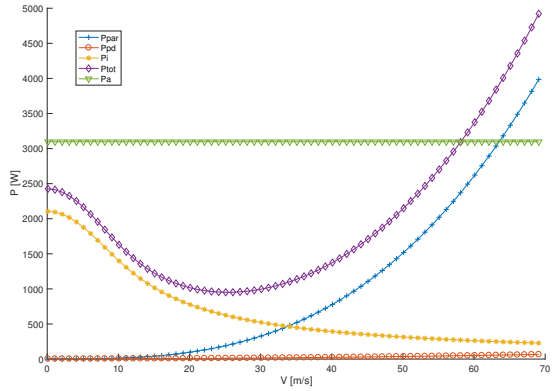

Figure 6.4: Power curve estimation of a helicopter.

Equations (6.8) and (6.9) are used to calculate the range and endurance. This is done by finding an equivalent $^{L}/_{D}$ ratio for helicopters at the maximum endurance and maximum range velocities. Prouty provides a graph in the book "Helicopter performance, stability, and control" relating velocity to a $^{L}/_{D}$ ratio [55].

6.2.7. Concept Trade-off

Table 6.12 shows the final trade-off between a helicopter and a fixed wing configuration, which was carried based on the criteria defined previously. As it can be seen, the payload is not taken into account as they payload subsystem is expected to be the same regardless of the configuration selected.

Table 6.12: Trade-off table between the helicopter and the fixed wing aeroplane.

	Endurance (2)[h]	Range (5)[km]	HP req. (4)[HP]	Cost (3)[€]	Manoeuvrability (1)[-]	Max. range speed (2)[$m\,s^{-1}$]	Stall speed (1)[$m\,s^{-1}$]	Total
Fixed wing	11	700	5.5	198,375		19	15	51
Helicopter	3.6	320	6.5	185,275		34	0	44

6.2.8. Financial Budget

This subsection is about the financial budget. This will be needed to evaluate the different concepts based on their costs, and to get a general overview on which subsystems are the most expensive. First, the different subsystems are evaluated on their costs, after which the total overview will be given.

The costs of the UAV can be subdivided into design, system payload and avionics, structure and the engine. The cost of each subsystem is described in table 6.13.

Table 6.13: Cost of each subsystem, and total cost of the payload and avionics.

	Cost [€]
Payload	24,000
Control sensing	23,500
Communication relay	18,500
OBC	3,000
Safety	125
Total	69,125

The total cost of the system payload remains the same for the three different concepts, which is €69,125 including contingency as described in the full payload overview table. The costs of the structure of the UAVs depend on two big factors: the cost of materials and the costs of manufacturing.

For the costs of materials, three materials were chosen to investigate further: carbon fibre, aluminium 2025-T6 and aluminium 7075-T6. These materials were chosen because these are some of the most used materials in aviation industry.

First, the material costs have to be determined, but the materials have different densities, costs and strengths. These parameters have to be taken into account when choosing a material and material cost, in order to get the cheapest and lightest design as possible. The material chosen will, however, not mean that only this material will be used, since this would limit the design too much. It is, however, a good estimation for the overall design.

For comparing the different materials, the SM, SS, cost SM (= $\frac{E}{[€/kg]}$), cost SS (= $\frac{\sigma}{[€/kg]}$), corrected (= divided by ρ) cost SM and corrected cost SS are used and tabulated in table 6.14. To determine the [$€/kg$], different products were taken from

stores and their price per kilo was averaged and taken as a reference. The products are taken for aluminium and carbon fibre preprag, fabric and layup.[31][32] After this, the parameters described before can be found in in table 6.14.

The specific modulus compares different material strengths based on their density. This means that for the same weight of material, the strength of a material can be compared. This method can also be applied to compare different materials for the same cost, and for the cost and weight, which are the cost specific modulus/strength and corrected cost specific modulus/strength.

Table 6.14: Parameters of materials.

	Carbon fibre	Aluminium 2025-T4	Aluminium 7075-T6
Density [10^3 GPa]	1.6	2.7	2.7
€/kg	220	27	27
Modulus of elasticity [Pa m^3 kg^{-1}]	142	73	71.7
Tensile strength [Pa m^3 kg^{-1}]	1.73	0.45	0.54
SM	88.8	27	26.6
SS	1.1	0.17	0.2
Cost SM	0.7	2.7	2.7
Cost SS	0.008	0.017	0.02
Corrected Cost SM	0.4	1.0	1.0
Corrected Cost SS	0.005	0.006	0.007

Table 6.15: The maximum material costs for different UAVs and materials.

	Carbon Fibre Materials [€]	Aluminium 2045-T4 [€]	Aluminium 7075-T6 [€]
Cost Conventional Single UAV	2600	320	320
Cost Conventional Multiple UAVs	2600	320	320
Cost Helicopter	2920	360	360

As can be seen from table 6.14, aluminium 7075-T6 has the best overall specific properties. If the UAV weight will be 25 kg, and the weight remaining from subtracting the weight of the known systems from this is the weight left for the structure of the UAV. If this weight is fully spent on the structure, the cost for the different materials will be as described in table 6.15. This will represent the maximum costs of the materials used for the UAV. Also, as can be seen in table 6.15, aluminium is the cheapest material by far if the whole weight would be used for the structure. This value, including a big reserve factor for manufacturing, is used for the procurement cost and is shown in table 6.16.

The total costs of the UAV, GS and the kite are described in table 6.16. The costs of the GS can differ for each concept because each require, for example, different recovery system are used for a conventional UAV and a helicopter.

Table 6.16: Total overview of costs for the different concepts.

Category	**Name**	**Single UAV Cost [€]**	**Multiple UAVs (n = 2) Cost [€]**	**Helicopter Cost [€]**
UAV	Design	-	-	-
	System payload	69,125	101,000	69,125
	Manufacturing	2,100	4,200	6,300
	Engine	20,000	40,000	24,500
	Subtotal	*91,225*	*182,450*	*99,925*
GS	Extra screen, case, batteries, etc	6,950	6,950	6,950
	Central computer	3,500	3,500	3,500
	Transceiver+antenna	9,000	9,000	9,000
	Generator	800	800	800
	Launcher	20,000	20,000	N/A
	Recovery	1,800	2,600	-
	Subtotal	*42,050*	*42,850*	*20,250*
Kite	Kite-Transceiver+antenna	8,100	8,100	8,100
	Kite	50,000	50,000	50,000
	Kite transponder	5,000	5,000	5,000
	Tether	2,000	2,000	2,000
	Subtotal	*65,100*	*65,100*	*65,100*
Total		**198,375**	**290,400**	**185,275**

6.3. Number of fixed wing UAVs

After the cost estimation of different concepts a reasonable conclusion can be drawn on the optimal number of UAVs deployed within the UAS. In general, the UAS can fully function and meet all requirements with only one UAV deployed. This follows also from the deployment of a pseudo-satellite discussed in chapter 12. The added value of adding more UAVs consists of two factors:

[31] https://alcobrametals.com/

[32] http://www.carbon-vertrieb.com/shop/

First of all, in case more than one UAV is used, the mission does not fail when a single UAV fails. When only one UAV is used, failure of that UAV will make the entire UAS non-operational, resulting in full mission failure. Even when the solely deployed UAV is repairable, during the reparation time the UAS will be non-operational and results in downtime. Also, when one UAV is on the ground to refuel, (an)other UAV(s) will still be in the air, able to respond to a manual commands or situation change momentarily. A second obvious advantage of deploying multiple UAVs is an increased mapping rate. Higher mapping rates make the UAS more valuable to SAR teams. The two disadvantages of multiple UAVs are the increased costs of the UAS and the decreased transportability because of increased system size and mass. This second disadvantage results in a limit of two UAVs, because 3 or more UAVs do not comply with **REQ.U.SYS.21**. Because of the advantages of deploying two UAVs and the limited cost increase of deploying a second UAV, it is decided to have two fixed wing UAVs deployed in the UAS. With this choice, the costs stay well within the limits defined in **REQ.O.SYS.10**.

6.4. Subsystem design

This section deals with design options for the fixed wing UAV. These are the aeroplane configuration, the propulsion, take-off and landing subsystems.

6.4.1. Aeroplane Configurations

A few options are plausible for the integrated fuselage and propeller placement. These are listed below.

A Single tractor propeller with single fuselage
B Single tractor propeller with twin booms
C Single pusher propeller with single fuselage
D Single pusher propeller with twin booms
E Two propellers with single fuselage
F Two propellers with twin booms

Configuration A has the disadvantage that the propeller is ineffective in the case that a net landing is used, [32]. The advantage is the clean air the propeller feels which gives a higher efficiency. A disadvantage is the interference with the payload that is mounted in the front. On top of this, a higher trim drag is assumed due to the moment caused by the heavy weight of the tractor propeller.

Configuration B has the same layout as configuration A, but with two booms instead of the tail section of the fuselage.

Configuration C has a pushing propeller at the back which does not interfere with the FOV. Additionally, there is no contamination of the payload. Wake impregnation, however, lowers the efficiency of the propeller and generates more noise. The weight of the propeller and the long fuselage at the back lead to an aft CG, [29].

Configuration D has a more forward CG compared to configuration C since the fuselage has partly been changed to rods as in configuration B.

Configuration E has two propellers placed either up front, at the back or on the wing. This results in a complex and challenging control and stability since there has to be accounted for single engine failure.

Configuration F is the same as configuration E, only with two rods like configuration B.

Fuselage layout and propulsion trade-off

This subsection discusses the trade-off between the six options mentioned above. To make a decision for the possible design of the location of the propeller and whether to use a single fuselage or a twin boom, there were some criteria that were determined, along with their weights to make the decision. The following are the trade-off criteria:
Mass (4) : Mass is an important parameter, as it would help determine how much lift is required. The lighter the structure, the better it will be for the design. As the two propellers will have two engines with them, the mass of configuration E and F would be the most, on the other hand, configuration A would be the lightest, as the propeller would be near the engine, and thus, a lot of mass will not occur.
Maintenance (1) : Maintenance means the ability to change the propulsion system easily. As during the mission, if there is a defect in the propulsion system, the ability to change the propulsion system would be very helpful. In this case, Configuration A and B are very good, as it is easy to change their propulsion system as they are independent of the entire system. In addition, for configuration D, as the engine would be with the propellers, it would be easy replacing it. On the other hand, for configuration C, It will be very hard, as the engine would be connected to the propeller with a shaft, which will be going through the tail.
Sensor field of regards (3) : Assuming that the payload and the cameras are placed up front, sensor field of regards is how the position of the propeller would affect the view. It can be noticed for the propellers in the nose (Configuration A and B), it is not very efficient, as the propellers would interfere with the images of the camera. However, for the other configurations, there will be no interference by the propellers in front of the camera.
Transportability (1) : As the UAV has to be moved around a lot depending on the disaster, therefore it is important to look at the transportability of the UAV for the configurations. While making the decision, it is initially assumed that the UAV would be a single piece and as a result no assembly is required. Also, the single fuselage design (configurations A, C and E) are easier to transport as these configurations will be shorter in design compared to the twin boom configurations (configuration B,D, and F0

Launch & recovery (3) : This criterion determines how the affected design would affect the possible launch and recovery system. The front propellers are not very effective for net landing, as the propellers would interfere with it. As a result (configurations A and B) are not affected. In addition, for configurations E and F, having the propellers on the wing may have no effect on the landing with the net. Lastly, having a propulsion on the back would mean that the fuselage would protect the net from the propeller and allow a safe landing.
Parts count / complexity (2) : Configuration A will have the least number of parts as it is a simple configuration. On the other hand, the two propeller configurations (configuration E and F) will be more complex due to the number of parts that are present in them. As a result, they will affect both the aerodynamic and structural complexity of the design.
Safety & Risk impact (3) : Safety and risk impact is how the placement of the propeller affects the payload in the fuselage. Assuming that the payload is in the front, having the propeller in the nose could affect the payload, if there is any leakage from the engine. Having the engine so close to the payload is a risk for the sensors and instruments [29].
Control & Stability (3) : This parameter is of importance as it has a direct effect on the location of the centre of gravity. Having the propeller in the nose results in a forward shift of the centre of gravity, which is desirable for a stable flight (configurations A and B). On the other hand, having the propeller in the back would mean that the centre of gravity would be shifted to the aft direction. Having a twin boom would help shift the aft propeller more towards the centre of gravity.
Based on these criteria table 6.17 was derived.

Table 6.17: Number of propellers and propeller location trade-off.

	Mass (4)	Maintenance (1)	Sensor field of regards (3)	Transportability (1)	Launch + Recovery (3)	Parts count/ complexity (2)	Safety + Risk impact (3)	Control & stability (3)	Total
A	3	3	1	3	1	3	1	3	42
B	2	3	1	2	1	2	1	3	35
C	2	1	3	3	3	2	2	1	43
D	2	3	3	2	3	2	2	2	47
E	1	2	3	3	2	1	3	2	41
F	1	2	3	2	2	1	3	2	40

6.4.2. Empennage

There are multiple configurations possible when it comes to the empennage. The H-tail configuration has the shape of an H and is connected by two booms. The H-tail also has two rudder surfaces. The π-tail is similar to the H-tail, but has the horizontal surface on top of the vertical tail. Lastly, the Δ-tail has an inverted V shape. This configuration cause the stability and control of the UAV to be relatively complex.

Table 6.18: Trade-off table for the empennage of the UAV.

	Mass (2)[-]	C&S (3)[-]	Aerodynamic characteristics (2)[-]	Failure/Stall Tolerance (3)[-]	Total
H-tail	2	3	2	3	26
π-tail	1	3	3	1	20
Δ-tail	3	2	3	2	24

6.4.3. Main Wing Planform

The planform of the aeroplane is also an important design parameter to trade-off. Firstly, elliptical wings have proven to be performs highly with respect to drag. However, their shape is complex and causes difficulties in manufacturing. Moreover, elliptical also have unfavourable stall characteristics which may jeopardise the success of the mission, [51]. Semi-elliptical wings, on the other hand, have similar drag performance as fully elliptical wings and have more favourable stall characteristics. These are also easier to manufacture than fully elliptical wings.

Rectangular wings are the simplest and cheapest wings to manufacture. However, they aerodynamically inefficient though w.r.t. drag compared to elliptical wings. Moreover, rectangular wings stall at the wing root, which is beneficial for controllability since control surfaces are at the wing tips.

Furthermore, tapered wings have better drag performance w.r.t. the rectangular wings but are worse compared to elliptical wings. The stall also initiates more towards the wingtips; too much taper yields unfavourable stall characteristics. Finally, tapered planforms are more complex than rectangular wings.

Back-swept wings are beneficial to high speed aircraft. Their aerodynamic characteristics are therefore not preferable for the UAV for this mission and will therefore not be considered in the trade-off.

Similarly to back-swept wings, front-swept wings show good drag performance at high speeds. However, front-swept wings do not show tip-stall problems at low speeds. Their design also inrease structural weight and complexity due to aeroelastic coupling between bending and torsion, [64].

Table 6.19: Trade-off table for the planform of the UAV.

	Drag performance(3)[-]	Stall behaviour(3)[-]	Complexity/Costs(1)[-]	Total
Elliptical	3	1	1	13
Semi-Elliptical	3	2	2	17
Rectangular	1	3	3	15
Tapered	2	3	2	17

The wing has been chosen to be mounted on top of the fuselage. This top-wing configuration presents stability advantages and also has an efficient span-wise lift distribution. This presents many advantages with respect to endurance. Additionally, the wing is less likely to get damaged during take-off or parachute landings. The downside of this configuration is the structural support needed to mount the wing which adds weight.

6.4.4. Aerofoil Selection

Different types of aerofoils have been investigated in a trade-off. These can be seen in table 6.20. For the aerofoils, it was chosen to trade off a cambered/semi-symmetrical, a reflex cambered, a symmetrical and a high thickness aerofoil. A cambered/semi-symmetrical aerofoil is an aerofoil that provides lift at zero AoA, whereas a symmetrical aerofoil does not. The reflex cambered aerofoil is an aerofoil that reflects back at the trailing edge and is typically used for flying wing configurations, e.g. a configuration without a tail. A high thickness aerofoil tends to have greater stability compared to the others.

Table 6.20: Trade-off table for the aerofoil of the UAV.

	Cruise speed (3)[-]	Maximum L/D (3)[-]	Maximum achievable lift (3)[-]	Stability (2)[-]	Stall characteristics(3)[-]	Total
Cambered/ Semi-symmetrical	3	3	2	2	2	34
Reflex camber	2	1	3	3	1	26
Symmetrical	2	2	1	2	2	25
High thickness	2	2	3	1	3	31

6.4.5. Propulsion Subsystem

A schematic of the propulsion system that will be used is shown in fig. 6.5. Several engines have been traded off based on weight, power, power per unit mass and efficiency as shown in table 6.21. The winner of the trade-off is the DA 150 EFI [33] which will be used for the final design. The engine will come with a 325 W generator.

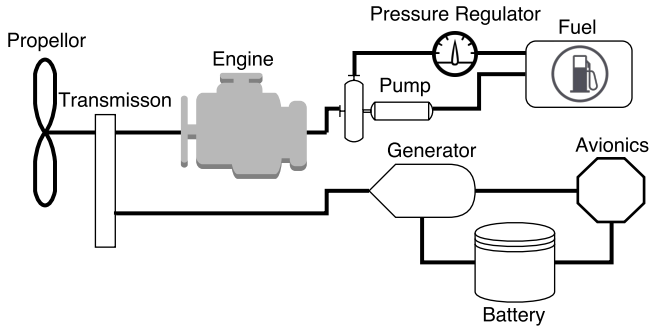

Figure 6.5: Propulsion system of the UAV.

Table 6.21: Trade-off table for the engine of the UAV.

	Mass (4)[kg]	HP (2)[HP]	$\frac{HP}{kg}$ (5)	Efficiency (2)[-]	Total
DA 150 EFI	1.6	13.3	8.313	0.82	39
Evolution engines 116 Gx 2	1.82	8.5	4.670	0.94	32
Graupner G 26	1.63	8.5	5.215	0.943	37
3W-55i CS	1.937	5.73	2.958	0.565	19
3W-75i CS	2.454	7.89	3.215	0.552	21
3W-212i B4 CS	5.72	21.19	3.705	0.596	24

6.4.6. Take-off Subsystem

Different solutions that were considered, such as: take-off from runway/road, from roof or van, throwing by hand and with the use of a catapult system.

[33] https://www.unmannedsystemssource.com/shop/propulsion/da150efi-uav-engine/

It is not realistic to use a runway or road due because of the unpredictable quality of the ground surface. Moreover, using the roof of a vehicle is not an option either. Often times, SAR teams rely on volunteers and arrive only with their equipment. It cannot be ensured that the team will have access to a suitable car to launch the UAV. Furthermore, throwing by hand cannot happen due to the high weight UAV of 25 kg. Therefore the only viable option that is left is the catapult launch. This catapult launch is reflected in requirement **REQ.U.SYS.12**. This requirement gives a maximum take-off distance ensuring the flexibility of the launch and having a limit on the length of the catapult.

6.4.7. Landing Subsystem

Among the different possible landing methods, the options considered were parachute landings, conventional runway landings, vertical landings and skyhook landings. Requirement **REQ.U.SYS.13** limits the landing distance to 2 m and discards runway landings immediately. The trade-off for the landing subsystem is summaried in table 6.22.

The skyhook (developed by Boeing [34] for example) has the disadvantage of being extremely costly and large in volume. It is therefore not viable for this mission.

Net landings are a proven concept that cost little. On top of this, inflatable poles can be used to limit the size of the sub-system.[35] However, it may difficult to comply with the requirements **REQ.G.SYS.5** and **REQ.U.SYS.21**. It should therefore be easily disassembled and stored to optimise the use of space in the van.

Finally, parachute landings are an option which may be used at all times. The disadvantages are that no particular landing position can be achieved and that it adds weight to the UAV. Furthermore, in wind conditions over 10 m s^{-1} there is a high chance of dragging the UAV over the ground when landed.

Table 6.22: Trade-off table for the landing system of the UAV.

	Costs (3)[-]	Ease of use (2)[-]	Mass (4)[-]	Safety (5)[-]	Size (3)[-]	Off the shelf (2)[-]	Total
Skyhook	1	2	1	2	1	3	30
Net	3	3	3	2	2	2	47
Parachute	3	3	2	3	3	3	53

In conclusion, taking table 6.22 into account and considering all the pros and cons, it was chosen to opt for a net landing with a parachute on-board for emergencies and as redundancy.

6.4.8. Mass Budget

Former trade-offs have lead to different UAV subsystems. A final mass budget is now derived including each subsystem. Structural and fuel mass is taken into account, based on a preliminary estimations. Structural mass specifically includes the masses of the wing, the fuselage, the tail and the twin booms. Moreover, the fuel system includes fuel, the fuel-tank and its peripherals. The mass budget is shown in table 6.23.

Table 6.23: Mass budget of the UAV.

Group	Component	Mass [kg]
Structural	(Detailed design phase)	10
Propulsion System	Engine	1.6
	Generator	3.3
	Propeller	0.20
	Batteries	0.05
Fuel System	(Detailed design phase)	4
Mapping Payload	RGB	0.36
	IR	0.15
	LIDAR	0.56
	Gimbal	0.15
Communication Payload	Tranceiver	0.12
	Antenna	0.50
Control Sensing	Radar	0.05
	GPS/IMU	0.18
	Pitot Tube	0.16
OBC	Processors	0.10
	Breakout boards	0.20
	Storages	0.04
	Thermal management units	0.40
	Micro Controllers	0.05
Safety	Lights	0.2
Total	Excluding Contingencies	22.37
	Including Contingencies	25

[34] http://www.boeing.com/history/products/scaneagle-unmanned-aerial-vehicle.page
[35] https://www.youtube.com/watch?v=bnFJDUgfsPE&feature=youtu.be&t=1m46s

6.5. Ground station subsystem design

The GS is used to monitor data flux and to control the UAV in emergency situations. According to **REQ.U.SYS.6** it has to communicate over 50 km with the UAV. According to **REQ.O.SYS.1** it needs to have an open communication relay of 72 h. It should be portable and easy to use.

Requirement **REQ.U.SYS.6** poses the hardest challenge since the altitude the UAV flies at poses problems for the line of sight (LOS). A lot of characteristics determine the range of quality of transmission. One of them is the placement of the antenna. This is shown in fig. 6.6. Several options are explained below.

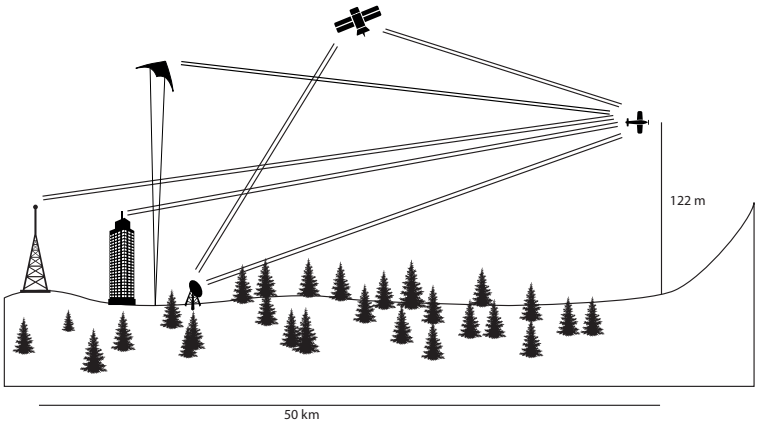

Figure 6.6: Ground station communication scheme concept.

A telecommunication tower or tall building provides direct line of sight, but is unreliable because it is unsure whether tall buildings have survived natural disasters. A directional antenna in the ground is possible to provide a high range. It has the disadvantage not to be able to communicate with multiple UAVs. Calculations show that at 50 km range, the angle of the directional antenna should be 1.4°. This interferes with too many obstacles. A pseudo-satellite can be launched everywhere and does not interfere with obstacles. Using a satellite as a relay provides long communication but the frequency range that can be used is limited and it comes with at an expensive price. Furthermore, new channels may occupy these satellites for news feed. Table 6.24 depicts the trade-off for the antenna placement used for the GS. It was chosen to go for a pseudo-satellite.

Table 6.24: Trade-off table for antenna placement.

	Range (4)[-]	Reliability (4)[-]	Cost effectiveness (3)[-]	Total
Tall buildings	3	1	5	21
Directional Antenna	3	3	3	22
Pseudo-satellite	4	5	4	33
Satellite	5	3	1	23

Two regulations are particularly important for the use of a pseudo-satellite. The operational height of a kite differs among the globe. If a higher altitude is required, licenses have to be obtained and air traffic control needs to be aware of it. SAR teams have an operational service ceiling of 300 m.[36] Moreover, the visibility of the tether at higher operational height becomes more and more vital. Above 30 m the tether needs to equipped with an obstacle avoidance light every 15 m.

Three different kites have been explored and the trade-off is shown in table 6.25. All kites are stable in high wind conditions and are set up fast. A magnus kite is a proven concept as it is used by a Portuguese company called Omnidea.[37] It is a very stable configuration at low wind speeds but it is hard to control at high wind speeds. A fixed drone stabilises itself continuously but is heavy and takes time to deploy.[38] A sled kite is transportable and is able to withstand high wind speeds. It is self stabilising, hence does not require control devices. It was chosen to go for the sled kite. *However, later on in this report, it was found that a sled kite does not perform well in zero wind conditions or very strong wind conditions. This is discussed in further detail in subsection 12.3.3.*

Table 6.25: Trade-off table for the kite.

	Stability (5)[-]	Weight (3)[-]	Fast deployment (4)[-]	Wind speed range (4)[-]	Cost (2)[-]	Total
Magnus kite	3	2	2	3	3	47
Fixed drone	5	2	1	5	1	57
Sled kite	5	5	4	3	3	74

[36] https://info.publicintelligence.net/FAA-DisasterAirspaceManagement.pdf
[37] http://omnidea.net
[38] http://www.skypoint-e.com/multicopter/

Several sub-components were selected for the pseudo-satelitte. Such as a transponder that is needed to warn other aircraft near of its location. A transceiver that is needed to transmit information to and from the UAV. Tether cables need to be designed to attach the pseudo-satellite to the ground. Wind is used as power source to generate energy for the battery. *However, in the final report it was found that this form of providing energy does not suffice (subsection 12.3.2)*. The possible antennas that can be used are the omni or the directional antennas or a combination of both. Two specialised antennas using the diversity system will be used. One of the antenna will have a higher gain to transmit over a longer distance and the other will have a conical radiation pattern pointing downwards to pick up SAR teams and also the UAV at close range. These will be designed using CST Studio Suite in the detailed design phase.

Central computer: Regarding the central computer that can be used, it would have to be able to withstand rough conditions, work for a long period of time to complete the mission cycle. The requirement for the laptop is to have a processor that clock speeds up to 2 GHz, have a RAM of at least 8GB to run multiple operations at the same time and storage of 512GB (36 hours of data, data should be transferred to an external drive for later analysis). After looking at some laptops, there were certain options that could be considered. The Panasonic Toughbook CF-31, GETAC B300G6 and Dell latitude C640. The Panasonic Toughbook CF-31 will be used for this system since it also has a dedicated graphics card which is needed for analysing the large mapping data.

Controller: A controller is needed in order to control the UAV in case where the control is switched to manual from autonomous. The controller that will used is a flight simulator controller for precision controls. An FPV interface is going to be coupled with this in order to translate the controls to the transmitter. The choice of controllers that is available are Thrustmaster Hotas Warthog, Saitek Pro X-56 rhino and X-Gyro 1500. The first two choices give six degrees of freedom. Out of these the Thrustmaster is taken for the design since it is more rugged and has more freedom in reconfiguring its buttons.[39]

Transceiver: To be able to send the data from the ground station to the pseudo-satellite, it would have to communicate in a certain frequency. And the information is send through a combination of transceiver and an antenna. The transceiver for this link can be less powerful than the ones used in the kite and the UAV. For this reason the ground link transceiver from uavfactory is used instead of the streamcaster series from Silvus technologies.

Antenna: The ground station needs an antenna to be able to transmit the information from the monitoring centre to either to the pseudo-satellite. The antenna should have a conical radiation pattern since it only has to communicate with the kite. A mono pole antenna from Cobham technologies is used for this purpose.

Generator: Depending on the power needed by all the components, a generator is needed to keep the monitoring station functioning for 72 hours. The generator has to be portable though. The generator is an optional portion as the search and rescue team might provide the possible generator for the operation. A 5 kW generator is enough to keep the ground station functioning.

[39] `http://www.thrustmaster.com/products/hotas-warthog`

Chapter 7: Aerodynamics

Chapter 7 will start by the main wing design in section 7.1. It will be followed by the design of the tail in section 7.2. The fuselage will be designed in section 7.3 and the propeller design will be given in section 7.5. The optimisation of the lay-out is documented in section 7.6 and verification and validation of the programmes and codes used can be read in section 7.8.

7.1. Wing design

This section will elaborate on the wing design. The aerofoil selection is documented in subsection 7.1.1 and the 3D wing planform will be given in subsection 7.1.2. A sensitivity analysis is given in subsection 7.7.1.

7.1.1. Aerofoil selection

The aerofoil selection is based on the application of XFOIL in MATLAB. Modifying the application resulted in a model to run multiple aerofoils in a sequence. As a first choice, it was chosen to go for a thick, cambered, semi-symmetrical aerofoil. This was chosen in subsection 6.4.3. Twenty-two aerofoils have been selected that comply with the aerofoil selection mentioned above. For legibility, the polar graphs of twelve of these aerofoils are shown in fig. 7.1a, fig. 7.1b, fig. 7.2a and fig. 7.2b. Table 7.1 shows the list of the twenty-two aerofoils that have been investigated.

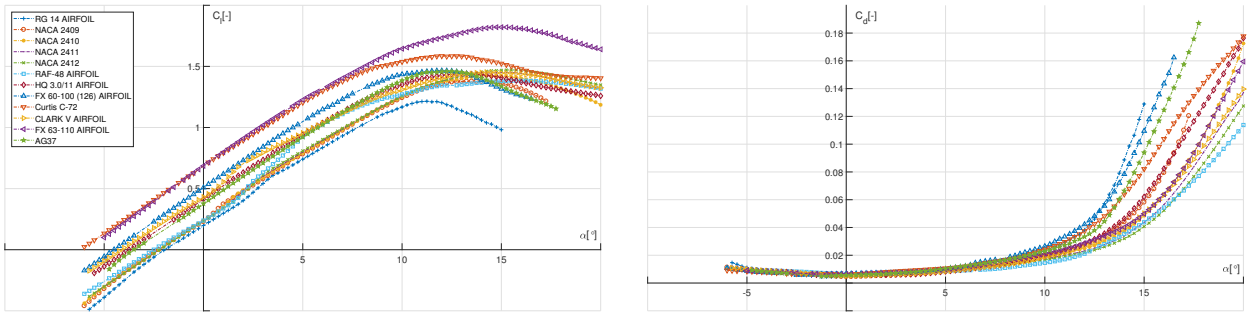

(a) C_l-α-graphs for different aerofoils.

(b) C_d-α-graphs for different aerofoils.

Figure 7.1: Lift- and drag polars for different aerofoils at Re = 800,000 and M = 0.12.

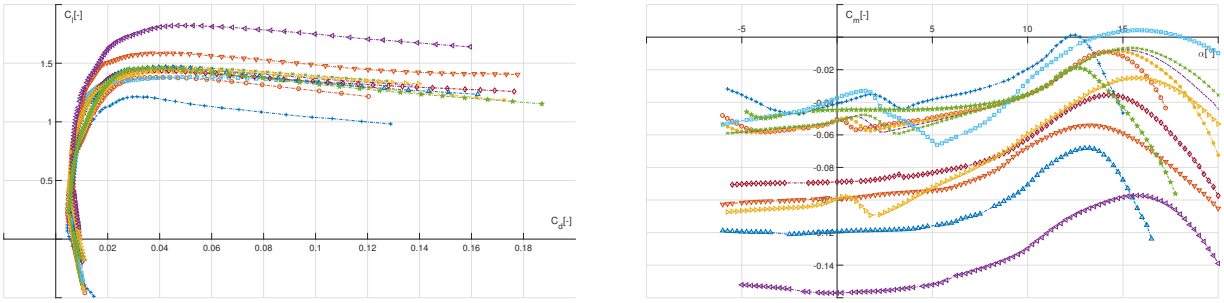

(a) C_d-C_l-graphs for different aerofoils.

(b) C_m-α-graphs for different aerofoils.

Figure 7.2: Lift-drag polars and moment diagrams for different aerofoils at Re = 800,000 and M = 0.12.

Figure 7.1a shows that all aerofoils roughly have the same C_{l_α}. This value was calculated to be 0.105. It was chosen to go for the Wortmann FX 63-110 aerofoil due to its high lift coefficient at high AoA. This aerofoil is depicted in fig. 7.4a. At zero AoA the FX 63-110 aerofoil has a 2D lift coefficient of 0.686. Taking a look at fig. 7.1b, it can be concluded that the aerofoil FX 63-110 scores reasonable in comparison to the other aerofoils. In cruise flight, which means flying at low angles of attack, it can be seen in fig. 7.1b that the drag for all chosen aerofoils is considered the same.

Figure 7.2a displays the lift to drag polar. It shows that for low drag the aerofoils are close to each other. However, for higher drag, the aerofoil FX 63-110 is able to provide more lift. Also, at cruise, with low drag. The FX 63-110 aerofoil has higher lift (it is displayed more to the top-left corner).

The high camber in the nose makes the aerofoil suitable for the low Reynolds number range that suits the FASAR mission. [56] It comes at a price since having the C_{m_α} being slightly positive as shown in fig. 7.2b, which means that it is a slightly unstable aerofoil in the positive AoA-range. The tail design will be designed in such a way that it counteracts the positive C_{m_α} of the wing.

7.1.2. Wing planform

A semi-elliptical wing planform was chosen for this mission. For the design of the main wing XFLR5 V6.38 was used. The main advantage of the semi-elliptical wing is the elliptical lift distribution which generates a minimal amount of induced drag. The dimensions of the wing planform are optimised with respect to chord and wingspan. This was done taking the tail size, structures and control and stability into account. For the dimensions of the wing the reader is referred to table 7.2. For the wing planform it was chosen not to choose for wingtips. Although a significant difference was shown in XFLR5 V6.38, the choice for no wingtips was primarily based on the hazards that came along for the structures department. The C_L - α curves of the configuration with wingtips or without wingtips were roughly the same whilst looking at the C_D-α curves, only a small decrease in drag was seen.

Table 7.1: Aerofoils selected for the main wing aerofoil.

Aerofoils			
RG 14	USA 48	S2027	FX 63-110
RAF-48	HQ3.0/11	GEMINI	FX 60-100
EPPLER E853	EPPLER 67	Curtis C-72	CLARK V
S40222	AG37	NACA 2408	NACA 2409
NACA 2410	NACA 2411	NACA 2412	NACA2413
NACA 2414	NACA2415		

Table 7.2: Final geometry values of the main wing.

Variable		Unit
Aerofoil	Wortmann FX 63-110	
c_r	0.408	[m]
S	0.777	[m^2]
e	0.9	[-]
A	7.56	[-]
b	2.423	[m]

In fig. 7.3a the main wing design can be seen. Flaps and ailerons have been designed and are more elaborated in chapter 8. The design for rolling can be seen in fig. 7.3b and the design with flaps and ailerons is depicted in fig. 7.3c.

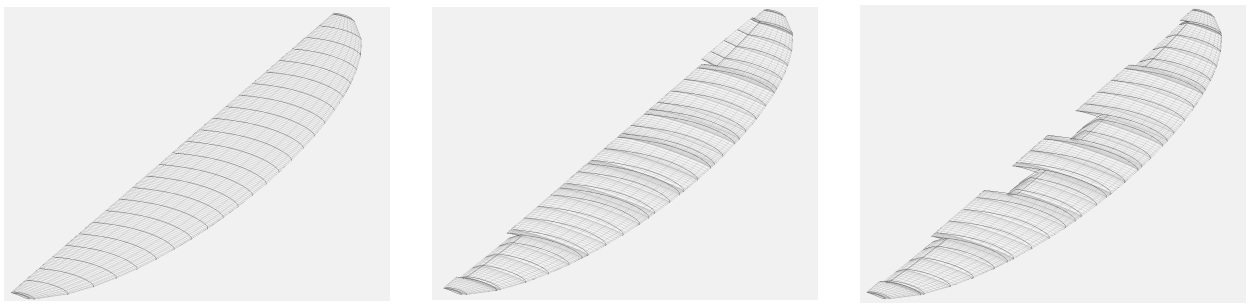

(a) Main wing planform in cruise configuration.

(b) Main wing planform in roll configuration,

(c) Main wing planform in stall configuration.

Figure 7.3: Different planform configurations at c_r = 0.408m, b = 2.423m, S = 0.777 m^2, AR = 7.56 and MAC = 0.347m.

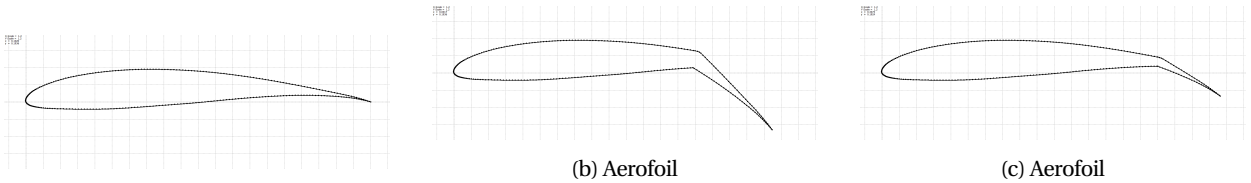

(a) Aerofoil: FX 63-110

(b) Aerofoil flaps: FX 63-110 bent at 70% chord, 35 °.

(c) Aerofoil aileron: FX 63-110 bent at 80% chord, 20 °.

Figure 7.4: Aerofoil FX 63-110 depicted in cruise configuration and shown with flaps and ailerons.

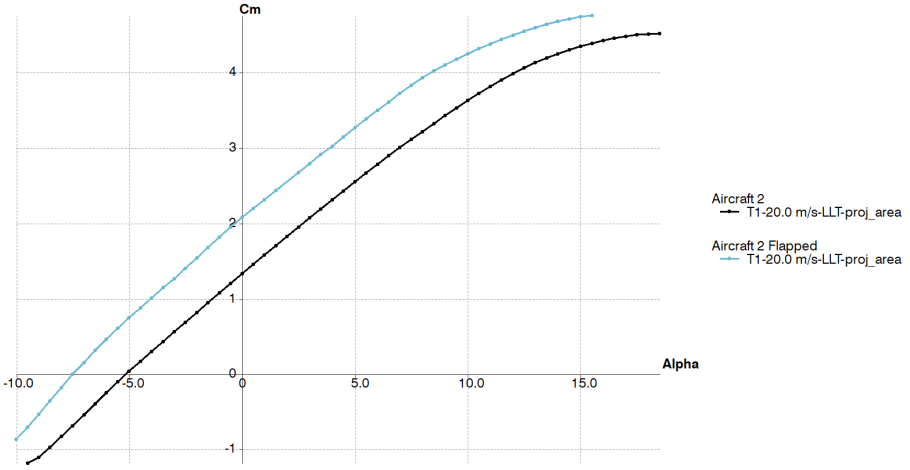

Figure 7.5: C_L - α curves with and without flaps and aileron deflected. Measured at 20 m s^{-1}, Re = 600,000.

7.2. Tail design

The tail is an important aspect for the stability and control and contributes to the aerodynamics of the aircraft. For the tail, the dimensions are determined, also the aerofoil used for the tail. The chosen horizontal tail configuration is the U-tail, using twin booms. In this section, the two vertical tail and the horizontal tail are designed for the certain configuration. To determine the geometry of the tail along the distance from the quarter chord to the tail, it is sized according to the horizontal and vertical tail volume coefficient [26].

7.2.1. Aerofoil selection

The aerofoil selection of the horizontal and vertical tail is done by using XFOIL in MATLAB. First, different aerofoils are chosen to do the evaluation on with XFOIL. A high C_{l_α} is desired for the horizontal tail and a low pitch moment is preferred. Taking this into account symmetric aerofoils are considered as they behave the same in both positive and negative angles of attack and the pitching moment is zero at zero angle of attack. The NACA0009, NACA0010, NACA0011, NACA0012, NACA63-012, NACA63-015, NACA63-018, NACA64-012 and NACA66-018 [62] are commonly used for tail sections and therefore analysed. The result of this analysis is shown in fig. 7.6. The different behaviours of the aerofoil can be observed in the graphs, and the gradients were analysed for these graphs. An aerofoil is chosen by looking at the required characteristics, which are high $C_L - \alpha$, low $C_D - \alpha$ and a wide range of $C_L - C_D$. [26]

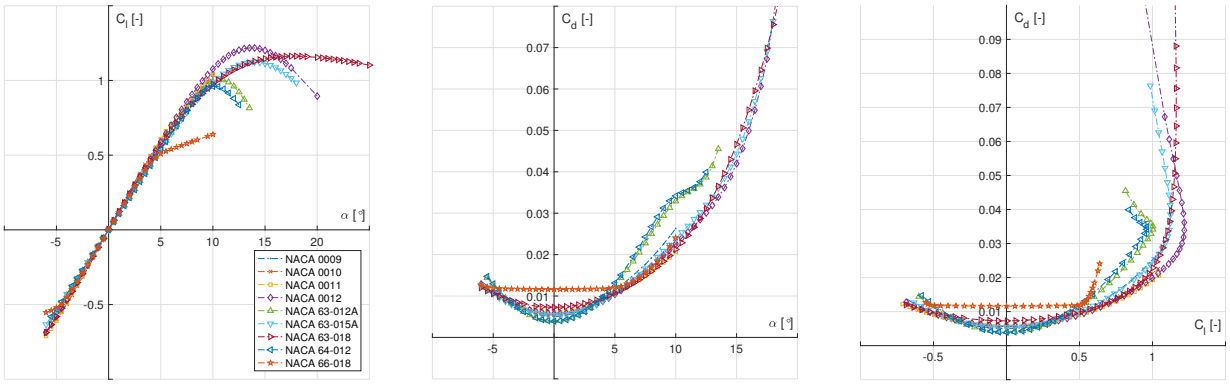

(a) C_L-α-graphs for different tail aerofoils (b) C_D-α-graphs for different tail aerofoils (c) C_D-C_L-graphs for different tail aerofoils

Figure 7.6: Polar graphs for tail aerofoils at Re = 500,000, M = 0.12.

Right before stall conditions of the wing the tail needs to operate at a C_l value of 0.951 (sea level) to counteract the moment still generated by the lift of the wing. It could be seen in the graphs that the NACA 63-018 performed very well in all these conditions. In order to have sufficient room for recovery after stall the NACA 63-018 aerofoil is chosen for the horizontal tail. This aerofoil has only a slight decrease of C_l after stall with also a high stall angle. Also, for the same reason, the aerofoil is chosen for the vertical tail too.

7.2.2. Tail planform

According to method three described in "General aviation aircraft design: Applied Methods and Procedures"[26] the tail is sized with an input of the horizontal- and vertical tail volume coefficient. This method is the initial tail sizing of the horizontal- and vertical tail simultaneously. This method is used because both tails have their centres of lift approximately at the same longitudinal position. The desired tail arm of 1.5 m is evaluated, from which the sizing was done. Once this tail arm was determined, the required area, span and average chord for the horizontal tail and the vertical tail is computed for with the method mentioned before. [26] The results are presented in table 7.3.

Table 7.3: Final geometry values of both the horizontal and vertical tail.

	Horizontal tail	Vertical tail (one)
Aerofoil	NACA 63-018	NACA 63-018
Span width [m]	0.7	0.11
Chord width [m]	0.194	0.194
Surface area [m^2]	0.136	0.043
A [-]	3.608	0.568

Table 7.4: Dimensions for the fuselage.

Parameter	Dimensions [mm]
Nose length	300
Total length	1,372
Height	200
Front width of fuselage	200
Aft width of fuselage	165

7.3. Fuselage design

The fuselage is needed to store the required payloads for the UAV and also to protect the payload from external factors. It is decided that the wing will be on the top of the UAV (see subsection 6.4.3), as a result, the fuselage will support the weight of the wing. Also, the fuselage is required to be able to carry the engine. After the placement of the payload is established as it can be seen in subsection 11.10.1, the cross sectional dimensions are determined. As the UAV is not flying at high altitudes, the inside of the UAV does not have to be pressurised. Thus, considering aerodynamic properties of several shapes, the final shape of the cross section is determined. The shapes considered for the cross sectional of the fuselage are the elliptical, rectangular, flat-sided with semi-circular top and bottom or a rhomboid shape, as it can be seen in fig. 7.7a[13]. An elliptical cross section is chosen because in small angles of attack and in side slip, the flow will not separate. As a non-pressurised fuselage is being used, the pressure loads will not be considered. Using an elliptical shape may not be very efficient for space utilisation. However, as the fuselage is going to be long due to the centre of gravity consideration, the space wouldn't be an issue. The sizing of the fuselage is done while considering the payload placement and that helped to determine the dimensions of the fuselage that needs to be used. When designing the fuselage, it is ensured that the fuselage should be as streamlined as possible. And as a result, a converging fuselage body is chosen: the shape which resembles a tadpole. The reason to choose the tadpole fuselage is that it does not generate a lot of drag: the front part of the fuselage is shaped in such a way that it is able to sustain a laminar boundary layer. This shape would produce pressure gradients that are favourable for the UAV. [26]

Furthermore, the design of the nose of the fuselage was considered too. There are several type of nose shapes that are possible for the UAV, and it can be seen in fig. 7.7b. [13]

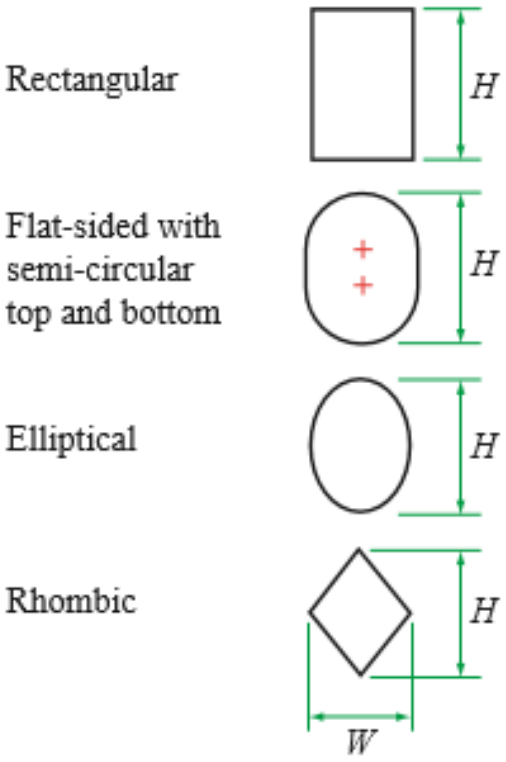

(a) Various options for the fuselage shape.

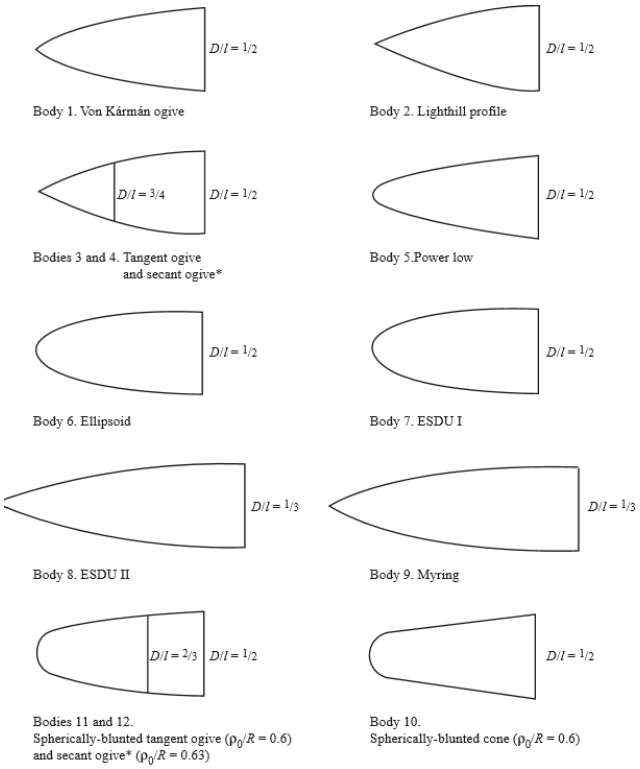

(b) Various options for nose design.

Figure 7.7: Possible options used for the fuselage and the nose.

Initially, a blunt nose is chosen instead of a pointed nose because the pointed nose produces flow separation, turbulence and drag. A rounded nose acts better in this scenario. After analysing experiments done on these nose shapes, it was seen that the ellipsoid nose would produce less drag than the other configurations. [47] Also, looking at reference values, the fineness ratio (Diameter/length) is chosen to be 0.5. [19] Thus the final dimensions, considering the payload placement and the aerodynamics, taken for the fuselage are table 7.4.

7.4. Drag calculation

A proper understanding of drag is needed for the designer. The drag calculations help to provide information about the required propeller needed for the UAV to be able to operate, and also about the performance of the UAV. The drag of the body in subsonic flight can be divided according to eq. (7.1). [26]

$$C_D = C_{D_0} + C_{D_f} + C_{D_i} + C_{D_w} + C_{D_{misc}} \tag{7.1}$$

Where, C_D is the total drag coefficient, C_{D_0} is the basic drag coifficient (pressure drag), C_{D_f} is the skin friction drag coifficient, C_{D_w} is the wave drag and $C_{D_{misc}}$ is the miscellaneous or additive drag.

For low subsonic UAV, it is possible to omit the wave drag. While making the calculations, the C_{D_0}, C_{D_f} and $C_{D_{misc}}$ are lumped together to the minimum drag coefficient or $C_{D_{min}}$. To analyse the drag characteristics of the UAV as a whole, the component drag build-up method is used. In the method, the flat plate skin friction is considered on the wetted area of the aeroplane. Also, it is considered that the entire UAV is under turbulent flow, as it assumes the worst case scenario for the UAV. To make the drag calculations, the body was initially divided into the fuselage, the wing, the horizontal tail, and the vertical tail, as they are in contact with air. The skin friction of these components was calculated and slightly modified using the form factor (FF) and the interference factor (IF). The form factor is the measure to determine the pressure drag due to viscous separation. The interference factor is the effect of the other components on each other. In addition, the drag of the antennas and the external payload is found. All these values are added and multiplied with a CRUD (Cumulative result of undesirable drag) value. This factor accounts for the contributions which are not possible to be analysed analytically, such as dents, small vents and outlets surface panel alignment. A factor of 25% is chosen for this purpose. [26] The final value that is obtained after this gives the minimum drag coefficient. To calculate the lift induced drag coefficient, a simplified $K \cdot {C_L}^2$ method is used. Thus, to calculate the value of the induced lift drag coefficient eq. (7.2) is used, where e is calculated by XFLR5 to be 0.9.

$$C_{D_i} = \frac{{C_L}^2}{\pi \cdot AR \cdot e} \tag{7.2}$$

Adding the $C_{D_{min}}$ along with the C_{D_i} will give the total drag coefficient which will be used in the calculations. An overview of the entire method can be seen in fig. 7.8. [26]

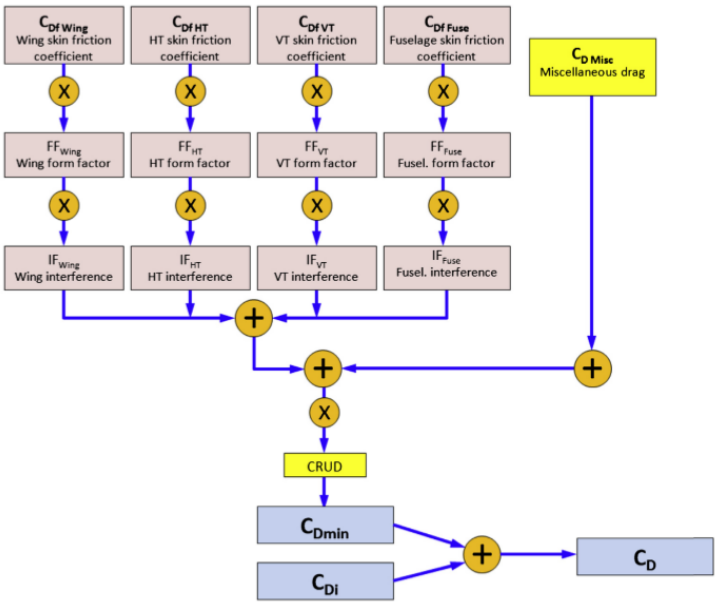

Figure 7.8: Method for calculating the drag coefficient.

Using this calculation, different drag force is calculated for different conditions, to account for each for the propeller design as seen in fig. 7.8.

From table 7.5, it can be noticed that the drag force would be the highest for the take-off configuration at it's cruise velocity for both the sea level and at 3500 m. and the drag forces would be the lowest during cruise. Thus, the thrust will need to be designed for these values.

Table 7.5: Drag force for difference scenarios.

Sea-Level		
Conditions	Velocity [m/s]	Drag [N]
Take-off	21	32.987
	33.8	83.732
Cruise	33.8	25.720
Landing	23.4	40.763
At 3500 m		
Take-off	21	23.547
	40.2	83.849
Cruise	40.2	26.022
Landing	23.4	29.091

Using this method, the drag versus the velocity calculations are done too to analyse the performance of the UAV, and to find out the minimum drag force present at a specific velocity, and can be seen in fig. 7.9.

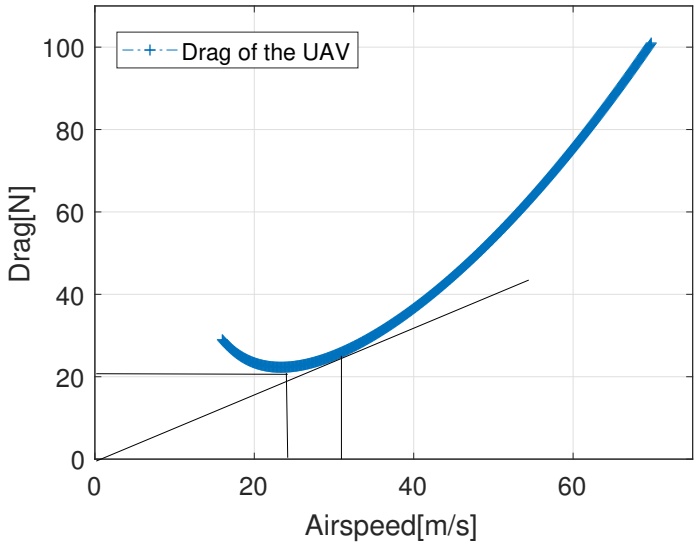

Figure 7.9: Drag force with the velocity.

From fig. 7.9, It can be seen that the minimum drag is at 23.3 m/s, and it has a drag of 22.3 N then. This value is used to calculate the endurance of the UAV.

7.5. Propeller blade design

In this section there will be elaborated on the propeller design. First, the Aerofoil is selected to have optimal lift and drag characteristics. Second, the design process to end up with a complete propeller blade and the geometry is shown. Third, a sensitivity analysis is performed on four design parameters, to find out what difference it makes to change the specific parameter.

7.5.1. Aerofoil selection

The aerofoil selection of the propeller blade is done by using XFOIL in MATLAB. First different aerofoils are chosen to do the evaluation on with XFOIL. The NACA6412, NACA4412, CLARK Y and ARA-D 10% [15, 61] are commonly used for propeller blades and therefore analysed. The result of this analysis is shown in fig. 7.10.

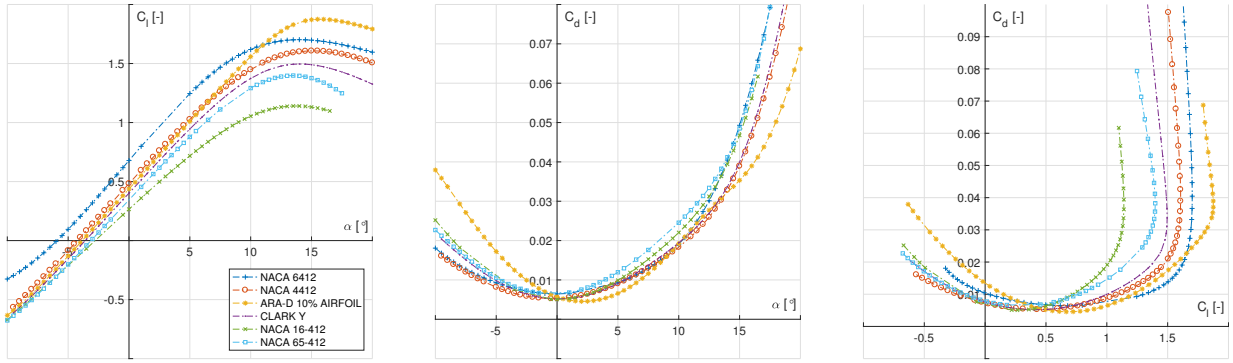

(a) C_L-α-graphs for different aerofoils (b) C_D-α-graphs for different aerofoils (c) C_D-C_L-graphs for different aerofoils

Figure 7.10: Polar graphs for propeller aerofoils at Re = 1,000,000, M = 0.12.

As for propellers a high range of C_l is beneficial at a low drag coefficient. A high $C_{l_{max}}$ at high angle of attack is an advantage in unexpected circumstances (e.g. high crosswinds). As in which the angle of attack of the blades increases and consequently the lift coefficient increases as well. Therefore, according to these criteria, the ARA-D 10% aerofoil (see fig. 7.11) is chosen as the most optimal one.

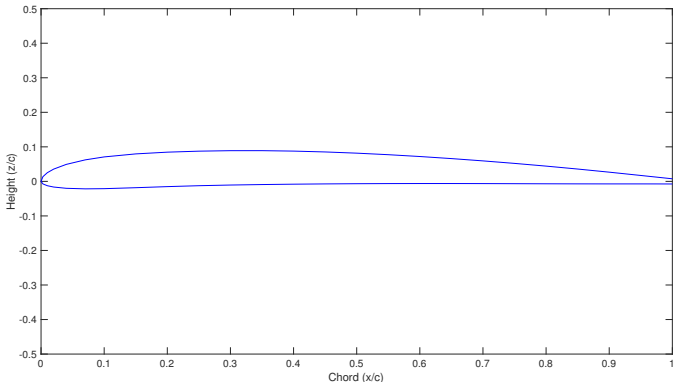

Figure 7.11: Propeller blade aerofoil choice.

7.5.2. Propeller blade geometry

With XROTOR, a blade geometry is designed for minimum induced losses. XROTOR uses the classical blade-element and vortex formulation [16]. Betz [7], Goldstein [24], and Theodorsen [65] formulated this method first and Larrabee reformulated the method later on [41]. The specific mission operating conditions are used as input and selected as follows. First, the flight speed is determined, by calculating the speed at maximum range. This will be used in the biggest part of the mission and therefore, the propeller is optimised for flying at that speed. Second, to design for a specific required thrust, the drag of the whole UAV is determined (see section 7.4). Setting the thrust equal to the drag gives the required thrust for which the propeller needs to be designed for. Third, a larger diameter makes the propeller more efficient [23]. Only the size is constraint by the ground clearance and the boom separation and therefore set at 0.6 m. Fourth, the C_l at maximum C_l/C_d is obtained from XFOIL. This is the most desired C_l to operate each blade section on. Therefore, each blade section is optimised for minimum induced losses at a C_l of 0.84. Furthermore, the number of blades, hub diameter and rotor rotational velocity (within boundaries of the engine) are iterated to find the lowest power required to operate the propeller.

After checking the geometry the tip chord appeared to be 0.0035 m, which according to Tracy [66] not possible to manufacture. The chord has to be at least 0.0060 m. Therefore, the last 9 sections of the geometry are modified to meet the tip chord requirement and have the least efficiency and required power difference. A few different tapers towards the tip are iterated with the final geometry presented in table 7.6. For this final geometry the optimal pitch angles are recalculated.

Table 7.6: Changes in tip geometry for manufacturing accommodation.

	Previous profile		Modified profile	
	η_p = 0.8311	$P_{r_{tot}}$ = 1.03 [kW]	η_p = 0.8086	$P_{r_{tot}}$ = 1.087 [kW]
R [m]	c [m]	β [°]	c [m]	β [°]
0.2895	0.0140	29.90	0.0150	25.82
0.2919	0.0130	29.74	0.0130	25.65
0.2940	0.0110	29.60	0.0110	25.51
0.2955	0.0095	29.48	0.0097	25.39
0.2970	0.0080	29.38	0.0084	25.29
0.2982	0.0065	29.30	0.0069	25.21
0.2991	0.0051	29.24	0.0063	25.15
0.2997	0.0041	29.20	0.0060	25.11
0.3000	0.0035	29.18	0.0060	25.09

With this modified geometry the final values are shown in table 7.7 for three blade sections.

Table 7.7: Final geometry of the chord and pitch angle of three blade sections.

	c [m]	β [°]
Root (hub)	0.062	72.83
0.5 · R	0.050	35.68
Tip	0.006	25.09

After all the blades are tested for different cases: take-off configuration at launch speed, take-off configuration at cruise speed (e.g. the flap actuators do not work), cruise configuration at cruise speed and the landing configuration at landing speed. The landing configuration is just before hitting the net. After the first touch, the engine is shut down. Mean sea level appeared to be the most limiting and therefore, table 7.8 presents operation conditions at sea level. The engine has a rotational velocity range of 1800 RPM to 6500 RPM and a maximum power available of 8.6678 kW. This means that the engine is able to provide the necessary power and rotational velocity ranges.

Table 7.8: Operation Conditions to Compensate Drag at MSL.

	V [m s^{-1}]	D = T [N]	Ω_{RPM} [RPM]	η_p	$P_{r_{tot}}$ [kW]
Take-off	21.0	32.99	2,724	0.6183	1.1205
Take-off	33.8	83.73	4,290	0.6730	4.2049
Cruise	33.8	25.72	3,000	0.8086	1.0873
Landing	23.4	40.76	3,021	0.6328	1.5072

7.6. Configuration optimisation

The configuration of the main wing and tail wing have been optimised with respect to the moment coefficient. This moment coefficient is calculated around the centre of gravity of the complete structure. The fuel tank is placed exactly on top of this centre. Therefore the most forward and aft centre of gravity position is at the same location. In cruise mode it is aimed for to reach the highest range. This means it is aimed for the highest glide ratio $\frac{L}{D}$, which is shown in fig. 7.12. By orienting the main wing with respect to the free-stream in such a way that $C_m = 0$ at $\left(\frac{L}{D}\right)_{max}$, no control surfaces have to be used in cruise condition and maximum range is reached. The best orientation was found with a tilted main wing of -2.34 °. Figure 7.13a shows the graph of C_m - α. It can be seen that the graph intersects at the correct point. Figure 7.13a also shows that the aircraft is stable with a C_{m_α} being negative. And by flying at an AoA of 2 °, the UAV flies without a moment. By looking at the C_L - C_m curve in fig. 7.13b it can be seen that the UAV is still providing positive lift.

It shows that the aircraft is indeed stable by looking at the C_{m_α} which is negative. The curve intersects at AoA of 2 ° and at 2 °, the $\frac{C_L}{C_D}$ - α is maximum as well with a value of 25.5.

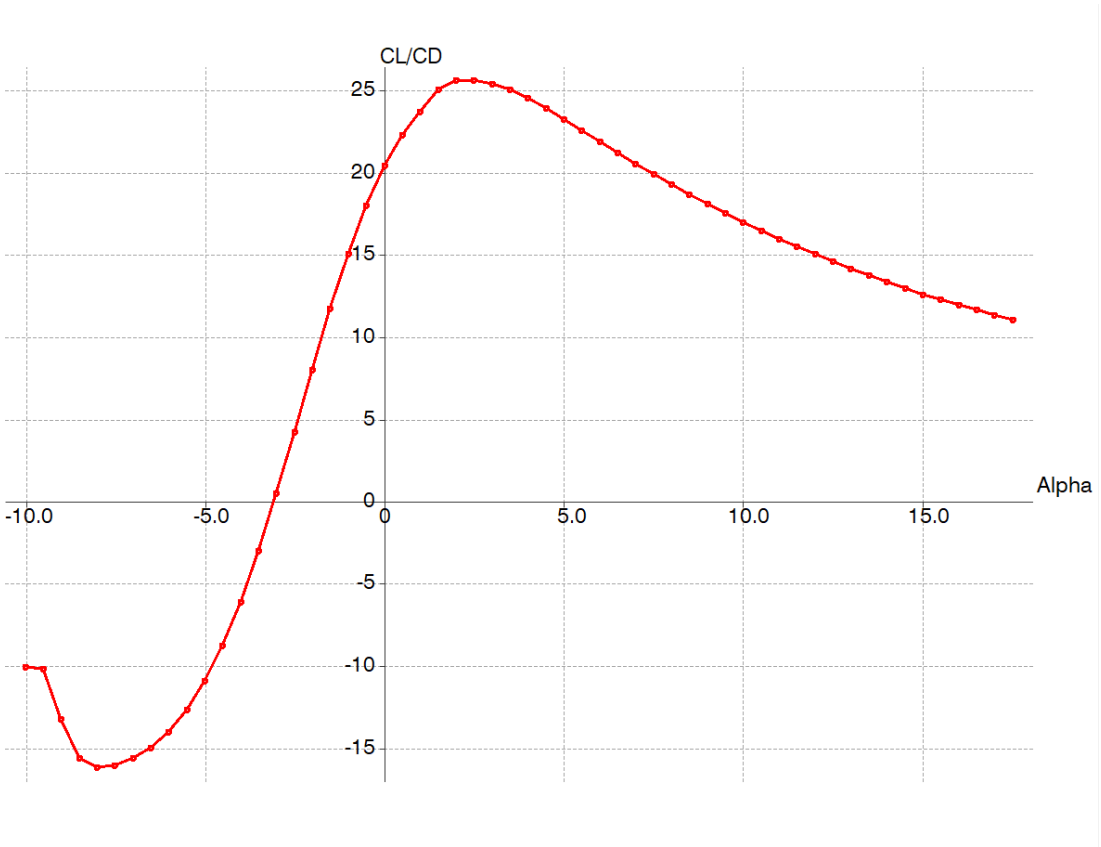

Figure 7.12: $\frac{C_L}{C_D}$ - α-graph for the entire configuration.

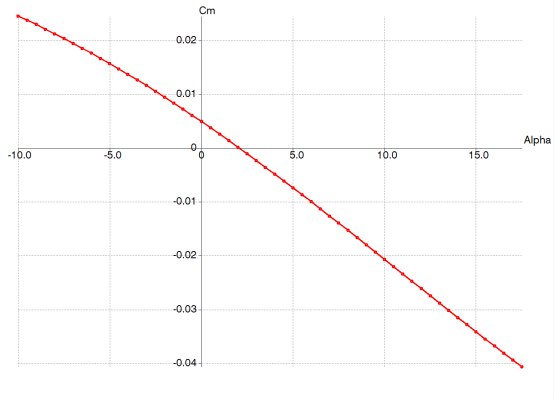

(a) C_m - α-graph for the entire configuration.

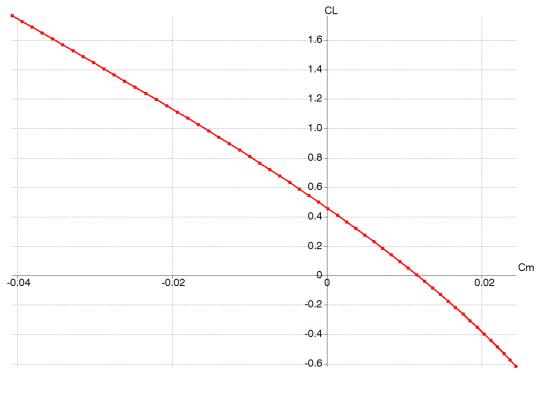

(b) C_m - C_L-graph for the entire configuration.

7.7. Sensitivity analysis

In this section the sensitivity analysis of the aerodynamics design is discussed. In order to make sure the design is robust the effect of change in certain design variables is analysed for the main wing, tail and propeller design.

7.7.1. Main wing sensitivity analysis

The sensitivity analysis for the main wing is focused on two parts. First, a look is taken at the change of root chord. Second, the aerofoil is changed to a different aerofoil selected from table 7.1. By changing the root chord by a factor of two, but still maintaining its span, it can be seen that the main surface area increases by a factor of 2. Figure 7.14a shows that increasing c_r the C_L - α is lower in the mid-range of AoA. It can be seen though that the bigger root chord gives a less positive C_{m_α}. Lastly, it can be seen that the optimum $\frac{C_L}{C_D}$ remains roughly the same. By changing the aerofoil of the main wing to the NACA 2410 aerofoil, it is found that the performance of that aerofoil is significantly less. Figure 7.15a shows that the FX 63-110 aerofoil outperforms the NACA 2410. Furthermore, the wing differs significantly in maximum lift over drag. The NACA 2410 however, is a lot more stable compared to the FX 63-110 aerofoil, as shown in fig. 7.15c. Overall, it is still flyable with these changes in root chord and aerofoil selection. However, the performance is significantly less.

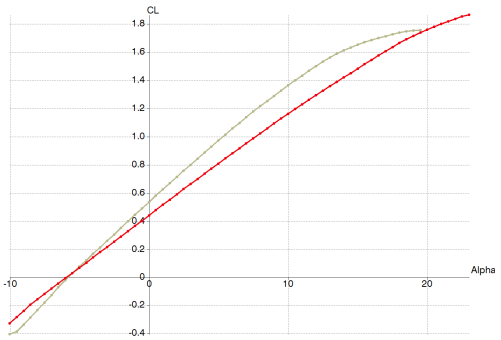

(a) C_L - α curve comparison for two C_r lengths.

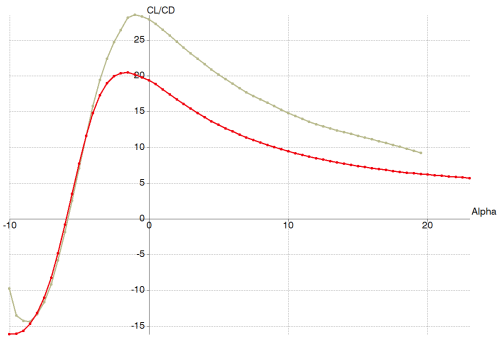

(b) C_L - C_D curve comparison for two C_r lengths.

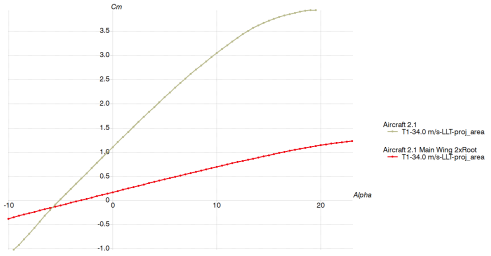

(c) C_m - α curve comparison for two C_r lengths.

Figure 7.14: Sensitivity analysis by changing the root chord by a factor of 2.

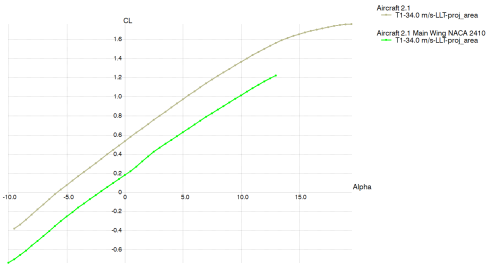

(a) C_L - α curve comparison for two aerofoils.

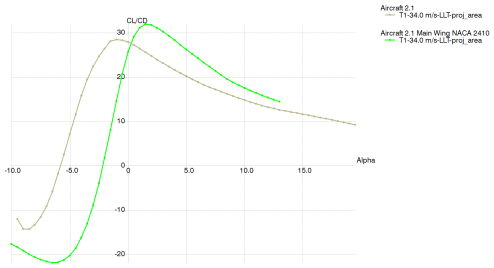

(b) C_L - α curve comparison for two aerofoils.

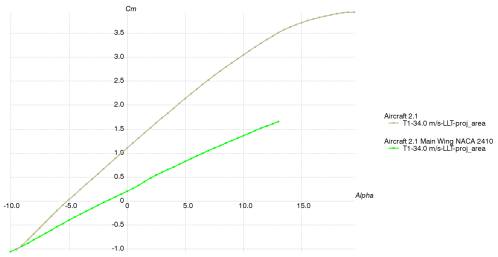

(c) C_m - α curve comparison for two aerofoils.

Figure 7.15: Sensitivity analysis by changing the aerofoil to NACA 2410.

7.7.2. Tail design sensitivity analysis

The sensitivity analysis helps to provide the knowledge about how a changing factors affects the design of the tail. For this sensitivity analysis, it is observed how the dimensions are changed when the volume coefficient and the chosen aerofoil is changed. Other parameters were not analysed, as the distance from the tail used was not the optimised value. Also, some other dimensions were not considered, as they were restricted by other departments, as a result, looking at their sensitivity would not provide the information.

Table 7.9: Analysis of horizontal tail with changing volume coefficient

V_h	S_h [m^2]
0.6	0.09
0.8625	0.14
0.95	0.15

Table 7.10: Analysis of vertical tail with changing volume coefficient

V_v	S_v [m^2]
0.01	0.012
0.035	0.043
0.050	0.061

From table 7.9 and table 7.10, It can be seen that the coefficient is directly proportional to the tail surface area. As a result, increasing the tail volume, would result in an increase of the surface area.

As for the aerofoil, the design choice is constrained to be a symmetric contour. Since the aerofoil with the best C_L - α curve was chosen, it can be seen that for an aerofoil with a lower C_{L_α} the size of both the horizontal and vertical tails would increase, however this size increase is not significant due to the small changes in C_{L_α}.

7.7.3. Propeller blade sensitivity analysis

The sensitivity analysis for the propeller is focused on four parts. First, the number of blades is changed from two blades to three. Second, the diameter is changed from 0.6 to 0.8 m. Third, the cruise airspeed is changed from 33.8 to 45 m s^{-1}. Fourth, the aerofoil is changed from ARA-D 10% to NACA 16-412, thereby implying a new design C_L from 0.8377 to 0.5436. The results in table 7.11 are, for every part, compared to the original design of subsection 7.5.2.

Table 7.11: Propeller blade sensitivity analysis compared to the original design.

	Blades	Diameter	Cruise airspeed	Aerofoil	
	2 –> 3 [-]	0.6 –> 0.8 [m]	33.8 –> 45 [m s^{-1}]	Ara-D 10% (0.8377) –> Naca 16-412 (0.5436)	
Efficiency	-2.82%	3.73%	3.10%	-5.18%	(Positive beneficial)
Power	8.80%	-2.79%	29.10%	5.42%	(Negative beneficial)
New Ω_{RPM}	3,000	1,800	3,100	3,500	
Blade maximum chord size	Smaller	Smaller	Bigger	Bigger	

As can be seen in table 7.11, a larger diameter will be beneficial, but as the design is restricted by the tail boom separation and ground clearance, this is not a possibility. The other changes result in more disadvantages relating to power and efficiency. As can be seen from the percentages in table 7.11 the propeller blade is not really sensitive to changes. The design of the propeller is therefore sensitive to changes in the design and will become less efficient. However, it is predicted that a suitable propeller may always be designed. This is highly beneficial in the case that real life data shows discrepancies between the estimated UAV design performance and its actual performance and requires to change the input data for the propeller design.

7.8. Verification and validation

XFOIL 6.99 is used for the development of the polar graphs. The program is verified/validated by referring to [17]. The procedure used in this paper shows that XFOIL is accurate in the linear region of the C_L -α curve. It was verified using aerofoil NACA 4415 at Re = 3,000,000. The results from their wind tunnel test were compared to [1].

XROTOR 7.55 is used for the development of the propeller blade geometry according to minimum induced losses. The verification and validation of the program is done by referring to [68]. This master thesis shows the process of using CFD and experimental results. The 'N250' propeller [49] and the 'NACA Prop III' [18] are used in this process. It is shown that comparing with the CFD analysis there is a bit higher estimation of thrust and a slightly higher estimate of power. Although, the small difference in $\frac{C_T}{C_P} \cdot J$ (also known as the propeller efficiency) is negligible, XROTOR is a good approximation method to design the propeller to minimise induced losses.

XFLR5 V6.38 is validated using reference [14]. David Communier et al. carried a study on merging CATIA V5 and XFLR5 and validated their XFLR5 software by means of an experimental validation method. They used the Price-Païdoussis wind tunnel for experiments. Different aerofoils were tested for validation and special attention was paid to the aerofoil NACA 0012 in particular. The aerofoils were tested using different velocities, namely 20 m s^{-1}, 25 m s^{-1}, 30 m s^{-1} and 35 m s^{-1}. These velocities are in the regime the FASAR UAV operates. It was found that the C_L was correct and the drag coefficient suffered from a negligibly small offset. Furthermore the offset in the slope of the C_m -α curve was negligible as well. From this it can be concluded that XFLR5 V6.38 is a proper programme to be used assuming the small offsets in the C_D - α curve and the slope of the C_m - α curve are inconsequential. XFLR5 V6.38 behaved as it should according to general knowledge of aerodynamics. Increasing the angle of attack in the linear range should lead to a higher lift for the aircraft. This is indeed the case. Furthermore, at the wingtips, it is expected to show vortices which is also shown in XFLR5 V6.38. According to knowledge obtained on aerodynamics, the programme XFLR5 V6.38 complies with what has been taught.

To calculate the drag of the body, an excel sheet is made to calculate all the values, and thus provides the drag for the different scenarios. The excel is checked with the values from the reference [26], to see if the value in the excel matches the one from the reference. Also, a sanity check is done with all the values that are obtained from the excel sheet, to see if the values obtained do make sense. The XLFR5 produced the C_D of the wing, and the excel for the wing matched that value too.

Chapter 8: Stability and control

In this chapter,the determination of tail size in order to achieve stability and control of the UAV is explained. Furthermore, the control surfaces are sized in section 8.3. Also the dynamic stability of the UAV is assessed in section 8.4.

8.1. Horizontal tail sizing

In order to determine the size and distance of the horizontal tail, it is necessary to evaluate the stability and controllability of the UAV. First, the tail volume needed for static stability is assessed in subsection 8.1.1. After this, the horizontal tail volume needed for controllability is calculated.

8.1.1. Stability curve

The stability margin is based on the longitudinal stability of the aircraft which is directly correlated to the location of the neutral point. For a conventional aircraft, the neutral point must be aft of the centre of gravity for longitudinal stability. This results in a stabilising pitch-down moment. The equation for determining the stability is shown in eq. (8.1), [57].

$$\frac{S_h}{S} = \frac{1}{\left[\frac{C_{L\alpha_h}}{C_{L\alpha_{A-h}}}\left(1-\frac{d\epsilon}{d\alpha}\right)\frac{l_h}{\bar{c}}\left(\frac{V_h}{V}\right)^2\right]}\bar{x}_{cg} - \frac{\bar{x}_{ac}}{\frac{C_{L\alpha_h}}{C_{L\alpha_{A-h}}}\left(1-\frac{d\epsilon}{d\alpha}\right)\frac{l_h}{\bar{c}}\left(\frac{V_h}{V}\right)^2} \tag{8.1}$$

Adapting this equation to find the required horizontal tail volume gives eq. (8.2):

$$C_{HT} = \frac{S_h l_h}{S\bar{c}} = \frac{1}{\left[\frac{C_{L\alpha_h}}{C_{L\alpha_{A-h}}}\left(1-\frac{d\epsilon}{d\alpha}\right)\left(\frac{V_h}{V}\right)^2\right]}\bar{x}_{cg} - \frac{\bar{x}_{ac}}{\frac{C_{L\alpha_h}}{C_{L\alpha_{A-h}}}\left(1-\frac{d\epsilon}{d\alpha}\right)\left(\frac{V_h}{V}\right)^2} \tag{8.2}$$

Where C_{HT} is the horizontal tail volume and S_h and S are the horizontal tail and wing surface areas respectively. $\frac{d\epsilon}{d\alpha}$ is the down-wash as seen by the tail, l_h is the relative distance between the wing and horizontal tail, $\bar{c}$ is the mean chord length of the wing. Furthermore, $\bar{x}_{cg}$ and $\bar{x}_{ac}$ are the centre of gravity and aerodynamic centre locations. Additionally, $C_{L\alpha}$ represents the lift gradient, subscript h is used for the horizontal tail and $A-h$ for the aircraft minus the horizontal tail. Finally, $\frac{V_h}{V}$ represents the ratio in airspeed between the horizontal stabiliser and the wing.

Also, because the propeller will blow air over the horizontal tail with a higher velocity than the velocity at infinite distance, $\frac{V_h}{V}$ is equal to 1 or higher. This could compensate for the downwash caused by the main wing. For this reason, it is assumed that $\frac{d\epsilon}{d\alpha} = 0$ and $\frac{V_h}{V} = 1$.

Using eq. (8.2), C_{HT} is calculated for the most forward and most aft c.g. positions. The aft position results in a larger C_{HT}, which is equal to 0.73. The largest horizontal tail volume is chosen since it is able to cope with all the flight conditions.

8.1.2. Controllability curve

The controllability curve determines the ability of the horizontal tail to trim the aircraft by counteracting the moment on the aircraft. The horizontal tail volume C_{HT} needed for controllability is determined by eq. (8.3), [58].

$$\frac{S_h}{S} = \frac{1}{\frac{C_{L_h}}{C_{L_{A-h}}}\frac{l_h}{\bar{c}}\left(\frac{V_h}{V}\right)^2}\bar{x}_{cg} + \frac{\frac{C_{m_{ac}}}{C_{L_{A-h}}} - \bar{x}_{ac}}{\frac{C_{L_h}}{C_{L_{A-h}}}\frac{l_h}{\bar{c}}\left(\frac{V_h}{V}\right)^2} \tag{8.3}$$

Where C_L is the lift coefficient. Other variables are as stated in subsection 8.1.1. Adapting this equation to find the required horizontal tail volume gives eq. (8.4):

$$C_{HT} = \frac{S_h l_h}{S\bar{c}} = \frac{1}{\frac{C_{L_h}}{C_{L_{A-h}}}\left(\frac{V_h}{V}\right)^2}\bar{x}_{cg} + \frac{\frac{C_{m_{ac}}}{C_{L_{A-h}}} - \bar{x}_{ac}}{\frac{C_{L_h}}{C_{L_{A-h}}}\left(\frac{V_h}{V}\right)^2} \tag{8.4}$$

After solving eq. (8.2), the largest tail volume needed to control the UAV is 0.77. This is also the largest horizontal tail volume needed, and is therefore selected to be able to accommodate for all conditions.

8.2. Aircraft static stability

Now that the layout of the UAV has been defined, its stability should be looked at in further detail. The longitudinal stability is first analysed thoroughly and is followed by an analysis of the lateral stability.

8.2.1. Longitudinal static stability

The longitudinal static stability can now be assessed by calculating the neutral point and the static margin. The neutral point is determined with eq. (8.5).

$$\frac{x_n - x_{ac}}{\bar{c}} = \frac{C_{L\alpha_h}}{C_{L\alpha}}\left(1 - \frac{d\epsilon}{d\alpha}\right)\left(\frac{V_h}{V}\right)^2 C_{TH} \tag{8.5}$$

This results in a neutral point of 0.80 m from the nose. By subtracting the most aft c.g. position from the neutral point, the stability margin can be obtained for the most aft c.g. position of the last iteration, which is 15 cm.

8.3. Control surface design

Proper control surface sizing is of utmost importance for the control performance of the aircraft. The UAV must achieve certain requirements such as for the roll rate but should not over achieve This is due to the fact that there must be a trade-off between stability and control.

8.3.1. Aileron sizing

In order to achieve roll control, the UAV is equipped with an aileron on each wing. control surfaces are necessary for manoeuvrability and must be designed for the most critical conditions. This occurs when the aircraft is flying towards an obstacle at top speed and must avoid it. It has previously been determined that the UAV shall achieve a turn radius of 65 m to avoid obstacles with a bank angle of 70°.

The Aerotenna μSharp obstacle avoidance sensor is able to detect obstacles at a distance of 120 m. Assuming a turn radius of 65 m and requiring a further 40 m to account for the possibility that the obstacle is moving towards the UAV, and 20 m if the object is static. In the remaining distance, a bank angle of 70° must be attained. Whilst travelling at top speed, this results in a roll rate requirement item **REQ.U.SYS.22** of 209 ° s^{-1}.

In order to achieve roll control, the ailerons must generate an asymmetry in moment around the longitudinal axis. In terms of stability derivatives, the steady state roll rate is expressed as shown in eq. (8.6), [25]. Please note that in this section, C_l represents a rolling coefficient, L is a rolling moment, F is a lift force and c_l is a lift coefficient.

$$\frac{pb}{2V} = -\frac{C_{l_{\delta_a}}}{C_{l_p}}\delta_a \tag{8.6}$$

Where p is the roll rate, b is the wingspan, V is the airspeed, $C_{l_{\delta_a}}$ is the aileron roll authority, C_{l_p} is the roll damping and δ_a is the aileron deflection. The roll authority is a term used to evaluate the responsiveness of the aircraft to an aileron deflection. Moreover, a damping term is used as the angle of attack along the wing varies with the roll rate. A higher roll rate results in a lower local angle of attack; hence the term damping.

In order to estimate the roll authority, one must consider the difference in lift provided by each wing. This is done by taking the aileron deflection δ_a and the lift gradient due to the deflection $C_{l_{\delta_a}}$ into account. Equation (8.7) expresses the lift coefficients of the up and down going wing with subscripts up and $down$ respectively. Furthermore , C_{l_y} represents the section of the wing which is being analysed at a distance y along the wingspan.

$$c_{l_{up}} = c_{l_y} + c_{l_{\delta_a}} \cdot \delta_a \qquad\qquad c_{l_{down}} = c_{l_y} - c_{l_{\delta_a}} \cdot \delta_a \tag{8.7}$$

The roll coefficient C_l is found by making the moment L dimensionless as shown in eq. (8.8).

$$C_l = \frac{L}{qSb} = \frac{L_{up} + L_{down}}{qSb} \tag{8.8}$$

Using the expression for the local C_l along the span of the wing, the lifting force generated by the wing can be determined. To calculate the lifting force, infinitesimal wing sections are considered with wetted area dS. This yields infinitesimal forces dF_{up} and dF_{down}.

$$dF_{up} = q\left(c_{l_y} + c_{l_{\delta_a}}\delta_a\right)c \cdot dy \qquad\qquad dF_{down} = q\left(c_{l_y} - c_{l_{\delta_a}}\delta_a\right)c \cdot dy \tag{8.9}$$

The moment of the section is calculated by multiplying the section force by its moment arm y. Doing so, simplifying the equation and integrating over the entire aileron wetted surface area yields the total moment L. The symbols b_1 and b_2 below represent the beginning and end of the aileron along the span of the wing starting from the longitudinal axis respectively.

$$L = 2q \cdot C_{l_{\delta_a}}\delta_a \int_{b1}^{b2} y dy \tag{8.10}$$

By substituting L into eq. (8.8) and differentiating with respect to δ_a, the roll authority is found as shown in eq. (8.11).

$$C_{l_{\delta a}} = \frac{2 \cdot c_{l_{\delta a}}}{Sb} \int_{b1}^{b2} y dy \tag{8.11}$$

Moreover, it has been mentioned that roll damping is present. Assuming a rigid wing with a roll rate of p, the linear velocity of the wing will vary along the span. As a result, this affects the velocity resultant and therefore impacts the local angle of attack of the wing. A complex derivation for this term can be found in [27] which results in eq. (8.12).

$$C_{l_p} = \frac{4\left(c_{l_\alpha} + C_{d0}\right)}{Sb^2} \int_0^{b/2} y^2 \cdot c(y) dy \tag{8.12}$$

Prior to performing the calculations, the aerofoil properties must be determined. Table 23.2.2 from [27] states that ailerons should have a chord length c_a between 0.20 and 0.35 of the wing root chord length. In order to determine the optimal c_a, different values were considered ranging from 0.20 to 0.35 of the root chord with deflection angles between 15 and 25°. Considering drag, lift and angle of attack at maximum lift by looking at fig. 8.1, an aileron chord of 20% root chord with a maximum deflection angle of 20° was chosen.

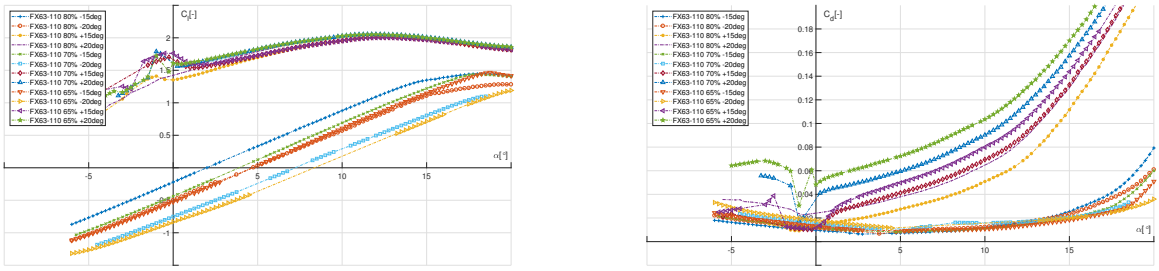

(a) $C_{l_a} - \alpha$-graphs for different aileron size and deflections.

(b) $C_{d_a} - \alpha$-graphs for different aileron size and deflections.

Figure 8.1: Lift and drag polars for different aileron size and deflections at Re = 800,000 and M = 0.12.

By rearranging eq. (8.6) for p and substituting eq. (8.11) and eq. (8.12) into the expression, the aileron can be sized by fixing b_2 and varying b_1. The maximum value of b_1 minimises the control surface area and is therefore preferable. The maximum value of b_1 that meets the roll rate requirement of 209° s^{-1} is therefore used. This yields a b_1 of 0.73 m and a b_2 of 1.11 m resulting in an aileron span of 0.38 m per wing.

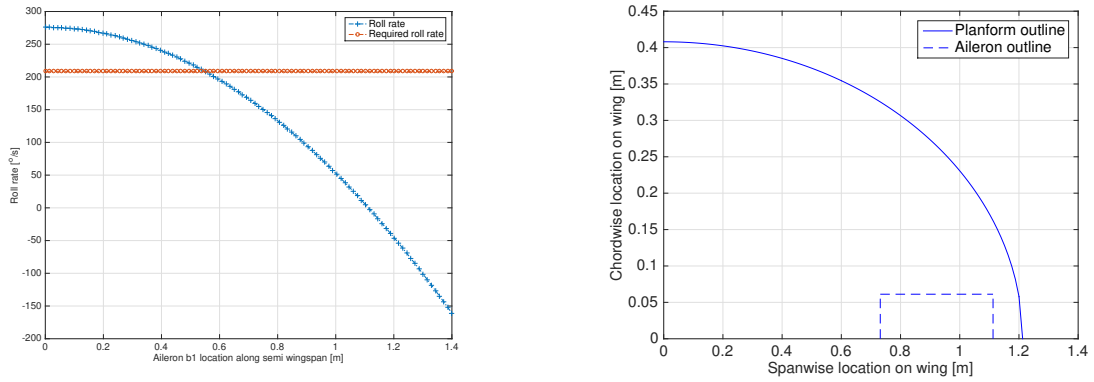

(a) Roll rate achieved by different aileron sizes.

(b) Sized aileron layout outline on wing.

Figure 8.2: Aileron sizing and performance.

Moreover, to check that the UAV has indeed rolled by 70° in its required time of 1 second, one must look at the dynamics of the UAV. Looking back at eq. (8.8), the moment coefficient of the aeroplane is given. The moment coefficient C_l is a function of the local angle of attack which varies the angular velocity of the aircraft. The wing rolling upwards experiences a lower angle of attack than that of the other due to the difference in the velocity vector component similarly to the roll damping explained earlier.

In order to take the roll rate into account in the calculations, one must consider the local angle of attack along the wing at every instant. This local angle of attack is calculated as shown in eq. (8.13).

$$\alpha(y) = arctan\left(\frac{p \cdot y}{V}\right) \tag{8.13}$$

Where y represents the location along the wing span and p is the roll rate. By considering the effect of the change in angle of attack into eq. (8.8), one can find that instantaneous moment coefficient. By multiplying the moment coefficient by the

dynamic pressure q and the moment arm of the aileron $\left(\frac{b_2-b_1}{2}\right)$) and the aileron wetted area S, the total moment generated by the ailerons is found as shown in eq. (8.14).

$$L = C_l(\alpha) q S_{ail} \frac{b_2 - b_1}{2} \tag{8.14}$$

The total moment is equal to the product of the mass moment of inertia I_{xx} of the UAV and its angular acceleration, α_{accel}. Rearranging this and solving for α_{accel}, the instantaneous angular acceleration is found as shown in eq. (8.15)

$$\alpha_{accel} = \frac{L}{I_{xx}} \tag{8.15}$$

By integrating eq. (8.15) twice with respect to time, the roll angle is determined. By requiring a roll angle of 70° and solving for time, it can be found that the UAV performs its 70° roll in 1.1 seconds. Obstacles can therefore be avoid but a distance of 4.5 m is lost from the safety margin due to the additional distance required to perform the manoeuvre. This is not perceived as a major issue as large safety factors have been taken when defining the safety distance.

8.3.2. Flap sizing

In order to lower the wing area and to maintain a stall speed of 18 m s^{-1} at an altitude of 3,500 m, hinged flaps will be used. In addition to the flaps, the ailerons will be operating as flaperons. Unlike for the ailerons, the flaps will be designed based on geometrical constraints rather than performance constraints. This means that the wing itself cannot be designed for a specific C_{Lmax} and achieving a high C_{Lmax} therefore becomes a goal and not a design parameter.

In order to limit bending loads, the flaps are to be placed close to the fuselage. For this reason, these will be place between the fuselage and the booms. The booms are located 35 cm from the longitudinal axis. Using a 1 cm clearance from the booms to allow for the boom/wing connection and a 13 cm clearance from the fuselage, a flap span of 21 cm is obtained.

Based on historical data from [27], it is known that the chord length of flaps c_f varies between 20 and 35% of the root chord and have a maximum deflection, δ_f, between 25 and 50°. Varying those values in XFLR5, an optimum combination of flap chord length and maximum deflection could be chosen as it was done in subsection 8.3.1.

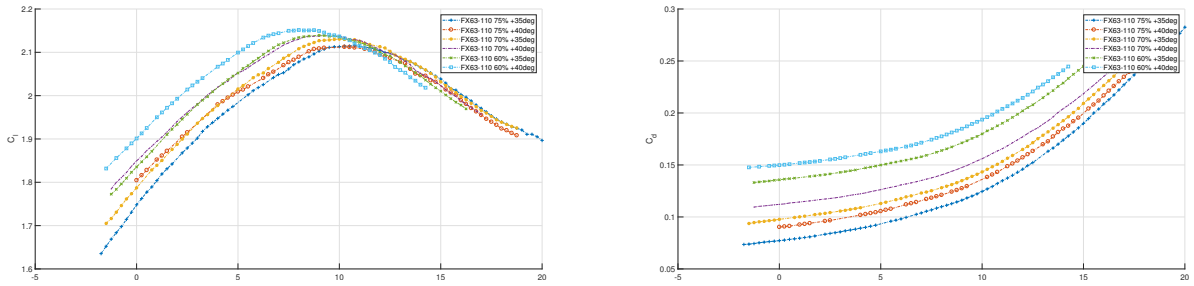

(a) $C_{l_f} - \alpha$-graphs for different flap settings.

(b) $C_{d_f} - \alpha$-graphs for different flap settings.

Figure 8.3: Lift and drag polars for different flap deflections and size at Re = 800,000 and M = 0.12.

Taking the polars as shown above in fig. 8.3a and fig. 8.3b into account, as well as keeping structural considerations, a maximum δ_f of 35° has been chosen with a c_f of $0.3c_r$.

Having sized the flaperons as well as the flaps, the C_{Lmax} of the wing can be estimated from 2D aerofoil characteristics as shown in eq. (8.16), [27]. The equation takes into account the different high lift surfaces on the wing, normalises the lift coefficient with the term S_{ref} (which represents the surface area of the wing) and multiplies the equation by 0.9 to consider losses in lift from 2D to 3D. Moreover, S_i in the equation represents the wetted area of the different sections being considered.

$$C_{Lmax} = \frac{0.9}{S_{ref}} \sum_{i=1}^{N_f} C_{l_{max_i}} \cdot S_i \tag{8.16}$$

Using this model, a C_{Lmax} of 1.74 is obtained. This value has been verified and validated with XFLR5 in section 7.8 and is therefore used throughout the design.

8.3.3. Elevator sizing

In order to control the UAV longitudinally, an elevator is required. For the sizing of the elevator, the elevator chord over horizontal stabiliser ratio $\frac{c_e}{c_h}$ and the maximum deflection determine the maximum lift the elevator can generate. The chord ratio can vary between 0.2 and 0.35 and the elevator can deflect to a maximum of 15 ° and 20 °[27]. Varying these values in XFLR5 gives the lift and drag curves for the different sizes and deflections.

As can be seen in fig. 8.4a when the elevator starts at 70% of the stabiliser (so the chord ratio is 0.3), the lift will not increase for larger elevators. As can be seen in fig. 8.4b, the drag does increase for a higher chord ratio, and therefore the chosen chord

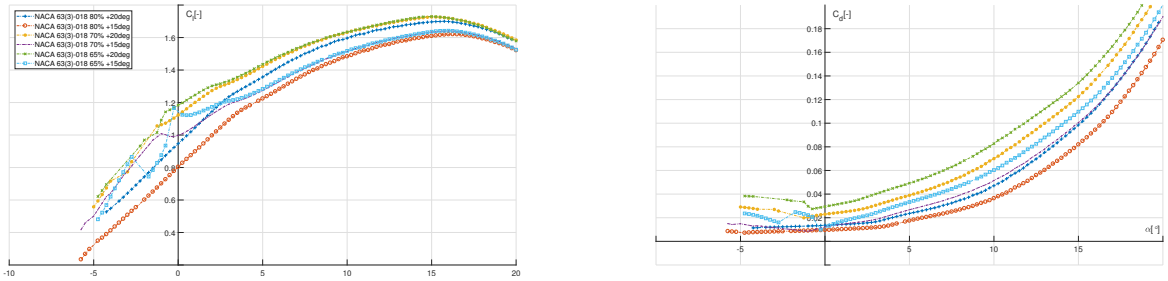

(a) Lift coefficient plotted against angle of attack.

(b) Drag coefficient plotted against angle of attack.

Figure 8.4: Lift and drag polars for different elevator deflections and sizes at Re = 800,000 and M = 0.12.

ratio will be 0.3 (since the elevator will start at 70% of the root chord). Choosing a bigger elevator would lead to a higher drag, without gaining extra lift. This extra drag would not be desired because this would lead to a higher fuel consumption and a less sustainable design. The maximum elevator deflection is 20° and the maximum lift is 1.72.

Furthermore, two critical situations normally determine the sizing of the elevator [62]. These are the ability to lift off and rotate the aircraft and the ability to trim the aircraft in flight. Since the UAV will be launched, it is not important to size the UAV for a conventional take-off. In addition, the most critical condition for the sizing of the elevator is the landing and the ability to control the UAV at this phase of its flight. Therefore, the equations from [62] have been rewritten to size for landing at the maximum altitude (=3,500 m), resulting in a required horizontal stabiliser lift $C_{L_{h_{tot}}}$ as formulated in eq. (8.17).

$$C_{L_{h_{tot}}} = \frac{C_L \cdot l_w + C_{m_{ac}} \cdot \bar{c}}{l_h} \cdot \left(\frac{V}{V_h}\right)^2 \cdot \frac{S}{S_h} \tag{8.17}$$

Where C_L is the lift of the wing, l_w is the distance from the wing to the centre of gravity and $C_{m_{ac}}$ is the moment coefficient of the wing around the aerodynamic centre. Filling in eq. (8.17) gives a $C_{L_{h_{tot}}}$ of 1.67. In addition, the total lift generated by the horizontal tail can also be expressed as described in eq. (8.18).

$$C_{L_{h_{tot}}} = \left(1 - \frac{b_e}{b_h}\right) \cdot C_{L_h} + \frac{b_e}{b_h} \cdot C_{L_{emax}} \tag{8.18}$$

Where $C_{L_{h_{tot}}}$ is the minimum lift coefficient of the horizontal tail (with the elevator) required to provide the control for the landing configuration. $\frac{b_e}{b_h}$ is the elevator span over horizontal stabiliser span ratio, which gives the span of the elevator with respect to that of the horizontal stabiliser. C_{L_h} is the maximum lift the horizontal stabiliser would give when there would be no elevator, and $C_{L_{emax}}$ is the maximum lift the part of the horizontal stabiliser with the elevator at maximum deflection gives. Equation (8.18) can be rewritten to get the required span of the elevator $\frac{b_e}{b_h}$ as shown in eq. (8.19).

$$\frac{b_e}{b_h} = \frac{C_{L_{h_{tot}}} - C_{L_h}}{C_{L_{emax}} - C_{L_h}} \tag{8.19}$$

This gives a $\frac{b_e}{b_h}$ of 0.89, which means that the elevator will run for 89% of the span of the horizontal tail.

Now the geometry of the elevator is determined, it can be verified by modelling this in XFLR5 to check whether the required C_{L_h} can be generated by the horizontal tail and elevator combination.

8.3.4. Rudder sizing

When designing the rudder, it is important to take into account different flight conditions such as spin recovery, coordinated turns, crosswind and so on. It has been determined that due to the high wind conditions the UAV has to sustain, crosswinds are the most critical parameter to size for. The method below has been derived from [62].

First of all, the total airspeed V_T must be determined in order to be able to analyse the problem. To do this, the approach speed U_1 and the wind speed V_W are considered, where U_1 is 1.3 times the stall velocity.

$$V_T = \sqrt{U_1^2 + V_W^2} \tag{8.20}$$

The side slip angle β is then found using simple geometry.

$$\beta = \tan^{-1}\left(\frac{V_W}{U_1}\right) \tag{8.21}$$

The force acting on the aircraft due to the wind F_W shall be calculated. C_{D_y} in eq. (8.22) represents the drag coefficient of the aircraft in the y-direction (side view) and S_S is the surface area the wind is acting on (surface seen in a side view of the UAV).

$$F_W = \frac{1}{2}\rho V_W^2 S_S C_{D_y} \tag{8.22}$$

A system of equations can now be defined (eq. (8.23) in order to solve for the rudder deflection δ_R and the crab angle σ. This is done considering the force acting on the fuselage and the force needed by the rudder to counteract it. The second equation takes the side force on the fuselage due to the movement of the aircraft into account.

$$\begin{aligned} &\frac{1}{2}\rho V_T^2 Sb\Big(C_{n_0} + C_{n_\beta}(\beta-\sigma) + C_{n_{\delta_R}}\Big) + F_W \cdot d_c \cos(\sigma) = 0 \\ &\frac{1}{2}\rho V_T^2 S_S\Big(C_{y_0} + C_{y_\beta}(\beta-\sigma) + C_{y_{\delta_R}}\Big) = \frac{1}{2}\rho V_W^2 S C_{D_y} \end{aligned} \tag{8.23}$$

The control derivatives $C_{y_{\delta_R}}$, $C_{n_{\delta_R}}$ as well as the sideslip derivatives C_{n_β} and C_{y_β} depend on the rudder chord length. An iteration process was therefore formed here and the values were determined using XFLR5. Starting with an assumed value of the rudder's chord to be 30% of the tail chord, the iteration eventually converged with a rudder the size of the vertical stabiliser. As a result, the full vertical tail will rotate and act as a rudder. A rudder deflection of 25° for each rudder is required during crosswinds at 8 Bft with a crab angle of 35°.

8.3.5. Control forces

Now that all the control surfaces have been designed, an actuation system must be designed for each of them. To size the actuators, the hinge moment of each control surface must be determined.

The hinge moment H_e is expressed as:

$$H_e = C_h \frac{1}{2}\rho V^2 S_{cs} c_{cs} \tag{8.24}$$

Where C_h is the hinge moment coefficient, and S_{cs} and c_{cs} are the control surfaces' area and chord length respectively. The hinge moment coefficient of each surface was determined with the use of XFLR5.

Using eq. (8.24), table 8.1 was created. A safety factor of 1.5 was used in order to ensure proper actuation is possible.

As it can be seen in table 8.1, the rudder requires a much higher torque than the other control surfaces, because the whole profile is being rotated. Due to this fact, it is decided to place the vertical fins above the boom and vertical tail attachments, in order to be able to implement a rotating mechanism, that otherwise would need to be too complex. This results in a U-shaped tail design.

The third column of table 8.1 shows the servo motors that will be used for each control surface. These servos are all taken from Volz.[40]

Table 8.1: Control surfaces hinge moment.

Control surface	Hinge moment [N m]	Servo motor
Ailerons	3.42	DA 10
Flaps	0.40	DA 10
Rudder	15.03	DA 20
Elevator	0.02	DA 10

8.4. Dynamic stability

In this section, the dynamic stability of the UAV will be assessed. This is done using XFLR5, whill gave the eigenvalues used to assess the eigenmotions of the UAV. This has been done throughout the design life-cycle to make sure the design is stable and the optimal design for different departments will not be unstable in the end, requiring changes in the final design. First the eigenmotions are discussed in subsection 8.4.1 after which the responses are evaluated in subsection 8.4.2.

8.4.1. Eigenvalues

The eigenvalues are an important measure in determining the response to the eigenmotions. These are listed for both the longitudinal and lateral eigenmotions in table 8.2.

[40] volz-servos.com/English/

Table 8.2: Eigenvalues for the different eigenmotions.

	Motion	Eigenvalues	Period [s]	Damping coefficient ζ	$T_{\frac{1}{2}}$ [s]
Longitudinal	Short motion	-4.034 +/- 5.256i	1.195	0.6088	0.1718
	Phugoid	-0.0063 +/- 0.328i	19.162	0.0012	110.585
Lateral	Asymmetric roll	-12.17	-	1	0.0570
	Dutch roll	-0.2965 +/- 3.267i	1.923	0.0904	2.3378
	Spiral	0.06221	-	-	-11.142

As can be seen, all the eigenmotions are stable, except for the spiral motion. This is due to the negative real part of the eigenvalue, which causes the oscillation to dampen out. The unstable behaviour of the spiral motion can be expected since this is an inherent unstable eigenmotion. The responses to the eigenmotions are shown in fig. 8.5 to fig. 8.9.

The period, damping coefficient and time to half amplitude are calculated using eq. (8.25), eq. (8.26) and eq. (8.27) respectively [33], [67]. Also, all the values for each eigenmotion are listed in table 8.2.

$$P = \frac{2\pi}{Im(\lambda)} \tag{8.25}$$

$$\zeta = \frac{-Re(\lambda)}{\sqrt{Re(\lambda)^2 + Im(\lambda)^2}} \tag{8.26}$$

$$T_{\frac{1}{2}} = \frac{ln(\frac{1}{2})}{Re(\lambda)} \tag{8.27}$$

8.4.2. Eigenmotions

Now the eigenvalues are known, the eigenmotions themselves can be reviewed. For each eigenmotion the responses are shown for the different important parameters, after which a short explanation is given about the eigenmotion.

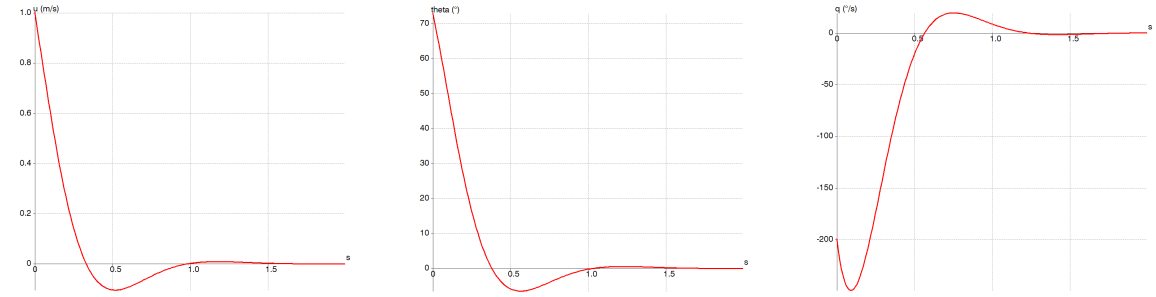

(a) Velocity difference [m s^{-1}] versus [s]. (b) Pitch angle [°] versus time [s]. (c) Pitch-rate [° s^{-1}] versus time [s].

Figure 8.5: Short motion eigenmotion responses.

The short motion is initiated by applying a step input to the elevator, which will increase the pitch-rate. This will cause the UAV to rotate, increasing the lift on the tail and decreasing the pitch-rate, making the UAV to oscillate.

In the fig. 8.5a, fig. 8.5b and fig. 8.5c u is the change in velocity (in [m s^{-1}]), θ (theta in the graph) is the pitch angle (in [°]) and q is the pitch-rate (in [° s^{-1}]). It can be seen in fig. 8.5 that the short motion is damped very quickly after just overshooting the end value. The quick convergence is due to the high damping coefficient, which will cause the response to half its amplitude after already 0.17 seconds.

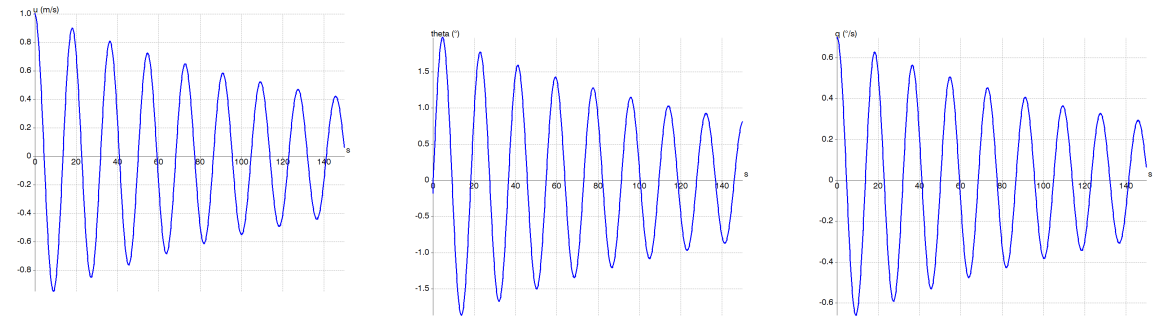

(a)
Velocity difference [m s^{-1}] versus time [s]. (b) Pitch angle [°] versus time [s]. (c) Pitch-rate [° s^{-1}] versus time [s].

Figure 8.6: Phugoid eigenmotion responses.

The phugoid is started by applying an impulse input to the rudder, after which the UAV starts to climb. The climb will cause the velocity to decrease together with the lift. This will make the pitch angle to decrease and the UAV to descend again. As a result, the velocity and lift will increase, and the motion to repeat. As can be seen in fig. 8.6, the phugoid is periodic and damps very slowly. This means that the motion is stable, because it will return to the equilibrium position. From the eigenvalues it can be derived that the period is 19.2 seconds, the damping ratio is 0.0012 and the time to half amplitude is 111 seconds. This confirms that the phugoid is indeed a slow eigenmotion, and damps slowly in this case since it will half the amplitude of its motion every 111 seconds.

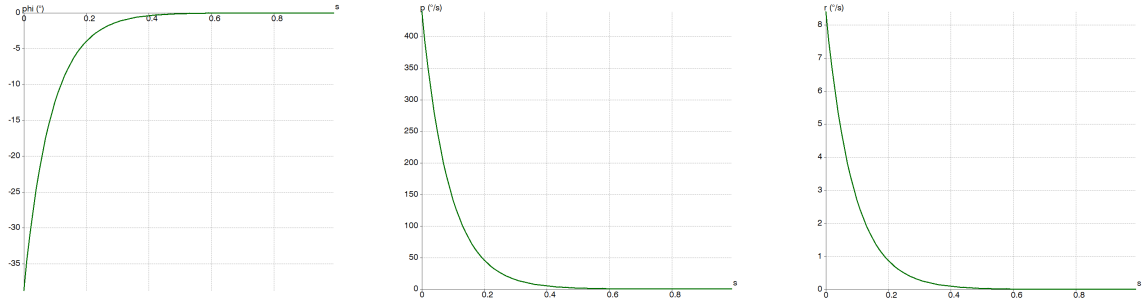

(a) Roll angle [°] versus time [s]. (b) Roll-rate [° s^{-1}] versus time [s]. (c) Yaw-rate [° s^{-1}] versus time [s].

Figure 8.7: Aperiodic roll eigenmotion responses.

In fig. 8.7a, fig. 8.7b and fig. 8.7c the roll angle ϕ (phi in the figure, in [°]), roll-rate p (in [° s^{-1}]) and yaw-rate r (in [° s^{-1}]) are plotted against the time (in [s]).

The aperiodic roll starts when a step input in the aileron deflection is applied. The UAV will start rolling to the left for a positive aileron input. Due to the rolling motion the effective angle of attack is increased on the left wing, increasing lift and causing a moment opposing this rolling motion. This means that the roll gets damped, as can be seen in fig. 8.7. There is no period since the eigenvalue does not have an imaginary part and that the damping does not induce an oscillation. Therefore the motion is critically damped with a damping coefficient equal to 1. Moreover, the motion gets damped very quickly with a time to half amplitude is equal to 0.057 seconds, which means that the UAV can stabilise itself in roll quickly.

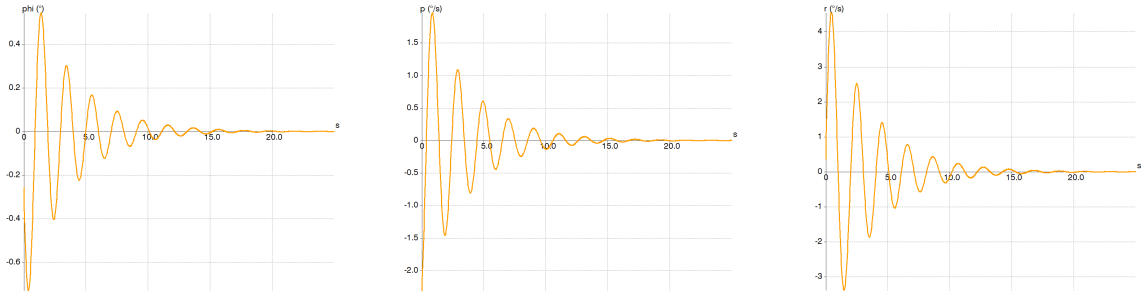

(a) Roll angle [°] versus time [s]. (b) Roll-rate [° s^{-1}] versus time [s]. (c) Yaw-rate [° s^{-1}] versus time [s].

Figure 8.8: Dutch roll eigenmotion responses.

The Dutch roll starts with an impulse input in the rudder, causing a yaw. This will cause the UAV to have more lift on the right wing, which again causes a rolling motion to the left. The rolling motion increases the effective angle of attack on the left wing and decreases the drag on the left wing (since the lift vector is tilted forwards). This will cause the UAV to yaw to the right and the motion starts over again. As can be seen in fig. 8.8, the Dutch roll motion gets damped rather quickly with a period of 1.9 seconds, a damping coefficient of 0.09 and a time to half amplitude of 2.34 seconds. It is important that the motion gets damped quickly, since this motion can be disrupting the payload measurements when a side-gust occurs.

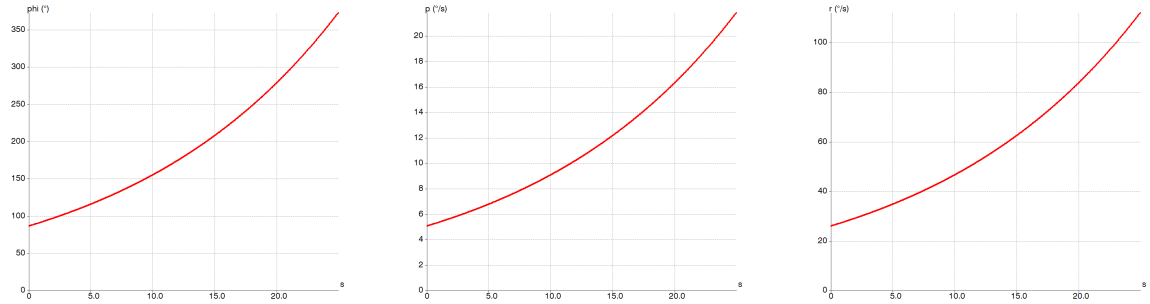

(a) Roll angle [°] versus time [s]. (b) Roll-rate [° s^{-1}] versus time [s]. (c) Yaw-rate [° s^{-1}] versus time [s].

Figure 8.9: Spiral eigenmotion responses.

The spiral motion is inherent to aircraft, since this starts when the UAV has a small bank angle. When the UAV is flying at this angle, it will start a slow turn. If the UAV starts a turn to the left, the right wing will fly at a higher effective velocity, it generates a higher lift, causing a rolling motion to the inside of the turn. As can be seen in fig. 8.9, the bank angle will increase further if not corrected, leading to high bank angles. The motion increases to twice the amplitude in 11.1 seconds, which gives enough time to correct for the bank angle.

8.5. Sensitivity analysis

As no prototype of the design has been made yet, nor have there been any wind tunnel tests, the design is subject to change once these are done. For this reason, it is important to predict how the design is affected by certain input changes.

In order to satisfy stability and controllability, the tail volume has to change with a changing UAV design. If the lift and lift slope of the main wing would increase, or those of the horizontal stabiliser would decrease, then the tail volume would decrease. Also, if the centre of gravity would move forward, this would result in a bigger tail volume. This would result in a smaller wing or a shorter tail boom. This can also work the other way around, which will cause a bigger tail, causing a higher mass and an aft moving c.g. position. This would again result in a higher tail volume, creating a snowball effect.

The flaps and ailerons are mildly sensitive to input variations. In the majority of cases, the ailerons can be expected to increase in width. If this is the case, a small increase in $C_{L_{max}}$ can be expected as well as a slight increase in drag. This may result in an additional iteration being required but is not expected to cause significant changes in the design of the UAV.

Similarly, the design of the UAV is relatively flexible and is not expected to affect the design much in case inputs have to be altered. On the other hand, the rudder is very sensitive to wind. An increase in wind required a larger surface area to control the UAV. However, a larger surface area also means a greater side force on the UAV meaning a greater moment arm is needed.

The elevator is more sensitive to a change in the required C_{L_h} at landing. This can be higher because of a more aft c.g. or due to a higher lift generated by the wing. Also, if the tail length would decrease, the elevator would have to increase. This would mean that the elevator would have to run across the whole horizontal tail or that the chord length must increase.

A snowball effect can be spotted here. It is of utmost importance to therefore validate the design with a wind tunnel as soon as a prototype is made.

8.6. Verification and validation

Verification and validation is an important step in order to determine the feasibility of the design. The verification process is used for the designer to determine whether the model at use works as expected and the validation ensures the results obtained are correct.

The horizontal tail volume was verified by using unit tests and hand calculations to check whether the MATLAB scripts were correctly programmed. Validation was done using XFLR5, and the calculations were validated to be correct. Also, the tail volume could be validated by comparing this with reference values from [26] and [43] and differed only by 0.07 from these reference values.

The dynamic stability was done using XFLR5, and will be verified in the future by theoretical values. The model can be validated further using a prototype UAV and record the responses for the various eigenmotions, and compare these to the outcomes of the outcomes of the models.

The control surface sizing were all verified using sensitivity analyses in combination with unit tests. Unit tests were performed by segmenting the MATLAB scripts and testing each segment individually. Sensitivity tests were then carried out on each unit by varying the input values and verifying the output varied as expected.

In order to then validate the control surfaces, reference data from [27] was used. The outcome was compared to historical data and allowed the validation of realistic values.

Moreover, as it has been mentioned in subsection 8.3.2, XFLR5 has been used to verify the CL_{max} of the wing. A 3D model has been made in XFLR5 which allowed for the verification of the equation. Furthermore, XFLR5 has been validated in section 7.8; thereby validating the model.

Chapter 9: Structural Design

This chapter discusses the structural design of the UAV. In order to meet requirement **REQ.U.SYS.1** and to achieve a sufficient performance, a lightweight structure has to be designed that can be manufactured with ease and can withstand the heavy loads that take place during heavy turns and high wind conditions.

First of all, the maximum load factors occurring during the mission are determined in section 9.1. These are of crucial importance to the structural design of the UAV. Secondly, a discrete structural model is constructed that is used to design the main wing, horizontal- and vertical stabilisers and is explained in section 9.2. The model allows the optimisation of skin thicknesses and web dimensions. When this vital model is explained, the design of the main wing, horizontal and vertical tail is discussed in section 9.4 and section 9.5. These are the main focus of the structural design. Next, the booms and fuselage are designed to achieve a fully integral design in section 9.6 and section 9.7. This concludes the structural design of the individual components. In order to confidently present this design as trustworthy results, a thorough verification is performed on the used models in section 9.9. Then, the strategy of assembly and disassembly of the UAV is explained in section 10.1, which is vital to the transportability of the product. Also, a preliminary production plan is designed in section 10.2. Finally, a sensitivity analysis on the used assumptions and different design inputs is provided in section 9.8, which concludes the structural design of the UAV.

9.1. Load Identification

The first step in designing the structure is identifying the loads that will occur during the lifetime of the UAV. The limit loads are defined as the loads at which the structure shall not interfere with the safe operation of the UAV. Ultimate loads are the design loads, at which the structure shall fail. The ultimate loads are equal to the limit loads multiplied by a safety factor. In general aviation this safety factor is 1.5 [46] for manned aeroplanes and 1.25 for drone design [29]. The minimum values the UAV has to be designed for are derived from FAA regulations Sec 23.337 [50], which require the usage of a minimum limit load factor of 4.4 and -1.8. These limit loads translate to ultimate load factors of 5.5 and -2.2 respectively, however certain in-flight scenarios have to be analysed to determine the highest limit load during the operation of the aircraft.

Air loads

The largest air loads on the structure happen during the following manoeuvres and scenarios:
Level turn: The level turn loads are driven by the obstacle avoidance requirement due to the fact that the UAV has to be able to make a turn with a certain radius at maximum velocity. The maximum velocity that the UAV will fly at during its operation is limited by regulations, however many sources, such as [29] define the maximum velocity using the dive speed, which is defined as 25% higher than the cruise speed. The load factor during a turn can be calculated using eq. (9.1) [46].

$$n_{turn} = \sqrt{\left(\frac{V_D^2}{R \cdot g}\right)^2 + 1} \tag{9.1}$$

Where V_D is the mentioned dive speed, R is the turn radius and g is the gravitational acceleration. For a maximum speed of 43 $m\,s^{-1}$ and a turn radius of 65 m the resulting load factor is 3.1. In order to reach a manageable ultimate load factor, iterations have been performed such that the turn radius still complies with the obstacle avoidance requirement **REQ.U.SYS.22**.

Steady pull-out: The steady pull-out loads are derived from a scenario in which the UAV is pulling up from a dive, when it is not yet at its lowest point. Equation (9.2) is used to determine the pitch up load factor [46].

$$n_{pull} = \frac{V_D^2}{R \cdot g} + 1 \tag{9.2}$$

The same turn radius is used for the pitch up manoeuvre as for the level turn, which results in a load factor of 3.9.

Vertical gust: Since the UAV is designed to be able to fly at high wind conditions, the gusts that occur at 8 Bft winds cause high load factors on the UAV. The maximum gust speed corresponding to those conditions is 9.4 $m\,s^{-1}$, which was evaluated during the mid-term phase using [39]. In chapter 6, fig. 6.1 shows the gust loading for different airspeed conditions based on eq. (6.2). A similar graph can be constructed using the aerodynamic values generated in chapter 7, such as C_{L_α} and the surface area. At a dive speed of 43 $m\,s^{-1}$ mentioned above, the resulting gust load factor is 2.5.

Gust loading during turn: A scenario that can occur during high wind conditions is a vertical gust during a level turn. For simplicity it is assumed to be a superposition of the two load factors previously mentioned. In high wind conditions this event is likely to occur due to the constant presence of gusts. Therefore, it is decided to design the structure for the resulting sum of the gust load factor and the level turn factor. This results in an ultimate load of 7 g, while taking a safety factor of 1.25 into account.

Other loads

Additional loads occur during launch and landing which are derived both from the flight characteristics of the UAV and from the design of the launch catapult and the net landing. The extra loads that have to be accounted for are the pull-back of the emergency parachute and the impact the UAV experiences when it hits the ground.

Launch: For take-off a catapult is chosen to launch the UAV, which results in inertial loads due to the acceleration of the UAV. Section 12.2 discusses the chosen catapult and the load factor associated with the acceleration which is 5.46 g and results in an ultimate load factor of 6.8 g.

Net landing: For the ground station a net is designed in which the UAV lands. This results in a compressive load factor along the X-axis due the deceleration of the UAV. Sub-subsection 12.1.1.3 deals with the load analysis of landing in the net. The result is a deceleration of 7 g, which means an ultimate load factor 8.75 g along the X-axis.

Parachute pullback: Since a parachute is included in the UAV for emergency situations, the force that acts on the UAV can be calculated using the parameters of the chosen parachute. The force of the parachute deployment can be calculated using eq. (9.3) [37]:

$$F = 0.5 \cdot \rho \cdot V_D^2 \cdot S_{\text{par}} \cdot C_D \cdot C_x \cdot X \tag{9.3}$$

Where V_D is the dive speed mentioned above, S_{par} is the surface area of the parachute and C_D is the drag coefficient, which is dependent on the type of parachute. The surface area of the chosen parachute is 10.5 m and drag coefficient for an annular parachute is 0.85 [37]. C_x is the shock load also dependent on the type of parachute and estimated to be 1.4. The factor X is a force reduction coefficient dependent on the UAV weight, parachute drag and surface area and according to [37] is estimated to be 0.08. This results in a force of 1,130 N, which corresponds to an ultimate load factor of 5.8. However, this load factor is not considered as a driving load case due to the fact that the force is a point load. Instead, reinforcements are added (explained in subsection 9.7.2)near the attachment point, where the point load acts on the primary structure of the fuselage.

Parachute impact: A possible impact load on the airframe occurs when the parachute is deployed and the UAV hits the ground. The parachute manufacturer provided the vertical speed of descent in case of deployment for a given weight, which can be used to estimate the force of impact.[41] The speed of descent is 4.22 m s^{-1} for a weight of 25 kg. In order to estimate the load factor resulting from the impact, a stopping distance has to be estimated. Since the parachute is mounted at the nose, the impact energy of 223 J is absorbed by the tail and boom structure, in order to protect the engine, electronics and most importantly the payload.

Assuming a deforming empennage hitting the ground, a 0.2 m stopping distance is a realistic value for the impact, which results in a limit load factor of 5.5 g, resulting in an ultimate load factor of 6.9 along the X-axis.

To summarise, the ultimate load factors along the Z-axis are +7 g for positive loading and -2.2 g for negative loading. The former is derived from a gust during a level turn. The latter is a requirement posed by regulations. Along the X-axis the ultimate load factor is 8.75 g, however the fuselage structure has to account for the force posed by the parachute deployment. The forces acting along the Y-axis are not used for sizing because they do not pose driving requirements on the structure, however they are accounted for to make sure no failure occurs.

9.2. Discretisation and assumptions

In order to design the main wing and the tail a model is created based on the skin panel method as can be seen in [29]. In this section the discrete model of the main wing is discussed and a list is shown which includes all assumptions made related to both the geometry and the process of determining the stresses in the structure.

The following coordinate system is used: the X-axis runs along the length of the fuselage pointing towards the nose, the Y-axis runs along the wing span and points towards the tip of the right wing and the Z-axis denotes height and is points upwards. The X-position of the origin is at the trailing edge of the root chord. The Y-position of the origin is at the centre of the fuselage. The Z-position of the origin is the centre line of the aerofoil, due to the fact that aerofoil data files are utilised. The coordinate system is shown in fig. 9.1.

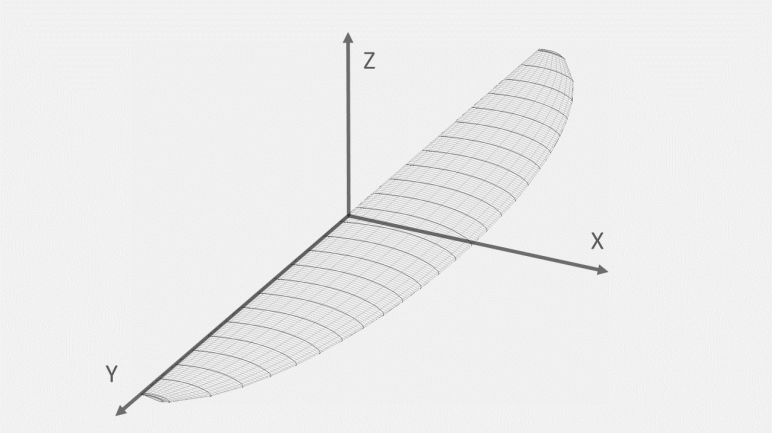

Figure 9.1: Coordinate system used in the structural model.

[41] http://fruitychutes.com/help_for_parachutes/parachute-descent-rate-calculator?term=IFC-144-S&weight=64

The wing is discretised along the chord and nodes are created which describe the contour of the aerofoil. The node positions correspond to the data of the chosen aerofoils: $FX63110$ for the main wing and $NACA63-018$ for the tail. The node positions are adjusted for the corresponding chord length along the span. Then, so-called panels are created to model the skin of the wing. Each panel is positioned between two nodes and has a length equal to the distance between the adjacent nodes. This is useful for modelling the geometry and also for applying different thicknesses to different panels.

Next, cross-section segments are created which contain the collection of panels at the corresponding location along the span of the wing. This allows the evaluation of cross-sectional properties along the wing such as cross-sectional area, centroid position and moments of inertia. It also enables the application of internal loads to any given cross-section. It is chosen to use 200 segments to ensure a sufficiently fine resolution while keeping computational times manageable.

One of the most important characteristics of the model is that the panels on the top part of the wing have a different thickness than the panels on the bottom part. Also, these thicknesses are allowed to vary along the span for every cross-section. Varying the thickness enables weight optimisation due to the fact that internal loads are expected to decrease towards the tip and the driving design factors are expected to be less critical in the bottom part of the skin due to different load factors in the positive and negative direction along the Z-axis. This is further elaborated on in subsection 9.4.2.

Optimising the wing structure for weight is a complex problem and requires several assumptions to be made both about the discretisation and the way the structure carries the loads. These assumptions can be seen in the following list. The impact of these assumptions is discussed in section 9.8.

- **A.1** The fuselage width at the wing root is 0.10 m and the wing is clamped at the fuselage.
- **A.2** The wing is cut into 200 segments with an equal width. Segments falling within the width of the fuselage are disregarded.
- **A.3** The panel thickness is constant.
- **A.4** Panels do not have an inclination w.r.t the X-axis.
- **A.5** I_{xz} is assumed to be zero.
- **A.6** The centroid of the cross-section does not change during the thickness optimisation algorithm.
- **A.7** Only Steiner's terms are used to evaluate moments of inertia during the thickness optimisation algorithm.
- **A.8** The skin only takes shear flow due to torsion. The shear webs carry all the shear loading.
- **A.9** Thin plate buckling is assumed for regions enclosed between webs.
- **A.10** Minimum allowed thickness is 0.4 mm due to manufacturing constraints.
- **A.11** Minimum allowed step-wise variation in thickness is 0.1 mm due to manufacturing constraints.
- **A.12** The lift distribution of the main wing is assumed to be fully elliptical.
- **A.13** The thickness optimisation algorithm does not take the effect of the normal force (due to the boom) into account.
- **A.14** The shear webs are assumed to be rectangular, even though flanges have to be added for attachment purposes.
- **A.15** The torsion caused by the boom is applied to the entire cross-section of the main wing.
- **A.16** For deflection calculations of the booms, the moment of inertia of the booms is considered to be constant at its minimum value.
- **A.17** The fuselage stress modes are assumed to be constant at its maximum value from nose to engine.

9.3. Material selection

The choice of material is a diverse decisions to make when designing the airframe. The available options for the lightweight structure are the use of aluminium, composites or the implementation of a honeycomb structure. Simplicity and the ease of manufacturing are highly prioritised, therefore even though composites can provide options resulting in less weight, aluminium alloys provide a sufficiently strong structure while meeting the mass budget for the airframe.

The chosen aluminium alloy is the aluminium 6061-T6, which is used for producing all graphs and diagrams in this chapter.[42]

9.4. Main wing

Designing a structurally reliable main wing poses one of the hardest challenges to this UAV's design, because of the large required wing surface area to take-off and land at low density conditions and the hostile wind conditions. Therefore, the structure is required to properly deal with the forces and moments induced by the large wing surface. The first step is designing the wing for bending (around X-axis) and shear (along Z-axis) as these are expected to be critical. Then, load resistance in other axes is checked and possible required reinforcements are incorporated in the structural design.

9.4.1. Loading Diagrams

To design the structure of the main wing, the shear and bending moments are identified along the span. This is done by estimating the lift distribution over the wing, creating the full load diagram of the wing (fig. 9.2a), producing a shear diagram of the wing (fig. 9.2b) and ultimately generating a moment diagram from this shear diagram (fig. 9.2c). These diagrams identify the internal shear and moment loads discretely along span-wise positions of the main wing.

[42] http://asm.matweb.com/search/SpecificMaterial.asp?bassnum=ma6061t6

The wing loading for bending consists of the lift distribution, the weight relief and the lift of the horizontal tail transferred via the twin booms. Also, the lift of the vertical tail transferred via the twin booms and a moment of the vertical tail transferred by the twin booms are considered in the loading diagrams. Within these five contributors, the lift distribution of wing is the most dominant. Yet, the other contributors should not be neglected and will be analysed to fully ensure structural integrity.

First, the lift contribution per panel of an elliptical lift distribution is analysed (see assumption **A.12**). It is given by eq. (9.4) [29]:

$$L(k) = L_{max} \cdot \frac{dy_{seg}(j)}{b} \cdot \frac{4}{\pi} \cdot \sqrt{1 - \left(\frac{2 \cdot y(j)}{b}\right)^2} \tag{9.4}$$

Equation (9.4) gives the lift distribution of an elliptical wing based on the maximum lift the entire wing generates. Knowing the lift contribution, the other four load distributions remain to be analysed. The lift of the horizontal tail transferred via the booms equals the maximum lift generated by the horizontal tail, which includes the same maximum load factor as the main wing. In this extreme condition, the horizontal tail lift equals 127 N: 63 N per boom attachment. This is visible as the load peak in fig. 9.2a. The horizontal force of the vertical tail transferred via the boom follows from the maximum horizontal gust and equals 32.6 N per vertical tail, resulting in the same force per boom attachment. This force is added when compression and tension in the skin is analysed via eq. (9.5). Also, since the horizontal and vertical tail act at a distance of 1.5 m from the attachment of the booms to the main wing, two additional moments are present. The moment about the Y-axis results in a torque on the main wing, this contribution can be seen at the boom attachment in fig. 9.2d. The moment about the X-axis is further analysed in subsection 9.4.5. Finally, the mass of the structure results in a weight relief, this weight relief initially is approximated and is than iterated several times, inserting the optimal thickness configuration found in subsection 9.4.2.

The wing loading diagram along the span is given in fig. 9.2a, the corresponding shear diagram is given in fig. 9.2b and the corresponding moment diagram is given in fig. 9.2c. Also, the torsion is given in fig. 9.2d. It should be noted that negative loads are only shown in the moment diagram. This is because the negative loads only pose structural requirements in bending, when negative loading could result in buckling of the bottom half of the wing. Shear and torsion are significantly more critical in positive loading, which is why only one graph is present in these diagrams. This graph corresponds to the positive loading case.

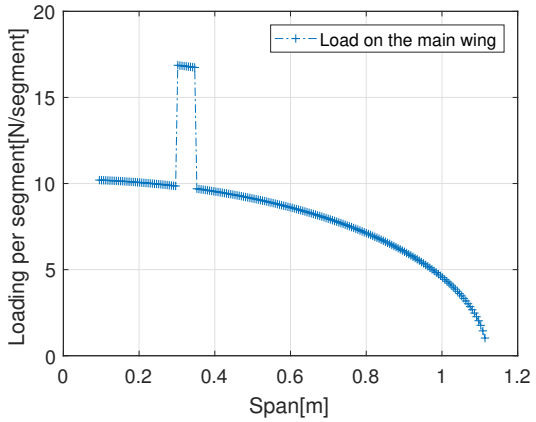

(a) Loading on the main wing varied by the span.

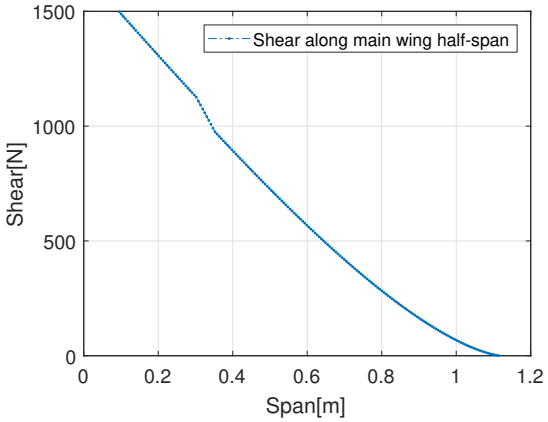

(b) Shear along main wing span.

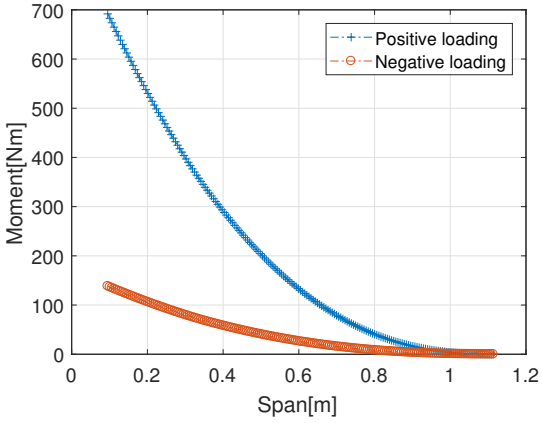

(c) Bending moment around X-axis along main wing span.

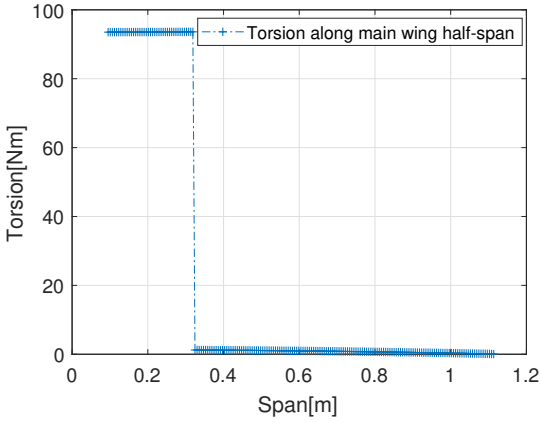

(d) Torsion around Y-axis along main wing span.

Figure 9.2: Main wing loading, shear, moment and torsion diagrams along the main wing span.

9.4.2. Bending and thickness optimisation

In the most common idealised structural models it is assumed that the skin carries only shear and not bending loads [46], however in order to achieve the lowest possible weight the skin thickness has to be optimised for both. As mentioned in section 9.2 the thickness is allowed to vary along the span and it is allowed to vary between the top and bottom part of the wing. This is necessary to ensure that the structural weight is constrained.

In general, bending causes normal stresses in the structure. Positive loading as shown in fig. 9.2c causes compression in the top panels and tension in the bottom panels, whereas the negative loading causes compression in the bottom panels and tension in the top panels. The formula describing the normal stress due to a bending moment is shown in eq. (9.5).

$$\sigma_{y_i} = \frac{M_x(z_i \cdot I_{zz} - x_i \cdot I_{xz})}{I_{xx}I_{zz} - I_{xz}^2} + \frac{M_z(x_i \cdot I_{xx} - z_i \cdot I_{xz})}{I_{xx}I_{zz} - I_{xz}^2} + \frac{P}{A} \tag{9.5}$$

Where I_{xx}, I_{zz} and I_{xz} refer to moments of inertia, M_x and M_z are the internal bending moments acting on a given cross-section, P is the axial load and A is the cross-sectional area. The subscript i denotes the ith panel in a cross-section, thus x_i and z_i denote the ith panel's position with respect to the centroid of the cross-section.

Moreover, if assumption **A.5** holds, then eq. (9.5) simplifies to eq. (9.6). Also, the axial load term in eq. (9.5) is neglected, due to its relatively small contribution.

$$\sigma_{y_i} = \frac{M_x z_i}{I_{xx}} + \frac{M_z x_i}{I_{zz}} \tag{9.6}$$

Designing the thickness for tension means making sure the normal stresses are kept below the yield stress of the chosen material. This requirement is easily satisfied as the stresses for minimum thickness are significantly below the yield stress of commonly used metals and composites. However, one also has to analyse the panels in compression due to the fact that buckling can occur at a much lower stress than the yield strength of the material.

As mentioned in assumption **A.9**, the wing skin buckling is approximated using a thin-plate buckling model based on [46]. The formula describing thin-plate buckling is shown in eq. (9.7).

$$\sigma_{crit} = \left(\frac{t}{b}\right)^2 \frac{K \cdot \pi^2 \cdot E}{12 \cdot \left(1 - V_e^2\right)} \tag{9.7}$$

Where t is the thickness of the plate, b is the short dimension of the plate, K is the buckling coefficient assumed to be equal to 8 [46], E is the Young's modulus of the chosen material and V_e is the Poisson ratio of the chosen material. The factor that has the largest impact on the critical buckling stress is the short dimension of the thin plate b, therefore the largest benefit of having two webs is the fact that they decrease b along the entire span of the wing. The other major factor is the panel thickness which is the design variable to be determined.

Another failure mode that can occur is column buckling. The governing equation to determine critical buckling stress for a beam fixed in one end (assumption **A.1**) is shown in eq. (9.8):

$$\sigma_{crit} = \frac{n^2 \pi^2 EI}{L^2 A} \tag{9.8}$$

Where n^2 depends on the mode of buckling and is equal to 0.25 for one end being clamped.[43] I is the moment of inertia with respect to the axis around which buckling occurs, and E is the Young's modulus of the chosen material. L and A are the length of the column and cross-sectional area of the column respectively.

In order to optimise the structure it is desired that when the ultimate loads are applied to the wing, buckling also occurs. This means that both the bottom and top thickness can be determined to satisfy these conditions. The thickness optimisation algorithm uses thin-plate buckling as a driving factor due to the fact that the critical column buckling stress is significantly higher along the entire span. Combining eq. (9.6) and eq. (9.7) for the top and bottom panels results in the following system of equations:

$$\begin{aligned} \left(\frac{t_{top}}{b_{top}}\right)^2 \frac{K \cdot \pi^2 \cdot E}{12 \cdot \left(1 - V_e^2\right)} &= \frac{M_{x_{top}} z_{max_{top}}}{I_{xx}(t_{top}, t_{bot})} \\ \left(\frac{t_{bot}}{b_{bot}}\right)^2 \frac{K \cdot \pi^2 \cdot E}{12 \cdot \left(1 - V_e^2\right)} &= \frac{M_{x_{bot}} z_{max_{bot}}}{I_{xx}(t_{top}, t_{bot})} \end{aligned} \tag{9.9}$$

Where t_{top} and t_{bot} are the thicknesses of the top and bottom panels respectively and I_{xx} is shown to be a function of both thicknesses. The locations $z_{max_{top}}$ and $z_{max_{bot}}$ are determined with respect to the centroid separately for top and bottom panels, as well. Using assumption **A.6**, this means the centroid is only updated once the thicknesses are determined, therefore for the solution an initial guess of top and bottom thickness ratio is determined. Also, the bending-term about the Z-axis is neglected due to the small magnitude of the moment M_z and due to the fact that moment of inertia about the Z-axis is

[43] https://ocw.mit.edu/courses/aeronautics-and-astronautics/16-01-unified-engineering-i-ii-iii-iv-fall-2005-spring-2006/materials-structures/gm12_13notes.pdf

much larger for the cross-section. Lastly, $M_{x_{top}}$ and $M_{x_{bot}}$ have to be evaluated separately due to the fact that compression conditions are analysed for both sides.

From eq. (9.9), the following system of equations can be derived by rearranging for t_{top} and t_{bot}:

$$\begin{aligned} t_{top}^3 \cdot A + t_{top}^2 t_{bot} \cdot B &= C \\ t_{bot}^2 t_{top} \cdot A + t_{bot}^2 \cdot B &= D \end{aligned} \tag{9.10}$$

In eq. (9.10), A and B are the thickness normalised Steiner's terms of the top and bottom panels respectively (assumption **A.7**) shown in eq. (9.11) and eq. (9.12). The terms C and D are shown in eq. (9.13) and eq. (9.14):

$$A = \sum_{i}^{n_{panels}} B_{top_i} \cdot {z_{top_i}}^2 \tag{9.11}$$

$$B = \sum_{i}^{n_{panels}} B_{bot_i} \cdot z_{bot_i}^2 \tag{9.12}$$

$$C = \frac{12 M_{x_{top}} z_{max_{top}} b_{top}^2 \left(1 - V_e^2\right)}{k \pi^2 E} \tag{9.13}$$

$$D = \frac{12 M_{x_{bot}} z_{max_{bot}} b_{bot}^2 \left(1 - V_e^2\right)}{k \pi^2 E} \tag{9.14}$$

In eq. (9.11) and eq. (9.12), B_{top} and B_{bot} represent to the length of each panel. Since eq. (9.10) is a non-linear system, a numerical solver is implemented that determines the optimum combination of top and bottom thicknesses for a given cross-section.

The optimised thickness for bending can be seen in fig. 9.3a. Adding the manufacturing constraints of assumption **A.11**, this results in the step-wise thickness plot in fig. 9.3a. Figure 9.3b shows stresses corresponding to the optimum thickness, whereas fig. 9.3c shows the stresses after taking the step-wise thickness into account. One can observe that for the top and bottom side of the wing the critical buckling stresses marginally exceed the stresses present in the structure.

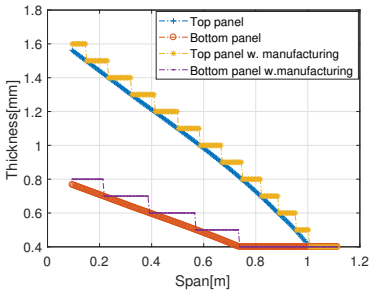

(a) Thickness optimisation of the skin.

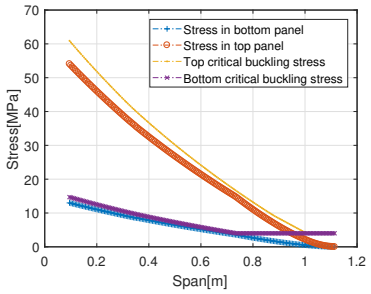

(b) Stress analysis of the skin

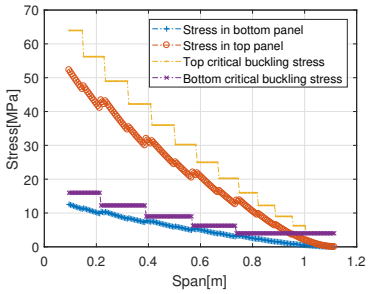

(c) Stress analysis of the skin after manufacturing discontinuities.

Figure 9.3: Skin thickness and stress diagrams of the main wing.

9.4.3. Shear

In order to design for shear the webs have to be sized based on assumption **A.8** and the skin has to be checked for its shear bearing capability. Two shear webs are placed that run along the span of the wing. The rear web location along the X-axis is driven by the flap chord dimensions, therefore it is placed at 30% of the root chord and kept at a constant distance from the trailing edge. The front web location is driven by the fact that the short dimension for thin plate buckling has to be minimised. Therefore the front web is placed at 65% of the root chord at a constant distance from the trailing edge. Due to the elliptical shaped leading edge both of the webs end at the points where the chord becomes smaller than the X-location of the webs from the trailing edge. The height of the webs is limited by the height of the aerofoil at different span locations. Equation (9.15) is the governing equation for shear flow in a cross-section under a given shear load [46].

$$q_s = -\frac{I_{xx} S_x - I_{xy} S_y}{I_{xx} I_{yy} - I_{xy}^2} \int_0^s t x ds - \frac{I_{yy} S_y - I_{xy} S_x}{I_{xx} I_{yy} - I_{xy}^2} \int_0^s t y ds \tag{9.15}$$

Equation (9.15) is applicable to a cross-section in the X-Y-plane, where S_x and S_y are the shear loads, I_{xx}, I_{yy}, I_{xy} are the moments of inertia and t is the thickness along a length of the integral.

For simplicity a rectangular shape is assumed for the shear webs as stated in assumption **A.14**. This allows the use of eq. (9.16) for a rectangular shape along with the assumption that the webs take all the shear caused by the direct shear loading. Also, shear loading in only one direction is used.

$$\tau_{max} = \frac{3V_z}{2t_{web}h_{web}} \tag{9.16}$$

Where V_z is the internal shear loading, h_{web} is the height of the web at the given cross-section, and t_{web} is the designed thickness. The required thickness can be determined, if one substitutes the shear strength of the material for τ. The required thickness for shear loading in combination with the thickness required by eq. (9.8) and eq. (9.17)(discussed in subsection 9.4.4) is calculated. However, the required resulting thicknesses are not allowed by manufacturing constraints. Therefore, the resulting web thickness is set to a constant 1 mm along the entire wing span for both shear webs in order to ensure sufficient stiffness.

For the mentioned web thickness, the normal stresses are calculated at the most critical positions. The normal stresses in the webs can be seen in fig. 9.4a. The maximum shear stresses are evaluated not for only for shear caused by direct shear loading, but also for shear caused by torsion mentioned in subsection 9.4.4. The maximum shear stress can be seen in fig. 9.4b.

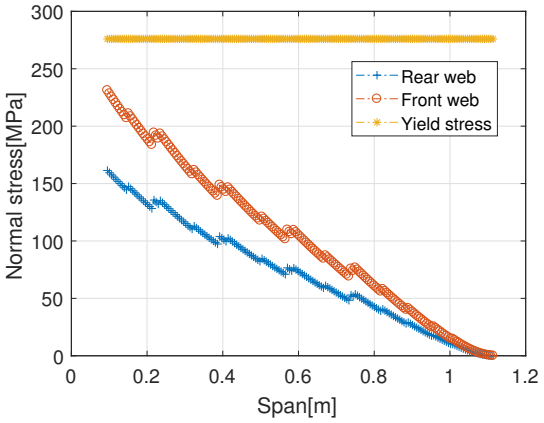

(a) Maximum normal stress in the shear webs.

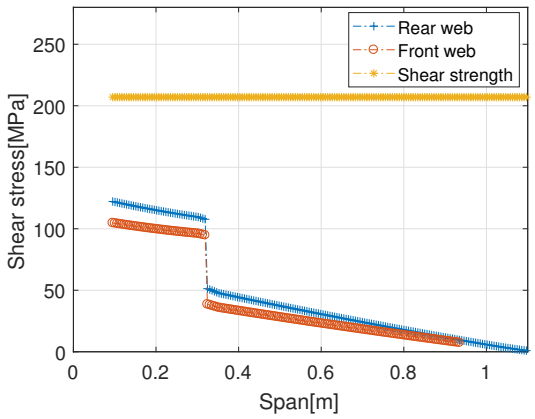

(b) Maximum shear stresses in the shear webs.

Figure 9.4: Normal and shear stresses in the main wing webs.

In order to ensure no failure occurs in the webs, they are checked for the Von Mises stress condition. The Von Mises stress in the webs is calculated using eq. (9.19)(see section subsection 9.4.4). The resulting Von Mises stress is shown in fig. 9.5a, and as can be seen the stress in the front web exceeds the yield stress of the material at the root up to about 140 mm from the centre of the fuselage. To achieve stresses below the yield stress the thickness of the front web has to be increased. Using several iterations the required thickness increment was determined. After an additional 0.2 mm thickness was added at the critical location the Von Mises stress was determined, which can be seen in fig. 9.5b.

It has to be noted that the Von Mises stress in the shear webs is evaluated using the maximum normal stress and the maximum shear stress along the height of the web, even though the positions of these critical stress do not coincide. In reality the maximum normal stress occurs at the edge of the webs, meanwhile the maximum shear stress occurs at the centroid of the web. However, this is not taken into account for simplicity, due to the fact that the result adds additional safety to the performance of the structure and only increases its weight marginally.

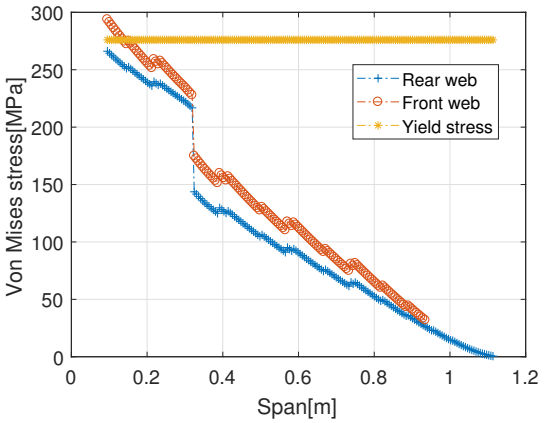

(a) Von Mises stress within the web without reinforcement.

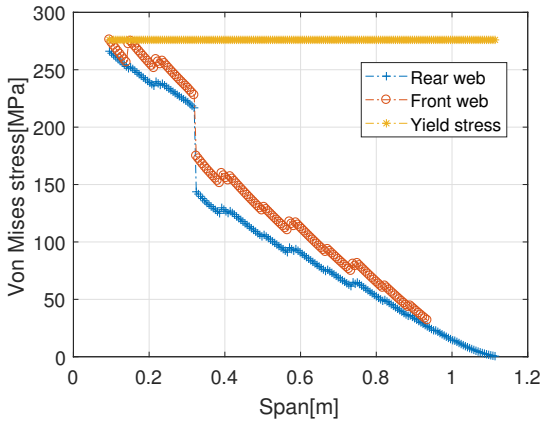

(b) Web Von Mises stress with additional thickness increment.

Figure 9.5: Von Mises stress within the webs with and without thickness increment.

9.4.4. Torsion & Von Mises

As can be seen in fig. 9.2d, most of the torsion originates from the presence of the boom connection. Additionally, there is a small contribution of the misalignment between shear and aerodynamic centres. The torsional load bearing capabilities of the structure are the result of the fact that the two webs create a closed section that performs well against torsion. In order to simplify the model it is assumed that the wing box in the centre of the cross-section takes all the torsional shear flow. This constant torsional shear flow is present in both shear webs and the top and bottom skin panels. The constant shear flow due to torsion can be calculated using eq. (9.17).

$$q_{s,0} = \frac{T}{2A_{enc}} \tag{9.17}$$

Where T is the torsion applied to a given cross-section and A_{enc} is the enclosed area of the wing section between the two shear webs. The shear stress present due to the shear flow can be obtained by dividing with the present skin thickness. This relation can be used to evaluate required thickness due to torsion by using the shear strength of the material.

In order the make sure failure does not occur in the skin, the shear stress due to the shear flow is determined, which means the Von Mises yield criterion can be obtained(eq. (9.18)).

$$Y = \sqrt{\frac{1}{2}\left[(\sigma_x-\sigma_y)^2+(\sigma_y-\sigma_z)^2+(\sigma_z-\sigma_x)^2\right]+3\tau_{xy}^2+3\tau_{yz}^2+3\tau_{xz}^2} \tag{9.18}$$

Since only normal stress along the Y-axis and shear stress along the XZ-plane is taken into account eq. (9.18) can be simplified to:

$$Y = \sqrt{\sigma_y^2+3\tau_{xz}^2} \tag{9.19}$$

This yield criterion analysis is shown in fig. 9.6b. From these graphs, it follows that the torsion, despite being significant does not cause the structure to fail.

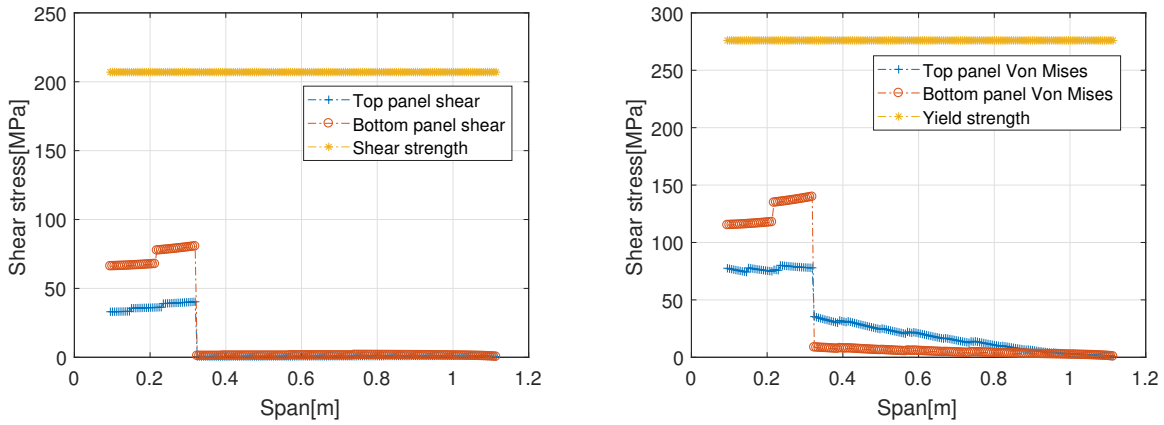

(a) Shear stress present in main wing skin

(b) Von Mises stress present in main wing skin

Figure 9.6: Torsional shear stress design.

9.4.5. Other forces and moments

So far, the structural analysis of the main wing has taken the forces in the Z- and Y-direction and moments around the X- and Y-axis into account. As such, the forces in the Y-direction, and the moments around the Z-axis seem not to be analysed. These forces and moments do occur however, especially during the strong acceleration and deceleration during take-off and landing. It is decided not to size the main wing for these forces as the moment of inertia around the Z-axis and the amount of material present on the X-axis of the wing are significantly larger than the X-axis moment of inertia and the Z-axis amount of material. Yet, a check for failure in bending or shear of the main wing in these directions is required to ensure full structural integrity of the main wing. With the current design thicknesses, stringers and webs, the maximum normal stress due to bending can be obtained using eq. (9.5).

In applying eq. (9.5), M_z follows from a point load transferred via the fuselage during take-off and landing. It is found, that at all points along the span-wise location of the wing, the σ_y during these loading conditions is significantly smaller than during regular flight, as was expected. This is primarily because of the I_{zz} which is significantly larger than the I_{xx} at every location along the span. As a reference, at the root, I_{zz} equals $1.411 \cdot 10^{-5}$ whereas the I_{xx} equals $2.795 \cdot 10^{-7}$.

Using the material defined in section 9.3, the final mass of the main wing including actuator mechanisms and the structural weight is estimated to be 4.035 kg.

9.5. Tail

The structural tail design is relatively similar to the main wing design and the same method is used. First, the lift distribution is analysed, from which a loading diagram is constructed. Next, the shear and moment diagrams are created. Although, the tail loading analysis is similar to the main wing load case, it is significantly less complex. This reduced complexity follows from the absence of bending forces from the boom, which were present in the main wing. Also, the smaller surface area of the horizontal and vertical tail compared to the main wing results in significantly smaller stresses present. Using the same method as during the main wing design, the loading, shear, moment and torsion diagrams are created. Only the internal shear and bending moment diagrams are shown, due to the fact that loading only serves as a tool for creating the shear and moment diagrams and the torsion acting on the tail is negligible.

9.5.1. Loading Diagrams

The loading diagrams of both the horizontal tail and the vertical tail are somewhat straightforward. This has numerous explanations. Yet, the most important one is that, opposed to the main wing, the planform of both the vertical and horizontal tail is fully rectangular. Therefore, the lift distribution is uniform along the span of both the vertical and horizontal tail. This highly convenient planform implies that the vertical and horizontal tail loading cases can be represented as simple beams. The horizontal tail is a beam with uniform loading, clamped at its two edges (the booms). The vertical tail is a beam subject to uniform loading clamped at its root location. From subsection 8.3.4 it follows that the entire vertical tail is required to rotate. In order to be able to freely move the vertical tail without interference of the horizontal tail it is decided place the vertical tail on top of the boom attachment, above the horizontal tail. Hence, the clamp location of the vertical tail is at its bottom. For these simple loading cases, the shear and moment diagrams of the horizontal and vertical tail are represented in fig. 9.7a, fig. 9.7b, fig. 9.7c and fig. 9.7d. The moment diagram of the vertical tail (fig. 9.7d) only consists of one graph since the left and right skin encounter the same maximum moments. The horizontal tail loading diagrams follow from the maximum and minimum load factors of 7 g and -2.2 g, the vertical tail loading diagrams follow from a maximum side gust. The magnitude of these forces have been estimated in subsection 9.4.1 for their effect on the main wing when transferred via the booms.

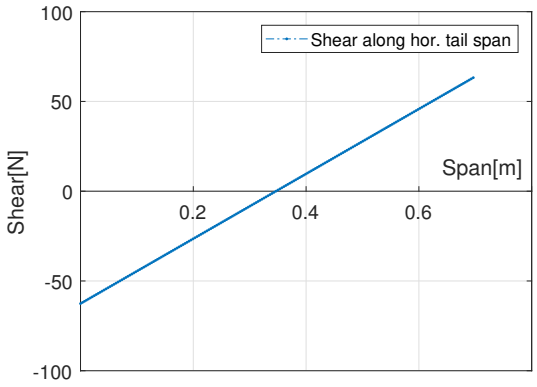

(a) Shear on horizontal tail.

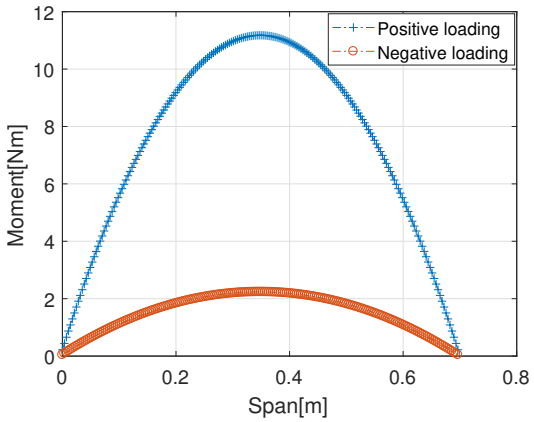

(b) Moment on horizontal tail.

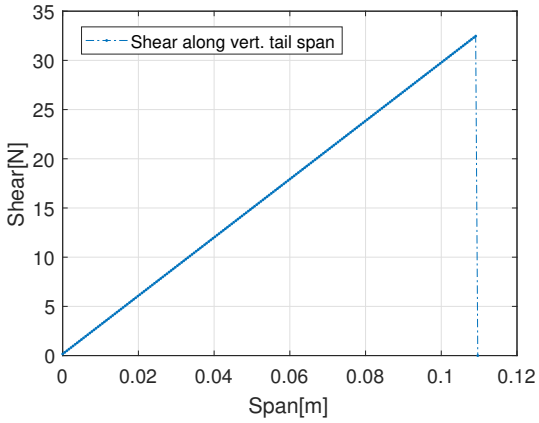

(c) Shear on vertical tail.

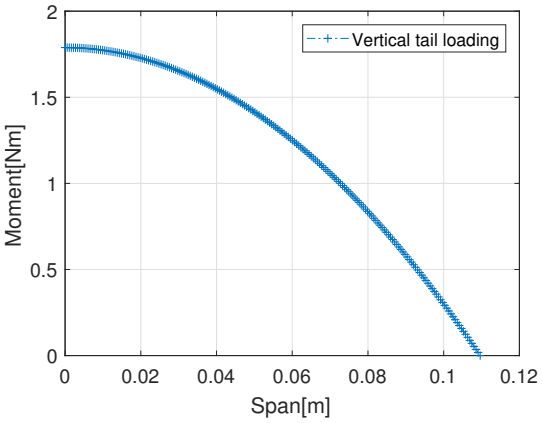

(d) Moment on vertical tail.

Figure 9.7: Shear and moment diagrams of both the horizontal and vertical tails.

9.5.2. Bending

To design the horizontal and vertical tail to withstand the loads identified in subsection 9.5.1, the same approach is used as during the main wing design. Again, a varying skin thickness is used along the span of the horizontal and vertical tail. This skin solely withstands the bending moments. The variation in skin thickness is found by the thickness algorithm applied throughout section 9.4 as seen in eq. (9.10).

Comparing fig. 9.2c with fig. 9.7b and fig. 9.7d the moments present in both the horizontal and vertical tail are significantly smaller than the moments in the main wing, as was expected. Therefore, the result found in fig. 9.8a, fig. 9.8b, fig. 9.9a and fig. 9.9b shows a small thickness required for the horizontal and vertical tail. In fact, the vertical tail is entirely constraint by its minimum manufacturing thickness of 0.4 mm(see assumption **A.10** derived in section 10.2). Because of this, the vertical tail is largely over-designed, which is visible in fig. 9.9b from the large gap between ultimate buckling stress allowed and maximum stress present in the skin. The same goes for the bottom skin of the horizontal tail, with its stress analysis in fig. 9.8b. Only the top skin of the horizontal tail has a varying thickness, reaching a maximum thickness of 0.6 mm.

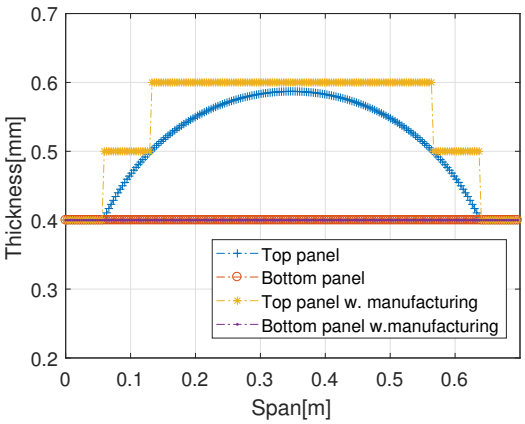

(a) Thickness optimisation of the skin

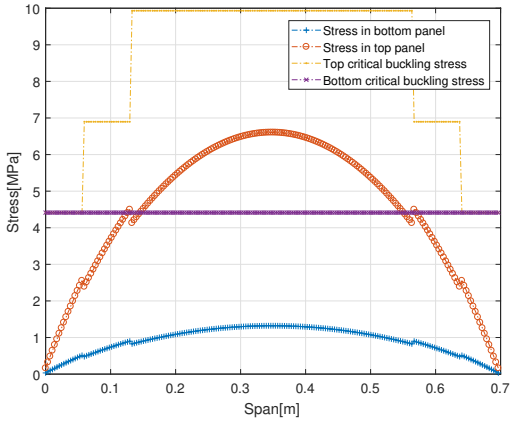

(b) Stress analysis of the skin after manufacturing discontinuities

Figure 9.8: Horizontal tail thickness optimisation with respect to the span.

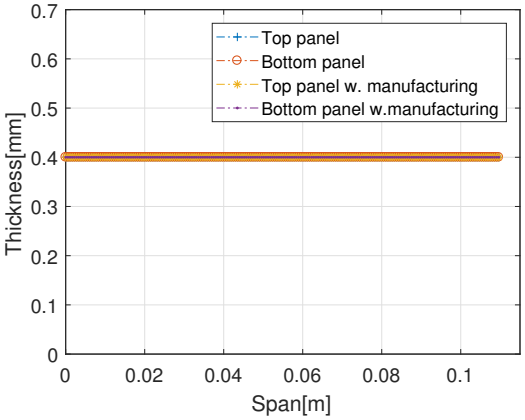

(a) Thickness optimisation of the skin

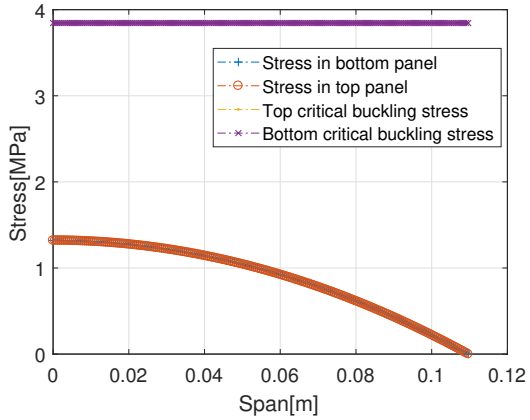

(b) Stress analysis of the skin

Figure 9.9: Vertical tail thickness optimisation with respect to the span.

9.5.3. Shear

As mentioned, for the tail design the same model was used as for the main wing. However slight modifications are made. The largest difference is the fact that only one shear web is included in both the horizontal and vertical tail structure. This choice was made due to the fact that little torsion is present in the loading of the tail and no closed wing box is required. The X-location of the horizontal tail shear web is driven by the elevator chord length, which is at 70% of the chord with respect to the leading edge. The shear web of the vertical tail is located at 25% due to requirements posed by joining the vertical fins to the horizontal stabiliser and the booms.

Similarly to subsection 9.4.3, the height of the webs can be determined by the height of the aerofoil at their respected X-location. Assumptions **A.8** and **A.14** are also held for the tail shear web design, which greatly simplifies sizing the thickness of the webs. The shear loading in both stabilisers is relatively low, as can be seen in fig. 9.7a and fig. 9.7c. Since the evaluation

of torsional shear flow is neglected for the tail, the required thickness is calculated using eq. (9.16). Similarly to the main wing the required thickness is insignificant compared to manufacturing constraints, therefore in order to ensure stiffness a 1 mm thickness is used.

Using the material defined in section 9.3, the final mass of the empennage including actuator mechanisms and the structural weight of both the horizontal and vertical tail is estimated to be 0.350 kg.

9.6. Twin booms

The twin booms need to withstand loads from the vertical tail in the Y-direction and from the horizontal tail in the Z-direction. The ultimate load case occurs when the maximum load factor of 7 g or the minimum load factor of -2.2 g applies in combination with a strong side gust. For structures like these booms, typically bending is the most critical failure mode, therefore the booms are designed to withstand bending. The shear and bending present throughout the boom results from the forces generated by the tail, analysed in subsection 9.4.1. They can be modelled as point loads. Then, the shear and moment diagrams are given by fig. 9.10a and fig. 9.10b respectively. From this point, the analysis will consider one of the two booms. The other boom will have an identical size.

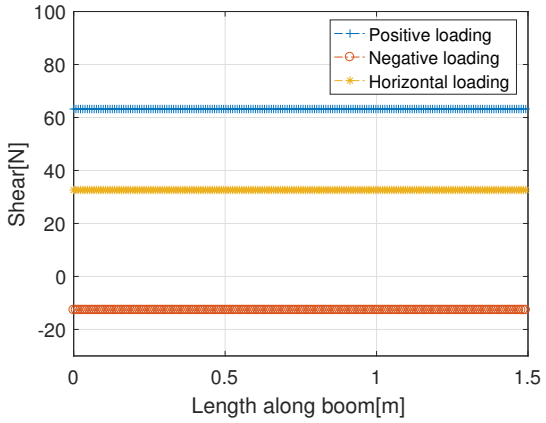

(a) Shear diagram of the boom.

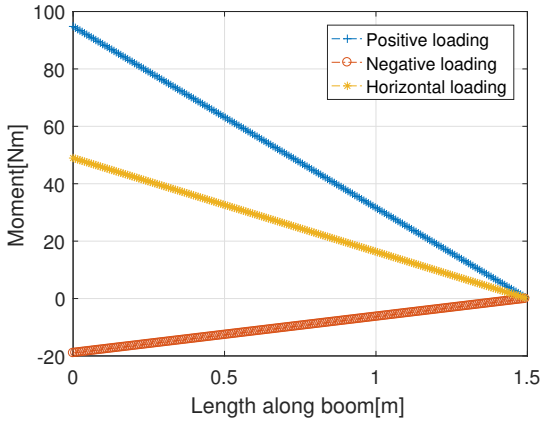

(b) Moment diagram of the boom.

Figure 9.10: Internal shear and bending moment diagrams of the booms.

9.6.1. Boom Sizing

It is expected that bending is more critical than shear, torsion or axial loads. In order to choose a design configuration, different cross sections of the boom are considered. From a pure bending perspective, the design of an I-beam typically is the most optimal. However, closed cross sections have the large advantage that cabling can be pulled through them and that they are rigid for torsion at only a small penalty in effective bending rigidity. Therefore, it is decided to limit the cross sectional possibilities of the booms to rectangular and circular cross sections. Of those, from an aerodynamics perspective, a circular cross section is preferable, which drives the design choice for a circular cross section. As discussed in section 10.1, the booms are required to be detachable to both the wing and the empennage. This gives constraints in the diameter of the circular cross section. Combining structural and assembly interests, it is decided to design for a tapered boom configuration with a diameter of 4 cm at the main wing connection and a diameter of 3 cm at the tail connection.

9.6.2. Bending and thickness optimisation

The booms are optimised for bending, using a varying thickness along the length of the booms. The bending analysis of the booms simplifies with the constant thickness along the cross section. Since a circular cross section is designed, I_{zz} and I_{yy} both equal $\pi r^3 t$. Then, using the bending formula eq. (9.5), the thickness can be optimised. The resulting thickness along the span is shown in fig. 9.11a. The discontinuous plot follows from the manufacturing limits(Assumptions **A.10** and **A.11** discussed in section 10.2). The boom consists of only two distinct thicknesses. Therefore, the penalty for using a constant thickness throughout the booms is little. Because of the increased ease of production of a constant thickness, it is decided to use a constant thickness of 0.5 mm. This thickness corresponds to the stress diagram shown in fig. 9.11b.

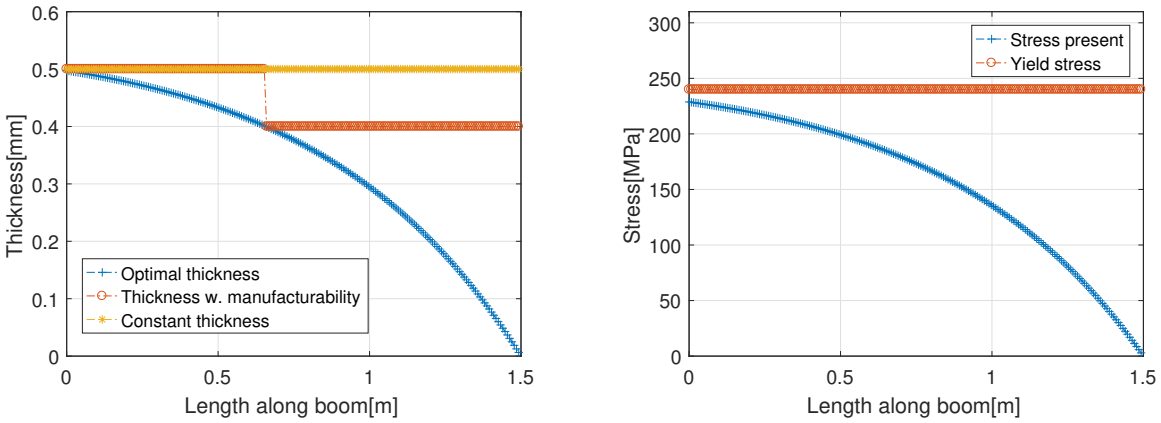

(a) Thickness optimisation of the boom's circular cross section

(b) Bending stress analysis of the boom

Figure 9.11: Horizontal tail thickness optimisation along the length of the boom.

9.6.3. Shear, torsion, buckling and axial loads

Shear, torsion and buckling are other relevant modes that need to be analysed. With the geometry defined in subsection 9.6.2, the maximum shear, torque and axial loads are analysed.

From the general behaviour of structures like this boom, failure in shear is amongst the more unlikely options. Shear forces actually act in both the X and Y-direction. However, for the purpose of proving the insignificance of shear, it will be assumed that it only acts in the z direction. The maximum allowed shear force for single shear failure follows from eq. (9.15) and equals 4,076 N. The actual maximum shear force present follows from fig. 9.10a and equals 63.2 N in the Z-direction and 32.63 N in the Y-direction.

Torsional loads will be very limited in the booms but some will be present from the horizontal tail forces that act at an arm of around 0.05 m. This load creates a maximum torque of 1.78 N m. The minimum torsional rigidity of the structure follows from eq. (9.17) and equals 5.22 N m for the booms. Therefore, torsional failure will not occur.

During regular flight, little axial loads will act on the booms. However, during landing and take-off, the booms will be loaded in compression and tension respectively. For the latter case, only yield failure needs to be analysed. For the former case, buckling failure can occur. The critical force at which the booms yield follows from eq. (9.5) and equals 7,247 N. The critical buckling force follows from eq. (9.8) and equals 578 N at its minimum point near the tail. The maximum axial load occurs when landing takes place at the 8.75 g analysed in section 9.1. However, at this high load factor, the boom is only compressed by the inertia of the empennage and its own weight. Therefore, the maximum axial load present equals only 206 N.

The summary of the failure modes other than bending can be found in table 9.1. Clearly non of these failure modes will be critical for the boom.

Table 9.1: Forces present and forces allowed in booms for different failure modes.

Failure mode	Loads allowed	Maximum loads present
Shear	4,076 [N]	63.2 & 32.63 [N]
Torsion	5.22 [N m]	1.78 [N m]
Column Buckling	578 [N]	206 [N]
Axial	7,247 [N]	206 [N]

9.6.4. Boom displacement

Since the booms are long beams with a relatively small cross-section, they typically have significant deflection due to the applied bending force. This deflection specifically is of major importance at the propeller location, as the booms may never interfere with the propeller. Therefore, it is decided to assess the maximum deflection of the booms in the Y and Z direction at the location of the propeller, which is 22 cm from the trailing edge of the main wing. To achieve a fully accurate estimation of the deflection, the varying moment of inertia due to a varying cross section has to be concerned. However, since this requires a double integral computation, it is decided to use the conservative assumption **A.16**. Consequently, the deflection in the Z and Y direction at the propeller location follow from eq. (9.20).

$$w_{prop} = \frac{F \cdot x_{prop}^3}{3 \cdot E \cdot I_{prop}} \tag{9.20}$$

Where w_{prop} equals the deflection in the Z or Y direction at the propeller, F is the point force due to the tail acting aft of the boom in the Z or Y direction, x_{prop} equals X location of the propeller from the trailing edge of the wing (as deformation only

starts there). E equals the Youngs modulus of the AL6061T6 alloy, I_{prop} equals the moment of inertia at the boom, assumed to be constant from there to the wing root.

From eq. (9.20) the maximum deflection occurring at the propeller equals 0.3 mm in the Z-direction and 0.15 mm in the Y-direction. This clearly forms no problem for possible interference with the propeller, as it has a clearance of over 5 cm from the booms. At the empennage, the boom deflection gets in the order of magnitude of multiple centimetres, however, at that location such large deflections will not have dramatic effects.

Using the aluminium alloy defined in section 9.3 the final mass of both booms is estimated to be 0.382 kg.

9.7. Fuselage

In this section the design of the fuselage is discussed. Since the focus of the structural analysis is the main wing, tails and the booms, the structure of the fuselage is designed in less detail. As such, the focus of the fuselage will be to assure a design that is capable of withstanding all loads, without optimising the design in high detail. For this small fuselage, typically a monocoque structure is used. That is, a structure in which the skin is the main load carrying part. As such, a monocoque design is used for the fuselage. However, local reinforcements are added in order to prevent failure when local loads are present and the skin alone is unable to withstand these loads.

9.7.1. Monocoque design

As any structure, the fuselage is prone to the different fundamental stress modes; bending, shear, axial and torsional loads. In designing the monocoque fuselage, a constant thickness is aimed at. Therefore, instead of constructing shear, moment and torsion diagrams from nose to engine, the maximum values in different stress modes are considered to apply everywhere from nose to tip. These values follow from section 9.1 and include a large safety factor of 2.0. They are given in the second column of table 9.2. Then, with these loads, a constant required skin thickness is given for all stress modes. These results are presented in the third column of table 9.2. The required thickness values are easily computed since a constant thickness is used. Then, the required constant thickness for bending, shear, axial yield, buckling and torsional loads follow from eq. (9.6), eq. (9.16), eq. (9.5), eq. (9.8), eq. (9.17).

Table 9.2: Required thickness of fuselage skin for different stress modes.

Stress Mode	Maximum load present	Required fuselage skin thickness [mm]
Bending	1,500 [N m]	0.052
Shear	2,000 [N]	0.015
Torsion	500 [N m]	0.019
Column Buckling	3,500 [N]	0.001
Axial	3,500 [N]	0.012

As follows from table 9.2, the required thicknesses are all significantly lower than the minimum thickness to avoid impact damage (section 10.2). Therefore, a constant thickness of 0.4 mm is used as the skin of the monocoque structure. However, this thickness is not taking into account high local point loads. These local point loads require structural reinforcements and will be discussed in subsection 9.7.2.

9.7.2. Fuselage reinforcements

There are additional point loads present on the fuselage during the operation of the UAV, which means reinforcements have to be added to certain critical positions within the structure. First, the reinforcement due to the parachute deployment are discussed, as they are the largest contribution to extra weight in the fuselage. Next, the design of the catapult attachment points is explained as well as the skin reinforcements required to transfer the launch loads to the airframe.

Parachute deployment

The largest point load on the primary structure of the fuselage is the force acting due to the deployment of the parachute. Unlike designing for the ultimate load factors used for the rest of the structure, the internal stresses resulting from parachute deployment have to be kept below the yield stress of the material. In case the parachute is deployed the payload and the OBC have to be protected from possible damage, both of which are placed in the nose cone of the UAV.

The maximum force acts right after deployment and was calculated to be 1130 N, for a worst case scenario in which the UAV flies at dive speed, at sea level and the same safety factor of 1.25 is used.

First, it is decided that a vertical plate is added that is able to carry the shear and bending loads that result from the deployment and is the structural element that transfers the loads to the rest of the structure. The best point to attach the parachute string is to the middle of the vertical plate. Since there is a hatch on the top of the UAV nose cone that opens for the deployment, as mentioned in subsection 11.10.2 and assuming the parachute strings are attached to the middle of the vertical plate, one can also assume that when the maximum force is acting on the aircraft the force of the parachute will point directly upwards (along the Z-axis), and a shear force in the opposite direction of flight (along the X-axis) due to the pull of the parachute on the string. Using these assumptions the thickness of the plate can be determined.

In order to determine the thickness, the maximum shear and maximum bending stresses in the plate are determined. The radius of the plate is the same as the radius of the fuselage. The required plate thickness is found using eq. (9.16) at the

midpoint of the plate. For simplicity constant thickness is used, which results in a plate that is 4 mm thick. Using the same material this plate adds a mass of 0.336 kg.

The loads from the parachute attachment point on the plate are transferred to the floor within the nose cone. The moment acting along the floor is the source of the most critical stresses and is therefore the driving criterion. If the thickness of the floor is increased in order to reduce the normal stresses, the mass of the floor overshoots the mass budget of the fuselage, therefore the floor thickness is kept at minimum thickness derived from manufacturing constraints and instead stiffeners are added to carry the normal stresses. The shear stress requirements are met with using the mentioned minimum floor thickness.

In order to size the stiffeners, the required moment of inertia is determined for the highest bending moment acting along the nose floor using eq. (9.6), in which the bending moment acting on the floor is derived from the parachute force acting at the vertical plate attachment. L-shaped stiffeners are chosen due to the fact that they are easily manufactured and easily attached to the floor, and the fact that they do not cause considerable obstruction for the placement of the packed parachute. The stiffeners are added to the top of the floor. The thickness and dimensions of these stiffeners can be determined using an iterative process, during which the mass of the structure is calculated for different combinations of thicknesses and stiffener heights.

The optimum condition is found at having two L-stringers with a constant thickness of 1 mm and with both length dimensions of 10 mm. This results in fig. 9.12a, which shows the stress along the fuselage floor in the nose cone. Figure 9.12b shows the CAD model of the floor and stiffeners, as well as the top part of the vertical plate. Since the model was created for illustrative purposes its geometry in the figure is simplified to a rectangular floor geometry (instead of the ellipse of the cone).

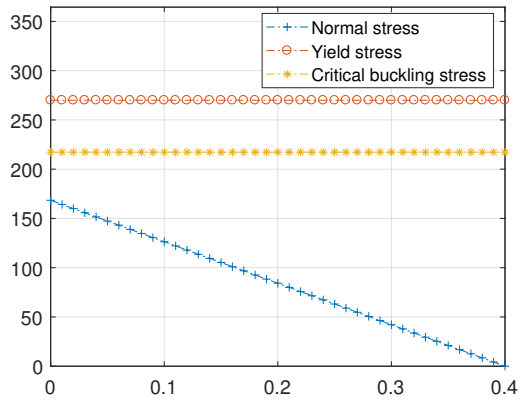

(a) Normal stress in the floor of the nose cone, using two L-shaped stiffeners.

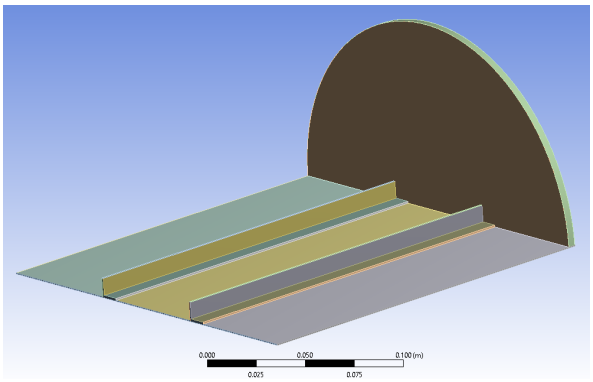

(b) Illustrative model of vertical plate and floor reinforcements.

Figure 9.12: Normal stress in nose cone floor and illustration of nose cone reinforcement.

Catapult attachment

In order to be able to launch the UAV using the chosen catapult, attachments to the clamps of the catapult have to be included. The catapult has two pairs of clamps that accelerate the airframe and fold down after deployment. It is chosen that horizontal fasteners are added to the lower side of the fuselage to which these clamps are attached. The fasteners add a small amount of extra drag, however they provide a simple, and most importantly a safe solution of carrying the catapult loads to the airframe.

Since the acceleration the catapult provides is known, the force acting on one fastener can be estimated and is equal to about 417 N. This force causes internal shear within the fastener as well as in the skin it is connected to. To make sure the skin can carry the shear load and due to stress concentrations around the fastener, the skin on the inner side of the fuselage has to be reinforced by adding extra thickness. In order to keep the fasteners close to the centre of gravity, it is decided to place them at the first and third quarter-point of the fuel tank along the X-axis. This placement also allows the load path to go through the fuel tank to the rest of the airframe, as no place for struts is available and the load has to be carried away from the skin.

The fasteners have to be sized appropriately to carry the force from the catapult clamps. The fastener diameter is sized in order to limit the shear stress. The allowable stress within the fastener has to be significantly lower than the shear strength of the fasteners, in order to avoid failure to fatigue. Equation (9.21) is used to approximate the bearing area stress within the bolt or pin.[44]

$$B = \frac{F}{t_{sk} \cdot d_f} \tag{9.21}$$

Where F is the force applied to the fastener, t_f is the thickness of the skin the fastener is attached to and is equal to 0.4 mm and d_f is the diameter of the fastener. It is determined that a 10 mm diameter is sufficient for the bolt to have significantly low stress. The length of the bolt however is driven by several factors: the width of the catapult clamps, the skin reinforcement thickness and the fuel tank thickness. According to the catapult manufacturer the clamps can be customised, which means

[44] http://www.engineersedge.com/material_science/bolt_single_shear_calcs.htm

the length required for the clamp can be determined for the given force. Using a length of 20 mm the present normal stress in the pin is 2.08 MPa and will therefore suffice for a preliminary approximation of the pin length outside the fuselage. As for the total pin length an additional 2 mm length is added to account for the thickness increment of the skin and possible fastening options from the inner side.

The size of the skin reinforcement patches are assumed to be 5 by 5 cm as a realistic estimation. For this size the thickness of the reinforced skin can be determined using eq. (9.22) which determines the stress within the skin due to the force acting on the pin:

$$\sigma_{skin} = \frac{F * \left(\frac{L_{pin}}{2} - t_{skin}\right)}{I_{zz}} + \frac{F}{h_{skin} \cdot t_{skin}} \tag{9.22}$$

Where F is the force acting on the pin, L_{pin} is the length of the pin, h_{skin} is the height of the reinforced skin patch assumed to be 5 cm and I_{zz} is the moment of inertia of the skin w.r.t the Z-axis. The variable t_{skin}, the thickness of the skin patch is the design variable. In order to make sure the stress in the skin never reaches the yield stress a safety factor of 1.25 is used, which means the maximum allowable stress is 217 MPa. After a few iterations, the required skin thickness is 1.7 mm, which results in a normal stress of 207 MPa. The resulting mass increment for the chosen aluminium alloy is 46 g and the additional small mass of the pins.

To summarise, four standard 22 mm pins or bolts are chosen with a diameter of 10 mm to which the catapult clamps can be hooked. These four points are placed on the bottom half of the fuselage near the fuel tank, such that the fuel tank can be attached to the skin reinforcements, which are four attached patches near the four pins with a thickness increment of 1.7 mm.

Using the aluminium alloy defined in section 9.3 the final mass of the fuselage including all reinforcements is estimated to be 1.98 kg.

9.8. Sensitivity analysis

This section discusses the sensitivity of the structural design to the assumptions made and possible changes in design inputs and estimations. The purpose of conducting the sensitivity analysis is to ensure that the outcome of the structural design is unsusceptible to small changes in design inputs, as well as to the application of assumptions.

9.8.1. Sensitivity to assumptions

In section 9.2, numerous assumptions have been done to idealise the loading situation and to be able to design the structure of the UAV. In the list below, the sensitivity of these assumptions to the design is evaluated.

- **A.1** is an large assumption. In reality, the wing will not be clamped at the edge of the fuselage but a rigid wing box will ensure that all loads are distributed to the fuselage. However, in the generated loading diagrams and the used buckling models the assumption that the fuselage is clamped is the closest approximation of what is happening to the real structure.
- **A.2** is a insensitive assumption to make. The number of 200 discrete panels is very fine. In fact, from 30 panels or more, adding more panels only increases computational time without clearly increasing precision.
- **A.3** is vulnerable to a lack of precision in production of the panels. When locally lower thicknesses are present, these minimum thicknesses might resulted in lower ultimate loads than anticipated.
- **A.5** is a safe assumption to make. The I_{xz} will be significantly smaller than I_{xx} and I_{zz} due to the fact that the chosen aerofoil is thin and is relatively close to being symmetric. Also, in case I_{xz} is not equal to 0, it will only add to the structural rigidity of the structure.
- **A.6** is a large assumption to make. During the application of the optimising algorithm the thicknesses of the top and bottom panels do change and as such, this assumption is only valid when the final centroid lies close to the original assumption. However, the assumed centroid has been checked to indeed lie close to the final centroid.
- **A.7** is a fair assumption to make. Even when principle moments of inertia contribute significantly to the entire moment of inertia, the structural performance will only increase. As such, this assumption only has a small risk of over-designing, not of failing at lower loads than anticipated.
- **A.8** is the large assumption on which the skin-web method is based. Although this is a proven design method, it is an idealisation. In reality, the shear force present will also result in a shear stress in the top and bottom panels of the wing. Therefore, the structural design is sensitive to the validity of this method. Still, the current shear stress is not expected to be critical be a large margin. This allows for some shear taken by the top and bottom skin panels.
- **A.9** is a common assumption for structural design. The skin of the wing and tail surfaces has little curvature, increasing the correctness of the thin plate approximation. Also, the curvature present in the skins will only have a structurally reinforcing effect. Therefore, this assumption does not pose risks to the structural integrity of the UAV.
- **A.10** follows from the manufacturing and impact thickness limits. In case this minimum thickness decreases, the design will get lighter. However, when this minimum thickness increases this will result in a heavier design. Although this would still allows a successful UAV design below the MTOW of item **REQ.U.SYS.1**, it would decrease the performance.

- **A.11** has the same sensitivity as assumption **A.10**. Only when the thickness step increases, the mass of the UAV structure will increase.
- **A.12** does pose a sensitivity risk to the structural design. Because the wing is semi-elliptical, the true lift distribution will slightly approach the lift distribution of a rectangular wing. This lift distribution has higher loads near the tip of the wing, increasing bending moment. It is expected however that these effects are very limited.
- **A.14** is a safe assumption to make. In reality, flanges will be added for assembling purposes, however, these flanges do not have structural purposes. As such, the design is not sensitive to the web not being entirely rectangular.
- **A.16** is a simplification. In reality, the inertia of the booms will be higher and thus the deflection will be smaller.
- **A.17** is a simplification. In reality, along the length of the fuselage, smaller stresses occur than what was assumed. This assumption was made primarily to show that the fuselage monocoque structure is limited by its minimum thickness.

9.8.2. Sensitivity to input changes

Except for the sensitivity to assumption, the sensitivity of the structural design should also be analysed regarding changes in inputs. As the design is considered to be conceptual, numerous inputs might change.

The first sensitivity that is apparent is the sensitivity to a change in loading factors. Higher loading factors occur when steeper turns, pull-ups and dives are required, but also when the system is required to operate at higher wind conditions or when a larger acceleration and deceleration during take-off and landing is required. All of these changes will increase the load factors. As the system currently is designed to just withstand all load factors (with a safety-factor), these increases in load factors will result in a higher required structural weight. Such a reinforced structure is can be designed provided the increase in load factors are within boundaries. The current wing structure is allowed to increase a few more kg at the costs of reduced performance as explained in section 4.1. Even when the systems exceeds the 25 kg from item **REQ.U.SYS.1**, taking aboard less fuel could be an emergency solution, again at the cost of decreased performance.

Also, the design is sensitive to the choice of material. Throughout the UAV, AL6061T6 has been used as an aluminium alloy. This design choice has been made because from numerous material options, it proved to be the most weight effective to this structural design. Therefore, when this aluminium alloy is not available for manufacturing, the structural weight of the UAV will increase. As such, the design is very sensitive to the availability of the used material. Still, AL6061T6 is a commonly used material for aerospace structures worldwide and for that reason, unavailability of the material is highly unlikely.

Finally, the sensitivity to changed inputs in dimensions needs to be assessed. Changes in aerofoil geometry, aspect ratio and the size of control surfaces require a different structural design. However, these geometry changes are expected to be little, if present at all. When such a geometry change occurs, the verified and validated model will simply have to be applied again to the new geometry arriving at a new optimal design that differs only slightly from the current design.

From this sensitivity analysis, it can be concluded that the structural design is not very sensitive to input changes. There is a sensitivity towards certain assumptions, however, none of the assumptions will alter the design drastically when they are excluded.

9.9. Verification and validation

In this section the executed verification and validation procedure is discussed. Since the structural design consists of numerous assumptions, calculations and a complex numerical model, both the intermediate and final results have to be verified and validated in order to ensure that the final structural design is capable of carrying the identified loads in a test environment.

Ultimate loads

The validity of the loads that the structure was designed for are crucial due to their influence on the internal bending and shear loads within the entire integral structure of the UAV. In order to verify that the load factor calculations were performed correctly and that no mistake was made in the scripts, hand calculations are performed using formulas from reference sources, as well as the original source. For both turning load factors and gust loading, the formulas from [46] are used, however verification is made by using calculations based on what is mentioned about the same loading scenarios in [11].

Validating the resulting load factors consists of analysing whether the load factors fall into a realistic range and checking whether similar small-sized UAVs are designed for similar load factors. For the negative load factor of -2.2 no validation is required, because it is derived from FAA regulations [50]. The confidence in the validity of the turn limit load factor is supported by [59], in which the load factors for small-sized UAVs is in a similar range than the limit case of 3.1.

Wing model

The discrete model created is rather complex and is prone to inconsistency and calculation mistakes. Therefore thorough verification has been performed by the use of unit tests and the application of simple reference geometry. Validation has also been performed, using finite element analysis as an assumed reference for structural test measurements. Special attention has been paid to make sure the FEA conditions are equivalent to that of the model.

Verification of discrete model

In order to make sure the discretisation of the wing geometry is correct and that the centroid and moment of inertia calculations are performed correctly for all wing segments, a simple rectangular geometry is inserted instead of the chosen aerofoil data. Determining the centroid and moment of inertia of a thin skinned rectangle can be performed by hand calculations. The chord along the span accordingly scales the cross-sectional geometry of the rectangle. The node positions, panel positions, panel lengths, centroid X- and Z-locations and lastly separate moment of inertia calculations for I_{xx}, I_{zz}, and I_{xz} are all verified using this method, as all results match the performed hand calculations.

The generated loading, shear, moment and torsion diagrams are easily verified by comparing simple load cases in the discrete model to their analytical solutions. This has been done for three different simple load cases: a point load case, a point and constant distributed load case and a point and varying distributed load case. The latter case closely resembles the actual loading diagram of the main wing.

As mentioned in subsection 9.4.2 a numeric solver is used to determine the top and bottom thickness of the skin. In order to verify the results of the numeric solver, the results obtained are substituted by hand to the governing equations to confirm the credibility of the solutions. This does not verify the thickness results to be the most optimal solution, but is does show that the obtained solution for thickness is a correct solution, which is the primary objective of verification.

The stresses obtained are also verified by hand calculations. For example the equation for normal stress due to a single bending moment (eq. (9.6)) is relatively simple and the results of the model can be checked by evaluating the maximum stress at a certain panel location for a certain location along the span. These point checks are performed at several different panels along the span.

Lastly, the mass estimation of the structure involves evaluating the cross-sectional area of a cross-section by summing all panel lengths along the chord and multiplying the panel length with their corresponding thicknesses. This means that the mass estimation is heavily dependent on the discrete model and also requires verification. After every iteration of the model, the total mass is verified by determining the average thickness along the span. The average circumference of the aerofoil can be determined using the aerofoil geometry and the semi-elliptical chord data. This provides a simple estimation of the total mass structure for a given material and this estimation is expected to be marginally higher than the mass determined by the discrete model. Indeed the difference between the mass approximation and the actual mass is very small, indicating a correct mass estimation method.

Validation of discrete model

The model is relatively hard to be validated without manufacturing and testing the designed parts of the wing assembly, however the results can be compared to the results of a finite element analysis done using one of the widely used tools in the engineering industry, such as Ansys or SolidWorks.

In order for the comparison to be valid, special attention has to be payed to defining the correct geometry, the correct boundary conditions and the same load case has to be analysed. This was done by using the discrete model to analyse a simple rectangular wing with a constant thickness clamped at one end. Two load cases were analysed: one with a constant pressure of 450 N/m^2 and one with a constant torsion of 90 N m throughout the span. A constant chord of 0.4 m and a wing span of 1.2 m and a thickness of 1 mm was used.

Since the discrete model uses the assumption that the wing is clamped at the fuselage (assumption **A.1**) the same boundary condition can be applied to the FEA model, as well. Figure 9.13a shows the normal stress evaluated using the discrete model used for the design of the wing structure, whereas fig. 9.13b shows the simplified geometry. Figure 9.14a shows the normal stress in the top panel evaluated using FEA in Ansys, whereas fig. 9.14b shows the same in the bottom panel.

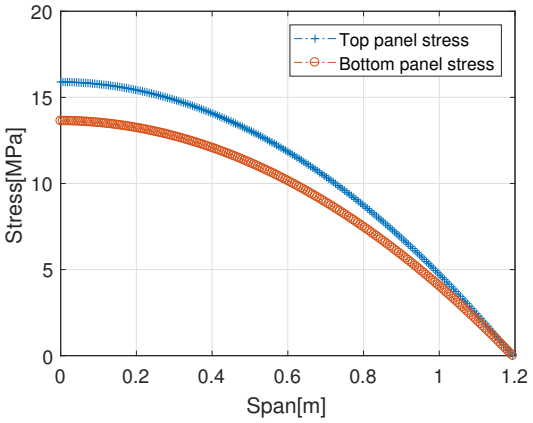

(a) Normal stresses due to uniform 450 N m^{-1} pressure.

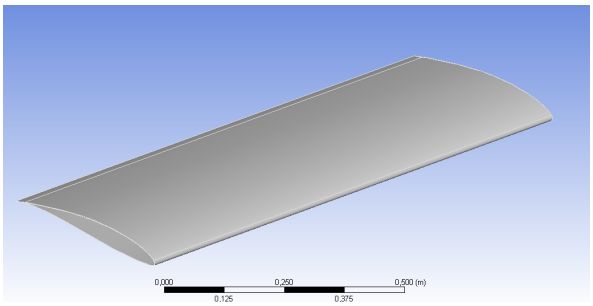

(b) Simplified wing geometry used for validation.

Figure 9.13: Normal stress determined using discrete model and the simplified geometry used for FEA.

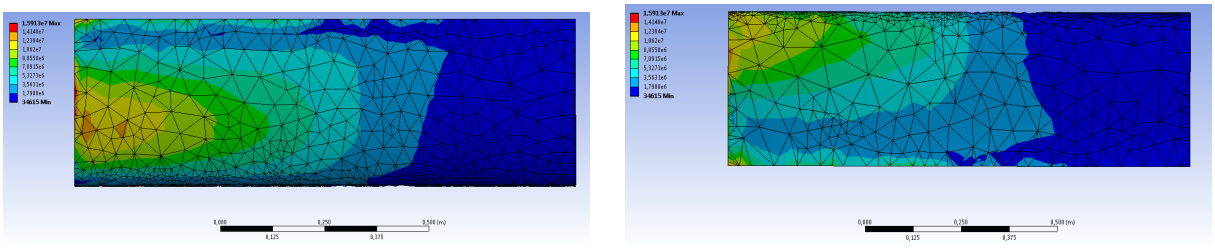

(a) Normal stress in top skin panel due to uniform 450 N m^{-1} pressure using FEA.

(b) Normal stress in bottom skin panel due to uniform 450 N m^{-1} pressure using FEA.

Figure 9.14: Normal stress in top and bottom panels evaluated using FEA in Ansys.

The maximum normal stress occurring in the top panel is 15.893 MPa using the discrete model and is 15.913 MPa using the FEA which results in a percentage error of 0.1%. In the bottom panel these values are 13.631 MPa and approximately 13 MPa respectively.

A similar analysis was done for torsion. As mentioned a constant torsion of 90 N m is applied to the structure. Figure 9.15a and fig. 9.15b show the Von Mises stress (also referred to as equivalent stress) in the structure due to this pure torsion calculated using the wing model and FEA respectively.

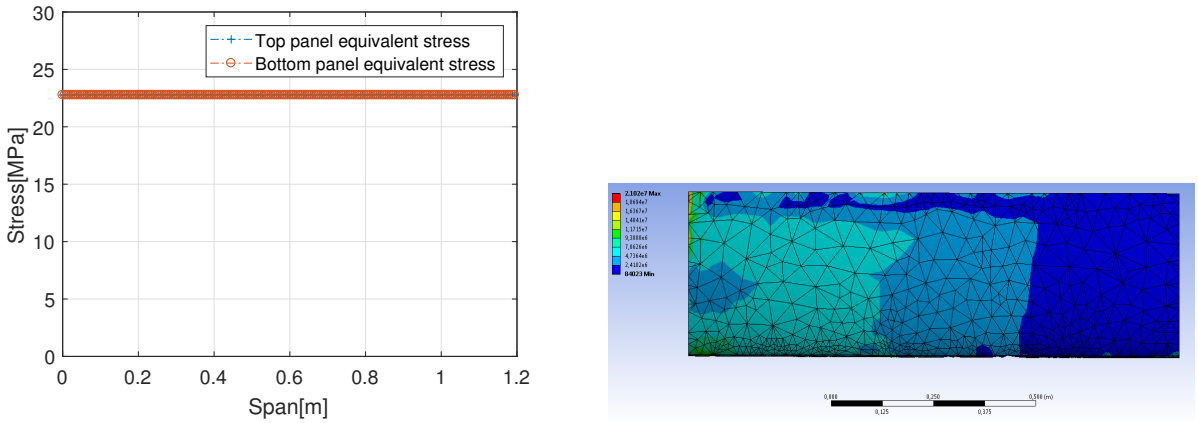

(a) Equivalent stress in the skin panels due to torsion using the wing model.

(b) Equivalent stress in top skin panel due to torsion using FEA.

Figure 9.15: Equivalent stress in the simplified structure due to torsion evaluated using both the wing model and Ansys FEA.

The maximum equivalent stress from the discrete model is 22.765 MPa, whereas the FEA equivalent stress due to torsion is 21.02 MPa, resulting in a percentage error of 7.7%.

In order to ensure that both bending and torsional load cases gave similar results, the test was run for multiple load cases, in which the magnitude of the pressure/torsion was changed. As a result, the ability of the constructed model to accurately predict normal stresses and torsional shear stresses in the skin is shown, however the validity of the thin-plate buckling theory used can not be assessed using this method. For further assessment of the model and the design outcome, more detailed numerical analysis of the design is required for the whole complex assembly. Furthermore, the parts are to be manufactured and the wing assembly (as well as the horizontal and vertical tails) are to be tested under the ultimate load cases.

Boom model

The boom model is different from the discrete wing and tail model and as such requires separate verification. The boom model however resembles the discrete model in most aspects, despite being significantly less complex. The boom model only optimises one constant thickness along the circular cross sections span-wise, whereas the discrete model optimises for both a top and bottom thickness. As such, only the bending equation is used to design the thickness. The verification consists of point checks of the moments of inertia, point checks of the local bending stresses at several span-wise locations and a system check for a simplified case of constant thickness and no taper. As was expected, the discretisation fully resembles the analytical solution of these point checks.

Chapter 10: Assembly and manufacturing

This chapter discusses the assembly and manufacturing of the UAV. In section 10.1, It is discussed how the assembly of the UAV takes place and what is the new design adapted for it. After which, the section 10.2 discusses the manufacturing of the UAV components.

10.1. Assembly of the UAV

As there is a volume requirement for the storage of the entire system. The UAV cannot be kept in one entire piece, instead, it has to be divided down into several pieces for the UAV to be kept inside a box to be able to transport it easily. The fuselage is going to be kept as an entire unit, as it includes the payload, and it is inconvenient for the user to assemble the payload during the mission. However, the wing and the tail section could be detachable, and could be kept in a more compact space. There were several possibilities analysed to be able to detach the wings. Some of the possibilities where to be able to attach the entire wing on the fuselage, or divide the wing into more than one structure. As the wing span is 2.422 m long, it is not possible to store the entire wing in the transportation vehicle, as the ground station system would be there too. As a result, dividing the wing into two separate wings would be a possibility, as it would meet the dimension requirement for the storage. Having more than two wings is a disadvantage for the weight, as dividing into more parts would increase the complexity of the structure, and increase the weight of the wings in total, as there would be more joints required to attach the structure. As a result, the wing would be divided into two separate parts. To make it easily attachable for the user, the fuselage will have a wingbox placed on the top, where the wing can be easily attached to the place. For the design of the wingbox, there were certain patents that were looked into, and the US patent 6,425,794 [44] meets all the requirements for the UAV. The attachment of the wing with the wingbox can be done with the help of dowel pins and also push and pull connectors to ensure easy placement and it can support the structure, as it can be seen in fig. 10.2a. The push and pull connectors ensure strengthened connections between the wing and the wingbox. There are several companies which produce this push and pull connectors. For instance, the Fischer, Yamaichi electronics and Weipu connectors.[45][46][47] The ones by Fisher can produce the connectors in every size, and can support high loads, as a result the ones by Fisher is going to be used. The push and pull connectors can be seen in fig. 10.1. The assembly of the wings to the fuselage should take three minutes by two people.

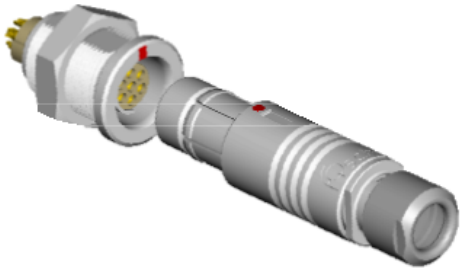

Figure 10.1: Push-pull connectors manufactured by Fisher [48].

In addition, due to the space left for transportation, the tail is going to be kept as a different unit too. the entire tail can either be kept together, or the booms can be divided from the empennage to have a more compact storage. As a result, a mechanism is added to the wing, to allow easy attachment of the tail to the wing. The mechanism that is going to be used for the tail attachment should be able to bare the loads, and the connectors should be able to be places in the wing easily, without causing any damage to the wings or to the booms during high loading cases. There were several mechanisms that were looked into when analysing the assembly of the tail to the wing. Some of the possible options for the use of the assembly were using push and pull connectors, or the use of the dowel pins and inserting them inside a hole, or using screws to screw the two structures together. However, as the assembly has to be done as quickly as possible, it is better to use the push and pull connectors, as they are able to bare high loads, easy to use and can ensure quick removal and insertion of the booms. As the booms on the wing side will have a diameter of 4 cm, the connector used has to accommodate this boom. Thus, a similar push and pull connectors as the one used in the wing is used, as it can be seen in fig. 10.2b. The boom attachment to the wing should take 2 minutes, and the boom attachment to the empennage should take 2 more minutes.

In addition, the propeller needs to be attached to the fuselage too, as the blades of the propeller should not be damaged when transporting the system, it will be kept as a separate unit. However to attach the blade hub to the engine, it is simply screwed in together. The attachment of the propeller should take 3 minutes.

As a result, the total time taken to assemble the entire unit should take 10 minutes when working with two people.

[45] https://www.fischerconnectors.com/
[46] https://www.yamaichi.de/
[47] http://www.weipuconnector.com/
[48] https://www.fischerconnectors.com/

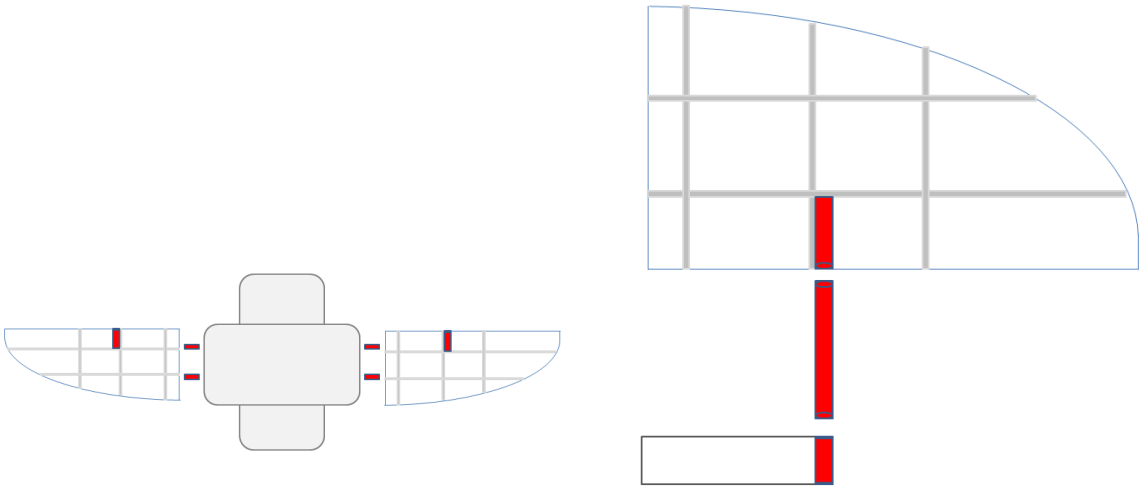

(a) Assembly of the wing.

(b) Assembly of the tail.

Figure 10.2: Illustration of the main wing and tail assembly.

10.2. UAV production plan

In this chapter the production plan of the UAV is documented. The production plan includes the manufacturing of the main wing, the tail and the fuselage. Manufacturing of other parts are discussed in subsection 10.2.4.

10.2.1. Main wing

The manufacturing of the main wing implies manufacturing of the skin, the ribs, the webs and the stringers and the assembly of these parts to obtain a wing.

The minimum thickness of the wing skin due to constraints is 0.4 mm [45]. This limitation in the thickness is due to several factors. First, it is to the prevent damage from stones, debris, mechanical tools and general handling. Secondly, manufacturing techniques such as forming and machining require a minimum thickness of aluminium. Face milling is used in order to vary the thickness of the top- and bottom panels over the span of the wing. It is advised to shear off a chip with a thickness of 0.1 mm.[49] This is why an increment in thickness of 0.1 mm is used over half the span of the wing as can be seen in fig. 9.3a.

For manufacturing purposes the skin of the wing is divided into three different sections: the top panel, the leading edge panel and the lower panel. This is done because forming techniques will be applied to the leading edge, while the top and bottom panels will be formed by riveting to ribs. First, the leading edge panel will be pre-cut in the elliptical shape of the leading edge as can be seen in fig. 10.3. Subsequently the panel will be formed according to the leading edge of the aerofoil. The shear-web which is located at the front of the wing will be the attachment point of the leading edge panel. Secondly, the bottom panel will be cut in the form of the wing planform without the leading edge section. Since the assembly of parts of the skin is required, an overlap between the top panel and the leading edge panel shall be present. Thirdly, the upper panel will also be cut in the form of the wing planform. However, since the aerofoil consists of a camber the upper panel shall cord-wise be larger than the lower panel by approximately 10%. The upper and lower panel shall be riveted to the trailing edge shear web.

The thickness shear webs of the wing are set to 1 mm(subsection 9.4.3). In order to rivet the skin of the wing to the webs, the top and the bottom of the web are formed to the inclination of the skin of the wing. The height of panel used to create the webs needs to be larger than the height of the web in order to create an area to which the skin can be riveted.

The ribs are mainly added for reinforcement purposes in order to connect the wing to the fuselage, to connect the tail to the wing and to maintain the shape of the wing. Firstly, there is one rib added near the assembly point with the fuselage. Secondly, there is one rib added at the point where the tail boom is connected to the wing. Thirdly, there are two ribs added to make sure the skin will remain in the shape of the aerofoil. Lastly, there is one rib added to maintain a proper shape at the wingtip. Consequently, for both wings, the number of ribs in both wings is equal to 10. The thickness of the ribs is 0.4 mm. The ribs are cut in the form of the aerofoil within wingbox created by the shear webs. Just as the manufacturing of the webs, the top and the bottom of the ribs are formed 90°and the height of panel used to create the ribs needs to be larger than the height of the web in order to create the areas to which the skin can be riveted.

Assembly of these parts will be done using riveting. First, the wing box will be produced by riveting the ribs to the front and the rear shear webs. Secondly, the leading edge panel will be formed in the approximate shape of the leading edge of the aerofoil. Lastly, riveting the leading edge panel, the top panel and the bottom panel to the ribs and the shear webs will form the panels into the shape of the aerofoil. The final main wing structure can be seen in fig. 10.3, in which the full wing span model is presented, however the wing box at the fuselage and the fuselage joints are not modelled.

[49] http://www.sandvik.coromant.com/en-gb/knowledge/milling/getting_started/milling_different_materials/aluminium_milling

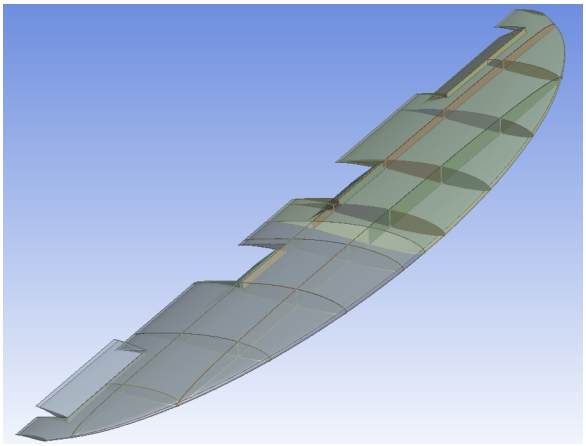

Figure 10.3: Final wing structure assembly.

10.2.2. Tail

The production plan of the tail is done in the same analogy as the production of the main wing(subsection 10.2.1). As can be seen in fig. 9.8a a thickness increment of 0.1 mm. is used again in the production of the top panel of horizontal stabiliser. The thickness of the bottom panel is limited by the manufacturing limit of 0.4 mm. The skin of the tail is manufactured and assembled in the same analogy as with the main wing. Instead, these panels can be cut in a rectangular shape. In the horizontal tail only one shear web included in the design along the line to where the elevator is attached. This means the leading edge skin panel shall only be riveted to the ribs and the bottom and upper panel shall be riveted to the ribs and the web. There are three ribs in the horizontal stabiliser: two ribs at the sides and one in the middle in order to form the sheet to the aerofoil.

For the vertical stabilisers the attachment point of the vertical to the horizontal stabiliser is the quarter cord line of the vertical stabilisers and the tip of the horizontal stabiliser. This is why the shear web of the vertical stabilisers is at 0.25c.

10.2.3. Fuselage

The fuselage consists of several different parts which create the final fuselage assembly. These parts are the main cylindrical body, the nose cone, the floor in the nose cone all three with the same thickness of 0.4 mm. Also the vertical plate separating the nose from the main body has a thickness of 4 mm. Additionally, there are two stiffeners that have to be attached to the nose cone floor and a back-plate on which the engine is mounted. The fuel tank is also considered part of the primary load bearing structure.

It is advised to manufacture the nose cane panels and the cylindrical main body in separate bottom and top panel parts. The thin skin body panels can be formed around the stiffening circular elements such as the reinforced vertical plate.

For the assembly, first all bottom panels have to be riveted to the vertical plate reinforcement. Then, after the two stringers are riveted to the floor panel, the nose cone floor has to be attached to the vertical plate also by the use of rivets. The fuel tank is attached placed onto the four patches of thick skin on the bottom panel of the main body. For the fuel tank, bolts can be used in case repairs are needed for the tank. These bolts can be combined with the fasteners used for the catapult launch as mentioned in subsection 9.7.2. The next step is adding and attaching the fuselage wing box to which the wings will be attached. Lastly, the top panels can be added to join the structure together

In order to place every subsystem in the fuselage three hatches are present which provide accessibility to all compartments and allow for wiring and mounting the engine.

10.2.4. Other parts

The manufacturing of the control surfaces, the joints, the propeller and the booms is not considered in this section as it will be considered in further development. When the manufacturing of these elements are proving to be difficult, a change in the design might be considered. This will not be a difficulty, as discussed in the sensitivity analysis in subsection 9.8.2.

10.2.5. Cost analysis of production

For the cost analysis of production a preliminary estimate is made using eq. (10.1), based on [29].

$$C = \text{e}1{,}319 \cdot W_E \cdot CEF \tag{10.1}$$

Where W_E is the empty weight of the airframe component and CEF is the cost escalation factor, estimated to be 2.2 based on [29]. This estimation is empirical and only accounts for the production of the airframe parts. The overall manufacturing procedure costs for the UAV consist of: manufacturing design and testing costs, raw material and off-the-shelf component costs, man-hours associated with the manufacturing and assembly process as well as the transportation and storage of the final products.

The preliminary cost breakdown of the manufacturing of certain parts can be seen in section 4.3.

Chapter 11: Electronics

This chapter discusses the chosen and design electronic components that are included in both the UAV and the kite. First, the avionics on-board the UAV are discussed along with the chosen payload and payload support. The implementation of a thermal management system is required to limit the temperatures in the OBC environment. The communication payload and communication system design are also presented, as well as the communication flow diagram. The communication link is summarised in the link budget. Lastly, the placement of all systems is elaborated along with the power distribution subsystem.

11.1. Avionics

The avionics system that is going to be used on-board is going to have a Service Oriented Architecture. In this architecture the different processor cores will be tasked with doing different tasks and the inter-connectivity will be dealt with in a data stream. What this means is that all the data is published into a hub which distributes it according to what is needed by the different components.[50]

11.1.1. Hardware

The simplest model that can be used is a segregated system where each computer has a sub-architecture. This model increases the computing resources available. This also makes the system safe with redundancies. However, adding more components adds more weight to the system. Hence, for avionics an architecture known as the integrated modular avionics (IMA) is used.[51] A few advantages to this architecture are:

- excellent portability
- excellent modularity
- efficient reuse of resources

Using this architecture helps with redundancy without the addition of multiple systems. Here there can be processors that are idle and is used on demand. Each processor has multiple cores (4 cores in this system) which is assigned for different tasks when not idle.

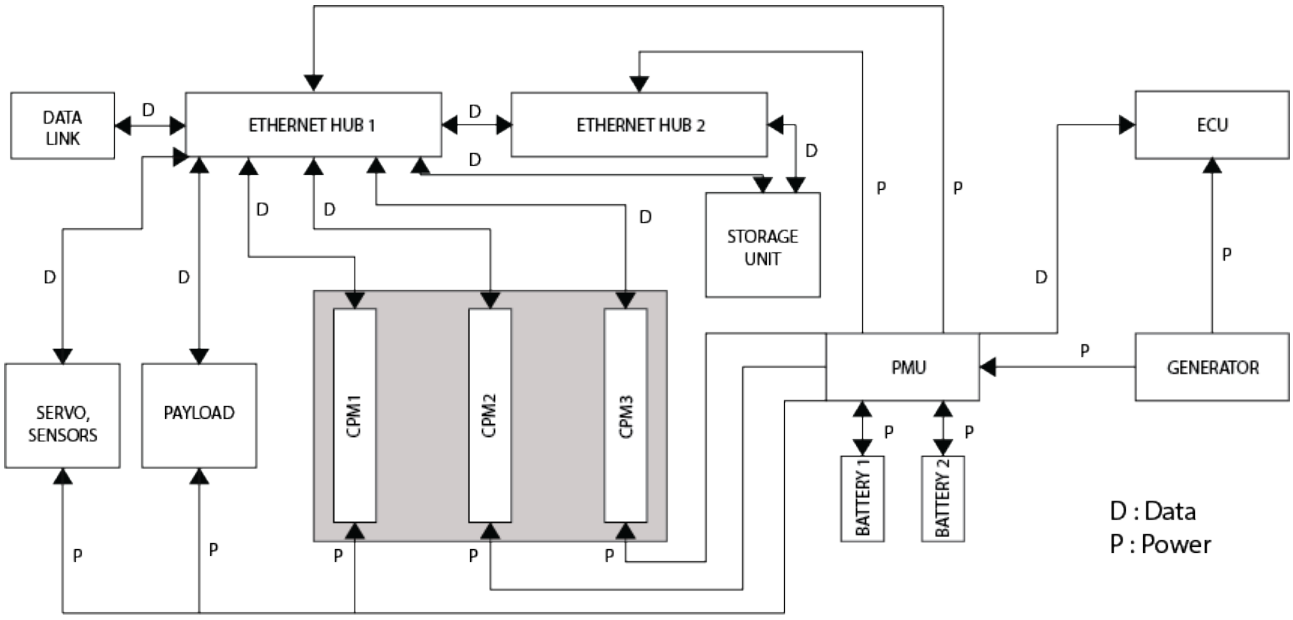

Figure 11.1: Schematics of the electronics on-baord the UAV.

Figure 11.1 shows the links and the architecture that is used in the FASAR UAV system. The different components are ellaborated below:

- CPM (computing processing modules): There are three computational units on-board the UAV. These processors in combination take the role of the flight control unit, flight management unit and payload management unit.
- Ethernet hub: Here is where all the data transfer takes place. The data is sent from the CPMs, sensors and payload here. The sensors and payload have an interface in order to be connected into the ethernet jacks of the hub. All the data has markers which helps it differentiate from the rest. When some information is needed by one of the subsystems

[50] https://upcommons.upc.edu/bitstream/handle/2117/8697/25_digital%20_avionics_pastor.pdf
[51] https://hal.archives-ouvertes.fr/hal-01102364/document

it either fetches it from here or sends a request. The advantage of such an information interchange system is that it simplifies the connection between the sub-systems and also a failure in one system does not break the link. There is also a second ethernet hub in parallel for redundancy. The gateway to the data link to the ground station is also present here. For redundancy and diagnostic purposes there is a storage unit that is connected to the hub. Here all the diagnostic information and the payload data is stored to be reviewed later or to be retrieved in case of communication breaks. It also takes in the sensor data so that it is available to all the processing units.

- PMU: The power management unit takes care of all the power voltage conversions for the different electronics on-board. It receives the power generated by the alternator and distributes it. It also stores the excess into batteries so that the power can be used in case of emergencies. The power is also used when the engine is switched off at the ground when running diagnostics.
- ECU: The engine control unit takes care of the engine operational settings such as the throttle, spark advance, mixture and cowl flaps. For this purpose the fuel pump is installed next to the ECU so that it can be operated together. The fuel pump is connected to the ECU so that it can regulte the fuel flow into the engines.

The CPM is divided into Flight management, flight control, payload management.[52] The module that is used in the system is Odroid-XU which comes with Exynos5 Octa Cortex™-A15 1.6Ghz quad core and Cortex™-A7 quad core CPUs. Having four cores and two processors in the same board help with minimising the size of the on-board computer and also distributing tasks such as payload control and obstacle avoidance. The Cortex-A15 can take up the heavier task being the faster processor. This processor has a power usage of 6 W. Along with the odroid-XU, pixhawk will be used as the autopilot module. The pixhawk also contains a module called Cube that will act as the redundant IMU module with 3 sets of accelerometers, magnetometers, gyroscopes and 2 sets of barometer.

Each control surface will be controlled by one servo motor each. They listen to data from the flight computer and makes changes accordingly. The servos that will be used are the 10mm form factor DA-10 from volz-servo.[53] These are specifically chosen because of their size and the throttle they produce which can withstand the deflection forces. The servo has enough torque to take the maximum loads on the control surfaces. Hence the flaps, ailerons and elevators are going to be hinged at one end by the servo axle and the other by a rotating rod. The rudder needed a bit more complex mechanism for deflection since the entire vertical surface moves. Thus, it requires additional support at the base. Figure 11.2 illustrates the mechanism used where the circular slots support the rudder. For the movement of the rudder in the slot, ball bearings are placed around the keyway of the shaft which is in contact on all sides. The motor shaft is present directly in the middle of the slot.

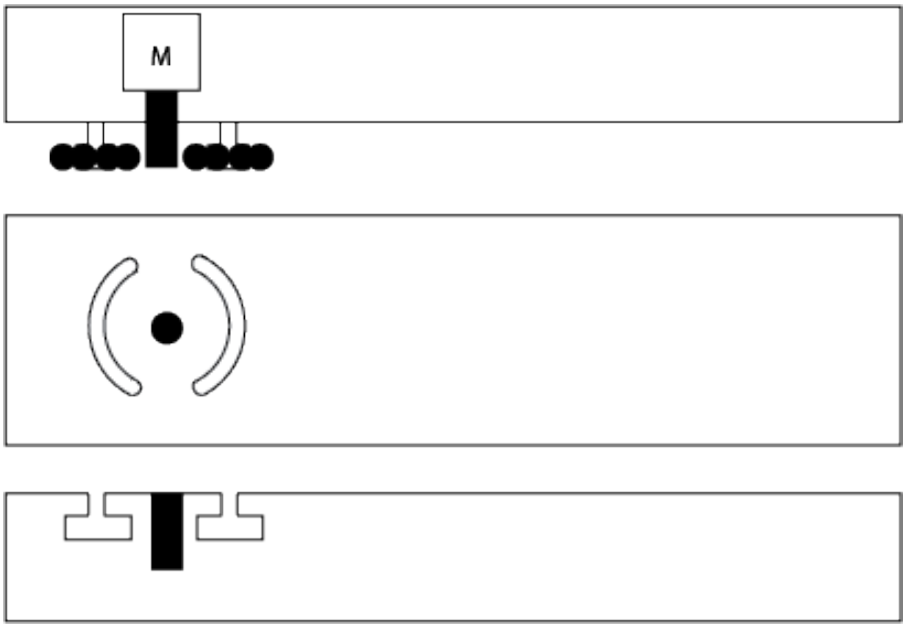

Figure 11.2: Servo mechanism for the rudder.

11.1.2. Software

Most of the operations for the flight control of the UAV require computations every 10 ms. For such a system use of real time operating system (RTOS) is required. These operations are not computationally intensive, but are done at high frequency. A RTOS works on programmed routines were actions are pre-programmed into the system to be performed at set intervals. In contrast a traditional OS will work on events which can cause delays which can be catastrophic to UAV operation. Since

[52] https://hal.archives-ouvertes.fr/hal-01102364/document
[53] http://www.volz-servos.com/English/resources/Downloads/DataSheets/DA-10_Datasheet_uni.pdf

in the hardware side multi-processor architecture is used the RTOS used is RTEMS (real time executive for multiprocessor systems). This is an open source RTOS used in embedded systems for space applications among many.[54]

11.2. Payload

The payload that is carried on board will be a LIDAR camera, an infrared camera and an optical camera. All the electronics including the payloads can be sensitive to vibrations that is introduced into the system by the engine. For this reason vibration damping plates will be used to which all the sensitive electronics will be attached to. Along with this the infrared and optical camera is going to be attached to a dual axis gimbal. This helps the infrared and optical cameras to have 180 degree view. This is especially important when it comes to the landing phase of the mission cycle where the camera needs to be facing forward. This will be elaborated more on chapter 12. The payloads will also include an interfacing module which comes with the kit. This is used to transfer the data to other devices after capture. In this case the ethernet jack in the interface module will be used to transfer the data into the ethernet switch. The payload data is also stored into SD cards to be used for further analysis later or in case some data is lost.

The LIDAR sub-system that is in use has a field of view of 360°around the lateral axis of the UAV and 30°in the other. The laser gets fired every 55.296 µs and has a rotational rate of 20 Hz.[55] This implies that the lasers are fired 904 times in a single rotation. Since only the beams fired downwards is of importance this reduces to 452 points. At a maximum height of 150m The area that will be mapped has a resolution of 1.04x5.025 m. Along the longitudinal axis this resolution gets finer due to the 409 beams firing when the aircraft moves forward. In the lateral direction only 16 beams are fired which does not give enough resolution for fine mapping. For this reason the UAV has to fly at 110 m altitude and have multiple passes in order to get accurate mapping details. The data rate of the LIDAR system is 0.5 Mbit s.

The optical camera (monochrome) will be used with a 6mm wide angle lens from Edmund that has a field of view of 58.97°. At a resolution of 1940 by 1460 the camera is capable of fine mapping with a resolution of 10cm at a height of 115m. A single picture already covers an area of 182.85x182.85 m, hence, at cruise speed photos need to be taken only at 5.5 s intervals. The data size of a single picture is 23 Mbit (taking a single pixel as 8bit). This is split into parts and sent every second. This amounts to a data rate of 4.18Mbit s.[56]

The infrared camera is used to send back video streams of the affected area. The camera is used with a 19mm stock lens which has a field of view of 32x24°. It has a resolution of 640x512. The camera is able to have a resolution of 1 cm at a height of 108 m. Each frame will have a data size of 2.6 Mbit. At the furthest distance of 50 km due to low data transfer only 5 frames per second will be transferred whereas at a distance of 10 km up to 20 frames per second can be transferred.[57]

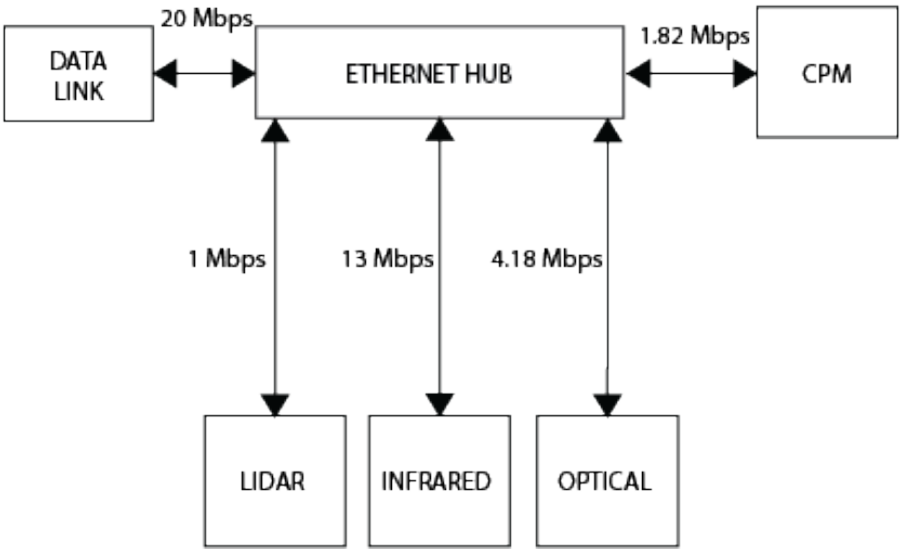

Figure 11.3: Data handling block diagram

11.3. Thermal management

With the amount of data section 11.2 that the processors need to process it tends to heat up quickly. For instance it is true that a 6W processor does not produce much heat but when the system is completely insulted the heat will build up over the duration of the mission of. There are different ways to cool such a system:

[54] https://www.rtems.org
[55] http://velodynelidar.com/docs/manuals/63-9243%20Rev%20B%20User%20Manual%20and%20Programming%20Guide,VLP-16.pdf
[56] http://www.imperx.com/wp-content/uploads/B1942_2MPHD_CCDCamera_Specs.pdf
[57] http://www.flir.eu/suas/vuepro/

- A water cooled system with water circulating through pipes can be used to cool the processors. This is not ideal since the pipes used here are not the most rigid. Moreover, in case of crashes or impacts they can get damaged thereby flooding the avionics unit.
- The simplest method used in different industries is a air cooled duct system where air enters through a duct and carries the heated air through an exist duct. In the application at hand the UAV might have to operate in volcanic regions where the ashes could enter/clog the air ducts and/or contaminate the electronics inside. Hence a sealed enclosure is required thereby crossing out this option.
- Air cooled copper plates that conduct heat fast and increase the surface area of radiation can help with cooling as well. This can be set up in a way that it fits into an enclosure and still be able to cool the system. Hence, a modified version of this system is used in the design of the thermal management system.

The requirement that is put forth is that the electronics cannot be contaminated with the outside air. It needs to cool all the processors on board with a maximum power of 6 W each.

Thus the setup is as follows: a copper heat sink is placed in the top leading edge of the fuselage nose which can be seen in fig. 11.13. The airflow outside assists in cooling the heat sink. The heat from the processors is transferred to a copper plate clamped to the top of the processor module and this is transferred to the heat sink outside through copper pipes. The heat pipe has three layers - the outer copper casing, an inner wick and the working fluid. The heat is absorbed by the fluid at one end and evaporates. This then flows to the cooler end and condenses. Subsequently the condensed fluid is absorbed by the wick and flows down to the region to be cooled. Since the ideal temperature for the processor is around 40°C, water is used as the working fluid since it has an operational range between 30°C and 100°C. The pipes are also made such that they are very robust.[58]

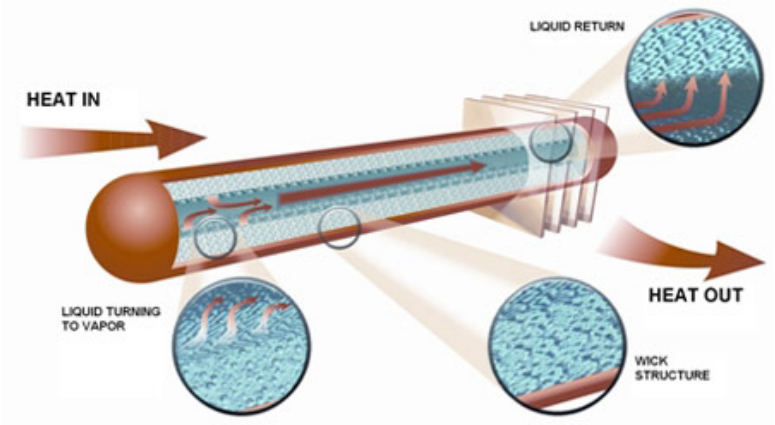

Figure 11.4: Heat pipe structure [59]

For the sizing of the heat pipe an online calculator from Advanced Thermal Solutions was used based on the pipe length, evaporation region and the condensing region. For the sizing of the heat sink a model was created on CATIAV5®and then exported into Ansys.[60] The thermal dissipation was then studied with the flow passing over the heat sink. An assumption is made here that the maximum thermal energy is transferred to the heat sink through the heat pipes. In reality some of the energy dissipates before it gets to the heat sink. So the assumption made is the absolute maximum value that can get transferred. From fig. 11.5 it is clear that the heat completely dissipitates through the heat sink.

[58] https://f.nordiskemedier.dk/283t6bife5vb3wha.pdf
[59] http://www.thermacore.com/news/multi-kilowatt-heat-pipe.aspx
[60] https://www.1-act.com/resources/heat-pipe-calculator/

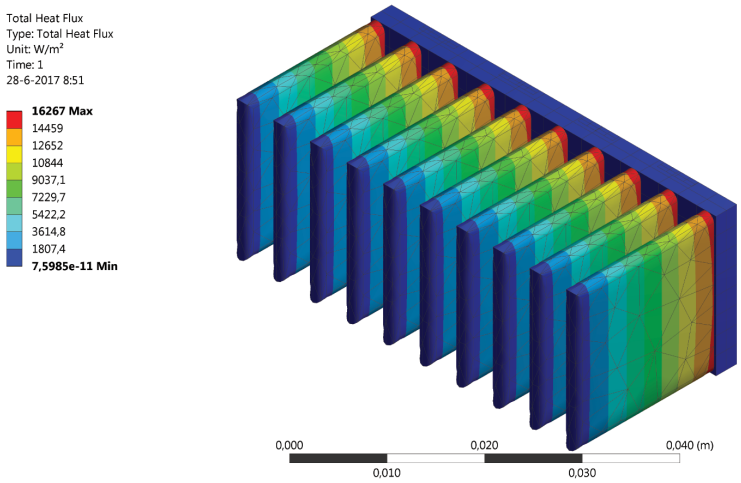

Figure 11.5: Heat sink Ansys simulation.

11.4. Communication

The biggest hurdle that was faced in the communication system was to have an antenna that could fulfil the requirements set forth by the mission.

11.4.1. UAV

The UAV will have two sets of patch antennas. One of the patch antenna is going to be facing downwards and will pick up communication from the SAR team. This antenna will also be used for data link with the monitoring station when it is in line of sight with the monitoring station.

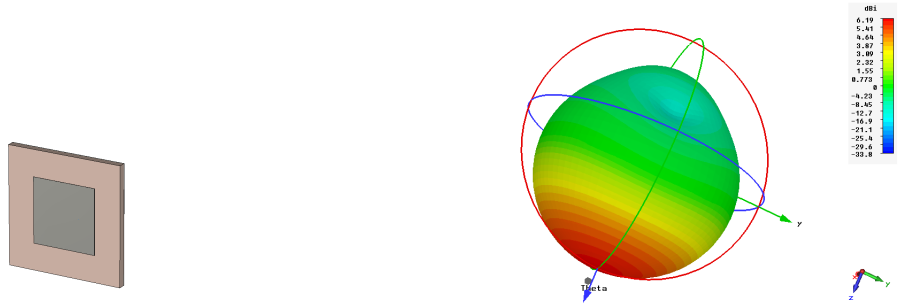

(a) 3D drawing.

(b) Radiation pattern.

Figure 11.6: Patch antenna.

The second set will have four patch antennas that has a single feed.The patch antennas have a radiation angle of 100°. The radiation of a single patch was first modelled in CST Suite (computer Simulation Technology Suite). From this the radiation spread and the gain of the antenna was found. This antenna can be used for communication with the SAR teams on the ground and also the monitoring station at close proximity. The next step was to get an antenna design that could communicate over a maximum distance of 50 km regardless of the orientation of the UAV. For this reason four patches oriented in four directions oriented outwards was used for establishing the communication link. The same patch antenna for the downward communication was used for the simulation. The interference of the four antenna was then simulated in CST and then was fine tuned by changing angles to get a good radiation pattern.

11.4.2. Kite

Similar to the UAV, the kite needs to have two sets of antennas as well. One of the antenna is the same as the one used in the UAV for communication with the SAR team. The patch antenna will be used on the kite facing down to relay data to and from the monitoring station. They can also relay data from the SAR teams that are in range of the kite. At a height of 300 m it will be able to pick up signals from over 5 km range.

The requirement for the second set of antenna that the kite needed was to intercept data from and relay data to the UAV. For communication within a small radius many off the shelf antenna can be used but the mission has to be performed up to a distance of 50 km. Hence a new antenna design had to be made and simulated. As a starting point [53] was used to set up the initial setup since the antenna had good gain in a small form factor and had directivity in 360°. The dimensions had to be

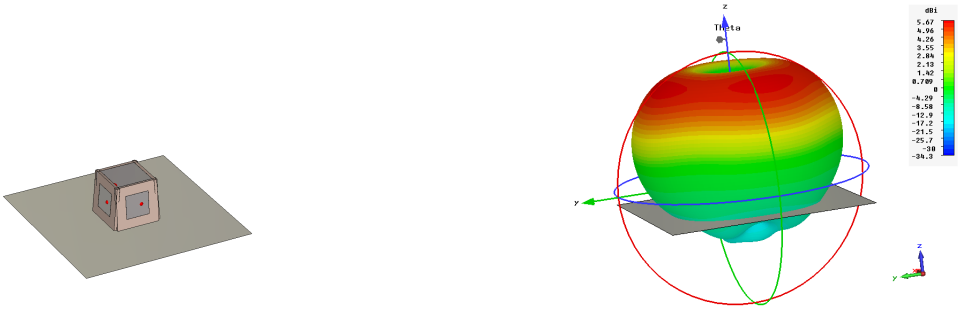

(a) 3D drawing.

(b) Radiation pattern.

Figure 11.7: Multiple patch antenna.

tweaked by running the simulation on loops to find the patch and connection dimension at which maximum power is radiated. It was found that the patch and the connection both needed a dimension of 31 mm for maximum efficiency. The beam in this case is also bent at an angle of 6° which is better for the design since a radiation pattern that directs above the kite is not needed.

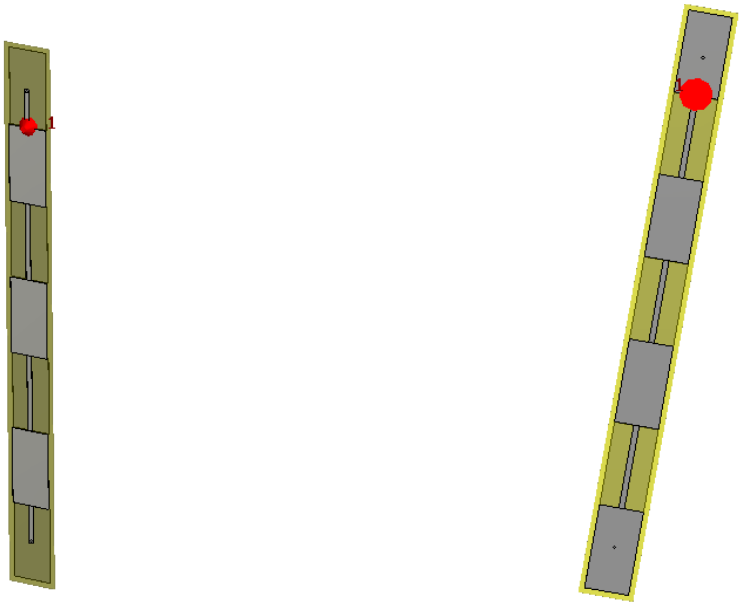

(a) 3D drawing of the front side of the collinear patch antenna.

(b) 3D drawing of the back side of the collinear patch antenna.

Figure 11.8: Drawing of the front and back side of the collinear patch antenna.

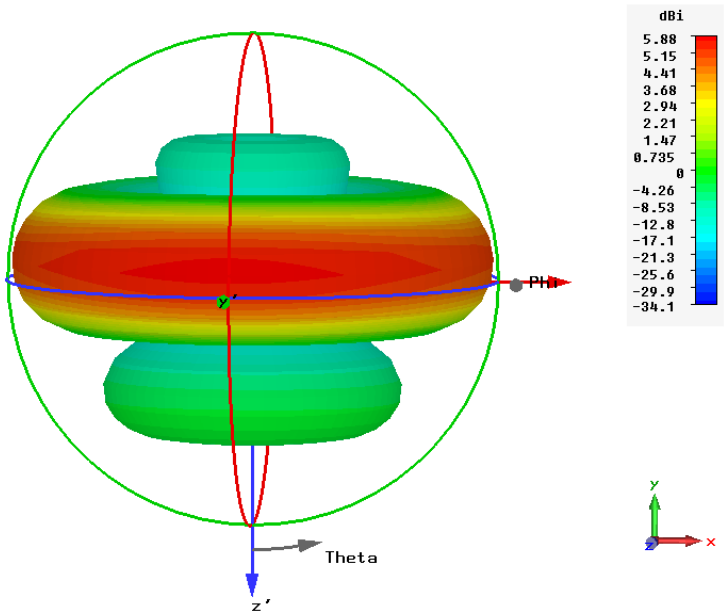

Figure 11.9: Collinear patch radiation pattern.

11.5. Validation

Two software were used in order to design and create models for the antenna design and the heat sink. Computer Software Technology Suite (CST) was used for antenna design and Ansys was used for designing the heat sink.

11.5.1. CST

In order to model the collinear antenna, a research paper on collinear patch antenna was consulted [53]. The research paper also included experimental data that was performed on its design. For validation the exact geometry was recreated in CST and the radiation patterns were generated. This then was compared to the experimental data as shown in subsection 11.5.1. From the comparison it is evident that the main lobe of the radiation is very similar between the experimental and simulated results The directivity difference between the experimental and simulation is only 0.15 dB.

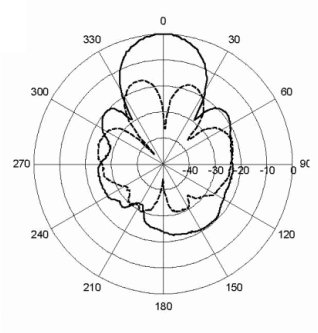

(a) Collinear patch experimental data.

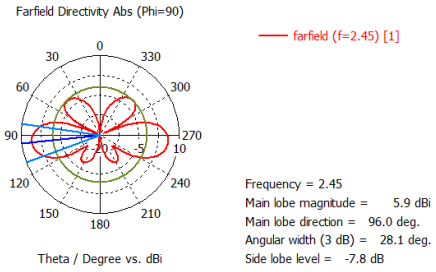

(b) Collinear patch simulated data.

Figure 11.10: CST validation.

11.5.2. Ansys

For the validation of Ansys, [61] was consulted. The paper shows the verification and validation procedures done on the software and the standards to which these tests are kept. There are also validation problems on the fluent workbench (workbench that is used for the model) for validation purposes.

11.6. Sensitivity analysis

It is important to have a sensitivity analysis to make sure that unexpected changes do not cause fail the system. From the communications stand point there is a safety margin of 4 dB included in the SNR calculations. In terms of angular deflections

[61] http://www.ansys.com/-/media/Ansys/corporate/images/other/nafems/NAFEMS-Verifying-and-Validating-Ext-Abstract_FINAL.pdf

the gain changes by 0.05 every degree. The simulation done in section 4.6 shows the variation with different angles of UAV orientation.

The LIDAR carried on-board the UAV is sensitive to changes in height. The height determines the resolution of the data gathered which in turn determines the amount of overlap needed in data collection. In terms of longitudinal resolution the fine mapping is met by a factor of two. But in lateral direction of the UAV there are only 16 beams fired which results in a lower resolution. This is reason for multiple passes of the UAV in order to collect enough data for better resolution.

11.7. Bill of components

Table 11.1 shows all the off the shelf products that are used in the avionics system.

Table 11.1: Bill of components.

Name	Company	Model	Quantity
On-board computer	HardKernal	Odroid-XU4	2
Flight autopilot	Pixhawk	PX4	1
Optical Camera	Imperx	B1942	1
Infrared Camera	Flir	Vue Pro	1
LIDAR	Velodyne	Puck LITE	1
RADAR	Aerotenna	mu Sharp Patch	1
IMU	ACME systems	Daisy-7	1
IMU (redundant)	Pixhawk	Cube	1
Pitot tube	Swiss Air-data system	PSS-8	1
Alpha and Beta veins	Swiss Air-data system	SMV-1	2
Thermal heat pipes	Advanced Cooling technology	copper/ water system	5
PMU	Millswood engineering	250W PMU	1
Batteries	Venom power	Venom 15C 3S	2
Ethernet switch	Curtis Wright Defence Solutions	KAD/SWI/108	3
Transciever	Silvus Technologies	Streamcaster 4200	2
Transponder	uAvionix	echoESX	1

11.8. Communication flow diagram

In this section the communication flow diagram is discussed which can be used to demonstrate the functioning of the communication system. It relays information on which systems/sub-systems are linked and where the information interchange takes place. The information transferred are the collected data, the communication packets, critical diagnostic information and the commands for the UAV to perform the mission.

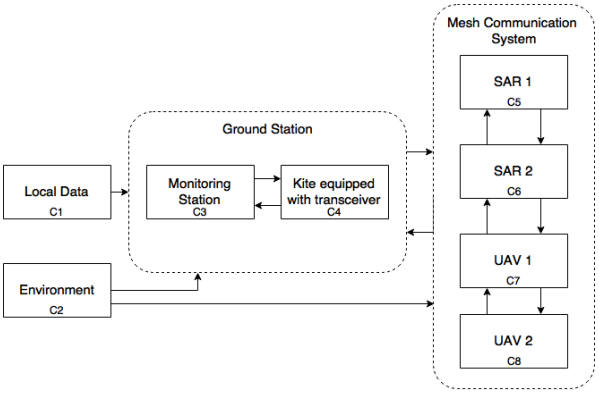

Figure 11.11: Communication flow diagram.

The system works with two deployed UAVs and a kite system that is connected to the monitoring station as seen in fig. 11.11.
Local Data (C1): Before launching the system, the entire mission can be made more efficient by gathering some data about the situation. There could be areas in the disaster zone that are already cleared by locals or volunteer groups. If known, the UAV can be redirected to other regions and there will not be any overlap in the data gathered. The topological data from local archives could also be used to get the lay of the land. The gathered information is then fed to the ground station. This can be then relayed to the UAV either at start up or/and relayed during mission cycle. Data is constantly collected during the mission duration to keep the system up to date.
Environment (C2): Environmental data gathered through various measurement devices on board is essential for the operation of the UAV. Data regarding obstacles (through RADAR), attitude (IMU), weather conditions (pitot tube) are required to make the system autonomous. The ground station also requires weather data to make sure that the crew and the system are not functioning in an unsafe environment. Temperature and wind speed measurement needs to be taken periodically for the operability of the kite.

Monitoring Station (C3): The monitoring station will be a central link in the system. It receives the data gathered from the UAV through the kite and will be the unit that interprets the unprocessed/pre-processed data received. Depending on the data gathered, rendering can be done here and then relayed through the kite to teams that need it. Live feed from the UAV is fed into this subsystem and from observation flight controls can be tweaked or changed. In cases where the UAV is in close proximity the monitoring station can directly communicate with the UAV without using the kite.
Kite equipped with transceiver (C4): The monitoring station is linked to the adjacent kite that is moored to the ground with tether cables. All the communications go through the kite since it has line of sight with the UAV, being at a higher height except for when the UAV is very close to the kite. The communication to and from the UAVs and the SAR teams are collected here and re-transmitted.
SAR (C5, C6): The SAR teams need to communicate with each other to consolidate search and rescue operations. This is done through a mesh system fig. 11.11 where signals are relayed through the closest system (UAV, SAR teams) to the target recipient. Thus the UAVs and SAR teams creates a closed loop communication network.
UAVs (C7, C8): As said in the previous subsection the UAVs form a closed loop with the SAR teams for communication. One of the primary function of the UAV being mapping, it has to transmit the gathered data to the ground station for processing and interpretation. For operational and redundancy needs it has to transmit diagnostic data to the ground station as well. Both the UAVs are equipped with transponders to send out location data to other aerial vehicles and also other air traffic monitoring stations.

The communication link for the ground teams still follow the multi-hop architecture where the closest node transfers data to the next node and so forth. In this case the two UAV along with the ground SAR teams form a mesh system where all the nodes act as a relay. The data that is transferred through this architecture is the communication link of the ground teams.

11.9. Link budget

An initial estimate for the link budget was already calculated during the mid-term phase. Now that the antenna has been designed there are accurate values that can be put into the link budget calculations. The link budget that is calculated is for a normal mission cycle at different distances from the ground station. For links during unexpected cases and large manoeuvres refer to the communication simulation in the performance chapter.

For this first the distance to horizon had to be calculated. Since both the receiver antenna on the kite and the transmission antenna on the UAV are airborne, the distance to the horizon increases.

$$d = \sqrt{h(2R+h)}$$

where d is the distance to the horizon, R is the radius of the earth and h is the height of the observer. From this it is found that the distance to the horizon is 101.3 km, which is more than what we require with our mission. Next the fresnal zones were calculated to take into account the reflection and refraction zones which is shown in table 11.2.

Table 11.2: Horizon and fresnal zone distances.

Distance	Value
Distance to horizon [km]	101.3
Max first fresnal zone radius [m]	39.5
Max second fresnal zone radius [m]	55.9
Max third fresnal zone radius [m]	68.4

With the new gain values of the antennas and their radiation orientation table 11.3 was populated. The user data traffic was obtained from section 11.2. The data rate from the payloads was then added to the diagnostic data to get the final throughput value. As before the environment that the system will operate at is free space with the assumption that at the current altitude there are not many obstacles and there is direct line of sight. The transmitter used for communication can operate at different frequencies between 400 MHz and 5800 MHz. This allowed a large choice for frequency. 2450 MHz is widely used for data transmissions and can be used in multiple countries, hence was chosen as the operating frequency. The co-linear antenna that was designed has a gain of 5.88 and the patch array antenna has a gain of 5.67. A safety margin of 4 dB was used due to the assumption that was made in regards to free space.

Table 11.3: Given link parameters.

Inputs	Value	Unit
Environment	Free Space	
Frequency	2,450	MHz
Max TX power	40	W
TX power control	Adaptive	
TX cable loss	0.1 [62]	dB
TX antenna gain	5.67	dBi
Number of RX antennas	2	
RX antenna gain	5.88	dBi
RX cable loss	0.3 [63]	dB
TX antenna height	150	m
RX antenna height	300	m
Objects in first Fresnel zone	No	
Target Distance	10 - 50	km
Safety margin	4	dB
User data traffic	18.18 -	Mbps

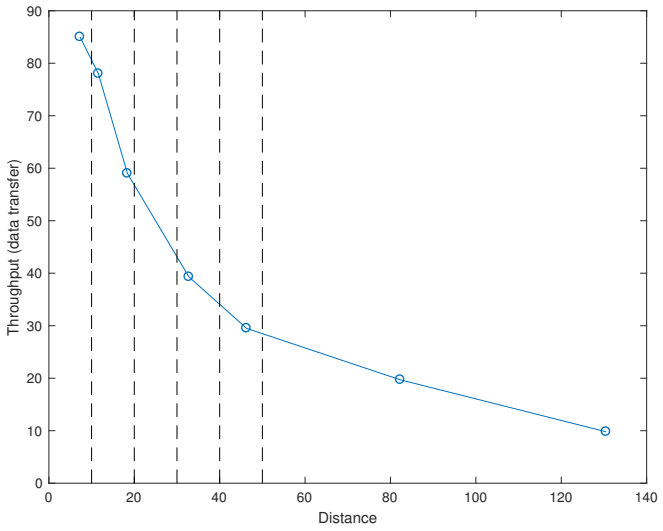

Figure 11.12: Throughput at different distances.

From fig. 11.12 it is evident that with decreasing distance the amount of data that can be transferred also increases. Since at the longest distance the user data traffic is already met, thus at lower distances the infrared camera video stream can be transmitted with a higher frame rate along with decreased transmission power. The duty cycle shows how much the sub-system will be burdened with the transmission. At 10 km there is a 26% load in the sub-system.

Table 11.4: Link-performance values at different distances.

Link Performance Results	**10** km	**20** km	**30** km	**40** km	**50** km
RSSI [dB m]	-69	-75	-78	-81	-83
SNR [dB]	24	18	15	12	10
MCS [-]	13	11	11	10	9
Link Capacity [MB s^{-1}]	78	39	39	29	20
Duty cycle [%]	26	51	51	68	102

11.10. Placement and power

In the section the placement of all of different subsystems is discussed, as well as the designed power distribution system.

11.10.1. Placement

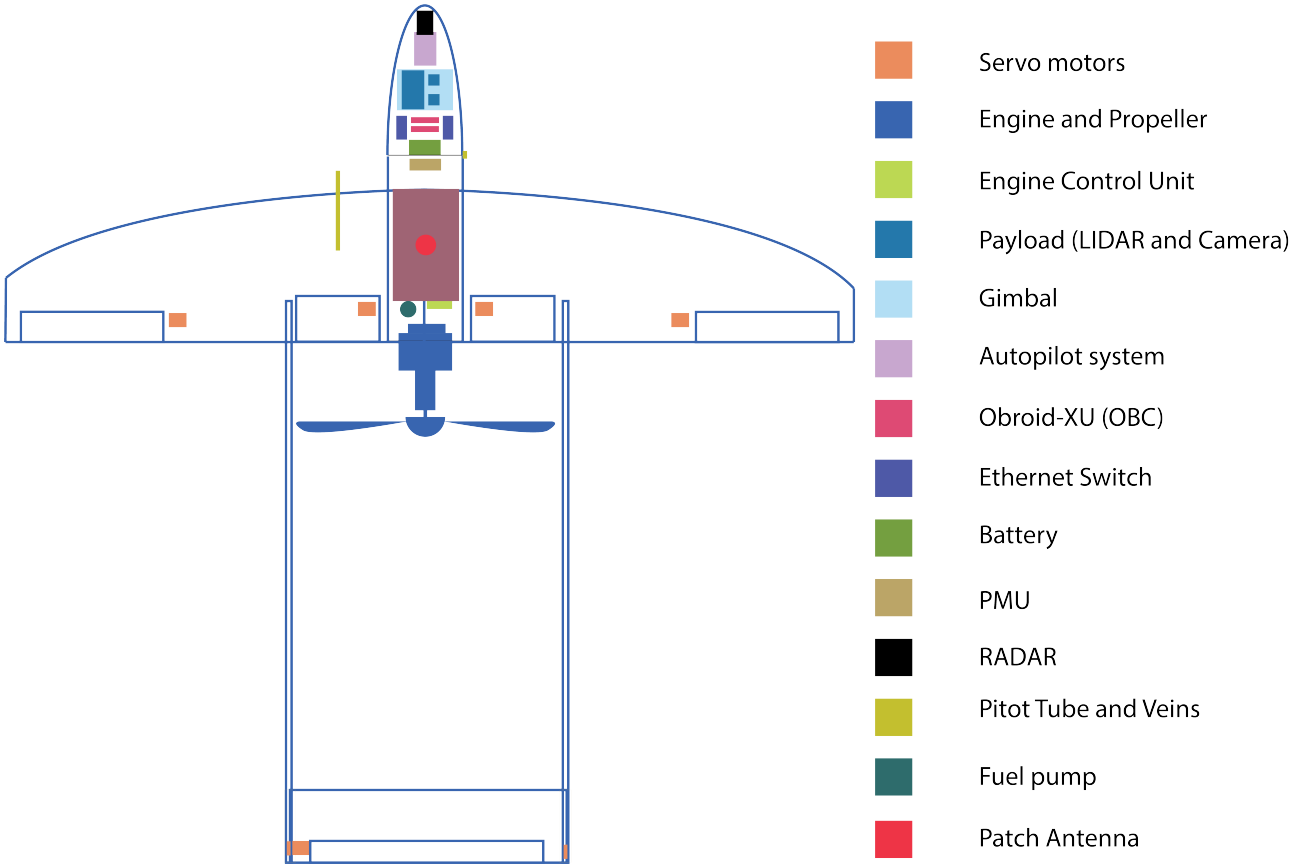

Figure 11.13: Placement of sub-components inside the structure.

The placement of the different sub-systems was a topic that was visited in the beginning of the design process. This process was done in iteration with the other designs in order to have it integrated into the entire design. In the first iteration some of the sub-systems placement were fixed since they can only perform efficiently at a certain configuration. For instance the payload (camera and LIDAR) position was fixed to 0.225 m from the leading edge of the UAV. This was set so that the cameras can have a tilt of up to 180°, which is important in landing procedures. This also provides the LIDAR sensor with 180°field of view. Accordingly the radar is placed at the tip of the nose so that obstacle avoidance can be realised.

The other sub-systems were placed with respect to this. In the first placement the fuel tank was left out since this is the only component in the UAV that can have variable mass in the duration of the mission. For this reason it needs to be placed at the centre of gravity of the UAV. With approximations of the initial values the centre of gravity was found for the entire system.

The next iterations were done as an update to the old placement when the detailed design of each component(tail, wing, fuselage) was finished. Figure 11.13 and fig. 11.14 shows the final placement of the components inside the UAV.

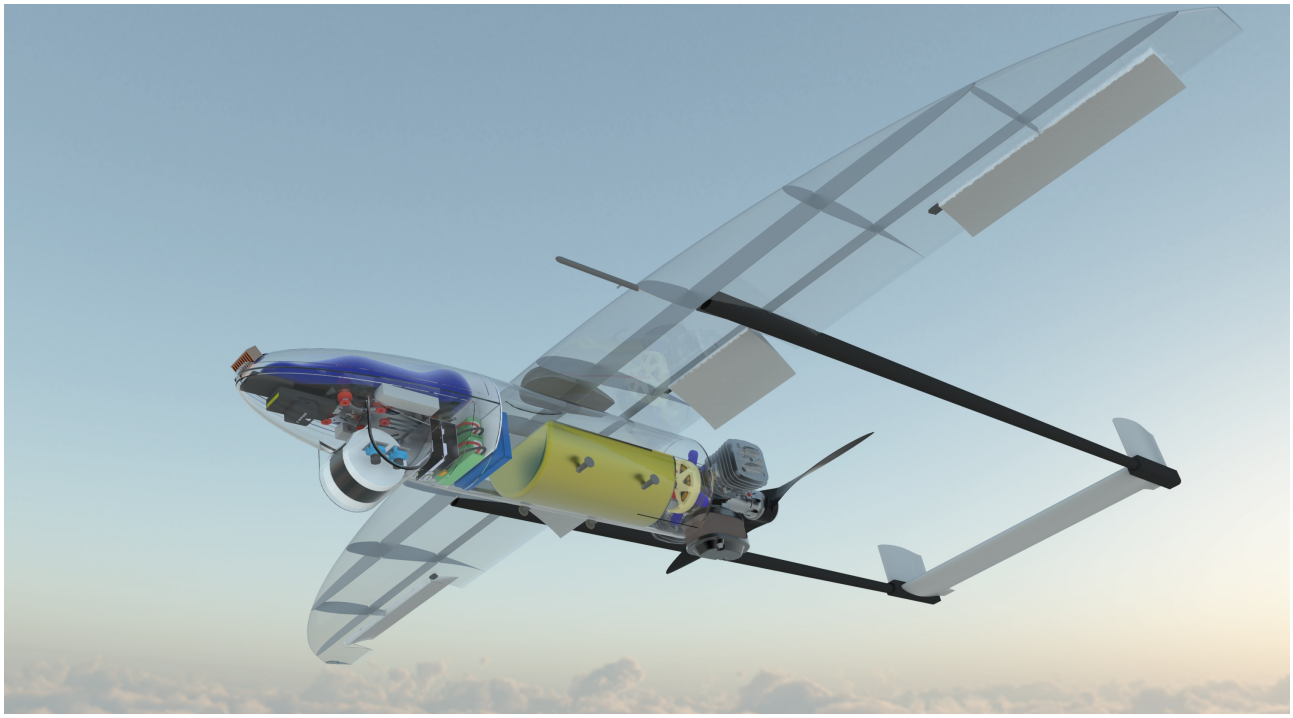

Figure 11.14: Transparent structure showing the sub-components inside.

11.10.2. Hatches

For a reliable completion of the mission the components in the UAV needs to be modular. The UAV is designed in such a way that the sub-systems inside can be accessed during the turn-around phase. Besides this there has to be a slot in the structure for refuelling the UAV. Three hatches are built into the system so that all the components are accessible. This has been illustrated in fig. 11.15. The hatch in the back opens downwards and gives access to the engine control unit, fuel pump and the fuel tank. Refuelling can be done through this hatch. The top side of the nose cone is where the parachute is placed. For packing and deployment of the parachute the top part of the cone opens up hinged at the leading edge. The bottom hatch slides to the front and then detaches downwards completely from the structure. This reveals the payload and the on-board computer so that parts can be switched and diagnostics done. This also gives access to the storage devices on-board so that further analyses can be done on the data collected.

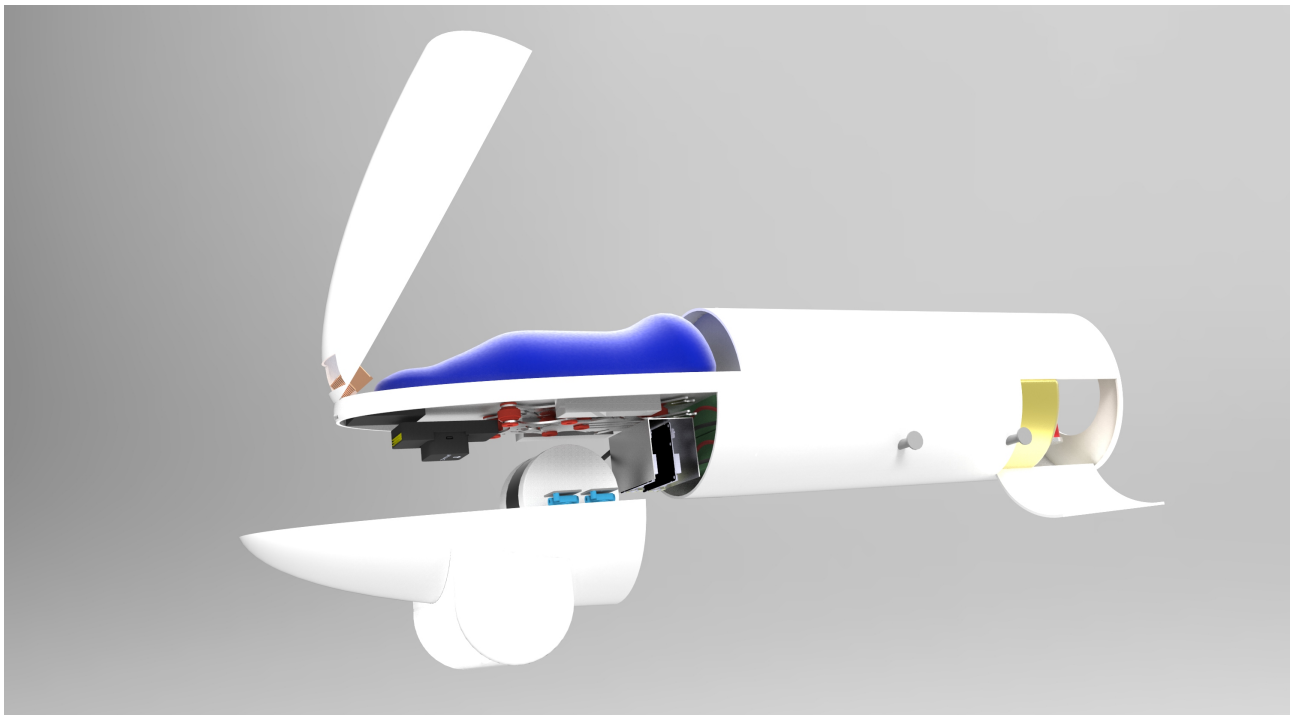

Figure 11.15: UAV hatches.

11.10.3. Power

The power requirement for the electronics is served by the generator attached to the engine. A 325W PMU acts as a central hub for the conversion and distribution of the power. It is also attached to 2 5S Lithium polymer batteries which can be used to relay power during start up as well. The importance of batteries comes in when the UAV has to be diagnosed at ground when the engine is not running and if there is an emergency during flight.

The power distribution works such that the fuel is burnt in the engine, which drives the generator connected to the PMU. This power is sent to a converter unit and transformer in the PMU that converts this power to a constant frequency that the aircraft can use, 400 hz. It ensures the system runs smoothly and records any faults. The PMU then converts the AC to DC at different voltages and supplies through its different ports to the electronics on-board. It also has two ports to recharge batteries to which the pair of 5S lipo batteries are connected.[64] The PMU can supply voltages from 5 to 21 VDC which is the range at which all the electronics on-board operates at as well.

[64] http://www.hfeinternational.com/wp-content/uploads/2016/07/250W_PMU_manual.pdf

Chapter 12: Ground station

In this chapter design of the ground station is reported. The ground station consists of several components; the landing subsystem which include the landing net and the parachute (section 12.1), the take-off subsystem which describes the launcher that is being used (section 12.2) and the pseudo-satellite subsystem which describes the configuration of the kites and the payload that is attached to it (section 12.3). The command station which is the point where all the information of the mission is being collected and the UAVs can be controlled (section 12.4). In section 12.5 the mass budget, size budget, cost budget, set up time and the amount of operators needed for the entire ground station is documented. Finally, a sensitivity analysis is carried out in section 12.6.

12.1. Landing

In this section the landing subsystem is discussed. The landing subsystem includes the landing net (subsection 12.1.1) and the parachute (subsection 12.1.2).

12.1.1. Net landing

A net is used to ensure a safe landing on varying locations without being dependent on a road or airport. A landing net is a proven concept which is used for UAVs of different sizes and masses. In this section the design of the net is explained. In sub-subsection 12.1.1.1 the general lay-out and set up of the net is explained. In sub-subsection 12.1.1.2 the landing technique itself is elaborated upon. In sub-subsection 12.1.1.3 a load analysis is performed on the net design.

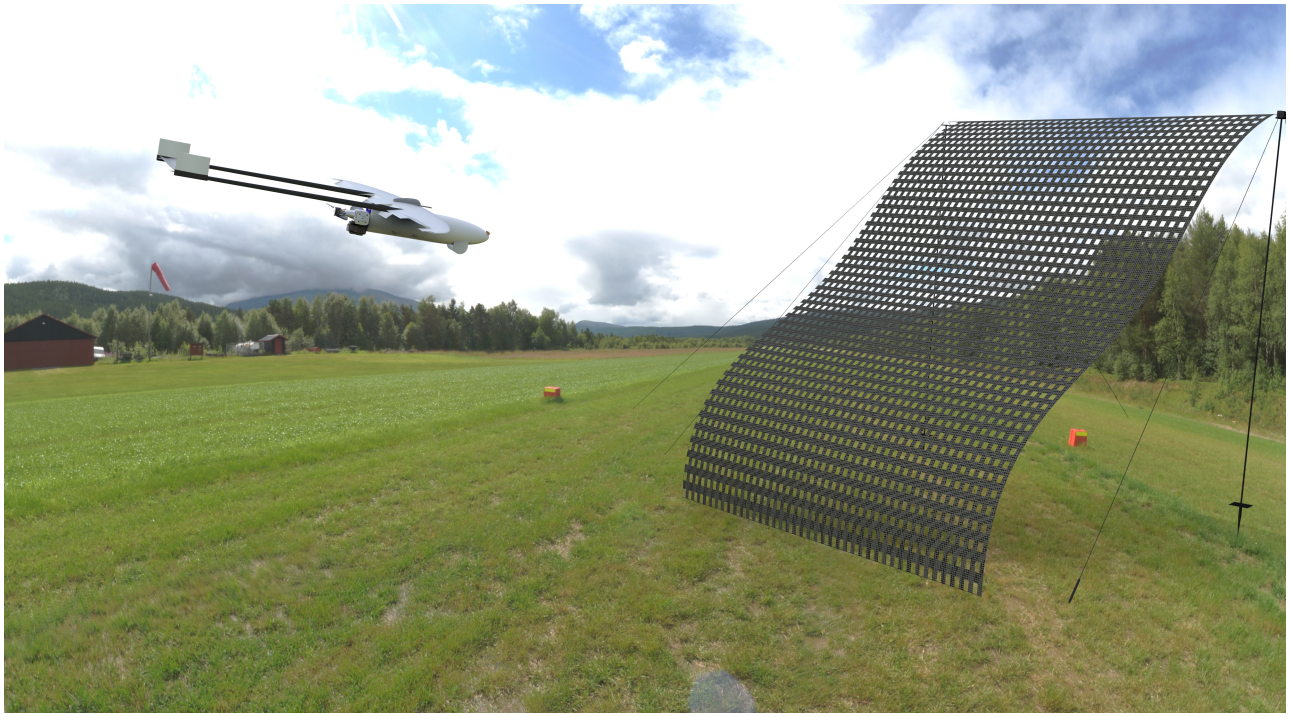

Figure 12.1: A render of the net (with exaggerated thickness) and the supporting structure.

12.1.1.1. Set-up

In the trade-off for the landing-subsystem in chapter 6 the net landing was chosen. The landing net has to be designed by the team because an off-the-shelf landing net does not exists. In fig. 12.1 a render of the drawing is presented. A frame of multiple tubes was chosen because it is easy to set up. Furthermore, using the net and two spring loaded reels, which are attached on top of the tube, the kinetic energy of the UAV is absorbed during landing. The spring reels have a brake such that there is no spring back after the impact has been absorbed. The net is attached to the ground at an angle of around 30° such in order to catch the UAV horizontally. The operators can then retrieve the UAV from the net.[65] Table 12.1 documents all the parts that are used to set up the landing net. This does include contingencies because for example the risk of losing a pin is very high.

[65] https://youtu.be/CwU5ZcbRDK8?t=2m1s

Table 12.1: The main parts that are used to build up the net.

Product	Dimensions [m]	Price [€]	Mass [kg]
UV-stabilized polyethylene net	0.0013 length x 7 width x 10.4 height	82.26	1.8
Spring Reel [2x]	0.28 diameter x 0.05 height	400	5
Ropes for attachment to ground [6x]	0.004 diameter x 10 length	59	2
Tension belts [6x]	0.035 width x 3 length	8	1.8
Tube [10x]	0.033 diameter x 1.75 length	75	46.7
Anchor tube[2x]	0.06 diameter x 0.75 length	50	3.6
Stormpin [20x]	0.02 width x 0.5 length	75	12
Wooden-pins [20x]	0.03 width x 0.4 length	25	8
Flat plate [2x]	0.4 length x 0.4 width x 0.008 height	35	0.2
IR emitter [3x]	0.3 length x 0.25 width x 0.01 height	240	3

How the net structure can be assembled is explained as follows. First the anchor tubes are anchored to the ground by hammering it into the ground. After that the hinge tubes are attached to the anchor tubes. Next step is to assemble the rest of the system flat on the ground. As soon that is done the assembled structure can be attached to the hinge tubes and raised. As final step the cords with stretch belts are attached to the ground and put under tension. The net is also attached to the ground at an angle of around 30°. During the design of the system, the mass of the system was always kept into account in order to allow the operators to move each part. The Netherlands Law on Working Conditions refers does not include a maximum mass.[66] However, it refers to the NIOSH-method to determine the mass that can be carried. A general guideline is 23 kg per person and a maximum of 50 kg for an object carried by multiple persons.

12.1.1.2. Landing in the net

In the first paragraph of sub-subsection 12.1.1.1, a short explanation is given about how the UAV lands in the net. This section explains it in further detail. The landing zone is programmed as a waypoint in the computer of the UAV. When the UAV approaches the landing zone the IR payload, which is attached to the gimbal, will be turned forward. The UAV is able to locate the landing net in three dimensions with an accuracy of 10 cm. So far differential GPS (DGPS) and real time kinetic (RTK) are both suitable systems for this but need extra antenna placement which is not desirable for the structures and control departments at this stage in the design. Instead of adding more weight to the UAV, IR emitters are used around the net which are powered by the generator. Furthermore the costs and power usage is on the low side.[67] The IR emitters will be attached to the top corners of the net structure and the ground as illustrated by blue circles in fig. 12.2. These IR emitters consist of three panels on which IR diodes are placed. Designing a lens for this system goes beyond the scope of this design phase but there are proven systems with a range of over one km.[68] The values used in table 12.1 have been derived from reference IR emitters. To ensure that the UAV has enough time to determine its relative position to the net and change its attitude accordingly, the IR emitters shall have a minimum range. The waypoint that is preprogrammed already guides the UAV in the correct direction. To eliminate as many risks as possible the UAV needs at least ten seconds to change its attitude. This led to requirement **REQ.U.LA.NET.3**. The IR camera will detect the three IR emitters and the on-board computer will compute its relative position and orientation. In combination with the altimeter the UAV lands in the net in the safe zone. The safe zone is the zone in which the nose of the UAV can land without causing damage to the UAV. When the UAV lands in the risk zone there is a risk of structural damage of the UAV. The red marked zone is the damage zone. If the nose of the UAV lands in these zone the UAV will get damaged. The dimensions of these zones are based on the wing span and length of the UAV. The damage zone at the bottom is larger because of the risk of the tail snapping off. By using these dimensions requirement **REQ.U.LA.NET.1** was derived which states that the UAV should be able to safely guide itself within these boundaries.

[66] `https://www.arboportaal.nl/onderwerpen/tillen-en-dragen`
[67] https://www.amazon.com/CMVision-IR200-Outdoor-Illuminator-Position-Adjustment/dp/B004V9Z7ZY
[68] `http://ronja.twibright.com/metropolis/dist.php`

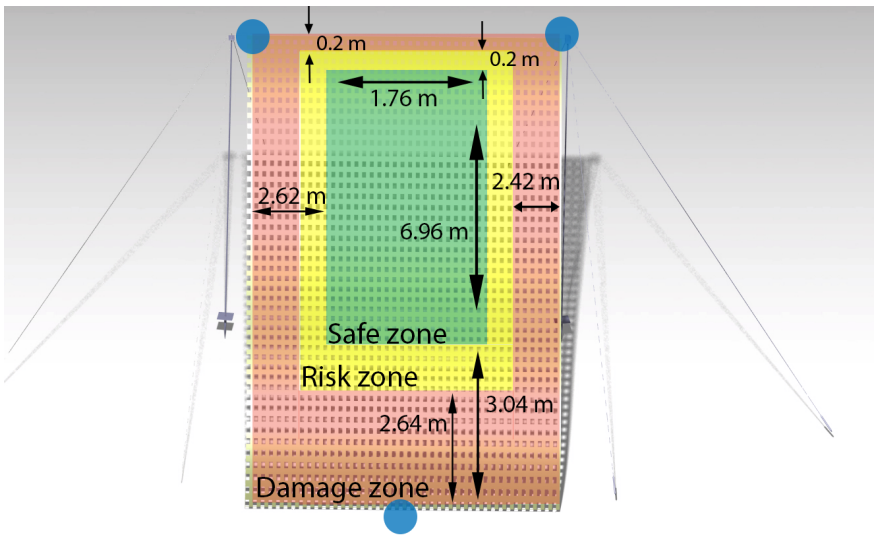

Figure 12.2: Illustration of safe, risky and damaging spots of landing. The blue circles denote the location of the IR emitters.

After the UAV has detected the IR emitters, approached the net and hit the net in the green zone, the net will absorb the kinetic energy and transfer that mainly to its top attachments to the spring loaded reels. The torsional springs will be winded up while a cable of four meter extends to create a braking zone for the UAV. This way the net will fold around the UAV such that the risk of hitting the ground is reduced. Besides that the spring loaded reels have a brake system such that there is no direct spring back. An illustration of this landing motion is depicted in fig. 12.3.

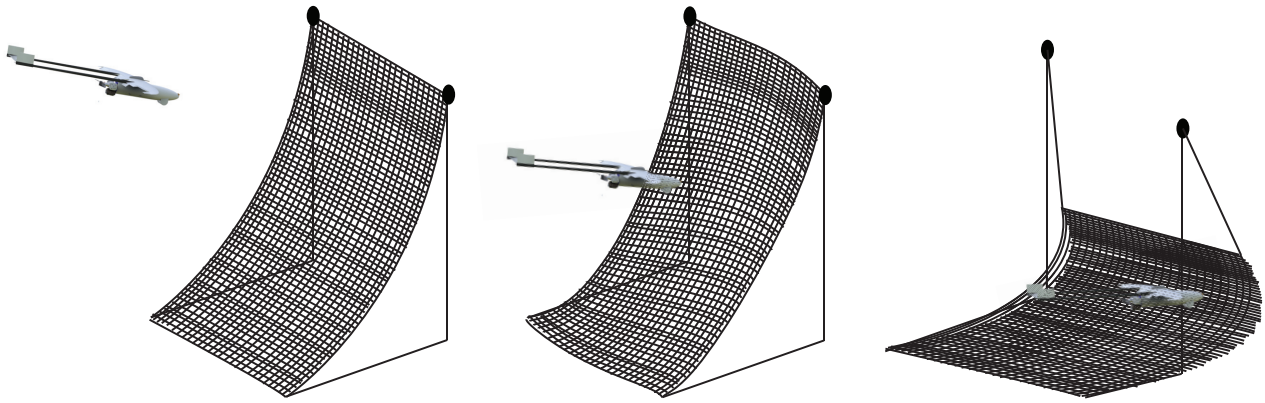

Figure 12.3: The net landing depicted in three different stages: the approach of the UAV, the first contact of the UAV with the net and the UAV in rest.

12.1.1.3. Load analysis

The impact energy was calculated and the springs in the reels are designed to absorb that energy. For these calculations, a stall speed of 18 m s^{-1} was used. However, the final approach speed shall not be equal to the stall speed. According to the Flight Safety Foundation the final approach speed is equal to 1.3 × stall speed [3]. This means that the landing speed to be considered is equal to 23.4 m s^{-1}. Consequently, the kinetic impact energy of the UAV which has to be absorbed by the net and the reel is 6,900 J. The reels will wind down a maximum of 4 m, which means that the deceleration of the UAV is 7g. The UAV has a horizontal margin of where it can land. Therefore, the spring in the reel should not be designed for the maximum 6,900 J it experiences when the UAV lands in the corner of the damage zone. A perfect landing in the middle was assumed such that the springs will not be designed too stiff. This means the spring loaded reels should absorb an energy of 3,450 J over a length of 4 m, leading to requirement **REQ.U.LA.NET.2**.

The impact energy is transferred through the net to the hook attached to the ground and the reel attached to the top of the tube. The cable which is attached to the top of the tube will therefore partly need to carry the loads induced by the impact of the UAV on the net. In order to select an applicable cable one needs to determine the required cable working loads.

This is done according to the following analogy. The force which the UAV exerts on the net is equal to the mass of the UAV times the deceleration. A UAV mass of 25 kg is used and a deceleration is determined using an approach speed of 23.4 m s^{-1}. The distance of deceleration of the UAV is determined by the configuration of the landing subsystem, which is 4 m in this case resulting in a deceleration of 68.4 m s^{-2}. An assumed constant force of 1,700 N will therefore act on the point of impact on the net. Because there is a risk that the point of impact of the UAV could be anywhere on the net, each of the

supports shall be able to handle the impact force. This means that the ground supports, the reels, the tubes and the cable shall be able to handle this impact force.

The working load of the cable depends on the impact force of the UAV, the angle with respect to the telescopic tube, the amount of pre-stress on the cable and the safety factor. The impact force of the UAV is 1,700 N. For the angle between the tube and the cable an angle of 45° is used. Due to an equilibrium in forces and considering a 45° angle, the force becomes 2,400 N. If one were to consider a pre-load of 200 N, one obtains a working load of 2,600 N. A typical safety factor for cables is 4, resulting in a required working load of around 10 kN.

Table 12.1 describes the general information of the designed net. The reasoning behind the dimensions can be found in sub-subsection 12.1.1.2. The attachment to the ground can be done by stormpins or wooden pins depending on environmental conditions. Stormpins are suitable for most types of hard surface. Wooden pins are very suitable for sandy and muddy surfaces. Including the other products adds up to a total volume of 0.1 m^3. However, in practice this efficient way of packing can never be reached and therefore a more realistic packing volume of 0.15 m^3 was chosen resulting in four different cases dedicated for specific parts each having a mass of around 20 kg.

12.1.2. Parachute landing

For emergency situations a parachute can be deployed. The parachute that is chosen is the "Fixed Wing Recovery Bundle" manufactured by Fruity Chutes.[69] Table 12.2 describes the main characteristics of this parachute. During selection of the parachute, a close look was taken at the impact energy and the loads that occur during deployment of the parachute. These load factors are documented in the structural design of the UAV. In addition, a deployment mechanism was briefly investigated. Different options are available such as a small pressured canister or the use of a spring. For simplicity and to limit weight, a spring is being used.

Table 12.2: Specifications of the chosen parachute.

Name	Mass [kg]	Costs [€]	Dimensions [cm]	Capability @ 4.6 m s^{-1}
Fixed Wing Recovery Bundle	1.2	716	13.97 diameter x 33 length	29 kg

12.2. Take-off

A choice was made to use a catapult for launch (chapter 6). Catapults for UAV-applications may use different techniques for launch. For example: a spring loaded catapult, a mass loaded catapult or using a compressor. The latter option is generally referred to as a pneumatic catapult launcher. The only type that falls in the scope of this design is the pneumatic launcher since it provides a high amount of power with a relatively low mass.

In contrast to a spring launcher, a pneumatic launcher has a near constant acceleration. This is beneficial for the design of the structure of the UAV. The chosen launcher is the "6 kJ Portable Pneumatic Catapult" developed by the UAV Factory.[70]

The launcher is depicted in fig. 12.4 with the rugged case next to the launcher. The contents of the rugged case is divided in two self-designed cases such that the weight of the system is divided and within regulations. The red clamps on top of the launcher are used to have a grip on the UAV to transfer the loads during the launch motion. These clamps can be custom made in collaboration with the manufacturer. The main focus of the clamps is that they allow clearance for the propeller. The clearance is ensured in two ways. Firstly, the height of the clamps is set such that the propeller does not touch the launcher. Secondly, the clamps fold forwards as soon as the clamps reach the end of the rail. The standard model folds the front two clamps down and the back clamps are completely let loose.[71] The customisation of the model ensures that both clamps fold down and stay fixed parallel to the launch rail instead of having a free spin. That way the propeller cannot come in contact with the clamps. The clamps themselves are holding the UAV by means of pins that are integrated in the fuselage. Section 9.7 elaborates more upon this integration.

Table 12.3: Relevant specifications of "UAV pneumatic catapult".

Rail length	Total weight	Launcher case dim.	Max. Launching energy	Max V_{launch} @ 25 kg	Set-up time	Cost
4 m	110 kg	1,313x704x543 mm	6 kJ	21 m s^{-1}	<10 min	€ 20,950

In the process of selecting an off-the-shelf catapult there are three main selection criteria: the launch velocity, the catapult rail length and the inclination of the catapult. These parameters define the acceleration the UAV has to endure during the launch. The load-factor is dependent on the maximum acceleration. The compressor will deliver 10 bar of pressure resulting in a velocity of 21 m s^{-1}. This is sufficient since the required take-off speed is 20.7 m s^{-1}, which is 1.05 times the stall speed(19.7 m s^{-1}).[72] This results in an acceleration of 5.46g.

[69] http://fruitychutes.com/buyachute/drone-and-uav-parachute-recovery-c-21/fixed-wing-bundle-c-21_22/fixed-wing-recovery-bundle-64lbs-29kg-15fps-p-137.html

[70] http://www.uavfactory.com/product/21

[71] https://youtu.be/UjUKY-8xQ50

[72] http://avstop.com/ac/flighttrainghandbook/takeoffperformance.html

The inclination of the catapult is important since it defines the initial climb angle after take off. This means the available power shall be sufficient in order to obtain a climb angle of 11°. According to the power equation (eq. (12.1)) for steady symmetric flight in climb the available power is linked to the maximum climb angle [60]. Using the velocity when the UAV leaves the catapult and a C_D at $C_{L,max}$, the required available power is determined to be 1.8 kW. This is sufficient since the engine available power is 9.7 kW(= 13 hp). Moreover, the engine does not need an external starter since this is already integrated in the system. The PMU that is chosen has the ability to start the engine.

$$\frac{P_a - P_r}{W} = RC = V sin(\gamma) \tag{12.1}$$

Besides the climb angle, a look was also taken into the performance in strong wind conditions. The launch speed and stall speed are relatively close together. Therefore, it is important to have the catapult directed towards the wind direction such that headwind is ensured. The flexibility of the orientation of the catapult guarantees that this is possible.

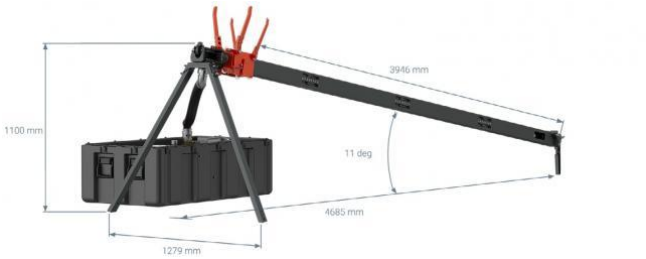

Figure 12.4: The UAV pneumatic catapult developed by the UAV Factory.

12.3. Pseudo-satellite

In chapter 6 it was decided that a kite shall be used as pseudo-satellite. Prior to the configuration choice and selection of the kite the payload of the kite has to be established as discussed in subsection 12.3.1. In subsection 12.3.2 the power supply of the payload to the kite is deliberated. At this stage, the mass of the payload is known, meaning that a kite can be selected as documented in subsection 12.3.3.

12.3.1. Kite payload

The purpose of the kite is to provide a communication relay between the ground station and the SAR-teams/UAVs. To fulfil this purpose, a communication payload is required on the kite. The payload including its components can be seen in table 12.4. To provide a communication relay a set of transceivers are needed: A transceiver to send information to the SAR-teams/UAVs which is able to reach 50 km and a transceiver which sends information to the ground station. Additionally, in order to prevent collisions with other air traffic, a transponder is added to the payload as well as a set of LED-lights. In order to transmit a signal, a set of antennas is needed, which contribute to the mass- and cost budget. Finally, these items require a power source, which will be discussed in this section.

Table 12.4: The payload of the kite.

Component	Weight [g]	Power consumption[W]	Cost[€]
Battery pack	1,900	-	500
Transponder	78	2.0	3,500
Transceiver	120	40.0	7,500
Transceiver	120	4.8	7,500
Antennas	400	-	-
LED	100	9.5	50
Total	2,718	56.3	19,050

12.3.2. Power supply

The payload needs a power supply to work. The power consumption of the payload can be found in table 12.4. This is the maximum power that is consumed when one of the transceiver needs to exchange information at the maximum 50 km range. Assuming this worst case scenario the following trade-off on power supply has been done. The options are: a power cable integrated in the tether, a wind turbine mounted on the kite, solar cells attached on top of the kite and a battery pack.

Power cable tether

To trade the power cable tether off, its feasibility had to be determined. Starting by checking the resistance of a very long cable (as it is required to be a couple of hundred meters long), a certain cross-sectional area was derived. Using that cross-sectional area with the length and density of copper, a mass estimate was derived for the cable. Usually the cables consists of three different cables woven together. A typical area is 3 × 15 mm^2 = 75 mm^2 which translates to a mass of 3 × 80 kg = 240 kg. Decreasing the area to an unrealistic 3 × 0.5 mm^2 translates to a mass of 3 × 2.6 kg = 7.8 kg with a power of 2.7 kW. This mass cannot

be pulled by the kite at low wind speeds. An option to save mass is to make increase the power and decrease the area further. However, this is unreliable and unsafe. Judging from these calculations, the use of a power cable tether is judged as not feasible.

Wind turbine

A wind turbine can be used to generate energy which can be stored in a battery for when the wind speed is too low. The standard power output equation for a wind turbine was used.[73] The used energy for reference corresponds to 8 hours of using the payload. An altitude of 3 km was used for the density and using a wind speed that corresponds to 4 Bft, a diameter of 1.1 m is needed for the covered circular area of the turbine blades. For a lower wind speed of 2 Bft, a diameter of 4 m is needed. Judging from these numbers, the wind turbine is not feasible since both kites will not be able to have a wind turbine of that size attached to it.

Solar cells

Solar cells can be attached to the kite to generate power. Some state-of-the-art solar cells are bendable and therefore attachable to the kite.[74] The power output of a solar cell has been computed using the standard equation with default values for the constants.[75] A worst case daylight solar radiation of 100 W m^{-2} was assumed. To charge the battery for a night of eight hours an energy of about 400 W h needs to be generated. This results in a required area of 27 m^2. This area is too large to fit on the selected kites and therefore solar cells are not a viable option.

Battery

A battery can also be used to power the subsystems of the kite. The disadvantages are that the battery adds weight and needs to be replaced when discharged. It is not possible fulfil the entire 72 hour mission with no recharge. From table table 12.4 the amount of energy needed in eight hours can be derived. This is $8 \times 56.3 = 450$ W h. This value has been taken as a reference point for the battery selection.

An investigation was done on different types of existing batteries and a choice was made for Panasonic NCR18650B.[76] In table 12.5 the specifications for this battery can be found. This means an added weight of 1.876 kg (including extra material needed to assemble these batteries together) needs to be pulled by the kite(s). This number includes a contingency for when the battery is not delivering its nominal voltage. Assuming worst case scenario, meaning wind still conditions, the pull force of the Helikite has to be sufficient. This in an iterative process which influences the sizing of the Helikite as documented in subsection 12.3.3.

Since increasing the capacity of the batteries increases the weight the batteries, there is a limitation on the maximum capacity possible. The batteries will be discharged after eight hours using the payload on maximum operational power. The system does not allow downtime because the UAVs would then become uncontrollable from ground thereby infringing **REQ.U.SYS.19**. Therefore, when one kite gets pulled in, the extra kite has to already have been deployed. A choice was thus made for multiple kites which is further elaborated upon in subsection 12.3.3.

Table 12.5: Relevant specifications of Panasonic NCR18650B.

Voltage [V]	Capacity [mA h]	Charge time [h]	Weight [g]	Price [€]
3.6	3,350	4	48.5	13

12.3.3. Kite selection

Using a defined payload of the kite, a selection of the kites can be performed. The most important factor in the configuration of the kite-system is the wind-speed. The kite-system shall be able to operate in windless conditions as well as 8 Bft conditions. The windless conditions impose a challenge to the kite design, since there is no wind to lift the kite, while the 8 Bft conditions impose a challenge on the kite design, since the pulling force can get high or the kite can drift away from the ground station. Since the kites can drift from the ground station, the cable has to be designed for this scenario such that the altitude of the kite is still 300 m. The most critical angle is 30° with respect to the ground surface. That results in a cable of at most 600 m. The cable is documented in table 12.6 and will be used for all the kites.

Certain regulations must be followed by the kite in terms of flying altitude and visibility. In different countries the maximum height of flying a kite without a permit is different. In emergency situations SAR operations have a ceiling of 600 m where operation transition takes place and an active zone ceiling of 300 m.[77] Therefore, the kite is designed to operate at a height of 300 meter. Visibility also plays an important rule. When the height of the kite is above 30 meters there has to be an obstacle avoidance light on the tether every 15 meter. On top of that the kite itself also has to have a light to increase its visibility.[78] As a solution reflective material can be attached or braided into the cable which will be enlighted by a laser system from the ground.[79]

[73] http://www.engineeringtoolbox.com/wind-power-d_1214.html
[74] http://www.altadevices.com/wp-content/uploads/2016/11/technology-performance-brief.pdf
[75] http://photovoltaic-software.com/PV-solar-energy-calculation.php
[76] https://www.conrad.nl/nl/panasonic-ncr18650b-speciale-oplaadbare-batterij-18650-li-ion-37-v-3350-mah-1410110.html
[77] https://info.publicintelligence.net/FAA-DisasterAirspaceManagement.pdf
[78] https://www.faa.gov/documentLibrary/media/Advisory_Circular/AC_70_7460-1L_.pdf
[79] http://www.kitepower.eu/home.html

Because there is no kite which can meet the requirement to operate either in a 0 Bft wind condition and an 8 Bft wind condition, a low and a high speed kite was chosen. The low speed kite is the Helikite which is explained in subsection 12.3.3. The high speed kite is the Delta kite which is elaborated upon in subsection 12.3.3. The amount of kites that is being used is described in subsection 12.3.3.

Helikite

The windless conditions require a solution which do not depend on the wind speed. This is why a Helikite is chosen to be included in the system.[80] This system is able to operate in windless conditions due to the lifting capacity of the helium. However, due to integration with an aerodynamic foil, the system is able to sustain a wind speed of 6 Bft. The netto lift the Helikite has in wind still conditions is most critical. This net force is 12.91 N, which is sufficient to climb to high altitudes. In subsection 12.3.1 the payload of 2.7 kg has been defined. The kite shall thus be able to lift its own mass in addition to the mass of the payload and the mass of the tether. In order to lift the mass a 7.0 m^3 kite is chosen as depicted in fig. 12.5.

Figure 12.5: The 7.0 m^3 Helikite developed by Allsopp Helikites.

In table 12.6 the most important products and their parameters are documented for this kite set-up. What stands out is that there are two Helikites bought such that once the batteries are drained of one set-up, the new kite is up and running.

Table 12.6: Size, mass and cost of the helikite set up.

Product	Dimensions disassembled [m]	Mass [kg]	Cost €
2 x Helikite Skyhook 7.0	1.75 length x 0.2 x 0.2	4	4,400
5 x 3.5 m^3 Helium gas	5 x 1.0 length x 0.22 diameter	114	1,950
3 x Kite and Kontiki Winch	2 x 0.4 length x 0.4 width x 0.3 height	66	2,925
2 x 2.2mm diameter rope x 1,000 m White Braiden Dacron	2x 0.6 length x 0.3 diameter	3	220

Delta kite

The kite chosen to operate in the wind range of 5 - 8 Bft is the Nighthawk Delta Kite as can be seen in fig. 12.6.[81] This kite is designed for fishing and is also proven to be suitable for steady aerial photography. This kite is characterised by its steady performance in high wind conditions.

[80] http://www.allsopp.co.uk/index.php?mod=page&id_pag=10

[81] http://www.kapshop.com/Lifters-Kites-Framed-kites/c75_3_55/p216/Paul&%2339s-Fishing-Kites-Nighthawk-(or-Kiwi-Delta)/product_info.html

Figure 12.6: The deltakite developed by Paul's fishing kites.

The kite has the payload of table 12.4 attached to it and an overview of the system can be found in table 12.7. Moreover, the cable used by the Nighthawk is the same as for the Helikite and is strong enough to cope with the loads.

Table 12.7: Size, mass and cost of the delta kite set-up.

Product	Dimensions disassembled [m]	Mass [kg]	Cost [€]
2x Nighthawk Delta Kite	1.50 length x 0.05 width x 0.05 height	1.8	264

Multiple kites

In subsection 12.3.2 the decision for multiple kites was made because a downtime in communication is not acceptable. This includes two Helikites and two deltakites. After 8 hours the kite will come down to charge the battery pack. Because the communication relay shall be provided during the whole 72 hours, a second kite shall already be deployed when the first kite will be retrieved. The second kite shall be deployed with a minimum distance of 20 meter perpendicular to the wind direction to the first kite due to interference between the two kites.

However, the use of two kites induces a problem: for a certain time frame there are two communication relay-systems active. This problem is being solved by a command from the ground station in which the payload of the first kite will be switched off and the payload of the second kite will be switched on.

12.4. Command Station

Besides the landing, take-off devices and the kite, the ground station consists of a control environment in which operators can analyse data, select targets, programme a flight path and intervene with flying in emergency situations. This section elaborates on the lay-out of this command station. Subsection 12.4.1 describes the generator chosen for power supply. Subsection 12.4.2 outlines what command station is used. Subsection 12.4.3 elaborates on the applications of the command station. Figure 12.7 gives a summarising illustration of the ground station.

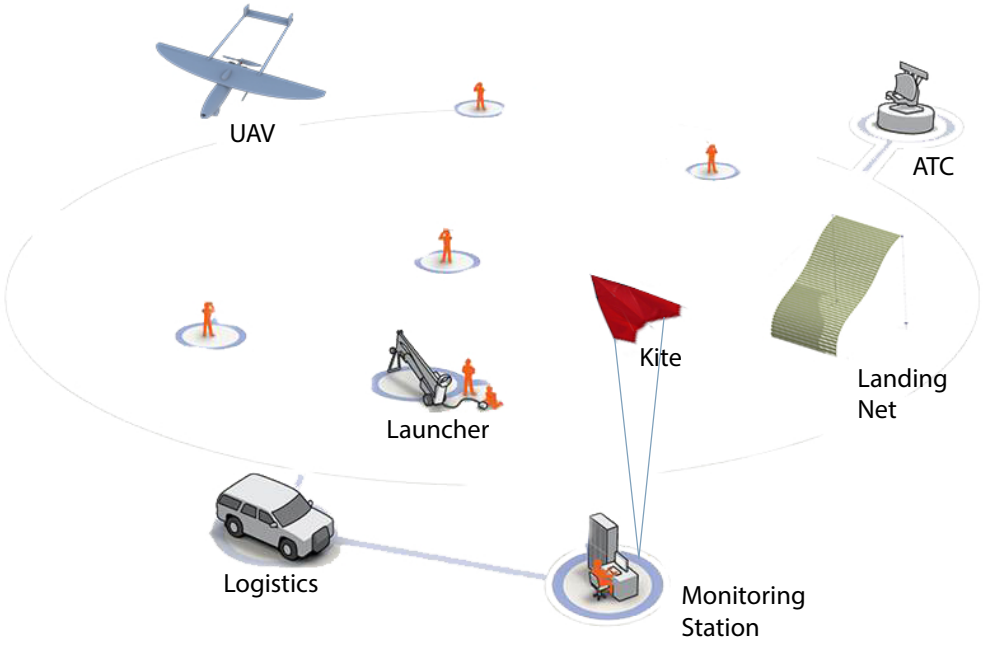

Figure 12.7: An illustration of a typical ground station set-up.

12.4.1. Power supply ground station

The power supply for the ground station will consist of a generator. Although in most cases this generator might already be present at the SAR command station itself, the system will contain a generator in case there is no power supply present. This generator is chosen according to the devices it needs to supply with power. The four most power consuming devices are the battery chargers, the computers, the catapult and the kite winch. All these systems combined will have an power consumption of 1.3 kW when running simultaneously.

The selected product is the GP2200i from Generac.[82] In table 12.8 the specifications of the GP2200i are shown. As can be seen the 1,700 W is sufficient to provide the power to run all the devices simultaneously. The runtime will be around 10 h when running at 25% of the running power, which is realistic. As discussed in sub-subsection 12.1.1.1, the maximum weight an operator can carry is 23 kg. As can be seen in table 12.8 an operator is allowed to carry this device alone according to the Netherlands Law on Working Conditions and it can be carried by two persons or more. The fuel that this generator uses is included in the UAV budget where also the fuel of the UAV can be found. This is mainly because the designated volume for the ground station does not leave more room while the UAV volume budget does. This is reported in subsection 4.3.1.

Table 12.8: The specifications of the selected generator.

Generator	Running power[W]	Starting power[W]	Fuel tank capacity[L]	Approx. run time[h]	Weight[kg]	Price [€]
GP2200i	1,700	2,200	4.5	10.8	21.1	539

12.4.2. Command station

The control panel will consist of two portable ground stations illustrated in fig. 12.8. This ground station is integrated in a durable military case. The advantage of buying this off-the-shelf integrated system is that it works like a docking station.[83] On the left a laptop can be docked. On the right numerous hardware can be attached in the modular hardware compartment. Most universal types of cables are already integrated in the casing of the ground station. The top right monitor can be used for different kinds of information. The manual controllers can be put on top of the modular hardware compartment. All the hardware in this case is automatically linked to the docked laptop. In essence, it is a plug and play system. Furthermore this ground station can be set up anywhere and can resist tough weather conditions. In the case of the rare event that two UAVs need to be manually controlled by the ground station by two different operators. To meet the regulation requirements two ground stations are needed to control both UAVs separately. The controllers used is the Thrustmaster Hotas Warthog.[84] The laptop that is being used is the Panasonic Toughbook CF-31 which is fully compatible with the control station and resistant

[82] http://www.generac.com/all-products/generators/portable-generators/gp-series/gp2200i
[83] http://www.uavfactory.com/product/16
[84] https://www.consoleshop.nl/product/114506/thrustmaster-hotas-warthog-a-10c-aircraft-controller-replica-pc.html?tid=pla-285101642602&ref=359869&label=22706-AGI-45823735852-ASI-285101642602-114506&gclid=CjwKEAjwj6PKBRCAy9-07PeTtGgSJAC1P9xG6DGtLxYnGbMfxeKdF94kGfE6CnzRwAmDvcOzeoLiqxoCOonw_wcB#product_specifications

to any weather condition.[85] All of these hardware are documented in table 12.9. In the modular hardware compartment a hard-disk is mounted. This hard-disk needs to store at least 36 hours of data and therefore a capacity of at least 512 GB is needed. For contingency and backups five hard-disks of 1 TB will be used. Furthermore a data link system is implemented to ensure data transfer between the pseudo-satellite and the ground station.

Table 12.9: Main components used for control station.

Product	Price [€]	Mass [kg]	Dimensions [m]
Panasonic Toughbook CF-31 [2x]	2,613	3.7	Incl. in control station case
Thrustmaster Hotas Warthog flight stick [2x]	229	6.35	0.32 x 0.26 x 0.44
Portable Ground Control Station [2x]	2,013	18.9	1 x 0.42 x 0.17
Harddisk 1TB [5x]	305	0.5	Incl. in control station case
Data link	2,950	0.1	Incl. in control station case
GP2200i generator	539		0.250 x 0.110 x 0.210

12.4.3. Command station applications

The ground station receives the mapping data. This mapping data has to be analysed by the operator. After the operator has done its analysis the important information can be send to the SAR teams. This can be done by voice communication. However, depending on the hardware the SAR teams are carrying, also visual information can also be send. The latter is of great value because the risk of misunderstanding is mitigated. In such a case a controller can for example mark on the touchscreen the ground station the areas of high interest and the optimal route to get there and send that to the SAR teams. That way the ground station becomes an extension of the headquarters of the whole mission with a much better logistic overview than nowadays procedures.[52] The information that is exchanged during the missions is also vital for an emergency helicopter because the pilot knows before hand the location of a found injured person and what spot is suitable for landing. An additional application of visual information is the use of IR payload to detect humans. For LIDAR, the software that comes along with the sensor and will be used to have a live render of the point cloud. This is for example very useful for forest fires as the LIDAR sensor can look through the canopy of a forest. Besides that the three dimensional mapping ability of the LIDAR can be useful for missions with a high density of casualties such as partially collapsed apartment buildings. How all of this goes into practice is roughly found in the mission simulation documented in chapter 4.

As already briefly touched upon in subsection 12.4.2, the UAVs must have the ability to be manually controlled simultaneously during emergency situations. The options that operators have are manually controlling the aircraft using the video stream as feedback and deploying the parachute. A look has been taken into beyond line of sight manual control regulations. So far there are not hard laws yet but a general rule is that there should be a video live stream and the operator can always overrule manually the controls of the UAV. [35] This means the combination of the live stream and the controllers that are plugged into the ground station are used for controlling the UAVs.

The command station can also receive meteorological information about the disaster area. Upcoming weather conditions can have a crucial influence on the mission. Having this information centralised at the command station of the UAVs can reduce the risk of SAR teams getting trapped in dangerous weather but also prevent the UAVs from flying in challenging weather conditions.

Figure 12.8: Monitoring station with an example configuration of the modular electronic compartment included.

12.5. Total cost, size, mass and time budget ground station

This section includes the total cost and size budget of the whole ground station. All the subparts are broken down in the respective section in this chapter. Table 12.10 shows the total budget. During derivation of the size budget a close look was taken at whether the calculated volume is realistic due to inefficient packing. It is important to pack as efficient as possible

[85] http://www.micronordic.eu/toughbook_cf_31_spec_sheet.pdf

since the maximum volume is a hard constraint. Besides that, during packing or unpacking parts shall not get lost easily. To mitigate that risk the subparts are fitted in designed cases. These cases are used for volume estimation and therefore the total volume is realistic. Also, a check was done whether the cases are not too heavy to be carried according the working condition laws as mentioned before. The size does meet **REQ.G.SYS.5**, which states that the maximum volume for the ground-station should be 1.25 m^3. During the derivation of that requirement already the risk of inefficient packing was taken into account. By means of these conditions it can be assured that the packing volume will not cause problems.

The cost requirement is met with a safe margin. Requirement **REQ.G.SYS.6** states a maximum price of ground station of 70,000 €. Table 12.10 shows a total cost budget of 54,415. Furthermore, requirement **REQ.G.Com.K.2** states the maximum price of the kite should be 70,000 €. This requirement is also easily met. On top of that, the cost of the kite system is included in the total ground station budget (as opposed to what the wording of both mentioned requirements imply).

Table 12.10: Total volume, cost and mass budget of ground station.

Subpart	Volume [m^3]	Price [€]	Mass [kg]
Total control station	0.114	8,649	50.1
Total landing net	0.158	1,046	97.5
Total redundant parachute	0.005	800	1.2
Total catapult launcher	0.500	20,950	110.0
Total kite payload	0.002	19,001	2.7
Total kite	0.365	10,149	96.2
Total	1.144	60,595	357.7

The ground station can be operated by three persons. One pilot who analyses the data that is being collected and operates the ground station. In case of emergency he/she can control the UAV manually. One extra pilot is idle and switches with the working pilot after twelve hours or helps when the working pilot is in an emergency situations by the UAVs. A different person is needed to operate the kite and the landing and take-off subsystems. This person will be mostly idle and therefore can assist the pilot in analysing data. That means that two persons are working at the same time while one person is resting.

To set-up the system the following time budget was derived. The compressor takes 10 minutes to be filled which can be done concurrently with setting up the rest of the catapult. That will take 10 minutes in total to set up with two persons. After that the two same persons build up the net which takes about 20 minutes. Meanwhile the third person has 30 minutes to set up one kite, attach the payload, run diagnostics for the kite payload and launch the kite. While the winch unwinds automatically the third person can join up with the other two persons to set up the ground station in 10 minutes. After that the UAV is assembled and diagnostics is run in 15 minutes. Then the UAS is ready. All this is summarised in table 12.11.

Table 12.11: Time budget to set up the ground station.

Activity	Time needed [min]	Persons
Filling compressor	10	0
Setting up catapult	10	2
Building up net	20	2
Setting up kite	30	1
Setting up control station	10	3
Running diagnostics	15	3
Total time	55	

The turn-around time budget was also derived. As soon as the UAV lands in the net it takes about two minutes to retrieve. To tension the net one minute is needed. Meanwhile the UAV can be re-fueled in three minutes. After that diagnostics are done in five minutes. It is assumed that programming the computer of the UAV is already done during operation since then the new targets will be known. After that the UAV is attached to the catapult and launched. This total turn-around time budget is shown in table 12.12

Table 12.12: Time budget of turn around time.

Activity	Time [m]	Persons
Retrieve UAV from net	1	3
Tension net	1	1
Re-fuel UAV	3	2
Diagnostics	5	3
Attach to catapult	1	3
Launch from catapult	1	3
Total time	12	

12.6. Ground station sensitivity analysis

In order to check the design on its robustness a quick sensitivity analysis was done on the stall speed, the main parameter of the ground station, that has influence on the design of the UAV. The stall speed has an influence on both the take-off and landing subsystems. Increasing the stall speed will have an effect on the take-off speed. The current catapult launcher is

not able to increase the launch speed above 21 m s^{-1}. To increase the launch speed to a maximum of 24 m s^{-1} the heavier edition of the catapult launcher has to be used.[86] However, this catapult launcher is larger (0.98 m^3 and will cause the total volume budget to overshoot the requirement mentioned in section 12.5.

The stall speed also has an influence on the landing net. When the stall speed increases the landing speed also increases. As an example the stall speed is increased to 20 m s^{-1}. That means a landing speed of 26 m s^{-1}. If the same brake distance, i.e. the extension of the cords of the reels, of 4 m is used the load factor will be 8.6g. For the original stall speed the load factor was 6.9g. To get the load factor down to that value an increase in brake distance to almost 5 m is needed. That ultimately results in the net structure being increased at least 1 m in height because otherwise the risk of the tail hitting the ground is too high. On top of this, the reels have to be able to absorb this increase of kinetic energy to a total of 8,450 J.

Judging from above analysis the main challenges that come with a higher stall speed are finding or designing a launcher that does not overshoot the volume requirement and the net structure that becomes larger. Therefore during the design process there has been close contact with other departments. It can be concluded from this sensitivity analysis that the ground station design does change but not to an unacceptable extend when certain parameters are changed. There is a chance that it will cause the ground station to overshoot the volume budget. However, the system will still work if a different type of transportation is found. This can be for example multiple mini-vans.

[86] http://www.uavfactory.com/product/78

PART III
Product assessment & project design logic

The third and final part includes an assessment on how concurrent engineering has been applied to the final design phase. Additionally, part III includes a risk assessment analysis of the product. Moreover, an assessment of the sustainability of the product is made. Following the sustainability, an investigation on reliability, availability, maintainability and safety is also carried out. To conclude, the project design logic for continuation of the project is described; including a cost break down analysis.

Chapter 13: Concurrent engineering strategy

Concurrent engineering is a method that is used during designing and developing products, in which the different departments run simultaneously. Following this method, the product development time decreases and an improved productivity is obtained.[87] Before the final design, the team first discussed the required outputs that needed to be obtained. After which, these required outputs were divided into several technical sections, which would elaborate on the values and conditions into more detail. The team was divided into electronics, control and stability, aerodynamics, structures and ground station. Information from one department is useful to one or more departments, and an N2 chart is made to visualise the iterations needed. This is of tremendous importance to know the required values for every department in order to complete their design process.

Electronics	Power for servos/actuators	antenna placement payload placement	placement: position + volume + mass payload position electronic connections and cut-outs	capability of landing sensors software output data handling
Power for servos/actuators Number of sensors/actuators (+power)	**Control & Stability**	tail size, Control surface size, fuel size	tail, volume, surface area tail, tail span control surfaces: rudders, elevators, ailerons, C_{Lmax}, control surface position dimensions	
	C_L ,C_{L_alpha} drag polars c_l-alpha main wing surface area	**Aerodynamics**	span, chord, taper, shape, airfoil thickness wing position, tail dimensions, tail position, C_L, C_{L_alpha} ,boom separation, L_h	wingspan stall/landing speed t/o speed
Distributed system or Safe payload position	Wing parameters, c.g. position maximum l_h allowed moments of inertia fuel placement	minimum fuselage size wing parameters tail parameters material properties	**Structural**	t/o limiting loads impact energy of parachute sizing of system
sway of kite (for antenna) landing net instruments + dimensions data handling details	manual control	Stall speed	take-off catapult rails, dimensions catapult loads net landing loads parachute landing	**Ground station**

Figure 13.1: N2 chart depicting the required values needed by there departments.

A constant communication link between each department was assured to make sure the values taken were up-to-date. If there was an iteration needed, everyone with a connection to the corresponding value value was made aware that an iteration was going to take place. During the design phase, a master sheet was created and maintained in which, every department put there values. Everyone could obtain required up-to-date values while designing there own part. In case a change was made in the sheet, the value was highlighted in a different colour to make sure all the departments were aware of the changes being made. The concurrent engineering worked robust as everyone communicated with each other, and everyone followed the prescribed procedures. However, the iterations could have been more efficient. Sometimes the iterations took longer than they should have with as a result, the number of iterations increased unnecessarily. If this process was done more efficiently this number could have been more optimal.

[87] http://www.concurrent-engineering.co.uk/

Chapter 14: Risk assessment

In this chapter, the risk analysis is discussed. Analysing the risk of the operation is an important task to take care off while designing the UAV, as it will help to figure out what should be done in case of some trouble or inconvenience, and what can be done to solve this problem. This is done by first listing the most important technical risks. The risks can be seen in table 14.3, and an overview can be seen in table 14.1. After this, the effect of the mitigation's is shown in the risk assessment shown in table 14.2.

In the tables the impact is also shown in colour, which is a combination of the probability and the effect of the risks. The red colour shows the highest impact and the blue one the lowest. The colours were inspired from [5] and adapted by looking at how critical the combination of effect and probability is. For example, the highest effect (catastrophic) will always be regarded as critical for the project regardless of the probability, and has the highest impact (red).

Table 14.1: Risk assessment matrix before mitigation.

		Probability				
		1 (remote)	2 (rare)	3 (unlikely)	4 (possible)	5 (likely)
Effect	1 (no effect)					
	2 (negligible)					
	3 (marginal)			8	20	
	4 (critical)			4, 12, 18		
	5 (catastrophic)	3, 14, 27	1, 2, 7, 10, 19, 25, 26	16, 17, 24	5, 6, 11, 13, 15, 21, 22, 23	9

Table 14.2: Risk assessment matrix after mitigation.

		Probability				
		1 (remote)	2 (rare)	3 (unlikely)	4 (possible)	5 (likely)
Effect	1 (no effect)	10	9		5	
	2 (negligible)	27	19, 25		3, 20, 21	
	3 (marginal)	8	1, 2, 18, 26	24	6, 23	
	4 (critical)	7, 14, 12	11, 4, 17			
	5 (catastrophic)	3, 13, 15, 16, 22				

Table 14.3: Technical risk management.

ID	Cause	Event	Consequence	Probability[88]	Effect[88]	Impact	Mitigation
1	The UAV is out of range and the antenna not powerful enough to transmit the signal.	Signal is lost	If redundancies not present the UAV can crash. The data collected during this stage is lost.	2	5	5	Have a pre-planned flight path and fly back. This can be done if there is no check command received for short time (for example, 10 seconds). Also, on-board storage can be present to store data temporarily. This will reduce the effect from catastrophic (5) to marginal (3), since this area can not be mapped as easily as another area.
2	Interruptions in the signal or poor transmission power	Loss of data packages	Incomplete data and a lot of noise in the data, resulting in unusable data.	2	5	5	On-board storage can be used to store data to be transmitted when a clear communication can be set-up. Also, the data can be relayed through other UAVs. This will reduce the effect from catastrophic (5) to marginal (3), since this area can not be mapped as easily as another area.
3	The structure is very complex	The design is not manufacturable	The structure contains components that are too intricate to be manufactured thus resulting in a failed design	1	5	5	Create a CAD drawings to check if the design is manufacturable, and have regular checks on the full assembly. This will decrease the probability, but since there is no number lower than remote, and CAD drawings are to be used anyway, there will be no effect in the risk assessment matrix.
4	Not enough protection for the external and internal components of the UAV.	Thermal failure	The structure and/or internal components fail due to excessive cooling or heating.	3	4	4	Investigate the environmental factors that are present during the operation of the UAV. A thermal shielding can be attached to the critical areas of the UAV. After this, the probability will go down from unlikely (3) to rare (2).
5	Midair collision	Structural damage and/or damage to vital sensors and actuators	The UAV can crash or subsystems fail	4	5	5	As the system will include two UAVs, if there is a bird strike that occurs on one of the UAV, the second UAV can be deployed and used to continue with the tasks. This will cause the effect to go down from catastrophic (5) to no effect (1).
6	The legislation for UAVs in disaster areas changes	The UAV is not allowed to fly in certain conditions.	The UAV cannot fly or it shouldn't fly in certain conditions	4	5	5	Accounting for the trend in law and future changes to make a certifiable design. This will decrease the impact from catastrophic (5) to marginal (3). This is because the UAV can be changed faster according to the change in the regulations.
7	Fuel trap/battery power loss	Sensors and actuators offline before end of mission and there is a lack of propulsion	The UAV can crash and data is lost	2	5	5	A small backup battery pack on-board that could be used to return to the ground station. For a fuel propelled UAV, an extra filter can be used. Maintenance is needed to reduce the chances of a fuel trap occurring. These mitigations will decrease the effect from catastrophic (5) to critical (4), since it is still a problem. Also, the probability will decrease from rare (2) to remote (1) because of the maintenance.
8	Different parties use the same bandwidth	Communication interference occurs	There is no possibility to communicate	3	3	3	Define clearly at the beginning of the mission which bandwidth is to be used by different parties. This will decrease the probability from unlikely (3) to remote (1).
9	UAV flies in clouds/-fog/smoke or deterioration of camera occurs	Camera failure/no visual	Mapping is not possible	5	5	5	As one of the criteria used to trade-off the cameras used was the visibility. This was taken into account, thus this has no affect on the cameras . This will cause the effect to go from catastrophic (5) to no effect (1). However, for the RGB cameras, they do get affected by the clouds present, as a result, this will cause the effect to go from catastrophic (5) to negligible (2).
10	The user suffers from health issues or does not perform it's work properly	User Fall-Out or a wrong user input	The system is not monitored (properly) which could cause mapping of the wrong area. The configuration of the system can be performed worse, resulting in a bad performance of the mission.	2	5	5	Make sure that the user will not be in charge of the system for more than a certain amount of time. Also, a backup operator should be present to take over if something goes wrong. This together will decrease the probability from catastrophic (5) to marginal (3) and the probability from rare (2) to remote (1).
11	Bugs are present in the ground station software	Ground station malfunctions occurs	The ground station is inoperative and can not be used.	4	5	5	Testing the ground station system and make sure there is a back-up system (software version) present. This will reduce the probability from catastrophic (5) to critical (4), since it may take a while to set up the backup system. Also, the probability will decrease from possible (4) to rare (2).
12	A limited storage space is present in the system.	Data overload of this storage	The data can not be stored and is lost	3	4	4	Add extra storage space for the data by, for example plugging in an extra flash drive (safety factor). Also, unit tests for the payload have to be done in order to accurately know the storage space needed for the data. Also, test the whole system like this. This will reduce the probability from unlikely (3) to remote (1).
13	Air traffic is present in the area, like rescue helicopters	The UAV collides with the air traffic	The UAV and/or the air traffic has received damage and may not be able to fly anymore/crashes.	4	5	5	Maintain good contact between the SAR teams and have the ground station operate in/as the central command for the total SAR operation. The UAV may have a "radio signal localisation system". This will locate the helicopters based on their radio signal emitted. The UAV will also have an obstacle avoidance sensor to help with the oncoming traffic that may be present .This will cause the probability to decrease from possible (4) to remote (1).
14	Debris is falling down, for example in case of a volcano eruption	Debris hits the UAV	The UAV critical systems or sensors have received damage and may not be able to complete its mission anymore (crashes).	1	5	5	Hide the most crucial systems in the core structure or below the UAV, making them more shielded to debris. This will decrease the effect from catastrophic (5) to critical (4).

Continued on next page.

[88] Ranked from 1 (low) to 5 (high).

Table 14.3: Technical risk management.

ID	Cause	Event	Consequence	Probability[88]	Effect[88]	Impact	Mitigation
15	The system is not watertight and it rains, or a battery/fuel tank is leaking	There can be a short circuit	The (electrical) systems can break and the UAV may crash	4	5	5	Have a (rubber) casing in which the electronics will be placed to avoid water exposure. Also, the fuel tank/lines can be encased in a rubber casing to avoid leakage. This will decrease the probability from possible (4) to remote (1).
16	Dust/ash/ice/dirt accumulation at rotating points, or actuator rods/cables wearing out or breaking	Engine failure or actuator stuck	Loss of control or thrust	3	5	5	Maintain the UAV regularly, preferably at least before/after every mission. Also, rotating parts like control surfaces may be covered (partially). The UAV(s) shall be covered when stored. this will reduce the probability from unlikely (3) to remote (1).
17	There is fatigue in the primary structure, or the automatic pilot makes too harsh manoeuvres for the structure.	Structural failure occurs	The structure is unable to carry the load and the UAV may crash	3	5	5	Design the structure with a safety margin. Limiting the automatic pilot in the load factor of a manoeuvre (except for emergency situations, like avoiding a helicopter). In maintenance an extra check for fatigue should be performed. Also, redundancy can be included in the design. This will decrease the probability from unlikely (3) to rare (2) and the effect from catastrophic (5) to critical (4).
18	Parachute malfunction.	In case the parachute is not able to deploy during landing	This may cause a harm to the UAV, as the speed of the UAV would be very high.	3	4	4	As there is a net present on the ground, this will still help in the landing of the UAV, also the parachute should be checked before it is taken off. This decreases the effect from critical (4) to negligible (2).
19	Catapult malfunction	In case there is a malfunction in the catapult due to some error.	The whole missions would now be possible if the catapult would not be able to work.	2	5	5	Always check how the catapult works before departing it somewhere. This decreases the effect from catastrophic (5) to negligible (2).
20	Unable to communicate through sled kite	In case, the wind conditions are too high for the kite	Unable to send information to and fro the UAV, and acting as a communication system for the SAR teams.	4	3	3	Have another which can withstand high loads, and with the presence of bleed valves, it will be able to withstand the forces. This decreases the effect from marginal (3) to negligible (2).
21	Harm to the kite	In case a bird/UAV hits the rope that is moored to the kite.	Unable to send information to and fro the UAV, and acting as a communication system for the SAR teams, and the kite may not be able to used again.	4	5	5	Using lights on the rope to make it more visible for the birds/UAV to see. This decreases the effect from catastrophic (5) to negligible (2).
22	Not enough power is provided for the components on the pseudo-satellite	If there is not enough wind to power the windmill enough to provide energy for the entire components.	Unable to send information to and fro the UAV, and acting as a communication system for the SAR teams, and the kite may not be able to be used again. Additionally, many important components would not be able to work.	4	5	5	Having a battery on board would help mitigate this risk, in case there is not enough power provided by the windmill on board. This decreases the probability from critical (4) to no effect (1).
23	Single engine failure	If the engine fails due to some cause	Not able to propel and complete the mission.	4	5	5	The parachute would then be deployed, so the UAV can safely land, and no further harm is done to the UAV. This decreases the probability from catastropic (5) to marginal (3).
24	The kite would not be able to get to the required altitude	The kite is entangled when it is going up or it is entangled with the other kite.	Unable to send information to and fro the UAV, and acting as a communication system for the SAR teams, and the kite may not be able to be used again.	3	5	5	Having the winch mechanisms far apart from each other and looking at the wind direction before putting the kite up might help reducing the chance for the kites to get entangled. This decreases the effect from catastrophic (5) to marginal (3).
25	The kite would not be able to get to the required altitude	In case the winch stop working while bringing the kite up	Unable to send information to and fro the UAV, and acting as a communication system for the SAR teams, and the kite may not be able to be used again.	2	5	5	Carrying an extra winch on board would help. This decreases the effect from catastrophic (5) to negligible (2).
26	Unsafe landing	In case the IR emitters on the net stop working	The UAV would not be able to land in the safe zone of the	2	5	4	The UAV still has a parachute, it would still be able to land, but it would cause harm to the tail. Also, the user may be able to impact the UAV into the net by using the joystick. This decreases the effect from catastrophic (5) to marginal (3).
27	Difficulty in flight	In case the actuators stop working during flight	The UAV would have trouble flying	1	5	4	As the thrust on the UAV is very high, it would not affect the UAV very much. This decreases the effect from catastrophic (5) to negligible (2).

Chapter 15: Sustainability assessment

Sustainability becomes more and more important in everyday life. Due to the use of fossil fuel, they release green house gases which contribute to global warming. Thus, the need for sustainable products and energy is rising. Sustainability is defined as: "the balanced integration of economic performance, social inclusiveness, and environmental resilience, to the benefit of current and future generations." [22]. In order to address those issues, the design will be made according to the circular economy paradigm. A circular economy can be defined as: "A regenerative system in which resource input and waste, emission, and energy leakage are minimised by slowing, closing, and narrowing material and energy loops." [22]. Considering both sustainability and the circular economy paradigm, a sustainable development strategy is made.

Sustainability can be split up into two categories; namely product sustainability and the environmental footprint. Product sustainability focuses on the products balanced integration of economic performance, social inclusiveness, and environmental resilience, to the benefit of current and future generations. On the other hand, environmental footprint focuses on how other contributors to the sustainability are defined and dealt with. Even though sustainability is of great importance nowadays, for this product the sustainability is not a very high priority. Saving lives is the main priority and therefore using a bit more fuel to be able to do this faster is more important than being sustainable. However, this does not mean sustainability does not play a role in deciding whether to go for one concept or the other.

15.1. Product sustainability

According to the circular economy paradigm the UAS design should be easily maintained and repaired. Thus while designing the UAS, and making components for the UAS, it was made sure that the parts used are off the shelf, as it would be easy to assemble, save time for manufacturing and in case of any defects, it would be easily replaceable. As a result, the payload used in the UAV are all off-the-shelf, also a lot of the components within the GS are off-the-shelf too, as a result keeping the manufactured components to a minimum. Often manufacturing a new product from scratch results in many waste products (also from prototyping) and this to a large extend is avoided. Another way to accomplish this is by making parts easily accessible to spend the time as efficiently as possible. Furthermore, the longevity of each component must be taken into account as long-lasting parts will be preferred to reduce waste. For most of the off-the-shelf products the supplier provides a life span of the product and this is consecutively used to compare similar performing products.

15.2. Environmental footprint

To cope with sustainability, the following contributors to the footprint of the system are identified [29].

Basic operational equipment:

- UAV: As the UAV runs on fuel, it produces emission. This might not be an ideal scenario, but the engine used is beneficial for the mission, and able to fulfil the requirements. An option considered to make it more sustainable was to use electric propulsion, but due to its lower endurance, that option was disregarded. The current engine uses fuel, and provides a large endurance. It is important for the mission to be able to withstand in air for a longer time, to help SAR teams with communication, and to detect people in the disaster zone. It should be noted that different engines have different emission levels and for this reason a two stroke engine is used for the design.
- GS: The GS runs on a fossil fuel generator, as there was a constant power source required to keep it running. The GS always should be in contact with the UAV. As the GS is the heart of the operation, if it is not operational for any amount of time, the mission may become disastrous. The GS could have run on more renewable resources, such as solar cells or wind turbines. Due to the lack of knowledge on whether power is available in the disaster area, a generator must be included. A high efficiency generator was therefore chosen in order to minimise carbon emissions. Also, with the payload on the kites, there could be a wind turbine placed on it, or a solar panel. But, due to their size, and their inefficient nature, these choices were disregarded.

Examples of other contributors:

- Cleaning equipment
- System test equipment
- Wheel chocks and tow bars
- Storage cases
- Materials used
- Tools (hand tools and power tools, spare tools)
- Ground maintenance computer system
- Repair kits (composite materials, vacuum bags)
- Bathroom facilities

Daily assessments are done by the sustainability engineer to test whether the design process proceeds in a sustainable way. The basic operational equipment are of highest priority as these are a direct consequence of the design and chosen for longevity characteristics. The other contributors cannot be directly designed for. In a SAR mission the number and kind of products that are provided are determined by whatever is available at the disaster zone.

Chapter 16: RAMS characteristics

This chapter briefly discusses the reliability, availability, maintainability and safety characteristics of the UAS. First, the reliability and availability are discussed in section 16.1. This part is followed by a review of the maintenance activities in section 16.2. Finally, the safety characteristics of the UAS are discussed in section 16.3.

16.1. Availability and reliability

A high availability translates to being able to operate the system when it is needed. The operational availability is defined by:

$$A_o = \frac{MTBF}{MTBF+MDT} \tag{16.1}$$

Where MDT is the maintenance down time and the MTBM is the mean time between maintenance activities [29]. These values are determined by the large maintenance check of section 16.2. The amount of missions after which a large maintenance check has to be performed as discussed is 4, since the system will have to endure heavy operating conditions. However, because the system is not used continuously, the availability of the system depends on the frequency of use. When the system is used once each month, the system is unavailable for five days every four months. In this case the operational availability is equal to around 0.96.

This means that in 95% of the time, the system will be standing by to be transported and used in the disaster areas. In addition to this, the UAV will be in maintenance for 5% of the time. Taking into account that there are two UAVs which can be maintained separately from each other as described in section 16.2 to make sure there is always at least one UAV available in case a disaster occurs during the maintenance of the other UAV.

The reliability of the system on the other hand is defined as the probability that a system will perform in a satisfactory manner for a given period of time when used under specified operating conditions [63]. Therefore different reliability can be derived for the UAV the GS and as a result, the reliability of the entire system could be calculated.

In order to determine reliability, it has to be defined what satisfactory performance means for the UAS and what the expected operational conditions are.

The reliability of a system in general can be estimated using the failure rate, however since no data is available for the UAS operation, the approach to estimating the reliability of the system is to estimate the failure rate of critical sub-components that are likely to fail over time.

16.2. Scheduled and non-scheduled maintenance activities

In scheduled maintenance there are two types of checks: a small maintenance check and a detailed maintenance check. The activities performed in these checks are listed in table 16.1. The small maintenance check implies a basic check on the most critical systems of the UAV. These maintenance checks will be performed before and after each mission.

The large maintenance check involves a check of the entire system. This means the entire system will be checked whether or not it is airworthy. This also includes the activities performed in the small maintenance check. When a part is not functioning properly is will be replaced by a spare part or repaired.

Table 16.1: Scheduled maintenance checks.

Small maintenance check	Large maintenance check
Visual external inspection	Catapult parts
Payload check	Assembly joints
Control surface check	Engine/generator
Kite and net damage inspection	Avionics
Engine oil check	Fuel tank
Propeller damage check	Antennas
Parachute check	Net subsystem
Light check	Kite subsystem

During pre-flight inspection, the operator may discover that a component of the system is in need of servicing, repair, modification, or replacement outside of the scheduled maintenance. This is why spare parts need to be present at the ground station. The essential spare parts that are critical to be present at the ground station are shown in the following list:

- Catapult launcher clamps.
- Servos for control surfaces
- Propeller
- On board electronic system
- Hatches of parachute compartments
- Cables for kite
- Cables for electronics

A common maintenance metric is maintenance man-hours per flight hour(MMH/FH)[29]. For a small-sized UAV the MMH/FH can be assumed to be 1. This means that for every hour flown, there will be one man-hour of maintenance work. So after 4 missions of 72 hours the amount of man hours is equal to 288. A small maintenance check will be executed after each mission. 3 maintenance workers are working for 4 hours, for a total of 12 hours. This means after 4 missions 48 hours of small maintenance is performed. Consequently, there are 288 - 48 = 240 hours left for the large maintenance check. A team of 6 workers shall be working for 40 hours for the large maintenance check. A worker is working 8 hours per day, which means the UAS-will not be available for 5 days. This can be decreased by maintaining the UAVs separately from each other. Then the UAV can be available after already 2.5 days, while the other UAV will be in maintenance two missions later. This could be done if the team will want to be able to use the full system faster after a mission. Even if the system would be needed within the 2.5 days, at least one UAV will be available.

16.3. Safety critical functions

- Propeller stops turning when landing in the net. This is important, since the if the propeller does not stop turning, it may be ensnared in the net. The propeller will not be ensnared directly after the UAV is captured in the net, but when the net folds around it, it may be a real risk. For this reason the propeller should stop when it is about to be captured by the net based on the position and acceleration of the UAV.
- A parachute is added to function as a safety option when the key systems of the UAV fail and the UAV is not able to fly and land.
- The parachute deployment button is covered by a cap in the ground station. This will ensure that the operator does not accidentally deploy the parachute.
- A fuel leak can occur where the fuel will leak from the UAVs fuel tank. For this reason, the fuel tank and lines are sealed and there is a part to refuel to avoid leakage and spilling.
- The UAV is launched from a distance by the operator. This will avoid a fault during launch to damage equipment or endanger people. This will also ensure the safety of the operator, since the operator will be arming and activating the launcher from a distance.
- The UAV will always have the function to be manually controlled by the operator. This will ensure the UAV to remain in the safe flying zones. Also, the operator will be able to control the UAV in case of a malfunction on the UAV or determination of the flight path. Also the manual control switch is covered by a cap to avoid the operators accidentally assuming manual control.
- The winches of the kites are placed 20 m away from each other perpendicular to the direction of the wind. This is to avoid the kites to entwine with each other, which would cause a large downtime in the communications.

16.3.1. Redundancy philosophy applied

A redundant part or subsystem is used when the failure of the part has a critical effect on the mission such as a crash of the aerial system. Subsystems such as the GPS sensors are therefore designed fail-safe. However, larger subsystems such as the wing of the UAV are not fail-safe, since an additional redundancy of those systems would impact the performance of the UAV significantly. These items are thus made safe-life.

Chapter 17: Project design and development

17.1. Project design and development logic

The project design and development logic was created concurrently with the project Gantt chart. It shows the procedure that needs to be followed before the product can be put on the market. Note that the product design and development logic flow diagram is constructed with yellow boxes. These represent recommendations are optional for the user to apply. Three different levels are depicted in the flow diagram, these are shown by means of the dotted arrows. The diagram is shown in fig. 17.1.

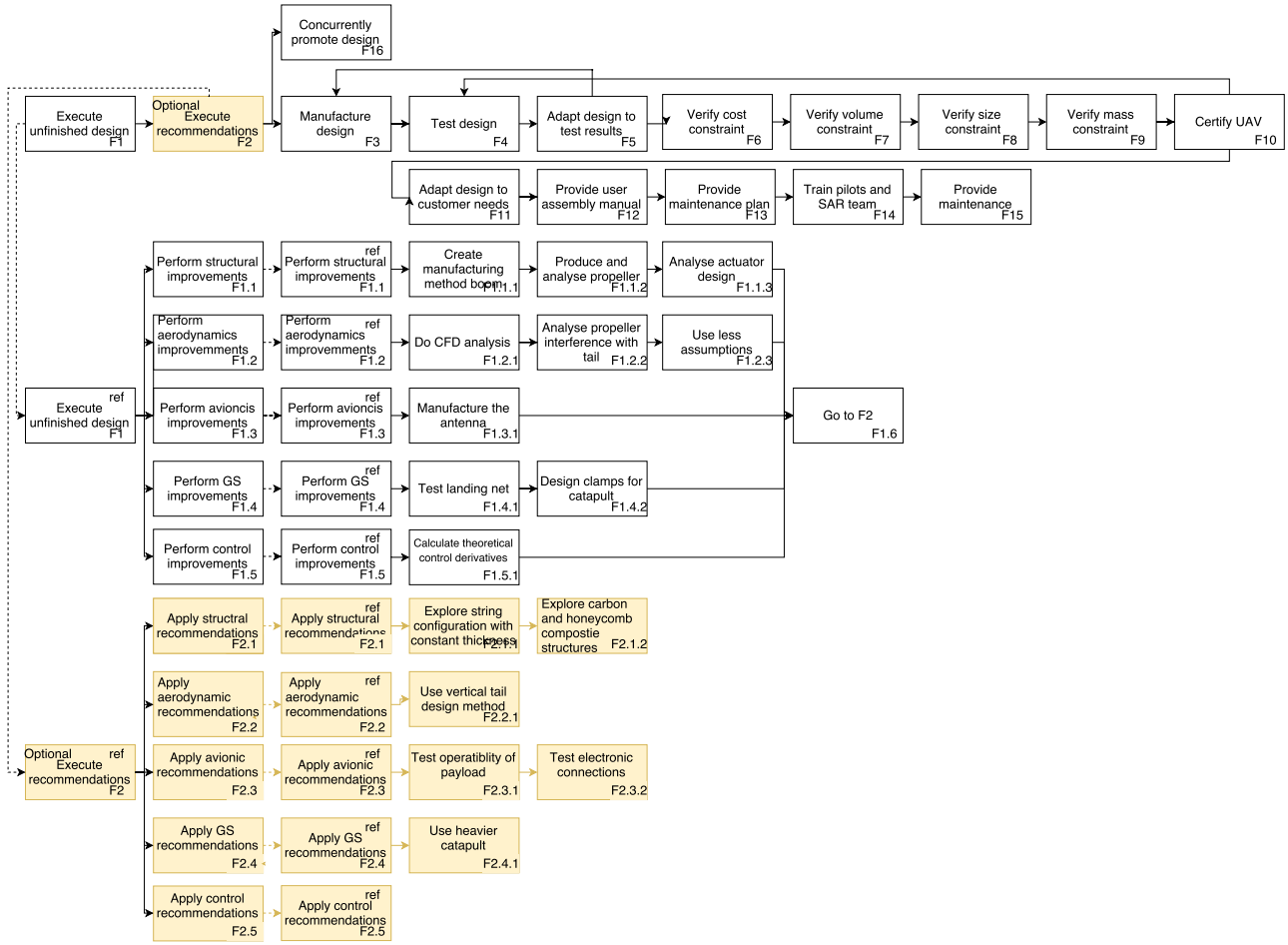

Figure 17.1: Flow diagram to show what needs to happen in the future before it can be sold on the market.

17.2. Project Gantt chart

This Gantt Chart roughly describes the steps to be taken after the third phase of this design project. It starts with implementing and designing all the things that could not be designed in the third phase of the project due to time, money and resource constraints. After these designs are delivered it is optional to execute (partially) the recommendations. When a model is build, tests can be performed and used to improve the design. Following up on those improvements the system can be manufactured and certified. As soon as the maintenance plan, assembly manual and the operator training has finished the product can be delivered to the customer. The product will be promoted on exhibitions and advertisements during the final stage.

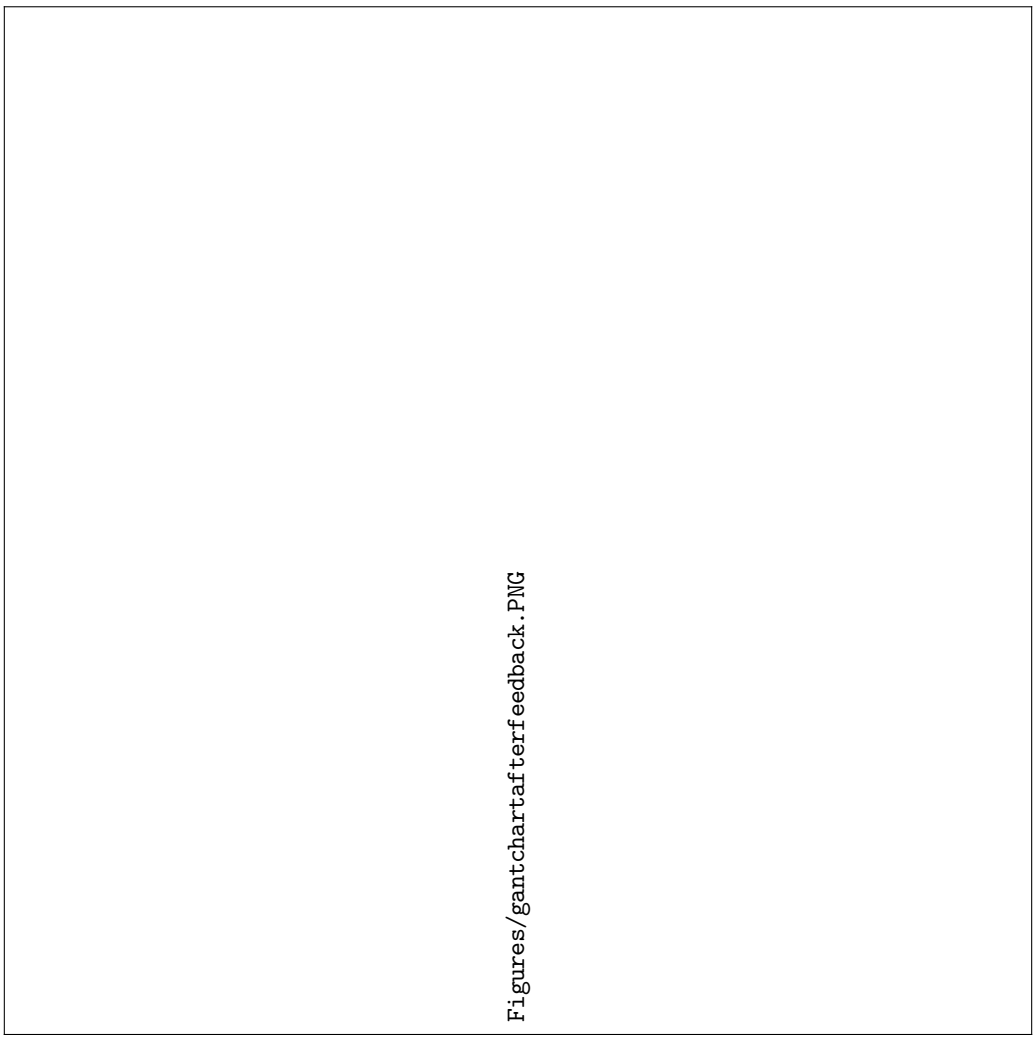

Figure 17.2: Gantt chart of the post-DSE phase.

17.3. Cost breakdown

The cost breakdown structure includes all costs factors for the post-DSE activities. This breakdown structure can be used to have an indication of the costs until the release of the product on the market and what costs come after the release of the product such as promotion and maintenance costs. The promotion costs will be mainly focused on before the product is released such that investors can jump in.

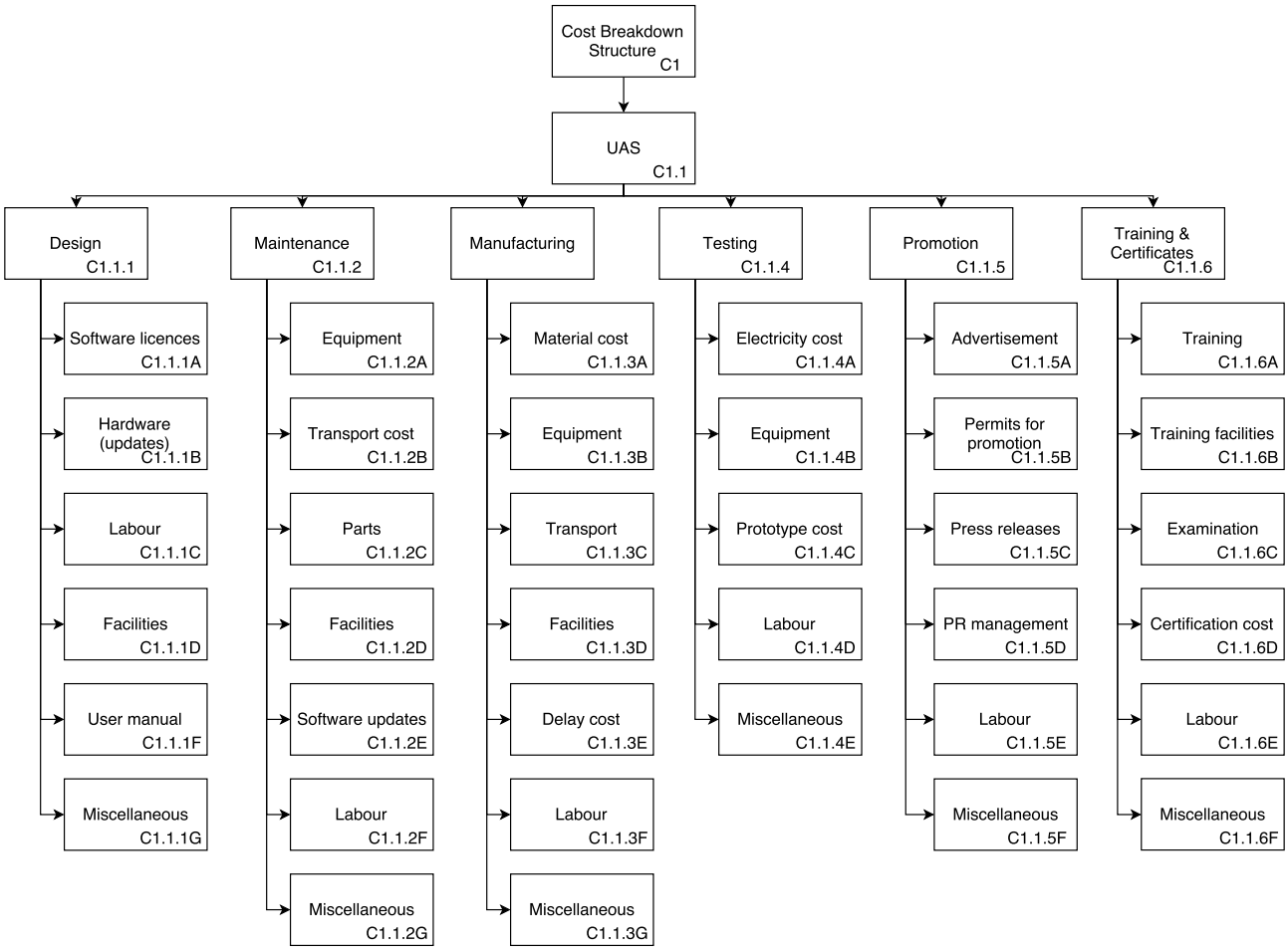

Figure 17.3: Cost breakdown structure showing the cost elements of upcoming activities.

Chapter 18: Conclusions and recommendations

By the end of the final report they aim was to have finalised the entire FASAR system. The system consists of two twin booms fixed wing UAVs with an U-tail. The UAVs are propelled by a two-blade propeller at the aft of the fuselage and powered by a combustion engine. Moreover, the system is also equipped with two kites that are part of the ground station and include transponders such as to create a communication network and allow communication between SAR teams. Additionally, the ground station includes a monitoring station for the entire system.

Once the configuration of the system had been determined, the team was divided into six departments; namely aerodynamics, stability and control, structural design, electronics, placement and power, and ground station. The team ensured concurrent engineering was carried out with the help of constant communication between each department.

Prior to finalising the design, a mission description and performance overview was carried out. A market analysis was first performed and provided a good overview to the team of what kind of product is required and allowed to set more requirements and constraints for the design to be attractive to customers and perform successfully in the market. During the market analysis it was found that as of today the UAS SAR market is €37.7 billion and is expected to increase to €79.82 billion by the year 2022. The target market for was analysed and a heat map was generated to visualise the global market. It was found that our persona are mainly located in Eastern Asia or on the West coast of America. Moreover, the UAVs can withstand wind conditions of up to 8 Bft which is significantly higher than other UAVs available on the market which can withstand a maximum of 6 Bft.

Following the market analysis, a requirement analysis was carried out for the system. This provided the designers information about what the system had to be designed for and provides understanding of which design options may be utilised for the design of the system. A compliance matrix shows that the vast majority of requirements have been met. However, **REQ.U.SYS.9**, **REQ.O.SYS.7** and **REQ.G.SYS.3** have not been met. The first has been relaxed from 10 Bft to 8 Bft due to the difficulties in meeting other mission requirements when designing for 10 Bft. Secondly, the circular economy paradigm could also not be fully integrated into the design due to the use of fossil fuels for the power the ground station and UAVs. It was assessed that using fossil fuels is highly beneficial to the mission and priority was set on saving lives rather. On the other hand, attempts at minimising emissions carried out and all other aspects of the system was designed according to the circular economy paradigm. Third and lastly, ground station takes 55 min to assemble with three individuals instead of 15 min with two. This is due to the fact that the ground station now consists of computers along with two kites. This change in requirement is deemed as reasonable and should not affect the performance of the mission greatly.

Subsequently, the performance of the UAV was analysed. The target performance is compared with the actual performance achieved. The UAV has a range of 840 km with a cruise speed between 31 and 34 $m\,s^{-1}$. It is also able to take off at altitudes up to 3,548 m with a ceiling at 5,000 m. Finally, an MTOW of 22.89 kg. Additionally, a budget for the ground station and the UAV system was also developed. The ground station will have a total volume of 2.26 m^3, have a cost of €222,600, total mass of 585 kg and a volume of 2.26 m^3.

For the final phase, the design started by analysing the aerodynamics of the UAV. In the aerodynamics department, the wing, the fuselage, the tail, and the propeller were designed for. With the use of XFOIL, twenty two aerofoils were investigated for the wing, out of which the Wortmann FX 63-110 aerofoil has been chosen as its characteristics matched the mission requirements best. Moreover, the dimensions of the semi-elliptical wing were determined and optimised with respect to the aspect ratio.

The tail was then designed for the U-tail configuration. It was chosen to use a symmetric aerofoil for both the horizontal and vertical tails. After careful analysis, the same NACA 63-0-18 aerofoil was chosen for both surfaces. Moreover, using optimised horizontal and vertical tail volume coefficients, the dimensions of the tail planform was determined.

The fuselage design depended greatly on the payload. The sizing was therefore performed accordingly and also considering the required location of the centre of gravity. Moreover, an elliptical shape of the fuselage is chosen, and the nose taken for the fuselage is an ellipsoid with a fineness ratio of 0.5, due to the drag contribution for sub-sonic flows.

To design the propeller of the UAV, the drag performance of the aircraft was first analysed to determine its required thrust. To calculate the drag, the component build up method is used, and it could be observed that drag is highest when the UAV is taking off. As a result, the maximum thrust of the propeller had to be thoroughly checked for take off. Finally, the propeller blade geometry, was designed to have minimum induced losses at cruise speed using XROTOR.

For the stability of the aircraft, the position of the wing is determined, as well as the tail coefficients to achieve stability and control. These coefficients were determined with the help of stability and controllability curves. Moreover, all control surfaces have been sized according to the requirements. Two flaperons along with two flaps are being used. Furthermore, the horizontal tail consists of an elevator and the vertical tail has two rudders which rotate the entire vertical tail. Finally, the dynamic stability of the UAV is analysed by using XFLR5 and it is concluded that the UAV is stable for all manoeuvres except for the spiral motion. Instability in spiral motion is normal and not considered dangerous due to its low instability.

During the structural design the focus was to obtain a lightweight structure for the ultimate loads identified for the lifetime of the UAV. A numerical model was constructed that determines the optimum skin thickness for the adaptable wing model in order to minimise weight. Taking manufacturing capabilities into account, the critical stresses in the structure were evaluated to ensure the structure is designed for its requirements. The fuselage was designed in coarse detail, however necessary reinforcements were added in critical locations. Also, possible wing attachment points for assembly were identified. The twin boom attachments were also sized for the load cases identified and overall resulted in a lightweight empennage.

For the structural parts, the aluminium alloy 6061-T6 was chosen that allows for a simple manufacturing procedure and keeps the total mass of the airframe within constraints.

The electronics of the UAV is discussed next. The power is divided into four categories. The actuators, payload, subsystem controllers and avionics systems and the sensors. The avionics system that is going to be used on board is going to have a service oriented architecture. In addition, a significant amount of computational power is required for the flight control. As a result, an RTOS system is required, and the architecture used will be RTEMS. Vibration damping plates will be used to which all the sensitive electronics are attached to decrease the effect of the vibrations. The infrared and the optical cameras will also be attached to dual axis gimbals. Moreover, as the processors heat up quickly, the fuselage nose will include a copper heat sink in the top leading edge. The airflow outside assists the heat sink to cool the processors down. Two sets of patch antennas on the UAV will used to fulfil the communication requirements. In addition, the kites also need two sets of antennas. Finally, it was ensured that the bill of components for each UAV consists primarily of off-the-shelf products.

The ground station is an important part of the system, as it handles the landing, taking off, the pseudo-satellite subsystem and the command station. For landing, a net landing is being used due to its reliability. The net will be used to absorb the kinetic energy of the UAV. For the UAV to detect the net, IR emitters will be placed on the net such that the UAV can detect the net. As a result, the UAV detects the IR emitters and is able to find the exact location of the net, and place itself in its safe zone. The UAV will be able to survive a deceleration of up to 7g, and the net will survive a landing of upt to 6,900 J. The impact energy is transferred through the net to the hook attached to the ground and the reel attached to the top of the support pole. The UAV will also carry a parachute for emergency situations.

For take off, an off-the-shelf catapult is used, which is able to launch the UAV. For the communication with the ground station to the SAR teams and the UAV, a pseudo satellite is required, which will include a communication payload to achieve this task. The payload will be connected to a battery pack and work with that. Two different types of kites are needed in order to be able to fly in all weather conditions. Up to 5 Bft, a helikite will be used and above that, a deltakite is utilised. Moreover, two kites of each kind are needed in order to achieve a mission with no downtime for the 72 hour mission as the battery packs will require charging. Finally, the ground station includes a power supply and the command station too, which are both going to be off-the-shelf products.

Bibliography

[1] Abbott, I. H., and Von Doenhoff, A. E. *Theory of Wing Sections, Including a Summary of Airfoil Data, by Ira H. Abbott and Albert E. Von Doenhoff*. Dover Publications, 1959.

[2] Administration, F. A. *Operation and Certification of Small Unmanned Aircraft Systems; Final Rule*, Vol. 81. Department of Transportation, 2016.

[3] and-landing Accident Reduction (ALAR) Task Force, T. F. S. F. A. The final approach speed. Briefing note, 2000.

[4] Anderson, S. B. "A look at handling qualities of canard configurations." *Journal of Guidance, Control, and Dynamics*, Vol. 10, No. 2, 1987, pp. 129–138.

[5] Bakker, H., Bosch-Rekveldt, M., and of Technology, D. U. Minor project management: Ct3101-i basic project management, lecture 9, 2016.

[6] Ballve, M. "COMMERCIAL DRONES: Assessing The Potential For A New Drone-Powered Economy." *Bussiness Insider*, 2014.

[7] Betz, A. "Airscrews with minimum energy loss." *Report, Kaiser Wilhelm Institute for Flow Research*, 1919.

[8] Boon, K., and Lovelace, D. *The Domestic Use of Unmanned Aerial Vehicles*, Vol. 134. Oxford University Press, USA, 2014. ISBN 978-0-19-935105-3.

[9] Bourtsev, B. N., Selemenev, S. V., and Vagis, V. P. "Coaxial helicopter rotor design & aeromechanics." *Twentyfifth European Rotorcraft Forum*, 1999.

[10] Brief, L. "Growth Opportunity in Global UAV Market." *Las Colinas, USA*, 2011.

[11] Bruhn, E. F. *Analysis and design of flight vehicle structures*. Tri-State Offset Co., 1965.

[12] Chandler, J. "Advanced rotor designs break conventional helicopter speed restrictions." *Professional Pilot*, Vol. 46, No. 9, 2012.

[13] Chappell, P., Clarke, A., and Porter, R. "Geometrical characteristics of typical bodies." *IHS ESDU*, , Vol. 77028, 1977.

[14] Communier, D., Salinas, M. F., Carranza Moyao, O., and Botez, R. M. "Aero structural modeling of a wing using CATIA V5 and XFLR5 software and experimental validation using the Price-Païdoussis wing tunnel." In *AIAA Atmospheric Flight Mechanics Conference*.

[15] Dhakad, A. S., Sawarni, A., Sahu, G., and Sahu, N. "Analysis Of NACA 6412 Airfoil (Purpose: Propeller For Flying Bike)." *IOSR Journal of Mechanical and Civil Engineering (IOSR-JMCE)*, Vol. 12, No. 1 Ver. II, 2015, pp. 115–124.

[16] Drela, M. "QPROP formulation." *Massachusetts Inst. of Technology Aeronautics and Astronautics, Cambridge, MA*, 2006.

[17] EDI, P., YUSOFF, N., and YAZID, A. A. "Airfoil Design for Flying Wing UAV (Unmanned Aerial Vehicle)," 2008.

[18] Evans, A. J., and Liner, G. A wind-tunnel investigation of the aerodynamic characteristics of a full-scale sweptback propeller and two related straight propellers. Research Note NACA RM L50J05, Langley Aeronautical Laboratory, 1951.

[19] Felkel, R. J. "Effect of Different Nose Profiles on Subsonic Pressure Coefficients." *American Institute of Aeronautics and Astronautics*, 2004, pp. 1–10.

[20] Fersch, T., and Buhmann, A. "The Influence of Rain on Small Aperture LIDAR Sensors." *GeMiC*, 2016.

[21] Fishpool, M. "Global Military UAV Market Forecast to 2022." *Market Forecast*, 2016.

[22] Geissdoerfer, M., Savaget, P., Bocken, N. M., and Hultink, E. J. "The Circular Economy – A new sustainability paradigm?" *Journal of Cleaner Production*, , Vol. 143, 2017, pp. 757 – 768. ISSN 0959-6526. doi:10.1016/j.jclepro.2016.12.048.

[23] Gerr, D. *Propeller handbook*. International Marine Publishing, 1989.

[24] Goldstein, S. "On the vortex theory of screw propellers." *Proceedings of the Royal Society of London. Series A, Containing Papers of a Mathematical and Physical Character*, Vol. 123, No. 792, 1929, pp. 440–465.

[25] Gudmundsson, S. Applied methods and procedures for the practicing aerospace engineer, 2011.

[26] Gudmundsson, S. *General aviation aircraft design: Applied Methods and Procedures*. Butterworth-Heinemann, 2013.

[27] Gudmundsson, S. Applied methods and procedures. In *General Aviation Aircraft Design*, pp. ii –. Butterworth-Heinemann, Boston, 2014. ISBN 978-0-12-397308-5. doi:https://doi.org/10.1016/B978-0-12-397308-5.03001-4. URL `http://www.sciencedirect.com/science/article/pii/B9780123973085030014`.

[28] Guha-Sapir, D., Below, R., and Hoyois, P. "EM-DAT: International disaster database." *Catholic University of Louvain: Brussels, Belgium*, 2015.

[29] Gundlach, J. *Designing Unmanned Aircraft Systems: A Comprehensive Approach*. American Institute of Aeronautics and Astronautics, Inc, 2012.

[30] Gursul, I. "Recent developments in delta wing aerodynamics." *The aeronautical journal*, 2004, pp. 437–451.

[31] Hanlon, M. "Schiebel next-generation UAV Camcopter." *New Atlas*, 2005.

[32] Howe, D., and Rorie, G. *Aircraft conceptual design synthesis*. Professional Engineering Pub., 2000.

[33] in 't Veld et al., A. *Lecture Notes AE3202 Flight Dynamics)*. TU Delft, 2013.

[34] Johnson, W. *Helicopter Theory*. Dover Books on Aeronautical Engineering Series. Dover Publications, 1994. ISBN 9780486682303.

[35] Jonathan D. Stevenson, Siu O'Young, L. R. "Beyond line of sight control of small unmanned aerial vehicles using a synthetic environment to augment first person video." *Procedia Manufacturing*, , Vol. 3, 2015, pp. 960–967.

[36] Kim, H. W., and Brown, R. E. "A comparison of coaxial and conventional rotor performance." *Journal of the American Helicopter Society*, Vol. 55, No. 1, 2010, pp. 12004–12004.

[37] Knacke, T. W. Parachute recovery systems design manual. Technical report, DTIC Document, 1991.

[38] Kong, W., Zhang, D., Wang, X., Xian, Z., and Zhang, J. "Autonomous landing of an UAV with a ground-based actuated infrared stereo vision system." In *Intelligent Robots and Systems (IROS), 2013 IEEE/RSJ International Conference on*.

[39] Krayer, W. R., and Marshall, R. D. "Gust factors applied to hurricane winds." *Bulletin of the American Meteorological Society*, Vol. 73, No. 5, 1992, pp. 613–618.

[40] Landolfo, G., and Altman, A. "Aerodynamic and Structural design of a small Nonplanar wing UAV." In *47th AIAA Aerospace Sciences Meeting including The New Horizons Forum and Aerospace Exposition*.

[41] Larrabee, E. E., and French, S. E. "Minimum induced loss windmills and propellers." *Journal of Wind Engineering and Industrial Aerodynamics*, Vol. 15, No. 1-3, 1983, pp. 317–327.

[42] Leishman, G. J. *Principles of helicopter aerodynamics with CD extra*. Cambridge university press, 2006.

[43] Leland M. Nicolai, G. E. C. *Fundamentals of Aircraft and Airship Design: Volume I Aircraft Design*. American Institute of Aeronautics and Astronautics Inc., 2010.

[44] Levy, A. V., and Palyka, I. Impact-absorbing wing connection system for model aircraft, July 30 2002. US Patent 6,425,794.

[45] materia, T. "Aircraft and Aerospace Applications: Part One." *Total materia*, 2004.

[46] Megson, T. H. G. *Aircraft structures for engineering students*. Elsevier, 2012.

[47] Milligan, A. V. "Drag of nose cones." *Peak of Flight*, , Vol. 345, 2013.

[48] Newswire, P. "Teal Group predicts worldwide UAV market will total $89 billion in its 2012 UAV market profile and forecast." *PR Newswire*, , Vol. 11, 2012.

[49] NLR. N250 propeller shoptest. Research note, Nationaal Lucht en Ruimtevaartlaboratorium; NLR, 1993.

[50] of the Federal Register US, O. *Code of Federal Regulations, Title 14, Aeronautics and Space, Pt. 23, Revised as of February 9 1996*. U.S. Government Printing Office, 1996.

[51] Okamoto, M., and Azuma, A. "Aerodynamic characteristics at low Reynolds number for wings of various planforms." *AIAA journal*, Vol. 49, No. 6, 2011, pp. 1135–1150.

[52] Poirier, A. Fema urban search and rescue teams: Considering an improved strategy for an evolving homeland security enterprise. Technical report, DTIC Document, 2012.

[53] Polivka, M., and Holub, A. "Planar version of Collinear Microstrip Patch Antenna." In *2006 International Conference on Microwaves, Radar Wireless Communications*. doi:10.1109/MIKON.2006.4345343.

[54] Prouty, R. *Helicopter Aerodynamics Volume I*, Vol. 1. Lulu. com, 2009.

[55] Prouty, R. *Helicopter performance, stability, and control*. PWS Engineering, 1986. ISBN 9780534063603.

[56] Riblett, H. "What Are Wortman Airfoils??" *EAA*, 1988.

[57] Rocca, D. G. L. Requirement analysis and design principles for a/c stability & control (part 1). TU Delft, 2017.

[58] Rocca, D. G. L. Requirement analysis and design principles for a/c stability & control (part 2). TU Delft, 2017.

[59] RODZEWICZ, M., and GŁOWACKI, D. "INVESTIGATIONS INTO LOAD SPECTRA OF LIGHT-WEIGHT UAV'S," 2014.

[60] Ruijgrok, G. Elements of aircraft performance, 1996.

[61] Rutkay, B. D. *A Process for the Design and Manufacture of Propellers for Small Unmanned Aerial Vehicles*. PhD thesis, Carleton University Ottawa, 2014.

[62] Sadraey, M. H. *Aircraft design: A systems engineering approach*. John Wiley & Sons, 2012.

[63] Smith, D. J. "Reliability, maintainability and risk: Practical safety-related systems engineering methods." *Training*, , Vol. 2017, 2011, pp. 08–21.

[64] Steenhuizen, I. D., and Elham, D. A. Wing design part 2, 2015.

[65] Theodorsen, T., et al. The theory of propellers. Technical report, Langley Memorial Aeronautical Laboratory, 1948.

[66] Tracy, I. P. *Propeller design and analysis for a small, autonomous UAV*. PhD thesis, Massachusetts Institute of Technology, 2011.

[67] Turteltaub, D. S. Lecture 3: Free vibrations of a damped, single degree-of-freedom system). TU Delft, 2017.

[68] Van Arnhem, N. Design and analysis of an installed pusher propeller with boundary layer inflow. Master's thesis, Delft University of Technology, 2015.

[69] van Holten, T., and Melkert, J. *Helicopter Performance Stability and Control: Ae4-213.* TU Delft, Faculty of Aerospace Engineering, 2002.

Appendix A: Functional breakdown structure: sublevels

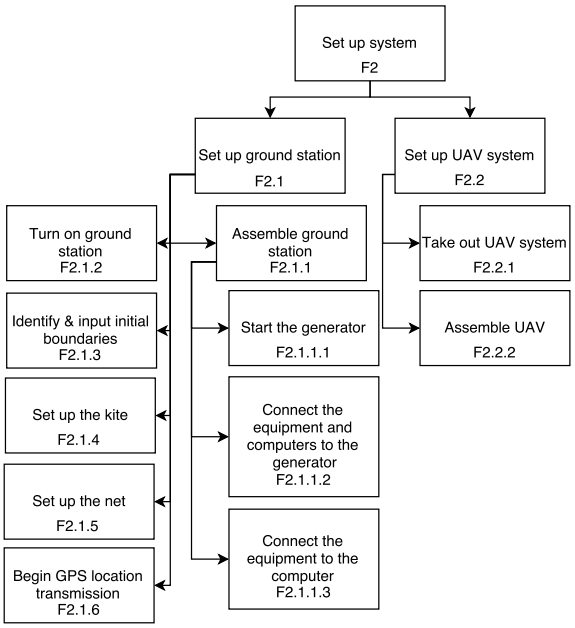

(a) Functional breakdown structure of setting up the system. Displayed up to the second sub-level.

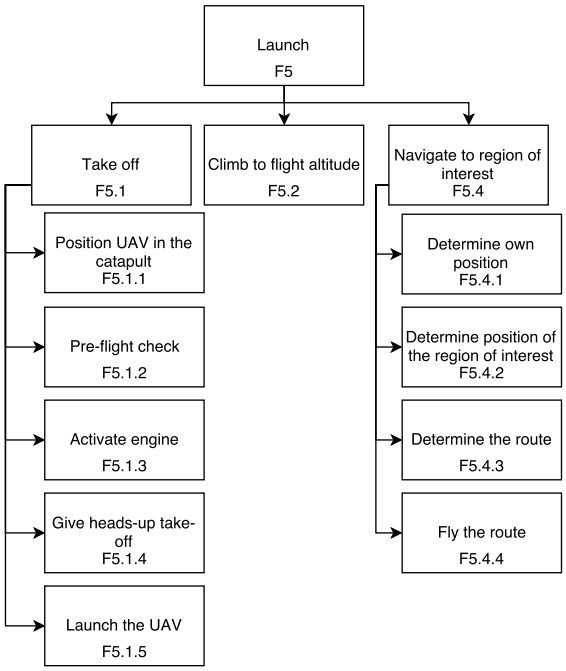

(b) Functional breakdown structure of the launch. Displayed up to the second sub-level.

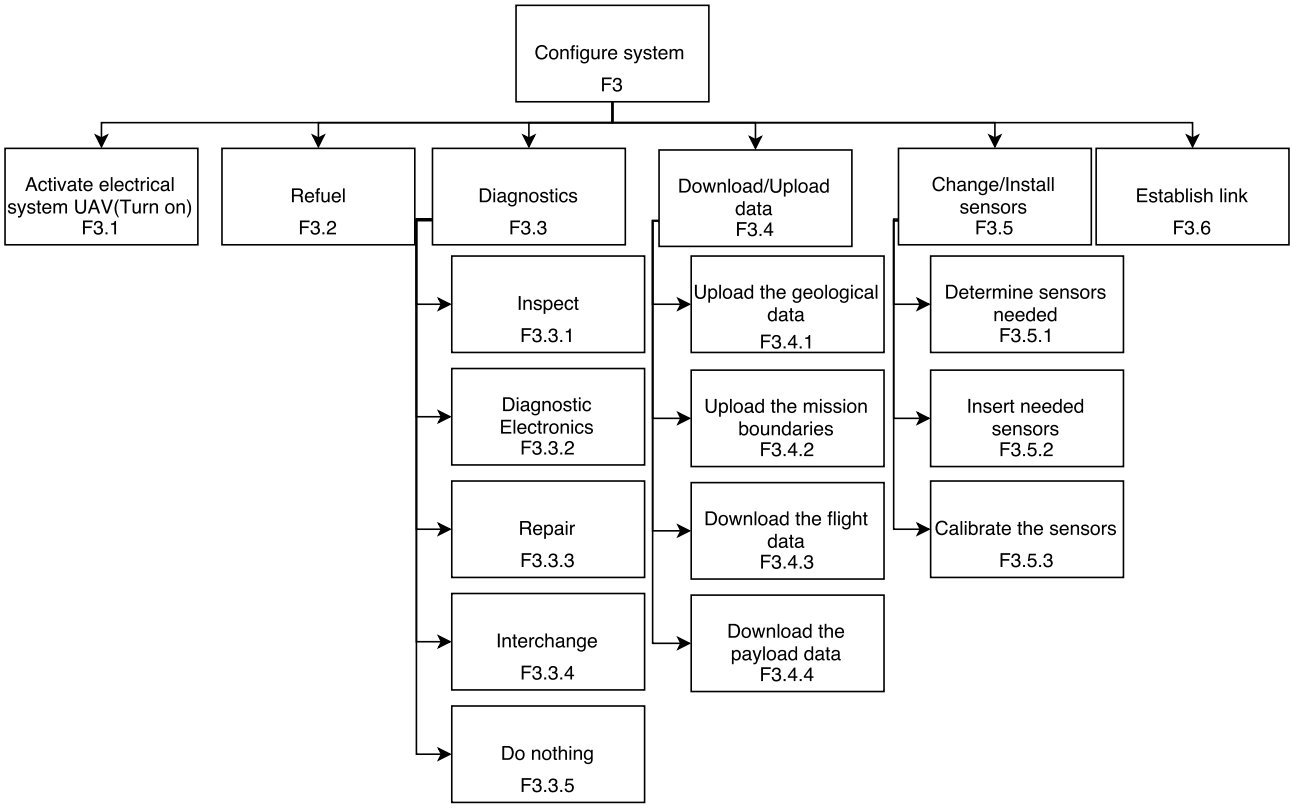

Figure A.2: Functional breakdown structure of the configuration of the system. Displayed up to the second sub-level.

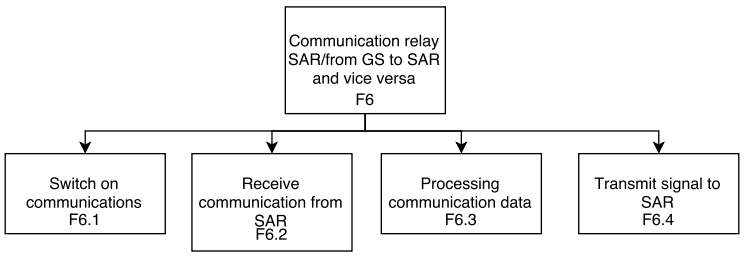

Figure A.3: Functional breakdown structure of the communication relay. Displayed up to the second sub-level.

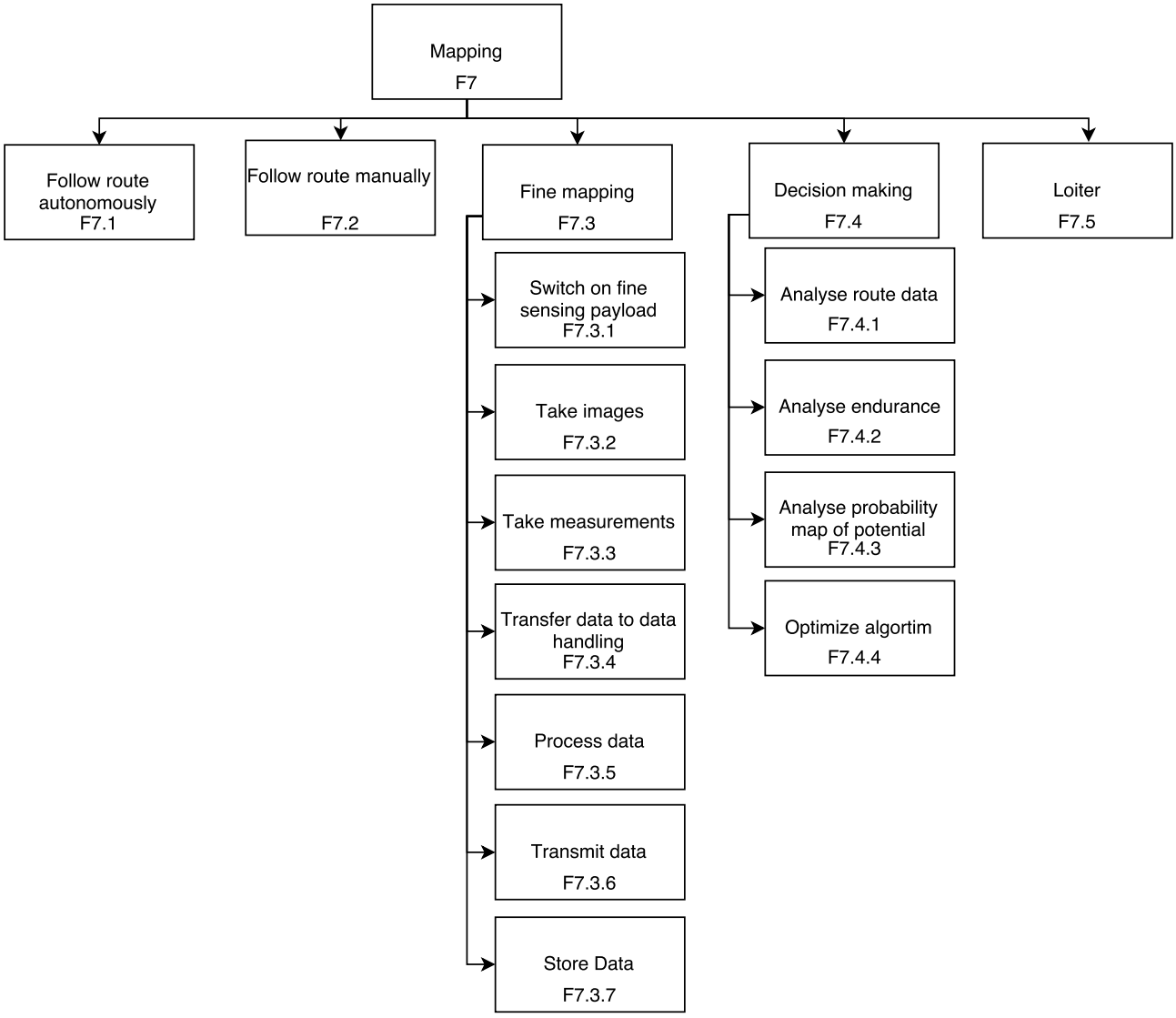

Figure A.4: Functional breakdown structure of the mapping system. Displayed up to the second sub-level.

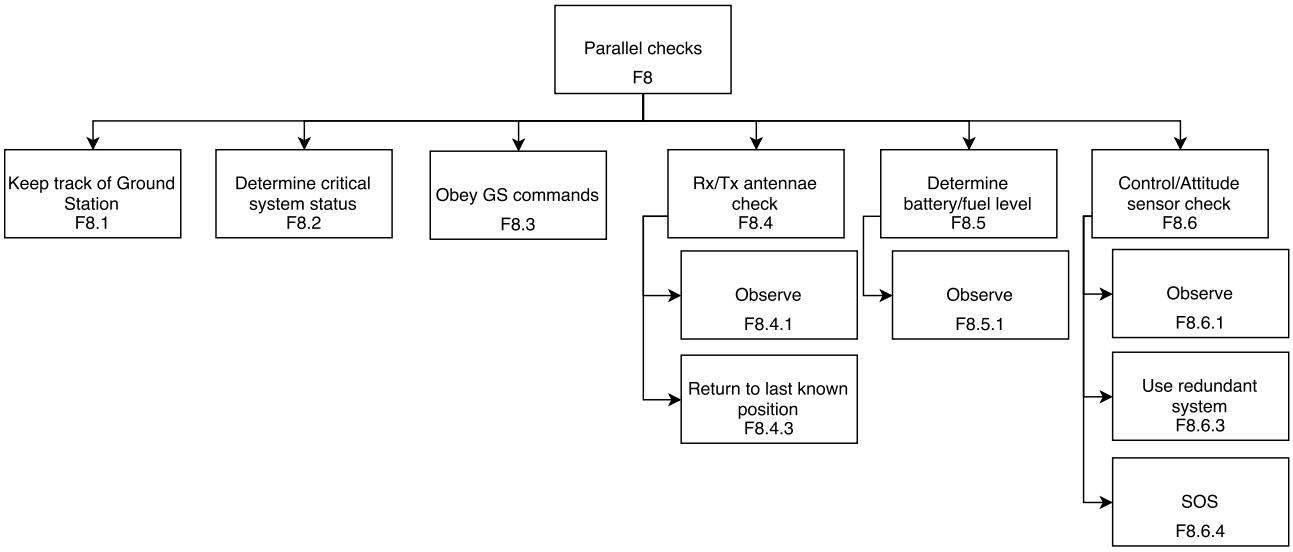

Figure A.5: Functional breakdown structure of the parallel checking system. Displayed up to the second sub-level.

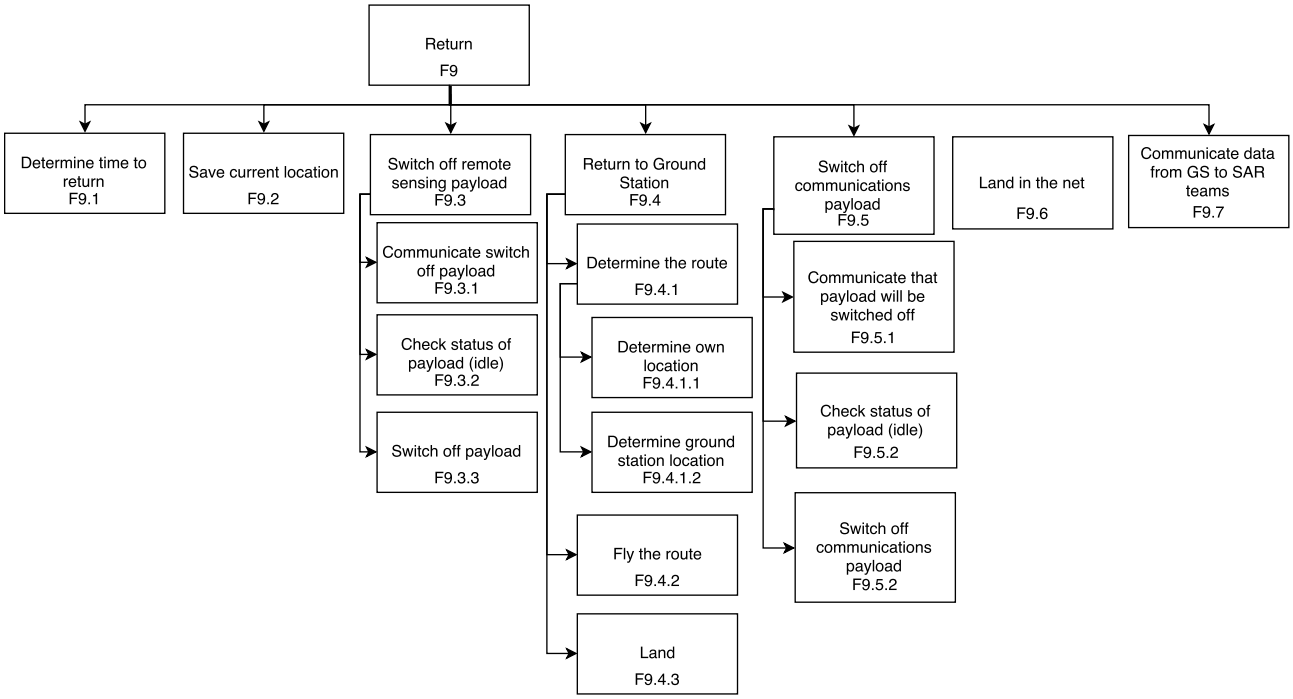

Figure A.6: Functional breakdown structure of the return procedure. Displayed up to the second sub-level.

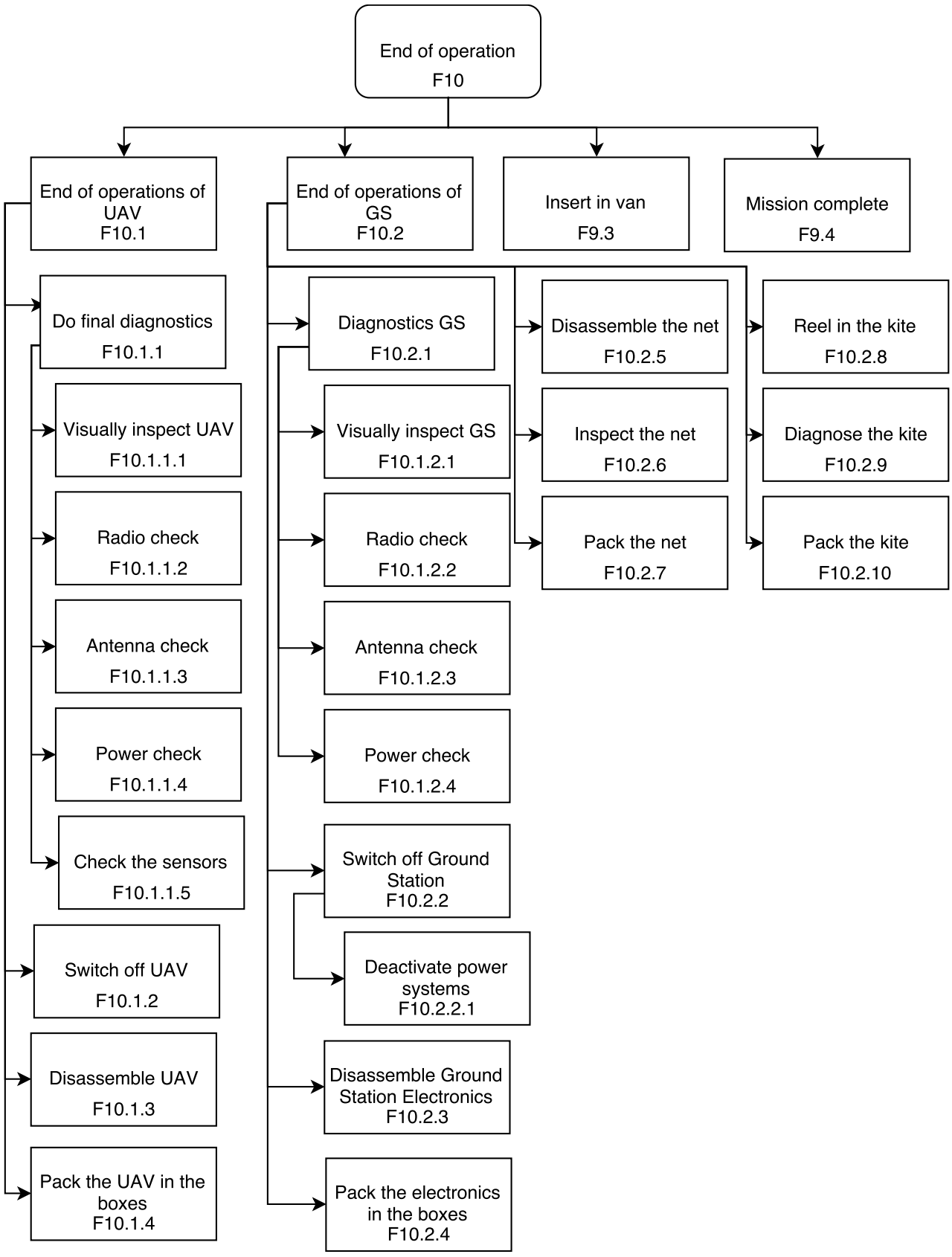

Figure A.7: Functional breakdown structure of the end of the operation. Displayed up to the second sub-level.